Behnam Mohammadi-ivatloo
Morteza Nazari-Heris *Editors*

Robust Optimal Planning and Operation of Electrical Energy Systems

Springer

Robust Optimal Planning and Operation of Electrical Energy Systems

Behnam Mohammadi-ivatloo
Morteza Nazari-Heris
Editors

Robust Optimal Planning and Operation of Electrical Energy Systems

Springer

Editors
Behnam Mohammadi-ivatloo
Faculty of Electrical and Computer Engineering
University of Tabriz
Tabriz, Iran

Morteza Nazari-Heris
Faculty of Electrical and Computer Engineering
University of Tabriz
Tabriz, Iran

ISBN 978-3-030-04295-0 ISBN 978-3-030-04296-7 (eBook)
https://doi.org/10.1007/978-3-030-04296-7

Library of Congress Control Number: 2018968118

This Springer imprint is published by the registered company Springer Nature Switzerland AG
The registered company address is: Gewerbestrasse 11, 6330 Cham, Switzerland

Preface

Considering the existence of uncertain factors in electric energy systems, such as load variation, power market price, and power generation of renewable energy sources, the results provided by the conventional deterministic optimal planning and operation of electric energy systems are not confirmed to be optimal framework for future power system conditions. Accordingly, studying uncertainties associated with parameters of electric energy systems is of importance for obtaining more effective and promising solutions of planning and operation of electric energy systems. In traditional approaches, probabilistic methods, interval-based analysis, and hybrid probabilistic and possibilistic methods are implemented for handling uncertainties associated with power system parameters. Recently, robust optimization (RO) and information gap decision theory (IGDT) methods are introduced as effective tools for the solution of power system problems. The RO and IGDT methods lead to more effective solutions and are promising for the robust planning and operation of electric energy systems. Such methods are capable to obtain optimal performance of the electrical energy systems in the worst-case condition. This book aims to study robust planning and operation of electric energy systems by employing RO and IGDT methods.

The *Robust Optimal Planning and Operation of Electrical Energy Systems* encourages scientific research on all topics pertaining to operation and planning of electric energy systems in the presence of uncertainties attaining a robust level using RO method and IGDT. This book presents the latest research being conducted on differing topics and recent developments and contribution of RO and IGDT methods to the robust optimal planning and operation of the power systems. The topics covered in this book are presented in the following:

- Information gap decision theory.
- Robust optimization method.
- Robust operation of multi-energy systems.
- Risk-constrained scheduling of solar ice harvesting system.
- Robust unit commitment.

- Robust scheduling of smart homes.
- Robust scheduling of electrical distribution networks.
- Robust microgrid and network expansion planning.
- Robust control of distributed energy storage systems.

The book contents are classified into two main parts, where the IGDT and RO method are discussed in the first and second parts, respectively. The aim of the first part is concentrating on definition and application of IGDT method in optimal operation and planning of electrical energy systems, which are summarized as follows:

A review on the application of IGDT in electrical energy systems is provided in Chap. 1, where modeling of uncertain parameter using IGDT is accomplished using a mathematical framework. The principles, fundamentals, applications, and advantages of the IGDT are discussed in Chap. 2. The main aim of Chap. 3 is to study the optimal operation of hub energy systems with the consideration of net price uncertainty using IGDT. Chapter 4 presents an IGDT-based framework for robust scheduling of an ice storage system, where the uncertain nature of building cooling load is studied. IGDT is implemented on a multi-period unit commitment problem in Chap. 5 aiming to maximize total profit obtained from selling electricity to consumers, where the uncertainty of electricity prices is modeled for assessing how market operator can make a risk averse decision at low market prices. Chapter 6 studies energy management of a renewable energy-based smart home, which contains a photovoltaic system for supplying a ratio of electrical demand of the considered home. In this chapter, the robust self-scheduling of a photovoltaic system panel installed in the smart home is formulated, and the best suited set point of all suppliers is obtained, where IGDT is applied for handling the uncertain power generation of the photovoltaic system. The main purpose of Chap. 7 is investigating the unit commitment problem in the presence of renewable energy sources and energy storage systems and modeling the uncertainties arising in this regard. Accordingly, the application of RO method, IGDT, and Taguchi's orthogonal arrays technique as well as their advantages and drawbacks for modeling the renewable energy sources and energy storage systems are studied. Chapter 8 introduces an IGDT-based robust security constrained unit commitment modeling of coordinated electricity and natural gas networks for managing uncertainty of wind power production. A comprehensive transmission system of natural gas, which delivers natural gas fuel to natural gas-fired plants, is considered in this chapter.

The second part aimed to study the application of RO method in investigating optimal robust operation and planning of the electrical energy systems as follows:

Chapter 9 studies a short-term electrical distribution network planning scheme, where a deterministic MILP model is transformed into a two-stage robust optimization model, and this complex trilevel optimization problem is handled using the column and constraint generation method. Chapter 10 presents a stochastic-robust optimization for robust microgrid expansion planning considering intermittent power generations and responsive loads. In this chapter, the presence of active microgrid in the electricity market is studied considering the IPGs/RLs and

contingencies uncertainties. The main purpose of Chap. 11 is studying the robust transmission network expansion planning considering the uncertainties associated with loads and wind power generation. Chapter 12 introduces a hybrid robust-stochastic method for coordinated optimal scheduling of natural gas and electricity cogeneration networks considering market price uncertainties. An optimal multi-agent-based distributed control model is proposed in Chap. 13, where the effects of uncertainties in power distribution system are investigated in terms of power and energy sharing. An optimal robust scheme for optimal day-ahead scheduling of distribution systems is proposed in Chap. 14 for minimizing the operation cost of the system considering load-responsive and renewable energy sources. The authors study uncertainty-based operation of multicarrier energy systems in Chap. 15 using a robust optimization method for dealing with severe uncertainty of upstream network price. Chapter 16 discusses the impact of power market uncertainty in optimal scheduling of the active distribution networks using RO method.

Tabriz, Iran

Behnam Mohammadi-ivatloo
Morteza Nazari-Heris

Acknowledgments

The editors of *Robust Optimal Planning and Operation of Electrical Energy Systems* extend sincere thanks to the invaluable experience of all scientists cooperated in the book and, more specifically, to all authors and reviewers of the book. We extend sincere thanks to the following reviewers list including individuals who have consistently and expeditiously delivered comprehensive, discerning, and valuable reviews.

The list of respectful reviewers is sorted in the following:

Geev Mokryani, University of Bradford, UK
Alireza Soroudi, University College Dublin, Ireland
Mousa Marzband, Northumbria University, UK
Kazem Zare, University of Tabriz, Iran
Amin Mohammadpour, University of Tabriz, Iran
Mahmoud Pesaran, University of Tabriz, Iran
Sajad Madadi, University of Tabriz, Iran
Saeed Abapour, University of Tabriz, Iran
Parinaz Aliaghary, University of Tabriz, Iran
Mohammad Jadid-Bonab, University of Tabriz, Iran
Sayyad Nojavan, University of Tabriz, Iran
Afshin Najafi-Ghalelou, University of Tabriz, Iran
Majid Majidi, University of Tabriz, Iran
Hamed Kharrati, University of Tabriz, Iran
Mohammad Amin Mirzaei, Sahand University of Technology, Iran
Hamdi Abdi, Razi University, Iran

Mehrdad Setayesh Nazar, Shahid Beheshti University, Iran
Milad Zamani, University of Tabriz, Iran
Farkhonde Jabari, University of Tabriz, Iran
Mohammad Hemmati, University of Tabriz, Iran
Farhad Samadi Gazijahani, Azarbaijan Shahid Madani University, Iran

Behnam Mohammadi-ivatloo
Morteza Nazari-Heris

Contents

About the Authors

Behnam Mohammadi-ivatloo is an associate professor at the University of Tabriz, Tabriz, Iran. Before joining the University of Tabriz, he was a research associate at the Institute for Sustainable Energy, Environment and Economy, University of Calgary, Calgary, Canada. He obtained MSc and PhD in electrical engineering from Sharif University of Technology, Tehran, Iran, in 2008 and 2012, respectively. He is head of the Smart Energy Systems Laboratory at the University of Tabriz. The main areas of his interests are renewable energies, microgrid systems, and smart grids.

Morteza Nazari-Heris is a research assistant in Faculty of Electrical and Computer Engineering at the University of Tabriz, Tabriz, Iran. He obtained BSc and MSc in electrical engineering from the University of Tabriz, Tabriz, Iran, in 2015 and 2017, respectively. He is a team member of the Smart Energy Systems Laboratory at the University of Tabriz. The main areas of his interests are microgrids, smart grids, integrated heat and power networks, and energy storage technologies.

Chapter 1
Introduction to Information Gap Decision Theory Method

Farkhondeh Jabari, Behnam Mohammadi-ivatloo, Hadi Ghaebi, and Mohammad-Bagher Bannae-Sharifian

1.1 Motivation

Nowadays, population growth and huge electricity consumption by residential, industrial, commercial, and agriculture sectors lead to more fossil fuel needed to drive thermal power plants and use of renewable energy resources such as solar, wind, geothermal, tidal and ocean waves, hydro, biomass, and biogas [1]. Moreover, gas, water, and power systems are interdependent [2] because natural gas is employed for heating applications such as boiling during power generation cycles, seawater desalting and fresh water production processes, and gas distribution networks. Similarly, pure water is used for cooling, heating, and powering. Meanwhile, uncertainties of renewables and variable nature of cool, heat, power, water, and gas demands may cause these systems to face energy crises and environmental issues, especially in water-stressed tropical regions [3]. Information gap decision theory (IGDT) has recently been discussed by scholars for robust design, operation, and scheduling of water-gas-electricity hybrid grids aiming to model uncertain parameters, evaluate their performance, maximize profit or minimize cost, and make risk-aversion and risk-seeker decisions under uncertain operating conditions. Application of IGDT in poly-generation systems can be classified into two general categories as follows:

- Robust systematic analysis by modeling uncertainties of renewables, loads, and energy tariffs
- Risk analysis of joint energy and reserve markets

F. Jabari (✉) · B. Mohammadi-ivatloo · M.-B. Bannae-Sharifian
Faculty of Electrical and Computer Engineering, University of Tabriz, Tabriz, Iran
e-mail: f.jabari@tabrizu.ac.ir; bmohammadi@tabrizu.ac.ir; sharifian@tabrizu.ac.ir

H. Ghaebi
Department of Mechanical Engineering, University of Mohaghegh Ardabili, Ardabil, Iran
e-mail: hghaebi@uma.ac.ir

B. Mohammadi-ivatloo, M. Nazari-Heris (eds.), *Robust Optimal Planning and Operation of Electrical Energy Systems*,
https://doi.org/10.1007/978-3-030-04296-7_1

1.1.1 Application of IGDT for Modeling Uncertainties of Renewables, Demands, and Energy Tariffs in Systematic Analysis

Rabiee et al. [4] used IGDT for long-term planning of wind products to model its variations. A loading margin index is also defined to improve the static voltage stability of the interconnected power system under uncertain wind generations. In [5], IGDT is implemented on a smart home to model electricity price fluctuations aiming to minimize daily operation cost of the building. In this study, smart home consists of fuel cell, backup, and auxiliary boilers for heat and power generation, battery pack for energy storage, and electrical appliances. Nojavan et al. [6] scheduled a solar photovoltaic-fuel cell-battery-local grid connected system for supplying both electrical and heat demands. They considered load uncertainty on building energy management strategy. A robust security-constrained unit commitment problem is solved by Nikoobakht and Aghaei [7] to model the wind generation uncertainty. Up and down ramp rates of thermal power plants, DRPs, energy storage units, and transmission lines switching are used for load-generation balancing in wind products shortage condition. In [8], pool market prices and electricity demand of distribution system buses have been considered as uncertain parameters using IGDT to enable system operator for making risk-aversion and risk-taker decisions in load flow problem. Ahmadigorji et al. [9] developed a multilayer robust distribution network planning approach via IGDT by considering loads, hourly prices, investment, and operation costs as uncertain variables. Amjady et al. [10] applied IGDT on multiyear transmission expansion planning problem. Impact of variations of loads and investment cost in transmission expansion process is evaluated by IGDT. In [11], optimal power flow problem is solved in huge power systems incorporating wind power uncertainties and considering some operational criteria such as HVDC voltage source converter, lines communication link, and feasible generation region of doubly fed induction generators. In [12], deviations of loads and power generation of distributed units in restoration of distribution grids after occurring a widespread disturbance are modeled by IGDT. In [13, 14], a short-term self-scheduling problem is solved for maximization of GenCo's daily profit under market price fluctuations. In [15], output power of wind farms and outages of transmission lines are modeled using IGDT as uncertain variables in design of wide-area power system stabilizers and robust control of inter-area oscillations. In [16], optimum size and installation time of distributed generation units in a microgrid are determined based on IGDT. Two types of uncertain parameters have been considered by authors: (a) random variables such as power generation of renewable energy resources and consumption of electrical loads, which are included by bilinear Benders decomposition technique-based chance constraints, and (b) nonrandom long-term growth of demand which is modeled by IGDT. In [17], optimal power flow problem is solved taking into account the steady-state voltage stability criterion and the wind power uncertainty for the worst-case analysis of the interconnected electricity grids. In this approach,

Table 1.1 Application of IGDT in poly-generation systems

References	Uncertain variables	Study fields
[19]	Electricity prices	Robust management of thermal and electrical demands in smart homes equipped with smart appliances, water storage tank, boilers, batteries, and fuel cells
[20]	Solar and energy tariffs	Optimal co-scheduling of heat and power in smart apartment buildings
[21]	Price and wind	Self-scheduling of wind generators
[22]	Wind	Unit commitment
[23]	Hear demand	Short-term scheduling of solar-driven industrial continuous heat treatment furnace
[24]	Pool price	Optimal mid-term selling/purchasing pricing strategy for electricity retailers
[25]	Electrical demand	Optimization of photovoltaic cells-battery-fuel cells hybrid multi-generation system
[26]	Chemical pollutants	Ecological risk management of chemical substances
[27]	Pool price	Optimal co-dispatching of combined heat and power units
[28]	Price	Day-ahead scheduling of aggregators of electric vehicles

maximum budget of uncertainty with minimum distance to voltage collapse point is found. In [18], it is proved that IGDT is a cost-effective scheme for managing the active distribution grids and providing the sufficient spinning reserves for upstream transmission system via modeling the variations of the renewable energy sources. Table 1.1 summarizes the taxonomy of its applications in different study fields.

1.1.2 Risk-Aversion and Risk-Seeker Decisions in Energy and Reserve Markets Using IGDT

In [29], the impact of electricity market price uncertainty in large consumers' energy procurement process is investigated. Various sources of energy suppliers such as battery, wind, photovoltaic, and local power system have been considered. Moreover, economic benefit of real-time demand response programs (DRPs) is proved using two case studies: (a) with IGDT and without DRPs and (b) with IGDT and DRPs. It should be mentioned that US Department of Energy (DOE) defines DRPs as effective and practical solutions to change the energy usage pattern of the residential, commercial, and industrial consumers considering the variations of electricity tariffs and incentive payments [30]. In [31], joint energy and reserve market is cleared by solving a robust unit commitment problem using IGDT. In this research, IGDT is applied on flexible loads to model their uncertain responses in offering consumption reduction capacities against hourly prices for participation in

reserve markets. In [32], hourly offering and bidding strategies of retailers is optimized, and real-time, fixed, and time-of-use market prices are determined by IGDT's robustness and opportunistic modes. In addition, a scenario-based stochastic methodology is proposed for modeling uncertainties associated with loads, ambient temperature, solar irradiance, and wind speed. An IGDT hybrid modified particle swarm optimization (MPSO) is employed in [33] to consider the uncertain prices, while price-taker producers participate in day-ahead market. In [34, 35], IGDT considers the price fluctuations in pool market for investigation of robustness and opportunistic aspects of energy procuring for large-scale consumers. In this analysis, distributed generation units, electricity purchasing from pool market, and bilateral contracts have been considered for supplying large customers. Nojavan et al. [36] solved this problem by considering DRPs. A weighted average squared error index-based variance-covariance matrix is also introduced by them [37, 38] to model the price uncertainty in solving the same problem. Alipour et al. [39] proposed an IGDT-based bidding framework for industrial applications with coproduction of heat and power, boilers, and power-only plants to participate in day-ahead electricity market. Kazemi et al. [40, 41] used IGDT for modeling day-ahead market price uncertainty and achieving optimum bidding curve of electric utilities with and without implementation of DRPs. Shafiee et al. [42] constructed a bidding-offering risk-constrained strategy for merchant compressed air energy storages and modeled unfavorable variations of day-ahead market prices using IGDT. Authors of [43] implemented IGDT on fuel, CO_2, and electricity trading problem and modeled the price uncertainty for robust scheduling of fossil fuel-driven thermal power plants.

Other sections of this chapter are structured as follows: In Sect. 1.2, a mathematical formulation is presented for uncertainty modeling by IGDT. Section 1.3 suggests some research fields as future trends and concludes chapter.

1.2 Mathematical Modeling of Uncertain Parameter Using IGDT

As mentioned in the previous subsection, information gap decision theory is a risk-assessed decision-making process, which makes some cost-effective and robust decisions against uncertain parameter using two robustness and opportunistic modes. The uncertain parameter of the optimization process can be adverse and causes the higher costs or lower profits or favorable with lower costs and higher profits. In other words, it addresses the robustness and the opportunity viewpoints of the optimization problem considering the variable nature of the uncertain parameter using the following requirements: objective function, performance investigation, and uncertainty analysis.

1.2.1 Objective Function

It is assumed that λ_t is an uncertain parameter for a minimization or maximization problem at operating time interval t. We consider that α refers to uncertainty variable and changes between 0 and 1 for decision variables $x_{i,t}$. Objective function, $F(x_{i,t}, \lambda_t)$, which indicates total cost (or expected profit) in a T-hour study horizon, should be minimized (or maximized). It evaluates all responses to choices of the decision-maker, $x_{i,t}$, and variable parameter, λ_t.

1.2.2 Implementation Requirement

In this subsection, expectations of system operator from objective function are stated in terms of total cost or profit and assessed by robustness and opportunity modes as Eqs. (1.1) and (1.2), respectively. According to relation (1.1), optimization problem is solved in robustness mode with maximum value of uncertainty variable, α, in a way that total cost cannot exceed from target cost or total profit cannot be lower than critical profit, F_k. Therefore, uncertainty variable, α, should be maximized as Eq. (1.3), in which F_k refers to a predefined target cost (or minimum expected profit) in robustness mode. By considering $\widehat{\alpha}(x_{i,t}, F_k)$, system operator makes a robust decision with less sensitivity to variations of uncertain parameter, λ_t, so that total cost is smaller than predefined target cost F_k or expected profit is more than critical profit F_k.

$$\alpha = \underset{\alpha}{\text{Max}} \left\{ \begin{array}{l} \alpha: \text{Maximum cost which is lower than the given target cost} \\ \text{or Minimum profit which is higher than the given critical profit} \end{array} \right\} \times \{\text{Robustness}\} \tag{1.1}$$

$$\beta = \underset{\beta}{\text{Min}} \left\{ \begin{array}{l} \beta: \text{Minimum cost which is lower than the given target cost} \\ \text{or Maximum profit which is higher than the given target profit} \end{array} \right\} \times \{\text{Opportunity}\} \tag{1.2}$$

$$\widehat{\alpha}(x_{i,t}, F_k) = \underset{\alpha}{\text{Max}} \left\{ \begin{array}{ll} \alpha : \underset{x_{i,j}}{\text{Max}}\ F(x_{i,j}, \lambda_t) \le F_k & \text{Cost minimization} \\ \alpha : \underset{x_{i,j}}{\text{Min}}\ F(x_{i,j}, \lambda_t) \ge F_k & \text{Profit maximization} \end{array} \right\} \tag{1.3}$$

A risk-taker decision-maker desires higher profit via implementation of opportunity function. As formulated in Eq. (1.4), variable β refers to minimum level of α aiming to pay lower cost and obtain higher profit as a result of decision variables, $x_{i,t}$. Note that F_w represents maximum cost or minimum profit in opportunity mode that is defined by decision-maker to pay less and obtain more profit under favorable deviations of uncertain parameter, λ_t, and is generally smaller than F_k.

$$\widehat{\beta}(x_{i,t}, F_w) = \underset{\alpha}{\text{Min}} \left\{ \begin{array}{ll} \alpha : \underset{x_{i,t}}{\text{Min}}\ F(x_{i,t}, \lambda_t) \le F_w & \text{Cost minimization} \\ \alpha : \underset{x_{i,t}}{\text{Max}}\ F(x_{i,t}, \lambda_t) \ge F_w & \text{Profit maximization} \end{array} \right\} \tag{1.4}$$

1.2.3 Uncertainty Formulation

For robust and opportunistic optimization processes, actual value of uncertain parameter can be calculated from information gap models as Eqs. (1.5a), (1.5b), (1.5c), (1.5d), and (1.5e) [44]:

- Energy-bound model: In this method, the uncertain parameter, λ_t, deviates from the forecasted or nominal value, $\tilde{\lambda}_t$, within some nested intervals with nesting parameter, α, as shown in Eq. (1.5a).

$$U\left(\alpha, \widetilde{\lambda}_t\right) = \left\{ \lambda_t : \int_0^{\infty} \left(\lambda_t - \tilde{\lambda}_t\right)^2 \mathrm{d}t \le \alpha^2 \right\}; \quad \alpha \ge 0, \quad \forall t \tag{1.5a}$$

- Envelope-bound method: In the envelope-bound information gap model, a known function ψ_t is used to determine the envelope shape of the uncertain parameter in a way that the distance of the actual value from the forecasted or nominal one is smaller than or equal to $\alpha\psi_t$, as stated in Eq. (1.5b).

$$U\left(\alpha, \tilde{\lambda}_t\right) = \left\{ \lambda_t : \left|\lambda_t - \tilde{\lambda}_t\right| \le \alpha\psi_t \right\}; \quad \alpha \ge 0, \quad \forall t \tag{1.5b}$$

- Fractional error approach: According to relation (1.5c), this model represents that the fractional deviation of the uncertain variable from the forecasted value is smaller than the scaler parameter α.

$$U\left(\alpha, \tilde{\lambda}_t\right) = \left\{ \lambda_t : \left|\frac{\lambda_t - \tilde{\lambda}_t}{\tilde{\lambda}_t}\right| \le \alpha \right\}; \quad \alpha \ge 0, \quad \forall t \tag{1.5c}$$

- Combined info-gap models: Integrating two energy-bound and envelope-bound models, the actual value of uncertain variable can be estimated as relation (1.5d).

$$U\left(\alpha, \widetilde{\lambda}_t\right) = \left\{ \lambda_t : \left|\lambda_t - \tilde{\lambda}_t\right| \le \alpha\psi_t \text{ and } \int_0^{\infty} \left(\lambda_t - \tilde{\lambda}_t\right)^2 \mathrm{d}t \le \alpha^2 \right\}; \quad \alpha \ge 0, \forall t \tag{1.5d}$$

- Non-convex information gap method: As inequality constraint (1.5e), if uncertain variable λ_t belongs to interval $[0, \pi]$, $\mathrm{d}^2\lambda_t/\mathrm{d}t^2$ will change between $-\omega^2$ and 0. Else if $\lambda_t \in [-\pi, 0]$, we have $-\omega^2 \leq \mathrm{d}^2\lambda_t/\mathrm{d}t^2 \leq 0$.

$$U(\alpha, \tilde{\lambda}_t) = \left\{ \lambda_t : \left|\lambda_t - \tilde{\lambda}_t\right| \leq \alpha\psi\left(\lambda_t, \frac{\mathrm{d}^2\lambda_t}{\mathrm{d}t^2}\right),\ \frac{\mathrm{d}^2\lambda_t}{\mathrm{d}t^2} = -\omega^2 \sin\lambda_t \right\};\quad \alpha \geq 0, \forall t \quad (1.5e)$$

1.2.4 Implementing Risk-Aversion and Robust Decision-Making Strategy

The robustness variable, $\widehat{\alpha}(x_{i,t}, F_k)$, operates as a risk-aversion tool and indicates the greatest amount of the uncertainty variable, α, while the maximum cost (or minimum profit) is lower (or higher) than the target value, F_k. Hence, a high value of $\widehat{\alpha}(x_{i,t}, F_k)$ corresponds to the higher cost (or lower profit), F_k, indicating that this decision is robust. Hence, it is expected that $\widehat{\alpha}(x_{i,t}, F_k)$ increases with the increase of F_k in cost minimization problem and decreases with the increase of F_k for maximization of expected profit. The uncertain parameter can be stated as Eq. (1.6). Positive sign is used if increasing rate of λ_t causes an increase in cost objective function. If decreasing rate of λ_t leads to a decrease in profit objective function, negative sign will be considered. According to Eq. (1.7), objectives are maximization of α for a minimum expected profit or a given maximum cost, F_k.

$$\lambda_t = \tilde{\lambda}_t \pm \alpha\tilde{\lambda}_t,\ \forall t = 1, 2, \ldots, T \quad (1.6)$$

$$\widehat{\alpha}(\tilde{x}_{i,t}, F_k) = \max_{\alpha}\left\{ \alpha : \max_{\tilde{x}_{i,t}} \text{cost} \leq F_k \text{ or } \min_{\tilde{x}_{i,t}} \text{profit} \geq F_k \right\} \quad (1.7)$$

1.2.5 Implementing Risk-Seeker and Opportunistic Design Making Strategy

The opportunity function, $\widehat{\beta}(x_{i,t}, F_w)$, assesses the feasibility of the low cost or high profit. Therefore, a small value of $\widehat{\beta}(x_{i,t}, F_w)$ is desired. According to Eq. (1.8), the opportunity variable is the least amount of α for minimization of total cost as low as F_w or maximization of expected profit as high as target profit, F_w. Therefore, it is expected that $\widehat{\beta}(x_{i,t}, F_w)$ increases with reduction of F_w for cost minimization approach and increases with increase of F_w for profit maximization problem as Eqs. (1.8), (1.9), and (1.10). If decreasing rate of λ_t causes a decrease in cost objective function, negative sign will be considered in optimization problem. Else if increasing rate of λ_t leads to an increase in profit objective function, positive sign will be used.

$$\widehat{\beta}(x_{i,t}, F_w) = \underset{x_{i,t}}{\text{Min}}\, \widehat{\alpha}(x_{i,t}, F_w) \tag{1.8}$$

$$\lambda_t = \tilde{\lambda}_t \mp \alpha\tilde{\lambda}_t,\ \forall t = 1, 2, \ldots, T \tag{1.9}$$

$$\widehat{\beta}\left(\tilde{x}_{i,t}, F_w\right) = \underset{\alpha}{\text{Min}} \left\{ \alpha : \underset{\tilde{x}_{i,t}}{\text{Min}}\, \text{cost} \leq F_w \text{ or } \underset{\tilde{x}_{i,t}}{\text{Max}}\, \text{profit} \geq F_w \right\} \tag{1.10}$$

1.3 Conclusion and Future Trend

In this chapter, information gap decision theory was introduced as a risk-assessment tool in power system studies. Firstly, advantages of IGDT technique in comparison with other uncertainty modeling approaches such as robust optimization, probabilistic methods, etc. were discussed. Then, uncertainty analysis using IGDT in power system and energy market researches was classified into two general categories consisting of "Application of IGDT for modelling uncertainties of renewables, demands and energy tariffs in systematic analysis" and "Risk-averse and risk-seeker decisions in energy and reserve markets using IGDT." Authors of this chapter are working on risk-constrained design and scheduling of a novel combined cooling and power generation system using IGDT. Uncertainty of ambient air temperature on power generation (supply side) and cooling load (demand side) of a benchmark industrial prosumer will be investigated. In other words, impacts of uncertainty of a variable parameter such as ambient air temperature on both generation and consumption sides will be analyzed for making robust and risk-seeker decisions and determining optimum operating point of power generation cycle and air conditioning unit. Moreover, implementation of IGDT hybrid robust optimization methods is suggested for modeling uncertainties.

References

1. Jabari, F., et al. (2016). Optimal short-term scheduling of a novel tri-generation system in the presence of demand response programs and battery storage system. *Energy Conversion and Management, 122*, 95–108.
2. Jabari, F., et al. (2018). Design and performance investigation of a biogas fueled combined cooling and power generation system. *Energy Conversion and Management, 169*, 371–382.
3. Jabari, F., Nojavan, S., & Mohammadi Ivatloo, B. (2016). Designing and optimizing a novel advanced adiabatic compressed air energy storage and air source heat pump based μ-combined cooling, heating and power system. *Energy, 116*, 64–77.
4. Rabiee, A., Nikkhah, S., & Soroudi, A. (2018). Information gap decision theory to deal with long-term wind energy planning considering voltage stability. *Energy, 147*, 451–463.
5. Najafi-Ghalelou, A., Nojavan, S., & Zare, K. (2018). Robust thermal and electrical management of smart home using information gap decision theory. *Applied Thermal Engineering, 132*, 221–232.

6. Nojavan, S., Majidi, M., & Zare, K. (2017). Performance improvement of a battery/PV/fuel cell/grid hybrid energy system considering load uncertainty modeling using IGDT. *Energy Conversion and Management, 147*, 29–39.
7. Nikoobakht, A., & Aghaei, J. (2017). IGDT-based robust optimal utilisation of wind power generation using coordinated flexibility resources. *IET Renewable Power Generation, 11*(2), 264–277.
8. Soroudi, A., & Ehsan, M. (2013). IGDT based robust decision making tool for DNOs in load procurement under severe uncertainty. *IEEE Transactions on Smart Grid, 4*(2), 886–895.
9. Ahmadigorji, M., Amjady, N., & Dehghan, S. (2018). A robust model for multiyear distribution network reinforcement planning based on information-gap decision theory. *IEEE Transactions on Power Systems, 33*(2), 1339–1351.
10. Dehghan, S., Kazemi, A., & Amjady, N. (2014). Multi-objective robust transmission expansion planning using information-gap decision theory and augmented ?-constraint method. *IET Generation, Transmission & Distribution, 8*, 828–840.
11. Rabiee, A., Soroudi, A., & Keane, A. (2015). Information gap decision theory based OPF with HVDC connected wind farms. *IEEE Transactions on Power Systems, 30*(6), 3396–3406.
12. Chen, K., et al. (2015). Robust restoration decision-making model for distribution networks based on information gap decision theory. *IEEE Transactions on Smart Grid, 6*(2), 587–597.
13. Mohammadi-Ivatloo, B., et al. (2013). Application of information-gap decision theory to risk-constrained self-scheduling of GenCos. *IEEE Transactions on Power Systems, 28*(2), 1093–1102.
14. Mathuria, P., & Bhakar, R. (2014). Info-gap approach to manage GenCo's trading portfolio with uncertain market returns. *IEEE Transactions on Power Systems, 29*(6), 2916–2925.
15. Ke, D., et al. (2018). Application of information gap decision theory to the design of robust wide-area power system stabilizers considering uncertainties of wind power. *IEEE Transactions on Sustainable Energy, 9*(2), 805–817.
16. Cao, X., Wang, J., & Zeng, B. (2018). A chance constrained information-gap decision model for multi-period microgrid planning. *IEEE Transactions on Power Systems, 33*(3), 2684–2695.
17. Rabiee, A., et al. (2017). Information gap decision theory for voltage stability constrained OPF considering the uncertainty of multiple wind farms. *IET Renewable Power Generation, 11*(5), 585–592.
18. Zhao, T., Zhang, J., & Wang, P. (2016). Flexible active distribution system management considering interaction with transmission networks using information-gap decision theory. *CSEE Journal of Power and Energy Systems, 2*(4), 76–86.
19. Najafi-Ghalelou, A., Nojavan, S., & Zare, K. (2018). Heating and power hub models for robust performance of smart building using information gap decision theory. *International Journal of Electrical Power & Energy Systems, 98*, 23–35.
20. Najafi-Ghalelou, A., Nojavan, S., & Zare, K. (2018). Information gap decision theory-based risk-constrained scheduling of smart home energy consumption in the presence of solar thermal storage system. *Solar Energy, 163*, 271–287.
21. Moradi-Dalvand, M., et al. (2015). Self-scheduling of a wind producer based on information gap decision theory. *Energy, 81*, 588–600.
22. Soroudi, A., Rabiee, A., & Keane, A. (2017). Information gap decision theory approach to deal with wind power uncertainty in unit commitment. *Electric Power Systems Research, 145*, 137–148.
23. Jabari, F., et al. (2018). Risk-constrained scheduling of solar Stirling engine based industrial continuous heat treatment furnace. *Applied Thermal Engineering, 128*, 940–955.
24. Charwand, M., & Moshavash, Z. (2014). Midterm decision-making framework for an electricity retailer based on information gap decision theory. *International Journal of Electrical Power & Energy Systems, 63*, 185–195.

25. Nojavan, S., Majidi, M., & Zare, K. (2017). Risk-based optimal performance of a PV/fuel cell/battery/grid hybrid energy system using information gap decision theory in the presence of demand response program. *International Journal of Hydrogen Energy, 42*(16), 11857–11867.
26. Yokomizo, H., et al. (2013). Setting the most robust effluent level under severe uncertainty: Application of information-gap decision theory to chemical management. *Chemosphere, 93* (10), 2224–2229.
27. Aghaei, J., et al. (2017). Optimal robust unit commitment of CHP plants in electricity markets using information gap decision theory. *IEEE Transactions on Smart Grid, 8*(5), 2296–2304.
28. Zhao, J., et al. (2017). Risk-based day-ahead scheduling of electric vehicle aggregator using information gap decision theory. *IEEE Transactions on Smart Grid, 8*(4), 1609–1618.
29. Bagal, H. A., et al. (2018). Risk-assessment of photovoltaic-wind-battery-grid based large industrial consumer using information gap decision theory. *Solar Energy, 169*, 343–352.
30. Qdr, Q. (2006). *Benefits of demand response in electricity markets and recommendations for achieving them.* US Department of Energy.
31. Ghahary, K., et al. (2018). Optimal reserve market clearing considering uncertain demand response using information gap decision theory. *International Journal of Electrical Power & Energy Systems, 101*, 213–222.
32. Nojavan, S., Zare, K., & Mohammadi-Ivatloo, B. (2017). Risk-based framework for supplying electricity from renewable generation-owning retailers to price-sensitive customers using information gap decision theory. *International Journal of Electrical Power & Energy Systems, 93*, 156–170.
33. Nojavan, S., Zare, K., & Ashpazi, M. A. (2015). A hybrid approach based on IGDT–MPSO method for optimal bidding strategy of price-taker generation station in day-ahead electricity market. *International Journal of Electrical Power & Energy Systems, 69*, 335–343.
34. Zare, K., Moghaddam, M. P., & Sheikh-El-Eslami, M. K. (2011). Risk-based electricity procurement for large consumers. *IEEE Transactions on Power Systems, 26*(4), 1826–1835.
35. Zare, K., Moghaddam, M. P., & Sheikh El Eslami, M. K. (2010). Electricity procurement for large consumers based on information gap decision theory. *Energy Policy, 38*(1), 234–242.
36. Nojavan, S., Ghesmati, H., & Zare, K. (2016). Robust optimal offering strategy of large consumer using IGDT considering demand response programs. *Electric Power Systems Research, 130*, 46–58.
37. Nojavan, S., & Zare, K. (2013). Risk-based optimal bidding strategy of generation company in day-ahead electricity market using information gap decision theory. *International Journal of Electrical Power & Energy Systems, 48*, 83–92.
38. Zare, K., Moghaddam, M. P., & Sheikh El Eslami, M. K. (2010). Demand bidding construction for a large consumer through a hybrid IGDT-probability methodology. *Energy, 35*(7), 2999–3007.
39. Alipour, M., Zare, K., & Mohammadi-Ivatloo, B. (2016). Optimal risk-constrained participation of industrial cogeneration systems in the day-ahead energy markets. *Renewable and Sustainable Energy Reviews, 60*, 421–432.
40. Kazemi, M., Mohammadi-Ivatloo, B., & Ehsan, M. (2015). Risk-constrained strategic bidding of GenCos considering demand response. *IEEE Transactions on Power Systems, 30*(1), 376–384.
41. Kazemi, M., Mohammadi-Ivatloo, B., & Ehsan, M. (2014). Risk-based bidding of large electric utilities using information gap decision theory considering demand response. *Electric Power Systems Research, 114*, 86–92.
42. Shafiee, S., et al. (2017). Risk-constrained bidding and offering strategy for a merchant compressed air energy storage plant. *IEEE Transactions on Power Systems, 32*(2), 946–957.
43. Mathuria, P., & Bhakar, R. (2015). GenCo's integrated trading decision making to manage multimarket uncertainties. *IEEE Power & Energy Society General Meeting*. (pp. 1–1).
44. Ben-Haim, Y. (2006). Chapter 2: Uncertainty. In Y. Ben-Haim (Ed.), *Info-gap decision theory* (2nd ed., pp. 9–36). Oxford: Academic.

Chapter 2
Information-Gap Decision Theory: Principles and Fundamentals

Navid Rezaei, Abdollah Ahmadi, Ali Esmaeel Nezhad, and Amirhossein Khazali

2.1 Introduction

Optimization problems have been defined and applied to various fields of science and technology. For simplicity, many of the variables and parameters that are involved in these problems are assumed to be deterministic variables with no variation in real time. Nevertheless, in reality, many of these parameters indicate stochastic behaviors or are totally ambiguous to the decision-maker. Therefore, making decisions in uncertain spaces is a usual matter. Nonetheless, the question is how the best decision can be made in this space to be resilient against deviations of uncertain variables from their forecasted amount. Information-gap decision theory answers this matter and also specifies how much uncertain variables can deviate while the performance of the system stays acceptable [1–3].

Dealing with these parameters such as deterministic variables and making decisions based on these erroneous presumptions can lead to undesirable results and impose excessive costs on the system. Therefore, implementing different approaches and methods which are capable of handling the uncertain space of the problems is

N. Rezaei
Electrical Engineering Department, University of Kurdistan, Sanandaj, Iran
e-mail: n.rezaei@uok.ac.ir

A. Ahmadi (✉)
School of Electrical Engineering and Telecommunication, University of New South Wales, Sydney, NSW, Australia
e-mail: a.ahmadi@unsw.edu.au

A. E. Nezhad
Department of Electrical, Electronic, and Information Engineering, University of Bologna, Bologna, Italy

A. Khazali
Electrical Engineering Department, Iran University of Science and Technology, Tehran, Iran

B. Mohammadi-ivatloo, M. Nazari-Heris (eds.), *Robust Optimal Planning and Operation of Electrical Energy Systems*,
https://doi.org/10.1007/978-3-030-04296-7_2

inevitable. During the last decade, different frameworks have been represented to incorporate uncertain characteristics in optimization problems such as probabilistic and stochastic programming, fuzzy optimization, interval optimization, and robust optimization. Each of these approaches has their advantages and drawbacks and is suitable for different types of optimization problems. Probabilistic and stochastic approaches are highly dependent on historical data of uncertain variables and the related probabilistic density function. Hence, in the case that these data are inaccurate or unavailable, the decisions made cannot be trusted. Furthermore, for the stochastic programming approach, while few scenarios cannot cover the whole uncertain space, increasing the number of scenarios increases the computational burden of the problem. The fuzzy optimization problem suffers from the similar problem and has to solve the optimization problem for different α-cuts. Interval and robust optimization both require uncertainty sets to be known in addition to this matter that robust optimization is a bi-level optimization problem which is usually difficult to solve [4]. Figure 2.1 shows how each approach deals with uncertainties. For the stochastic programming approach, the uncertain space is summarized as a number of scenarios. Fuzzy decision-making uses membership functions to handle the uncertainties of the system. Robust and interval optimization assume a certain space in which the uncertainties can vary and tackle the optimization problem according to this space. For the IGDT approach, an uncertain space is considered which is not determined and changes according to the characteristics of the optimization problem.

Despite all of these flaws, the information-gap decision theory (IGDT) does not require the exact interval of uncertainty sets. Indeed, according to the uncertainty budget, a decision is adopted to make the objective function robust against variations of uncertain variables. Figure 2.2 depicts the concept of IGDT compared with other optimization frameworks from the view of required data. As illustrated in this figure, according to the amount that the objective function can deviate (from the objective function which is acquired in the base case with deterministic variables), a specific portion of the uncertainty space can be handled [4].

Robustness and opportuneness are two main strategies for IGDT approach. These two conflicting concepts stem from uncertainties of different variables. While the robustness function estimates the resiliency to failure, opportuneness seeks the chance of a windfall. These immunity functions (robustness and opportuneness) are the main principals of IGDT [1]. These functions help the decision-maker to cope with various trade-offs and make a cost between the costs and reliability issues of the problem.

As explained, IGDT is a decision-making tool for uncertain circumstances. This method can be summarized in three main stages [1]:

1. Modeling the uncertain parameters

   In this section stochastic variables in which their deviation from forecasted amounts is salient have to be identified. As mentioned, no historical data or probabilistic density function is required for this approach.
2. Defining the desired strategy (robustness or opportuneness)

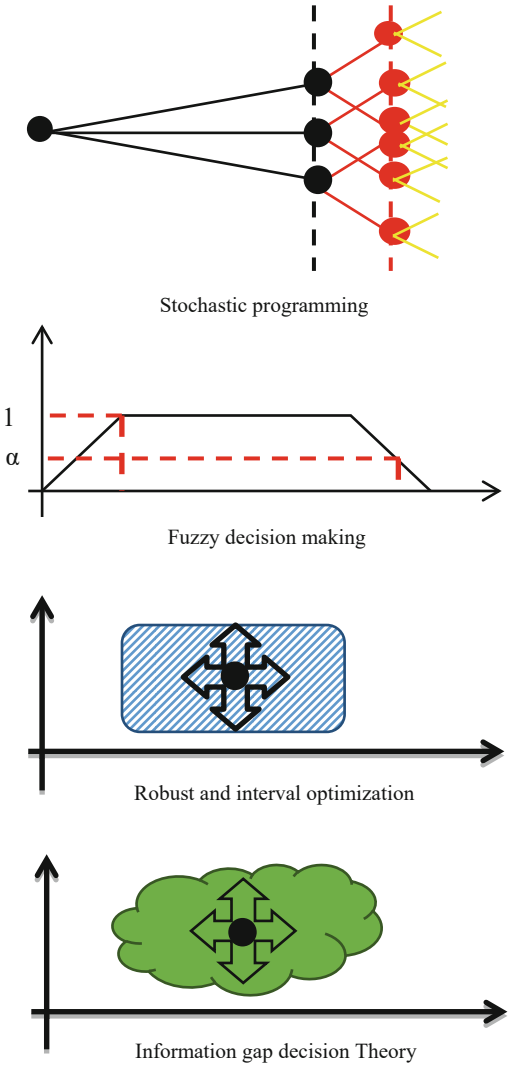

Fig. 2.1 Comparison between data required for different approaches

This strategy specifies as to what extent the uncertain variables and inputs can change while assuring the minimum income for the decision-maker (robustness strategy) or how should uncertain variables change to achieve a minimum windfall. Figure 2.3 shows a simple concept of robustness and opportuneness.

3. Analyzing to what extent uncertain parameters can deviate from their forecasted amounts according to the determined objective function

In this stage, the final decision is made, according to the minimum income, how much robustness is required, or on the other hand which option gathers the desired windfall according to variations of uncertain variables. Indeed, IGDT calculates the uncertainty horizon α around a forecasted amount u for a minimum

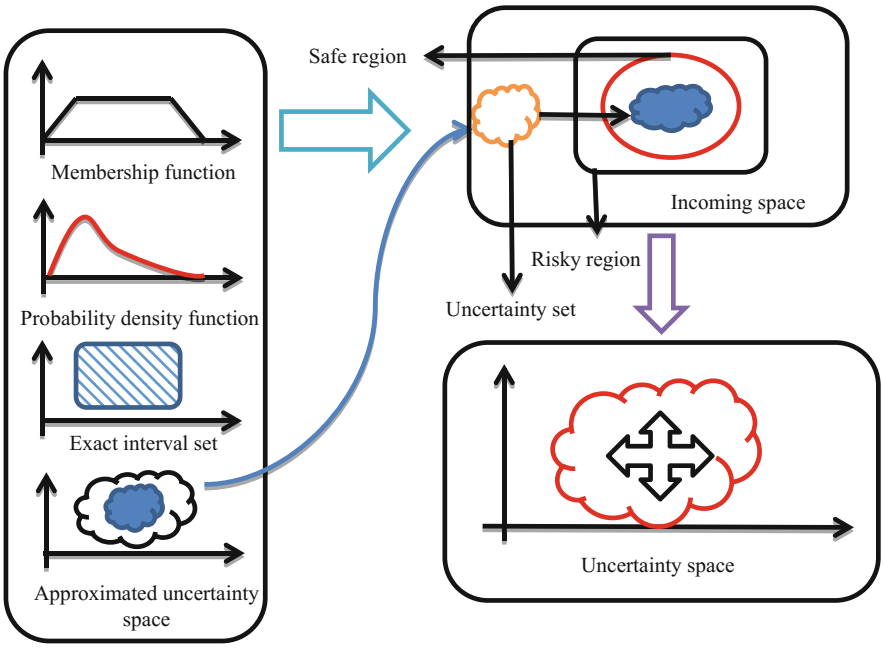

Fig. 2.2 Principles of IGDT

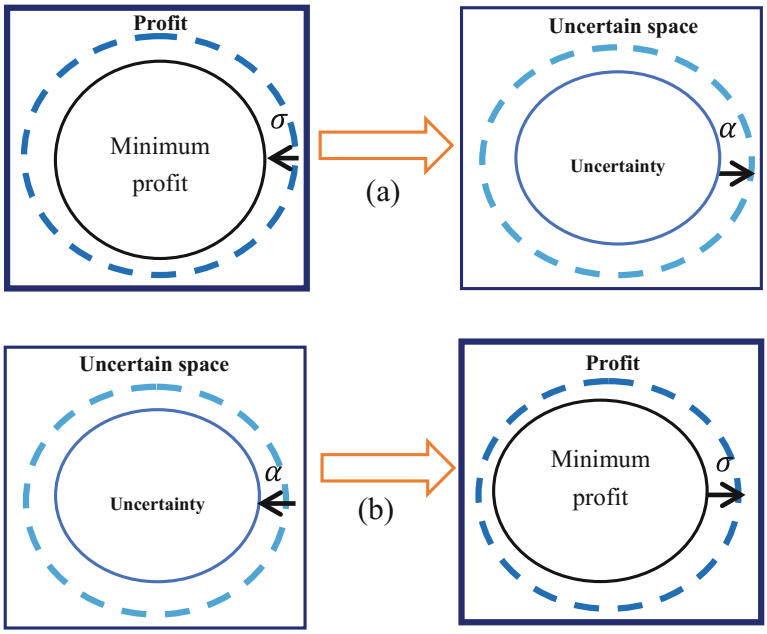

Fig. 2.3 Concepts of (**a**) robustness strategy and (**b**) opportuneness strategy

income (robustness) or the desired windfall. Figure 2.3 indicates a simple concept for robustness and opportuneness. In Fig. 2.3a the decision-maker is pessimistic and decreases the minimum profit (proportional to a coefficient such as σ) with the aim of handling a larger portion of the uncertain space. Nevertheless, in Fig. 2.3b the decision-maker is optimistic about the uncertainties of the system, and the more the uncertain variables deviate from the forecasted amount (in an advantageous way), the more profit is gained.

Despite probabilistic approaches which assign probabilities to each outcome, no probability is assumed in the IGDT approach, and only deviations from the forecasted amounts are considered. Furthermore, despite the min–max approach, it does not only consider the worst situation of the problem space.

After obtaining the robustness or opportuneness function, the decision-maker has to select the final amount. Although these functions are numerical, there is no numerical approach or a certain algorithm to choose the final decision based on the value of these functions. Hence, the decision-maker has to make a connection between these numerical amounts and the qualitative characteristics of the problem. It is definite that larger amounts of the robustness function α are more desired. The questions are how much should this function increase and what are the consequences of this increment? Despite the immunity function, determining how much is a solution desired can be interpreted as a qualitative judgment based on experience and knowledge of the problem [1]. Even using a probability P based on probabilistic theory decision needs a qualitative criterion. Larger amounts of P and α are desired, yet this cannot be used to select the final solution. The simplest way of making the final decision is considering previous experience with the system. Another approach is converting the immunity function α to a dimensionless parameter using a normalizing approach discussed in [1].

The other important issue about the immunity functions is the behavior of robustness and opportuneness functions against each other for different problems. For some problems, the decision-maker can concentrate merely on obtaining a minimum profit with a robust strategy. Still, the decision-maker can lose many opportunities in this way. Thus a question which arises is whether both of these functions can be improved simultaneously (the functions are sympathetic) or one of these functions has to be enhanced in the cost of exacerbating the other function (functions are antagonistic) [1].

2.1.1 Applications

IGDT has a vast application in different scopes of science, especially engineering. Many kinds of literature have been conducted on implementing IGDT to economics [5–7], project management [8–10], statistics, and biology [11].

Power system operation and planning optimization problems are usually accompanied with multiple uncertainties. With the increasing penetration of renewables

during the last decade in power systems, the uncertainty has become even severe. Therefore, one of the main fields that IGDT has been applied successfully is power system optimization problems including renewable sources. Generation and transmission expansion planning are usually high-dimension optimization problems with an enormous number of variables and constraints. In many of these problems utilizing other stochastic-probabilistic optimization, approaches can be extremely difficult or even impossible. Nevertheless, IGDT has appropriate compatibility with this type of optimization problems [12, 13]. Also, IGDT is used for planning lower voltage levels such as distribution expansion planning and planning distributed generations in microgrids. In the majority of these applications initially, the objective function is calculated for the base case according to forecasted parameters. After obtaining the objective function for the base case, a budget (proportional to the base case objective function) is dedicated, and by solving the optimization problem, it is calculated to what extent the immunity functions can be maximized. Bidding strategy for generation companies in power markets is the other application of IGDT for power system optimization problems [14, 15]. IGDT can be used whether to make a robust strategy to guarantee the minimum amount of profit or in an opportuneness framework to obtain the windfall caused by uncertain variables. In addition to generation companies, IGDT can also be a beneficial approach for independent system operators (ISO). IGDT has been used for unit commitment in the presence of high wind penetration [4]. Optimal power flow and security programming with high renewable generations can also be handled by information-gap decision theory [16, 17]. Designing power system stabilizers with the aim of damping local and inter-area oscillations is the other application of IGDT in power system optimization.

Structural engineering is another knowledge which uses the advantages of IGDT. Vibration amplitudes, natural frequencies, and loads such as earthquakes and wind. IGDT is utilized to improve structural immunity against variations of these uncertain parameters. Restricted information about the duration and expenditures can be a critical issue in the field of project management. However, IGDT can be used to adopt a robust approach for managing the finance of different projects.

2.1.2 Summary

Making decisions by solving optimization problems is a common practice. However, in reality, most of the optimization problems suffer from the lack of data or uncertainty of parameters. Therefore, it is inevitable to implement an approach which can deal with these deficiencies. The approach has to represent decisions which remain satisfying for different variations of uncertain variables in real time [4].

Information-gap decision theory is a decision-making approach to these situations. The method is capable of applying two different strategies. In the robustness strategy, the approach assures a minimum amount of profit for a certain amount of change in the uncertain parameters. On the other hand, in the opportuneness strategy,

the decision-maker intends to make benefits by the variations of uncertain variables [1].

The IGDT does not require historical data or probabilistic density functions and is compatible with the deficiency of exact data which makes it applicable to many optimizations and decision-making problems in reality. Indeed, despite other approaches such as stochastic or probabilistic programming which are extremely dependent on probability density functions, this approach can be implemented without knowledge of the stochastic behavior of uncertain parameters [4].

The results obtained by IGDT help the decision-maker to choose the final solution according to the dedicated uncertainty budget or the benefit that is predicted to gain. Hence, the IGDT does not provide a unique solution, but a group of solutions which the decision-maker can select according to the adopted strategies. Each solution has to satisfy all of the constraints while minimizing the required objective function. Therefore, the results are trustable and can be utilized to make the final decisions.

2.2 Challenges of IGDT

After introducing the principles and applications of information-gap decision theory, the advantages and flaws of this approach are discussed in this section. Also, a brief description is done about the future developments of this approach.

2.2.1 Pros of IGDT

As noticed in the previous sections, the main advantage of IGDT is that it can be implemented for optimization and decision-making problems which endure from the lack of historical data or carry imprecise data. Approaches such as stochastic programming and probabilistic approaches rely on historical data and probability density function. Any inaccuracy in these data can lead to undesired or even lethal results. Approximating probability density functions based on historical data is another challenging issue for these methods [1–4]. Any error in estimating the accurate probability density function with the proper parameters can result in disastrous results. Interval and robust optimization have the same problem. In these approaches at least, the interval of variations has to be determined to be used in these approaches. Despite these drawbacks that these approaches struggle with, IGDT is independent of historical data or probability density functions and can be applied with the least data about the variations of uncertain parameters [4].

Computational burden is another aspect that these approaches can be compared. For stochastic programming, while decreasing the numbers of scenarios can alleviate the decision, increasing the number of scenarios can extremely increase computation burden or even make the problem infeasible. Fuzzy optimization also tolerates the same problem where it has to be solved for different cuts. Nonetheless, IGDT is solved

in a deterministic framework for different budgets which reduces computational times. Furthermore, if the decision-maker is familiar with the intrinsic of the problem and the interval the budget varies, the execution time can even be shortened [2–4].

Giving the option to decision-makers on how to deal with their problems can be mentioned as another advantage of this approach. Decision-makers can opt whether to implement a conservative strategy (robustness) to assure the least profit or a strategy with more risk (opportuneness) to gain a windfall. Other decision-making approaches do not give the freedom to the decision-maker to choose the desired strategy such as IGDT.

2.2.2 Cons of IGDT

In the previous section, some advantageous aspects of IGDT were mentioned. However, in special situations, these benefits can become a serious drawback to this approach.

IGDT is a non-probabilistic approach. Thus, the assumptions which are made are fewer than other approaches which result in the ignorance of events with low probabilities. However, in reality, these events may occur and be outside the model. Stochastic and probabilistic approaches consider these situations according to their probability and cost they make. Also, if the nature of the problem is not known, selecting robustness strategy can establish the cause of losing other benefits and vice versa (adopting an opportuneness strategy can lead to failure).

The other con of this approach is related to the immunity functions. The amount of these functions cannot be interpreted simply. For example, when the robustness function equals to 0.5, merely this amount cannot give any sense and help the decision-making process. So, the decision-maker has to rely on other tools such as experience and sensitivity analysis [18].

Another concerning issue can be related to the uncertainty space of the problem. If this space becomes much larger than the approximated horizon of uncertainty, there can be upper or lower spikes in the outcomes, and the results can saliently differ from the estimated values [18].

A major criticism of IGDT is that since this approach works based on a point estimate, it is not appropriate for severe uncertainties. It is believed that for severe uncertainties, the approach does not have to be initiated from an estimated point, and instead, a universe of possibilities has to be considered [18].

2.2.3 Future Development

Decision-making under the deficiency of data or severe uncertainty has always been a challenging task to tackle by scientists. Although different approaches have been proposed to handle the uncertain space or lack of data, none of these frameworks

have been completely satisfying. Each of these frameworks has their pros and cons. Thus, using a combination of IGDT with these methods can be a perspective that has not been studied and implemented. Studying the severity of uncertainty that IGDT can handle can be another scope in which further development is required.

2.3 Statistics Related to Documents

This part presents the statistics related to documents in the field of IGDT. Terms such as "information gap decision theory" or "information-gap decision theory" or "info-gap decision theory" have been searched. The Scopus database has been used. It is worth mentioning that the results are reported by April 2018. This search resulted in 187 documents, and the VOSviewer software has been used to analyze these documents.

Figure 2.4 shows the number of published documents by year; it is clear that this field is a relatively new research filed, and the number of published documents was highest in 2016. Overall, the number of documents is increasing over the period.

Figure 2.5 shows the number of documents by source; *IEEE Transactions on Power Systems* and *International Journal of Electrical Power and Energy Systems* published nine documents in the field.

Figure 2.6 shows the number of published documents by authors; Y. Ben-Haim and K. Zare have published 25 and 16 documents related to IGDT, respectively.

Figure 2.7 shows collaboration between authors based on years. Y. Ben-Haim shown with blue color was the top researcher in this field in 2009, and A. Ahmadi shown with yellow color is one of the top researchers in 2018.

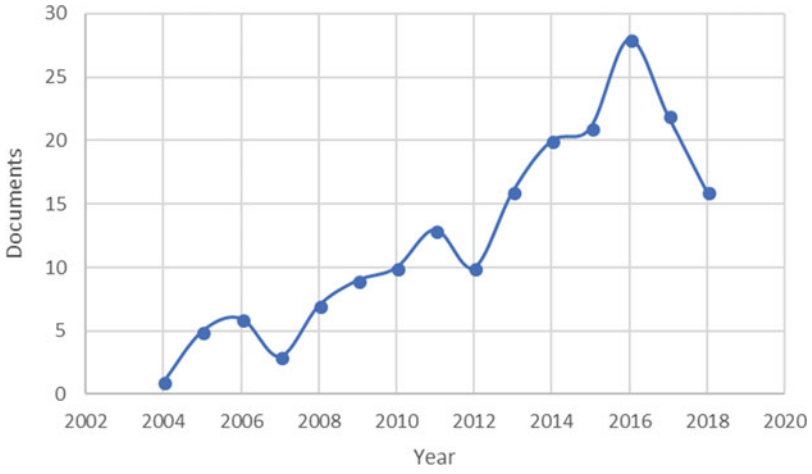

Fig. 2.4 Documents by year

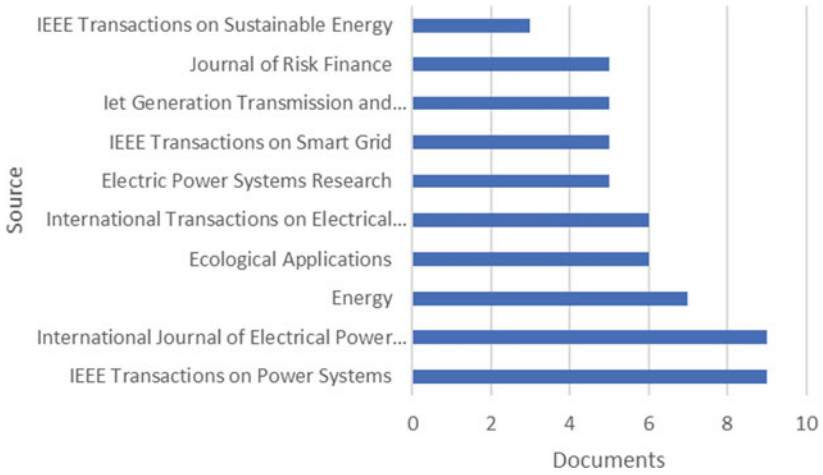

Fig. 2.5 Documents by source

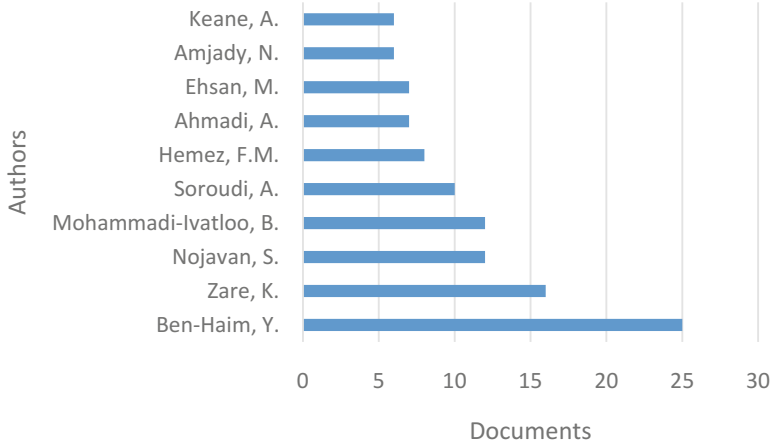

Fig. 2.6 Documents by author

Figure 2.8 shows the numbers of documents by type; 121 and 47 documents have been published as article and conference paper, respectively.

Figure 2.9 shows the number of documents by subject area; 116 and 73 documents were published in the engineering and energy fields, respectively.

Figure 2.10 illustrates the popular keywords based on years; the yellow color shows popular keywords in 2016. It is evident that information-gap decision theory, risk management, scheduling, self-scheduling, and electricity market are some popular keywords in 2016.

Table 2.1 shows the top ten popular keywords in the field; decision theory and information gap with 116 and 70 times of occurrence, respectively, are the top two popular keywords in the field.

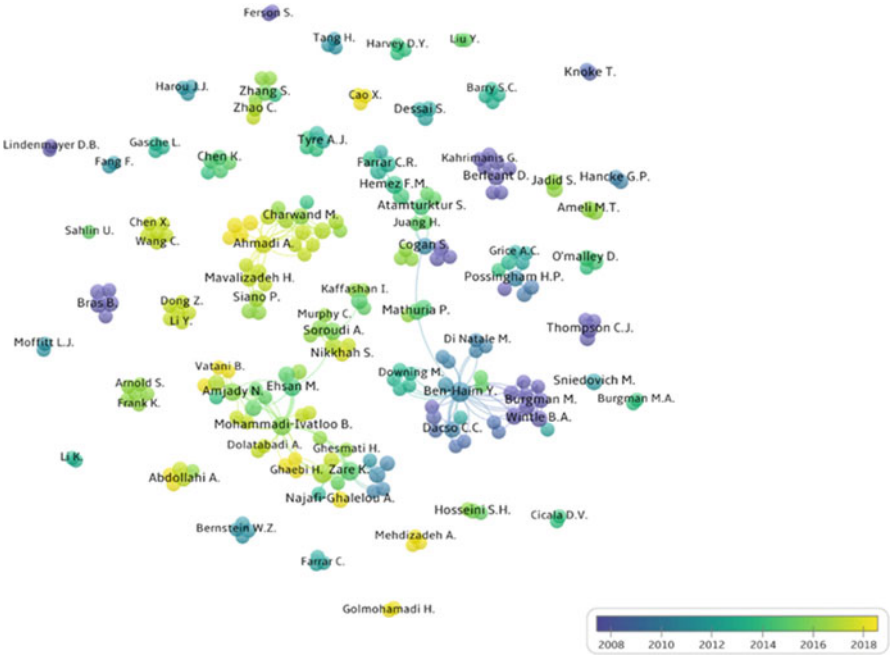

Fig. 2.7 Collaboration between authors

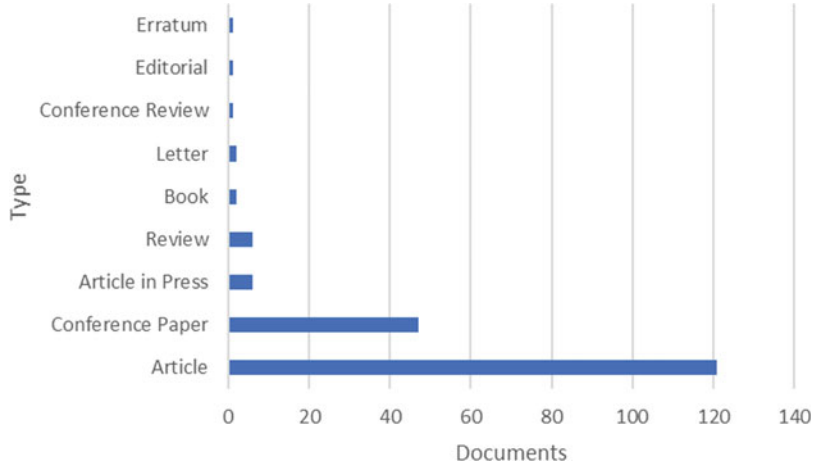

Fig. 2.8 Documents by type

Table 2.2 presents the top ten published documents in the field based on the number of citations. The book published by Y. Ben-Haim published in 2006 received the highest number of citations. Besides, Table 2.3 represents a taxonomy of the recent papers published in power systems.

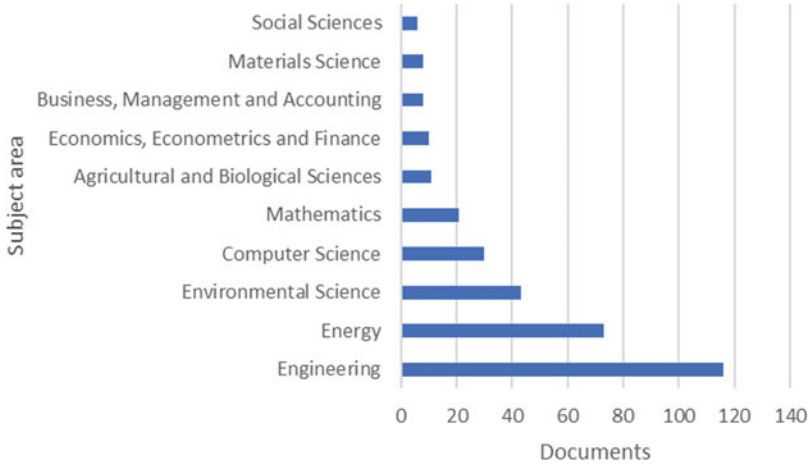

Fig. 2.9 Documents by subject area

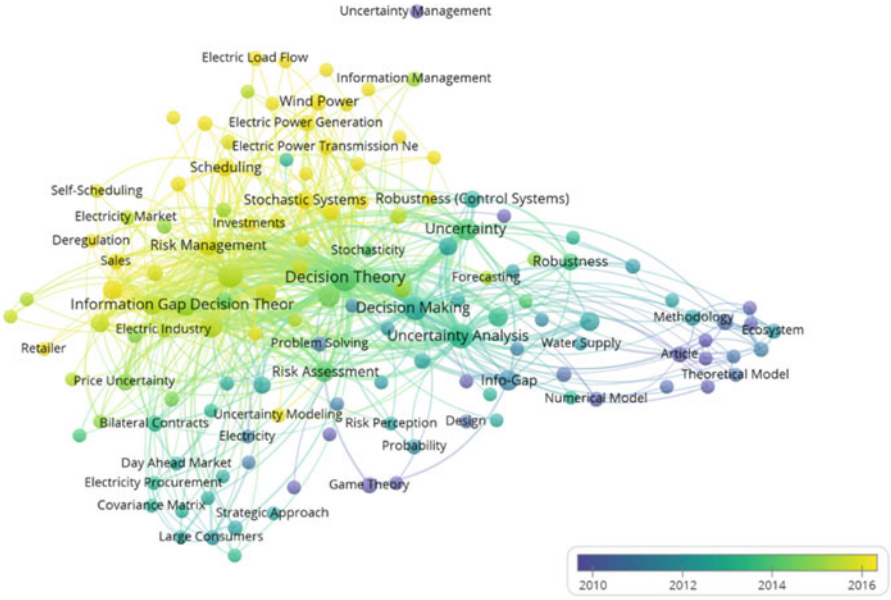

Fig. 2.10 The popular keywords

Table 2.1 The most popular keywords

Number	Keywords	Occurrences
1	Decision theory	116
2	Information gap	70
3	Uncertainty analysis	66
4	Decision-making	60
5	Uncertainty	38
6	Information-gap decision theory	35
7	Optimization	35
8	Costs	34
9	Commerce	32
10	Information-gap decision theory (IGDT)	27

Table 2.2 The top ten documents with highest citations in the field

References	Authors	Source	Citation	Year
[1]	Y. Ben-Haim	Academic Press	176	2006
[19]	Moilanen et al.	*Restoration Ecology*	118	2009
[20]	Soroudi and T. Amraee	*Renewable and Sustainable Energy Reviews*	115	2013
[21]	Mohammadi-Ivatloo et al.	*IEEE Transactions on Power Systems*	70	2013
[22]	Moilanen and B. A. Wintle	*Biological Conservation*	70	2006
[23]	Soroudi and M. Ehsan	*IEEE Transactions on Smart Grid*	63	2013
[24]	Moilanen et al.	*Ecological Modelling*	62	2006
[25]	E. Nicholson and H. P. Possingham	*Ecological Applications*	53	2007
[26]	Moilanen et al.	*Conservation Biology*	52	2006
[27]	E. McDonald-Madden et al.	*Journal of Applied Ecology*	51	2008

Table 2.3 The IGDT application to modern power systems

References	Subject	Uncertain parameter	Year
[28]	Reserve market clearing	Demand response	2018
[29]	Bidding strategy of microgrids	Load and price	2018
[30–32]	Smart building scheduling	Price	2018
[33]	Security-constrained unit commitment	Load	2018
[34]	Optimal scheduling of industrial furnaces	Heating demand	2018
[35]	Bidding and offering strategy of a retailer	Price	2017
[36, 37]	Scheduling of a hybrid energy system	Load	2017
[38]	Power system expansion planning	Demand and price	2017
[39]	Bidding strategy for generation companies	Price	2017
[40]	Bidding strategy for industrial consumers	Price	2017
[41]	Hydrothermal scheduling	Load	2016
[42]	Electricity procurement strategy of large consumer	Price	2016

2.4 Information-Gap Decision Theory Modeling

Generally, the info gap presents a critical presentation of the uncertainty happening in most real cases. In such real cases, the firm and optimal solution would be obtained provided that the data are available, while, indeed, a small part of the data is in access. If one wants to cast light on this problem, it can be stated that in most cases the gap between what is known and what is unknown is quite remarkable in different practical applications. Thus, it is needed to characterize this gap to make a robust and logical decision. Each IGDT-based problem includes three main parts as a system model, uncertainty modeling, as well as the performance requirements as follows.

2.4.1 System Model

The system model can be represented by $H(k, \gamma)$ which includes the input–output structure of the studied system. It is noted that k is the set of decision variables and γ is the uncertain parameter. $H(k, \gamma)$ can be alternatively described as the benefit that the decision-maker would gain for the selected values of k taking into account γ. It is worth noting that γ can be any uncertain parameter, such as the pool price, load demand, intermittent renewable energy power output, etc.

2.4.2 Uncertainty Modeling

In this respect, there are several models thus far presented for the IGDT technique. An uncertainty model based on the information-gap theory would be a cluster of nested sets which in most cases is unbounded. The information regarding the uncertain parameter would specify the form of the sets within an information-gap model. Usually, the architecture of the model of the information-gap theory is selected in order to represent the smallest or the most rigorous family of sets that their members are consistent with the previous information. However, in some cases, the innovative thinking may be necessary to represent the information-gap model with the capability of previous information capture. This would be partially linguistic with no unguaranteed presumptions.

Different information-gap models are as follows [1]:

- Energy-bound model
- Envelope-bound models
- Minkowski-norm models
- Slope-bound models
- Fourier-bound models
- Hybrid information-gap models: information gaps in probability functions

- Combined information-gap models
- Non-convex information-gap model: pendulum-like systems
- Non-convex information-gap model: linear system with uncertain coefficients
- Discrete information-gap models

In this regard, the two frequently used models in power systems are the energy-bound and the envelope-bound models.

2.4.2.1 Energy-Bound Model

Transient events are the most challenging ones to interpret compared to other dynamic events. Generally, the information of these phenomena is sparse, inaccurate, and not sufficient. It should be noted that an occurrence is not a mere individual number. On the contrary, it is a function of time or space or even both of them. In some cases, the structure of such a function would be a vector instead of a single-dimension scalar. In this regard, energy-bound uncertainty models appear in various conditions in which the energy is not exactly defined using a polynomial function of quadratic types, such as the energy per unit time related to an electric current that is quadratic in the current.

For a given function of scalar one, $c(t)$, fluctuating with an obscure behavior around the nominal function, $\tilde{c}(t)$, the energy-bound model can be defined as follows:

$$C(\alpha, \tilde{c}) = \left\{ c(t) : \int_0^{\infty} [c(t) - \tilde{c}(t)]\, \mathrm{d}(t) \leq \alpha^2 \right\}, \qquad \alpha \geq 0 \tag{2.1}$$

This function is a category of nested uncertain function sets in which α shows the uncertain parameter indicating the degree of nesting, such that $\alpha < \alpha'$ would infer $C(\alpha, \tilde{c}) \subset C(\alpha', \tilde{c})$. As $c(t) \vdash \tilde{c}(t)$ is a transient fluctuation supposed to be disappeared however asymptotically since the integral represented in (2.1) is constrained by the square of the uncertainty horizon which is finite. In this respect, the uncertainty of $c(t)$ is stated in a dual-level form where $C(\alpha, \tilde{c})$ determines the deviation of $c(t)$ from $\tilde{c}(t)$, which is not known. It is worth noting that α is unknown indicating the uncertainty horizon that is not known.

Besides, for vector-valued function, the energy-bound models would be represented as follows:

$$C(\alpha, \tilde{c}) = \left\{ c(t) : \int_0^{\infty} [c(t) - \tilde{c}(t)]^T B [c(t) - \tilde{c}(t)]\, \mathrm{d}(t) \leq \alpha^2 \right\}, \qquad \alpha \geq 0 \tag{2.2}$$

where B shows a real symmetric matrix which is known and positive definite [1]. The models represented in (2.1) and (2.2) are so-called cumulative energy-

bound models which are recognizable from the "instantaneous energy-bound model." The instantaneous energy-bound model is defined as a set of functions, while the energy is limited at each instant as below:

$$C(\alpha, \tilde{c}) = \{c(t) : [c(t) - \tilde{c}(t)]^T B[c(t) - \tilde{c}(t)] \leq \alpha^2\}, \qquad \alpha \geq 0 \tag{2.3}$$

where it should be noted that $c(t)$ and $\tilde{c}(t)$ are not necessarily the function of the variable t which is independent while they can be constant vectors. As intensively investigated in Refs. [1, 43], Eq. (2.3) can be rewritten as follows as the ellipsoid-bound info-gap model for vectors.

$$C(\alpha, \tilde{c}) = \left\{c : \left[c - \tilde{c}\right]^T B\left[c - \tilde{c}\right] \leq \alpha^2\right\}, \qquad \alpha \geq 0 \tag{2.4}$$

The two models represented above as instantaneous and cumulative energy-bound models can be easily discriminated by taking into consideration that the instantaneous energy-bound model includes functions that their magnitude is unbounded. The cumulative energy-bund model includes unrelentingly fluctuant functions.

2.4.2.2 Envelope-Bound Model

The envelope-bound model has been widely used in power system problems [44–46]. Accordingly, here the envelope-bound model is presented. Using this model, the variations of the uncertainty are restricted to an adjustable envelope. Hence, the expression for the scalar functions can be stated as below:

$$C(\alpha, \tilde{c}) = \{c(t) : |c(t) - \tilde{c}(t)| \leq \alpha\varphi(t)\}, \qquad \alpha \geq 0 \tag{2.5}$$

where the unknown function which specifies the envelope shape and the uncertainty parameter which specifies the size are denoted by $\varphi(t)$ and α, respectively. Besides, $C(\alpha, \tilde{c})$ shows the set of functions $c(t)$ such that their value does not deviate from the nominal function $\tilde{c}(t)$ by more than $\alpha\varphi(t)$. It is noteworthy that $\varphi(t)$ indicates the envelope function using the historical data. For example, if $\varphi(t)$ is selected 1, the deviation of the uncertainty would be limited to specific regions of t-values; otherwise $\varphi(t) = 0$ outside. The envelope function $\varphi(t)$ is utilized to show the relative degrees of the deviation in other realizations. It should be noted that the highest degree of deviation would be desired to vary proportionally to the nominal function; thus $\varphi(t) \propto \tilde{c}(t)$. Accordingly, the information-gap model represented in (2.5) turns into the set of functions $c(t)$ that their fractional variation around the nominal function $\tilde{c}(t)$ would not be greater than α. This issue can be mathematically represented as follows:

$$C(\alpha,\tilde{c}) = \left\{ c(t) : \left| \frac{c(t) - \tilde{c}(t)}{\tilde{c}(t)} \right| \le \alpha \right\}, \qquad \alpha \ge 0 \tag{2.6}$$

where the presented envelope is possibly constant everywhere for other situations, which means that the function mentioned above would be decreased to Eq. (2.7) used for the energy-bound model as well. In the case of Z-vectors, the envelope function can be presented by limiting each member of the vector as follows:

$$C(\alpha,\tilde{c}) = \left\{ c_z(t) : |c_z(t) - \tilde{c}_z(t)| \le \alpha\varphi_z(t), \quad z = 1,2,\ldots,Z \right\}, \qquad \alpha \ge 0 \tag{2.7}$$

It is worth mentioning that the envelope-bound information-gap models can be used for both constants c and functions $c(t)$. In the previous case, the expanding interval–uncertainty models were derived. Equation (2.5) would turn into the set of c-values in the expanding interval $\left[\tilde{c} - \alpha \quad \tilde{c} + \alpha\right]$, in which the size of the interval $\pm\alpha$ is uncertain. Regarding the vector case, Eq. (2.4), by using the mentioned intervals for every member of the vector c, a set of expanding boxes with the dimension Z will be generated. It should be noted that the scalar envelope-bound models are capable of being extended for the vector function using a different method. In this respect, Eq. (2.5) is rewritten as follows:

$$G = \{c(t) : \quad -\varphi(t) \le c(t) \le \varphi(t)\} \tag{2.8}$$

where the set of functions in a fixed envelop $\pm\varphi(t)$ which has been centered at zero is denoted by G. Therefore, assuming the set G and the real number α, the elements of G and α can be multiplied to derive the set αG as:

$$\alpha G = \{c(t) : -\alpha\varphi(t) \le c(t) \le \alpha\varphi(t)\} \tag{2.9}$$

where αG is zero-centered and shows the expanding envelope of the functions constrained by $\pm\alpha\varphi(t)$. Similarly, by summing up $\tilde{c}(t)$ and each element of the αG, the set $\alpha G + \tilde{c}(t)$ can be derived for any set αG and the function $\tilde{c}(t)$. Accordingly, Eq. (2.9) can be rewritten as below representing expanding envelope of functions which are shifted:

$$\alpha G + \tilde{c}(t) = \{c(t) : \tilde{c}(t) - \alpha\varphi(t) \le c(t) \le \tilde{c}(t) + \alpha\varphi(t)\} \tag{2.10}$$

Therefore, Eq. (2.5) would be rewritten as follows:

$$C(\alpha,\tilde{c}) = \{c(t) : c(t) \in \alpha G + \tilde{c}(t)\}, \qquad \alpha \ge 0 \tag{2.11}$$

It is worth noting that here the set G has two fundamental characteristics:

- G includes the zero function, i.e., $0 \in G$.
- G is also included in its expansions so that $0 < \alpha < \alpha' \in G$ states $\alpha G \subset \alpha' G$.

Equation (2.11) would be a general envelope-bound information-gap model for any set G of functions with respect to the abovementioned characteristics of the set G. This is a shifted expanding envelope of functions in which the set G specifies the shape. The properties of Eq. (2.11) which make it different relate to the fact that there is no necessity for the convexity of sets $C(\alpha, \tilde{c})$.

It is noted that the energy-bound and the envelope-bound techniques are highly correlated which can be even more extended using the Minkowski-norm models. The slope-bound models are used to take into account the rate of variations as the envelope-bound, energy-bound, and Minkowski-norm models have not considered the rate of variations. For instance, the envelope-bound model is possible to be used for the slope instead of the magnitude of the function to limit the rate of variations. In some cases, the knowledge about the partial spectral information to model the uncertain parameter is limited. In such cases, the Fourier-bound models can be used. The combined information-gap models are the combination of several models discussed above, for example, the combination of the energy-bound and the envelope-bound models. The non-convex information-gap models can be used both for the pendulum-like systems and linear systems with uncertain coefficients. Most of the dynamic systems existing in real life particularly in the natural, physical, and social fields besides the engineering problems would be characterized by a set of linear differential equations associated with constant coefficients. In such cases, the non-convex info gap for linear systems with uncertain coefficients can be utilized. It is noteworthy that for those parameters with a discrete variation of the uncertainty horizon, discrete info gap must be utilized. Ordinal preferences related to some alternatives can be determined using positive integers, while the low integer shows the desirability of the related alternative. In this respect, although the preferences can be uncertain, there is a discrete uncertainty, i.e., errors in the integer units.

2.4.3 Performance Requirements

In the presence of severe uncertainty, the IGDT technique would aid the decision-maker to adjust the values of the decision variables in a way that the minimum requirements of the system would be obtained and the related risk would be prevented [47]. There are two functions defined to this end, as the robustness function and the opportunity function.

2.4.3.1 Robustness Function

Profit Maximization

Assuming H_c is the lowest desired value of reward of the decision-making problem, the robustness function of the information-gap model can be interpreted as the

highest level of α in a way that H_c is obtained. Accordingly, this robustness function can be mathematically represented as follows:

$$\begin{aligned}\widetilde{\alpha}(k,H_c) &= \max_{\alpha}\{\alpha : \text{minimum requirement } H_c \text{ is always achieved}\} \\ &= \max_{\alpha}\{\alpha : \min\ H(k,\gamma) \geq H_c\}, \quad \gamma \in C(\alpha,\tilde{c})\end{aligned} \tag{2.12}$$

The robustness function in (2.12) implies the highest deviation from the nominal value such that the minimum performance is higher than a given value, H_c. The robustness function indeed models the risk-aversion behavior of the decision-maker when confronting the uncertainty. This function would be applicable when the decision-maker seeks to maximize the profit considering the highest level of the uncertainty. It should be noted that the decision made would be robust, risk-averse, and not affected by the uncertainty when the value of $\widetilde{\alpha}(k,H_c)$ is large. Otherwise, the decision would be crisp.

Cost Minimization

In case the system model (cost) is set to be minimized by the decision-maker, the robustness function can be rewritten as follows:

$$\begin{aligned}\widetilde{\alpha}(k,H_c) &= \max_{\alpha}\{\alpha : \text{minimum requirement } H_c \text{ is always achieved}\} \\ &= \max_{\alpha}\{\alpha : \min\ H(k,\gamma) \leq H_c\}, \quad \gamma \in C(\alpha,\tilde{c})\end{aligned} \tag{2.13}$$

2.4.3.2 Opportunity Function

Profit Maximization

On the other hand, the opportunity function denoted by $\widetilde{\beta}(k,H_w)$ is utilized to evaluate the chance of gaining the higher value of the objective function, e.g., profit which may be gained due to the variations of the uncertain parameter. This function can be stated as below [47]:

$$\begin{aligned}\widetilde{\beta}(k,H_w) &= \min_{\alpha}\{\alpha : \text{target performance } H_w \text{ may be met}\} \\ &= \min_{\alpha}\{\alpha : \max\ H(k,\gamma) \geq H_c\}, \quad \gamma \in C(\alpha,\tilde{c})\end{aligned} \tag{2.14}$$

where the deviation of the uncertain parameter from the predicted value by $\widetilde{\beta}$ may result in the targeted objective function value, e.g., profit. In other words, the opportunity function can be defined as the lowest value of α at which the decision made would endure and still get a high performance shown by H_w.

Cost Minimization

However, in the case of cost minimization, the opportunity function would be set as follows:

$$\begin{aligned}\widetilde{\beta}(k, H_w) &= \min_{\alpha} \{\alpha : \text{target performance } H_w \text{ may be met}\} \\ &= \min_{\alpha} \{\alpha : \max H(k, \gamma) \leq H_c\} \quad \gamma \in C(\alpha, \tilde{c})\end{aligned} \tag{2.15}$$

2.5 Conclusion

The uncertain parameters can be characterized by two general methods as the occurrence frequency of events by the probabilistic methods when the exact data are not available or as the subjective degrees of belief of the observer. However, the fuzzy logic theory has been widely used to characterize different kinds of uncertainties. This has been done by defining the fuzzy membership functions. In this respect, the commonly used probability models and fuzzy logic describe various points of view of incomplete or disjointed data, while any of them has been proposed for a different utilization with different performances. It should be noted that considering all the various features of the models, they are used to present the same concept using the mathematical functions which are normalized. In this respect, these functions can be either the probability distribution functions or the membership functions. The vague issue arisen here is how to provide the decision-maker with the required input data such as the probability distribution functions of the uncertain parameters. This would be of high significance in the realistic situations where the data of the input data may not be available or in case of the system vulnerability to underlying variations even when the data are available. Under such conditions, the historical data would be no longer useful. Hence, an efficient tool must be available to deal with the uncertainty as the decision-maker would face data which are much more fragmental. In this respect, the information-gap decision theory (IGDT) technique would be an effective and efficient uncertainty characterizing tool. This chapter highlighted applications, pros, and cons of IGDT.

References

1. Ben-Haim, Y. (2006). *Info-gap decision theory: Decisions under severe uncertainty*. San Diego: Academic.
2. Rezaei, N., Ahmadi, A., Khazali, A., & Guerrero, J. M. (2018). Energy and frequency hierarchical management system using information gap decision theory for islanded microgrids. *IEEE Transactions on Industrial Electronics, 65*, 7921–7932.

3. Khazali, A., Rezaei, N., Ahmadi, A., & Hredzak, B. (2018). Information gap decision theory based preventive/corrective voltage control for smart power systems with high wind penetration. *IEEE Transactions on Industrial Informatics, 14*(10), 4385–4394.
4. Soroudi, A., Rabiee, A., & Keane, A. (2017). Information gap decision theory approach to deal with wind power uncertainty in unit commitment. *Electric Power Systems Research, 145*, 137–148.
5. Bryan, B. S., & Thompson, C. J. (2007). Managing credit risk with info-gap uncertainty. *The Journal of Risk Finance, 8*(1), 24–34.
6. Stranlund, J. K., & Ben-Haim, Y. (2008). Price-based vs. quantity-based environmental regulation under Knightian uncertainty: An info-gap robust satisficing perspective. *Journal of Environmental Management, 87*(3), 443–449.
7. Yakov, B. H. (2005). Value-at-risk with info-gap uncertainty. *The Journal of Risk Finance, 6* (5), 388–403.
8. Ben-Haim, Y., & Laufer, A. (1998). Robust reliability of projects with activity-duration uncertainty. *Journal of Construction Engineering and Management, 124*(2), 125–132.
9. Meir, T., & Ben-Asher, J. Z. (2005). Modeling and analysis of integration processes for engineering systems. *Systems Engineering, 8*(1), 62–77.
10. Regev, S., Shtub, A., & Ben-Haim, Y. (2006). Managing project risks as knowledge gaps. *Project Management Quarterly, 37*(5), 17.
11. Carmel, Y., & Ben-Haim, Y. (2005). Info-gap robust-satisficing model of foraging behavior: Do foragers optimize or satisfice? *The American Naturalist, 166*(5), 633–641.
12. Dehghan, S., Kazemi, A., & Amjady, N. Multi-objective robust transmission expansion planning using information-gap decision theory and augmented ε-constraint method. *IET Generation, Transmission & Distribution*, *8*(5), 828–840. Available: http://digital-library.theiet.org/content/journals/10.1049/iet-gtd.2013.0427
13. Ahmadi, A., Mavalizadeh, H., Zobaa, A. F., & Shayanfar, H. A. Reliability-based model for generation and transmission expansion planning. *IET Generation, Transmission & Distribution*, *11*(2), 504–511. Available: http://digital-library.theiet.org/content/journals/10.1049/iet-gtd.2016.1058
14. Shafiee, S., Zareipour, H., Knight, A. M., Amjady, N., & Mohammadi-Ivatloo, B. (2017). Risk-constrained bidding and offering strategy for a merchant compressed air energy storage plant. *IEEE Transactions on Power Systems, 32*(2), 946–957.
15. Kazemi, M., Mohammadi-Ivatloo, B., & Ehsan, M. (2015). Risk-constrained strategic bidding of GenCos considering demand response. *IEEE Transactions on Power Systems, 30*(1), 376–384.
16. Rabiee, A., Nikkhah, S., Soroudi, A., & Hooshmand, E. Information gap decision theory for voltage stability constrained OPF considering the uncertainty of multiple wind farms. *IET Renewable Power Generation*, *11*(5), 585–592. Available: http://digital-library.theiet.org/content/journals/10.1049/iet-rpg.2016.0509
17. Rabiee, A., Soroudi, A., & Keane, A. (2015). Information gap decision theory based OPF with HVDC connected wind farms. *IEEE Transactions on Power Systems, 30*(6), 3396–3406.
18. Sniedovich, M. (2007). The art and science of modeling decision-making under severe uncertainty. *Mathematical Modeling; Severe Uncertainty; Maximin; Worst-Case Analysis; Robust Optimization; Info-gap*, *1*, 26.
19. Moilanen, A., Teeffelen, A. J. A. V., Ben-Haim, Y., & Ferrier, S. (2009). How much compensation is enough? A framework for incorporating uncertainty and time discounting when calculating offset ratios for impacted habitat. *Restoration Ecology, 17*(4), 470–478.
20. Soroudi, A., & Amraee, T. (2013). Decision making under uncertainty in energy systems: State of the art. *Renewable and Sustainable Energy Reviews, 28*, 376–384.
21. Mohammadi-Ivatloo, B., Zareipour, H., Amjady, N., & Ehsan, M. (2013). Application of information-gap decision theory to risk-constrained self-scheduling of GenCos. *IEEE Transactions on Power Systems, 28*(2), 1093–1102.

22. Moilanen, A., & Wintle, B. A. (2006). Uncertainty analysis favours selection of spatially aggregated reserve networks. *Biological Conservation, 129*(3), 427–434.
23. Soroudi, A., & Ehsan, M. (2013). IGDT based robust decision making tool for DNOs in load procurement under severe uncertainty. *IEEE Transactions on Smart Grid, 4*(2), 886–895.
24. Moilanen, A., et al. (2006). Planning for robust reserve networks using uncertainty analysis. *Ecological Modelling, 199*(1), 115–124.
25. Nicholson, E., & Possingham, H. P. (2007). Making conservation decisions under uncertainty for the persistence of multiple species. *Ecological Applications, 17*(1), 251–265.
26. Moilanen, A., Wintle, B. A., Elith, J., & Burgman, M. (2006). Uncertainty analysis for regional-scale reserve selection. *Conservation Biology, 20*(6), 1688–1697.
27. McDonald-Madden, E., Baxter, P. W. J., & Possingham, H. P. (2008). Making robust decisions for conservation with restricted money and knowledge. *Journal of Applied Ecology, 45*(6), 1630–1638.
28. Ghahary, K., Abdollahi, A., Rashidinejad, M., & Alizadeh, M. I. (2018). Optimal reserve market clearing considering uncertain demand response using information gap decision theory. *International Journal of Electrical Power & Energy Systems, 101*, 213–222.
29. Rezaei, N., Ahmadi, A., Khazali, A., & Aghaei, J. (2018). Multi-objective risk-constrained optimal bidding strategy of smart microgrids: An IGDT-based normal boundary intersection approach. *IEEE Transactions on Industrial Informatics*, 1–1. https://doi.org/10.1109/TII.2018.2850533
30. Najafi-Ghalelou, A., Nojavan, S., & Zare, K. (2018). Heating and power hub models for robust performance of smart building using information gap decision theory. *International Journal of Electrical Power & Energy Systems, 98*, 23–35.
31. Najafi-Ghalelou, A., Nojavan, S., & Zare, K. (2018). Information gap decision theory-based risk-constrained scheduling of smart home energy consumption in the presence of solar thermal storage system. *Solar Energy, 163*, 271–287.
32. Najafi-Ghalelou, A., Nojavan, S., & Zare, K. (2018). Robust thermal and electrical management of smart home using information gap decision theory. *Applied Thermal Engineering, 132*, 221–232.
33. Ahmadi, A., Nezhad, A. E., & Hredzak, B. (2018). Security-constrained unit commitment in presence of lithium-ion battery storage units using information-gap decision theory. *IEEE Transactions on Industrial Informatics, 99*, 1–1.
34. Jabari, F., Nojavan, S., Mohammadi-Ivatloo, B., Ghaebi, H., & Mehrjerdi, H. (2018). Risk-constrained scheduling of solar Stirling engine based industrial continuous heat treatment furnace. *Applied Thermal Engineering, 128*, 940–955.
35. Nojavan, S., Zare, K., & Mohammadi-Ivatloo, B. (2017). Risk-based framework for supplying electricity from renewable generation-owning retailers to price-sensitive customers using information gap decision theory. *International Journal of Electrical Power & Energy Systems, 93*, 156–170.
36. Nojavan, S., Majidi, M., & Zare, K. (2017). Risk-based optimal performance of a PV/fuel cell/battery/grid hybrid energy system using information gap decision theory in the presence of demand response program. *International Journal of Hydrogen Energy, 42*(16), 11857–11867.
37. Nojavan, S., Majidi, M., & Zare, K. (2017). Performance improvement of a battery/PV/fuel cell/grid hybrid energy system considering load uncertainty modeling using IGDT. *Energy Conversion and Management, 147*, 29–39.
38. Mavalizadeh, H., Ahmadi, A., Gandoman, F. H., Siano, P., & Shayanfar, H. A. (2017). Multiobjective robust power system expansion planning considering generation units retirement. *IEEE Systems Journal, 12*(3), 2664–2675.
39. Nojavan, S., Zare, K., & Mohammadi-Ivatloo, B. (2017). Information gap decision theory-based risk-constrained bidding strategy of price-taker GenCo in joint energy and reserve markets. *Electric Power Components and Systems, 45*(1), 49–62.

40. Alipour, M., Zare, K., & Mohammadi-Ivatloo, B. (2016). Optimal risk-constrained participation of industrial cogeneration systems in the day-ahead energy markets. *Renewable and Sustainable Energy Reviews, 60*, 421–432.
41. Charwand, M., Ahmadi, A., Sharaf Adel, M., Gitizadeh, M., & Esmaeel Nezhad, A. (2015). Robust hydrothermal scheduling under load uncertainty using information gap decision theory. *International Transactions on Electrical Energy Systems, 26*(3), 464–485.
42. Nojavan, S., Ghesmati, H., & Zare, K. (2016). Robust optimal offering strategy of large consumer using IGDT considering demand response programs. *Electric Power Systems Research, 130*, 46–58.
43. Schweppe, F. C. (1973). *Uncertain dynamic systems*. Englewood Cliffs, N. J.: Prentice Hall.
44. Aghaei, J., et al. (2017). Optimal robust unit commitment of CHP plants in electricity markets using information gap decision theory. *IEEE Transactions on Smart Grid, 8*(5), 2296–2304.
45. Murphy, C., Soroudi, A., & Keane, A. (2016). Information gap decision theory-based congestion and voltage management in the presence of uncertain wind power. *IEEE Transactions on Sustainable Energy, 7*(2), 841–849.
46. Ahmadigorji, M., Amjady, N., & Dehghan, S. (2018). A robust model for multiyear distribution network reinforcement planning based on information-gap decision theory. *IEEE Transactions on Power Systems, 33*(2), 1339–1351.
47. Zare, K., Moghaddam, M. P., & Sheikh-El-Eslami, M. K. (2011). Risk-based electricity procurement for large consumers. *IEEE Transactions on Power Systems, 26*(4), 1826–1835.

Chapter 3
Optimization Framework Based on Information Gap Decision Theory for Optimal Operation of Multi-energy Systems

Majid Majidi, Sayyad Nojavan, and Kazem Zare

Nomenclature

Indices	
t	Time periods index
Parameters	
η_{ee}^{T}	Transformer electrical efficiency
η_{ge}^{CHP}	Gas to power efficiency of CHP system
η_{ee}^{CON}	Converter efficiency
η_{ch}^{e}	Charging efficiency of battery storage system (BSS)
η_{dis}^{e}	Discharging efficiency of BSS
η_{ch}^{h}	Charging efficiency of thermal storage system (TSS)
η_{dis}^{h}	Discharging efficiency of TSS
$\alpha_{\min}^{e}$	Minimum capacity modeling coefficient of BSS
$\alpha_{\max}^{e}$	Maximum capacity modeling coefficient of BSS
α_{loss}^{e}	Loss of power coefficient in BSS
$\alpha_{\min}^{h}$	Minimum capacity modeling coefficient of TSS
$\alpha_{\max}^{h}$	Maximum capacity modeling coefficient of TSS
α_{loss}^{h}	Loss of power coefficient in TSS
A^{NET}	Coefficient for modeling upper network availability
A^{CHP}	Coefficient for modeling CHP system availability
A^{WIND}	Coefficient for modeling wind turbine availability

(continued)

M. Majidi (✉) · K. Zare
Faculty of Electrical and Computer Engineering, University of Tabriz, Tabriz, Iran
e-mail: majidmajidi95@ms.tabrizu.ac.ir; kazem.zare@tabrizu.ac.ir

S. Nojavan
Department of Electrical Engineering, University of Bonab, Bonab, Iran
e-mail: sayyad.nojavan@bonabu.ac.ir

B. Mohammadi-ivatloo, M. Nazari-Heris (eds.), *Robust Optimal Planning and Operation of Electrical Energy Systems*,
https://doi.org/10.1007/978-3-030-04296-7_3

$C_c^{st,e}$	Rated stored energy level in BSS
$C_c^{st,h}$	Rated stored heat level in TSS
C_r	Maximum operation cost of hub system in robustness function
C_o	Maximum operation cost of hub system in opportunity function
$g_{\min}^{net}$	Minimum rated capacity of gas network
$g_{\max}^{net}$	Maximum rated capacity of gas network
g_t^l	Residential gas demand
$p_{\min}^e$	Minimum rated capacity of electrical demand
$p_{\max}^e$	Maximum rated capacity of electrical demand
p_c^T	Rated limitation of transformer
p_c^{CHP}	Rated limitation of CHP system
p_c^B	Rated limitation of boiler
p_r	Rated power of wind turbine
p_t^{el}	Base electrical load
p_t^h	Heating demand
wa_t^l	Water demand in residential section
$wa_{\min}$	Minimum rated capacity of water network
$wa_{\max}$	Maximum rated capacity of water network
w_{ci},w_{co},w_r	Wind turbine cut-in, cut-out, and rated speeds
$w(t)$	Wind speed
x,y,z	Coefficients of power generation by wind turbine
$\widetilde{\lambda}_t^e$	Forecasted price of imported power from upper network
λ^{wi}	Operation cost of wind turbine
λ^g	Price of gas provided by gas network
λ^{wa}	Price of gas provided by gas network
λ_s^e	Operation cost of BSS
λ_s^h	Operation cost of TSS
Variables	
Cost	Total operation cost of hub energy system
$C_t^{st,e}$	Available stored energy level in BSS
$C_t^{st,h}$	Available stored heat level in TSS
g_t^{CHP}	Gas consumption of CHP system
g_t^B	Gas consumption of boiler
g_t^{net}	Total provided gas through gas network
$I_t^{ch,e}$	Binary variable; 1 if BSS is charging; otherwise 0
$I_t^{dis,e}$	Binary variable; 1 if BSS is discharging; otherwise 0
$I_t^{ch,h}$	Binary variable; 1 if TSS is charging; otherwise 0
$I_t^{dis,h}$	Binary variable; 1 if TSS is discharging; otherwise 0
p_t^e	Provided electric power by upstream network
$p_t^{ch,e}$	Charging power of BSS
$p_t^{dis,e}$	Discharging power of BSS
$p_t^{ch,h}$	Charging power of TSS

(continued)

$p_t^{dis,h}$	Discharging power of TSS
$p_t^{loss,e}$	Loss of electric power in BSS
$p_t^{loss,h}$	Loss of heat in TSS
p_t^{wi}	Power generated by wind turbine
wa_t^{net}	Procured water from water network
λ_t^e	Actual price of imported power from upper network
Functions	
$\widehat{\alpha}(C_r)$	Robustness function of IGDT
$\widehat{\beta}(C_o)$	Opportunity function of IGDT

3.1 Introduction

Hub energy systems are composed of different generation units to supply several energy demands. Combined heat and power (CHP) systems utilized in such systems are effective in increasing the efficiency of supplying heat and power load demands as much as 90% and reducing the pollutants gas emissions around 13–18% [1–3]. Stable operation of power systems including hub energy systems depends on various factors. One of the important factors that can make optimal operation of energy systems risky is uncertainty. Uncertainty of different fluctuating parameters like load [4, 5], market price [6–8], and other parameters can disturb predetermined scheduling and planning of hub energy systems. Uncertainty modeling of hub energy systems containing CHP system [9, 10], boiler [11–13], storage systems [14–17], and renewable generation units [18, 19] can be done to ensure a reliable power to energy demands.

3.1.1 Literature Review

Some research papers have studied multi-carrier energy systems in which brief summaries are reviewed in the following: Microgrid has been molded using hub energy concept in [20] in which optimal structures for storage system and converters are obtained. Optimal risk-based performance of hub energy system under uncertainty of market price, electrical load, and wind power has been evaluated using stochastic programming in [21]. Using Monte Carlo simulation in [22], scenario-based optimal performance of hub energy system in the presence of demand response has been studied. Also, stochastic programming has been employed in [23] to model uncertainty-based optimal performance of hub energy system in the presence of demand response and thermal energy market. An optimization framework based on robust optimization approach has been presented for hub energy system in [24]. To reduce fossil fuel consumption, renewable energy resources have been integrated using hub energy concept in [25]. Also, energy hub concept has been

used in [26] for optimum scheduling of microgrid in which operation cost of microgrid is minimized. Energy hub concept has been used to integrate energy resources at neighborhood stage in [27]. Several energy hub systems have been optimized and coordinated using multi-agent control approach in [28]. Various concepts of demand responses have been presented for smart hub energy systems in [29–32].

Optimal uncertainty-based operation of hub energy system has been scheduled using stochastic programming in [33] in which uncertainties of wind generation and pool price have been taken into account. Conditional value at risk measure is employed in [34, 35] to assess risk-based optimal operation of energy system under uncertainties. Optimal scheduling of a CHP-based microgrid has been studied considering the uncertainties of power market price and load demand using scenario-based modeling method in [36]. A novel model based on self-adaptive learning with time varying acceleration coefficient-gravitational search algorithm (TVAC-GSA) has been developed for economic dispatch problem of hub energy system in [37]. Using a new dispatch model based on fuzzy control and finite-state machines in [38], optimal scheduling of hub energy system has been investigated. Hub energy concept has been used to integrate fuel cell into a CHP system to gain economic benefits in [39]. Multi-carrier energy systems have been completely discussed and reviewed in [40]. Employing various optimization techniques and formulations, operation of hub energy system subject to operational limitations has been discussed in [41]. In order to assess uncertainty-based optimal performance of electrical-heat microgrid energy system in a deregulated market, probabilistic-based optimization framework has been presented in [42, 43] under demand-side programs [44].

Multi-objective optimization model has been presented for optimal eco-emission operation of hub energy system in [45, 46]. Optimal performance of smart hub energy system under demand response programs has been investigated in [47]. A multi-objective framework has been presented for optimal design, sizing, and operation of hub energy system in [48]. With the aim of maximizing profit, an optimization model has been developed for optimal performance of hub energy system in [49]. Optimum performance and operation of hub energy system under dynamic and real-time pricings has been studied in [50]. Adequacy of hub energy system has been studied in [51] in which dependencies of energy carriers at both demand and generation sides have been taken into account. Optimal economic performance of hub energy system has been studied in the presence of renewable energy sources and demand response in [52]. Furthermore, optimum performance of hub energy system has been studied with considering vehicle to grid technology in [53]. Optimal operation of hub energy system has been studied from reliability viewpoints in [54, 55]. The CHP economic dispatch problem has been studied using several mathematical methods and heuristic approaches such as genetic algorithm [56] and whale optimization algorithm [57]. A business model has been presented for hub energy system in the presence of renewable energy resources in [58].

In [59], a residential energy hub model has been presented for smart home in which plug-in hybrid electric vehicle as well as cogeneration units and combined heat and power system have been employed. A hierarchical energy management system including supervisory, optimizing, and execution control layers has been presented for optimal operation of hub energy system in [60]. Using a goal attainment-based technique, optimum energy flow problem of hub energy networks has been studied in the presence of several interconnected hub energy systems in [61]. Influence of optimizing heating network on the performance of hub energy system has been studied using teaching-learning-based optimization algorithm in [62]. Finally, using TVAC-GSA, optimum power flow of multi-carrier energy system has been studied within single and multi-objective optimization problems in [63].

3.1.2 Contributions and Novelties

In this chapter, optimal performance of hub energy system under severe uncertainty of upper network has been studied using information gap decision theory. The discussed uncertainty modeling methods do not provide any operating strategy for different possible conditions of uncertainty. The main feature of IGDT compared with other uncertainty modeling techniques is that it is composed of two immunity functions that model the whole aspects of uncertainty including the positive and negative ones. Robustness and opportunity functions of IGDT have been used to model and determine appropriate operating strategies of hub energy system. So, the contributions and novelties of proposed paper can be expressed in below:

- Economic performance of hub system is assessed under severe uncertainty of upstream network price.
- Uncertainty modeling of upstream network price is done by information gap decision theory (IGDT).
- Robust performance of hub system against uncertainty is assessed using robustness function of IGDT.
- Optimistic performance of hub system against uncertainty is assessed using opportunity function of IGDT.

3.1.3 Structure of Chapter

The rest of the proposed chapter is listed as follows: Information gap decision theory is briefly described in Sect. 3.2. Optimum performance of hub energy system under severe uncertainty of upstream network price is mathematically presented in Sect. 3.3. Simulations are done in Sect. 3.4 and the results are presented in the same section. Finally, this paper is concluded in Sect. 3.5.

3.2 Information Gap Decision Theory (IGDT)

IGDT is one of the powerful methods used for uncertainty modeling. This technique benefits from two immunity functions called robustness and opportunity functions. These functions determine appropriate operational strategies for stable operation of power system. In comparison with other uncertainty modeling techniques, this method doesn't need much more data for uncertainty modeling; therefore it doesn't make the problem much more sophisticated. Also, IGDT determines operating strategy for the operating systems under the desired taken policies against uncertainty. Generally, IGDT is composed of three sections which are expressed in below.

3.2.1 System Model

System model shows the input/output structure of studied system. This model can be expressed as function like $C(q,\rho)$in which q is decision variable and ρ is uncertain parameter.

3.2.2 Operation Requirements

Depending on the objectives of scheduling and planning, there are various expectations from each power system. These expectations are called operation requirements which are expressed based on robustness and opportunity functions:

$$\widehat{\alpha} = \max_{\alpha} \{\alpha\text{: maximum total cost which is is not higher than a specified cost}\} \tag{3.1}$$

$$\widehat{\beta} = \min_{\beta} \{\beta\text{: minimum total cost which is less than a specified cost}\} \tag{3.2}$$

Equation (3.1) expresses robustness function of IGDT. Robustness degree of system against possible increase of uncertain parameter is determined by this function. In fact, this function determines risk-averse strategies to be employed by operator of system for stable operation of system under higher levels of uncertainty. This function is mathematically expressed in (3.3) as follows [64, 65]:

$$\widehat{\alpha}(C_r) = \max_{\alpha} \{\alpha : \max(C(q,\rho)) \leq C_r\} \tag{3.3}$$

According to Eq. (3.3), $\widehat{\alpha}(C_r)$ expresses robustness level of system against increase of uncertain parameter. Since higher robustness levels are desired, higher values of $\widehat{\alpha}(C_r)$ are suitable.

On the other hand, reduction of uncertain parameter may provide some benefits for system which can be modeled using opportunity function (3.2). This function is mathematically expressed in (3.4) as follows [64, 65]:

$$\widehat{\beta}(C_o) = \min_{\beta} \{\alpha : \min(C(q,\rho)) \leq C_o\} \tag{3.4}$$

This function models the possible benefits and profits than can be achieved as a result of decisions. It should be noted that $C_r$and C_o are the maximum operation cost of system in robustness and opportunity function, respectively. It is obvious that C_r is greater than C_o.

3.2.3 *Uncertainty Modeling*

Information gap decision theory includes various uncertainty models. One of the most frequent types of these models is envelope-bound model which is expressed through Eq. (3.5) [4].

$$U(\alpha, \tilde{u}) = \left\{ u(t) : \left| \frac{u(t) - \tilde{u}(t)}{\varphi(t)} \right| \leq \alpha \right\}, \alpha \geq 0 \tag{3.5}$$

3.3 Problem Formulation

In this section, optimal performance problem of hub energy system under severe uncertainty of upper network is mathematically modeled.

3.3.1 *Electrical Limitations*

The power imported from upstream network plus the generation of wind turbine and CHP system as well as discharge power of BSS should be equal to electrical energy demand to satisfy electrical load balance limitation (3.6).

$$P_t^{e,l} = \begin{pmatrix} A^{NET} \times \eta_{ee}^{T} \times p_t^{e} + A^{CHP} \times \eta_{ge}^{CHP} \times g_t^{CHP} \\ + A^{WIND} \times \eta_{ee}^{CON} \times p_t^{wi} + p_t^{dis,e} - p_t^{ch,e} \end{pmatrix} \tag{3.6}$$

The power provided by upstream network should satisfy both network and transformer limitations which are expressed through Eqs. (3.7) and (3.8).

$$p^{e}_{\min} \leq p^{e}_{t} \leq p^{e}_{\max} \tag{3.7}$$

$$\eta^{T}_{ee} \times p^{e}_{t} \leq p^{T}_{c} \tag{3.8}$$

Electric power generation of wind turbine is expressed in Eq. (3.9). According to this equation, the generation of wind turbine is proportional with the hourly wind speed. According to each wind speed at each time, generation of wind turbine will be various within 0 and the rated power.

$$p^{wi}_{t} = \begin{cases} 0 & w < w_{ci} \\ p_r(z - y.w(t) + x.w^2(t)) & w_{ci} \leq w < w_r \\ p_r & w_r \leq w < w_{co} \\ 0 & w \geq w_{co} \end{cases} \tag{3.9}$$

Produced electric power by CHP system is limited by Eq. (3.10).

$$\eta^{CHP}_{ge} \times g^{CHP}_{t} \leq p^{CHP}_{c} \tag{3.10}$$

Equations (3.11, 3.12, 3.13, 3.14, 3.15, and 3.16) are used to model BSS.

$$C^{st,e}_{t} = C^{st,e}_{t-1} + p^{ch,e}_{t} \times \eta^{e}_{ch} - p^{dis,e}_{t} / \eta^{e}_{dis} - p^{loss,e}_{t} \tag{3.11}$$

$$\alpha^{e}_{\min} \times C^{st,e}_{c} \leq C^{st,e}_{t} \leq \alpha^{e}_{\max} \times C^{st,e}_{c} \tag{3.12}$$

$$p^{loss,e}_{t} = \alpha^{e}_{loss} \times C^{st,e}_{t} \tag{3.13}$$

$$\frac{\alpha^{e}_{\min} \times C^{st,e}_{c} \times I^{ch,e}_{t}}{\eta^{e}_{ch}} \leq p^{ch,e}_{t} \leq \frac{\alpha^{e}_{\max} \times C^{st,e}_{c} \times I^{ch,e}_{t}}{\eta^{e}_{ch}} \tag{3.14}$$

$$\alpha^{e}_{\min} \times C^{st,e}_{c} \times I^{dis,e}_{t} \times \eta^{e}_{dis} \leq p^{dis,e}_{t} \leq \alpha^{e}_{\max} \times C^{st,e}_{c} \times I^{dis,e}_{t} \times \eta^{e}_{dis} \tag{3.15}$$

$$I^{ch,e}_{t} + I^{dis,e}_{t} \leq 1 \tag{3.16}$$

Equation (3.11) states available stored energy of BSS which is limited in Eq. (3.12). Some percentage of stored energy in BSS is wasted as power loss which is expressed in Eq. (3.13). Equations (3.14) and (3.15) limit the charging and discharging power of BSS. Finally, Eq. (3.16) is used to avoid BSS from simultaneously being charged or discharged.

3.3.2 *Thermal Limitations*

Heat generation of CHP system and boiler as well as released heat from TSS should be equal to heating demand (3.17).

$$P_t^{l,h} = \left(A^{CHP} \times \eta_{gh}^{CHP} \times g_t^{CHP} + \eta_{gh}^{B} \times g_t^{B} + p_t^{dis,h} - p_t^{ch,h}\right) \tag{3.17}$$

Equations (3.18, 3.19, 3.20, 3.21, 3.22, and 3.23) are employed to model TSS.

$$C_t^{st,h} = C_{t-1}^{st,h} + p_t^{ch,h} \times \eta_{ch}^{h} - p_t^{dis,h}/\eta_{dis}^{h} - p_t^{loss,h} \tag{3.18}$$

$$\alpha_{\min}^{h} \times C_c^{st,h} \le C_t^{st,h} \le \alpha_{\max}^{h} \times C_c^{st,h} \tag{3.19}$$

$$p_t^{loss,h} = \alpha_{loss}^{h} \times C_t^{st,h} \tag{3.20}$$

$$\frac{\alpha_{\min}^{h} \times C_c^{st,h} \times I_t^{ch,h}}{\eta_{ch}^{h}} \le p_t^{ch,h} \le \frac{\alpha_{\max}^{h} \times C_c^{st,h} \times I_t^{ch,h}}{\eta_{ch}^{h}} \tag{3.21}$$

$$\alpha_{\min}^{h} \times C_c^{st,h} \times I_t^{dis,h} \times \eta_{dis}^{h} \le p_t^{dis,h} \le \alpha_{\max}^{h} \times C_c^{st,h} \times I_t^{dis,h} \times \eta_{dis}^{h} \tag{3.22}$$

$$I_t^{ch,h} + I_t^{dis,h} \le 1 \tag{3.23}$$

Produced extra heat by CHP system and boiler is stored in TSS which is expressed by Eq. (3.18) and restricted by Eq. (3.19). Some percentage of stored heat in TSS is lost which is expressed by Eq. (3.20). Equations (3.21) and (3.22) are used for charging and discharging limitation of TSS, respectively. Finally, binary variables used in Eq. (3.23) are employed to limit charge and discharge of TSS at the same time.

Heat generation of boiler is restricted by Eq. (3.24) which is expressed as follows:

$$\eta_{gh}^{B} \times g_t^{B} \le p_c^{B} \tag{3.24}$$

3.3.3 *Limitations of gas and water networks*

Total provided gas by gas network is expressed and limited by Eqs. (3.25) and (3.26), respectively.

$$G_t^{l} = g_t^{net} - g_t^{B} - g_t^{CHP} \tag{3.25}$$

$$g_{\min}^{net} \le g_t^{net} \le g_{\max}^{net} \tag{3.26}$$

Water demand is satisfied through the provided water by water network which is expressed and restricted through Eqs. (3.27) and (3.28), respectively.

$$Wa_t^{l} = wa_t^{net} \tag{3.27}$$

$$wa_{\min} \le wa_t^{net} \le wa_{\max} \tag{3.28}$$

3.3.4 Objective Function Without Uncertainty

In this chapter, optimal performance of hub energy system is set to be the objective function in which total operation cost of hub energy system is minimized (3.29).

$$\text{Min}\, Cost = \sum_{t}^{H} \begin{pmatrix} \lambda_t^e \times p_t^e + \lambda^{wi} \times p_t^{wi} + \lambda_s^e \times \left(p_t^{ch,e} + p_t^{dis,e}\right) \\ +\lambda_t^e \times \left(p_t^{ch,e} - p_t^{dis,e}\right) + \lambda^g \times g_t^B + \lambda^g \times g_t^{CHP} \\ +\lambda_s^h \times \left(p_t^{ch,h} + p_t^{dis,h}\right) + \lambda^{wa} \times wa_t \end{pmatrix} \tag{3.29}$$

As expressed in the objective function, total operation cost of hub energy system is composed of costs of imported electric power, gas and water from electricity, and gas and water networks as well as operation costs of CHP system, boiler, TSS, and BSS plus the cost/revenue of exchanged power.

3.3.5 IGDT-Based Optimal Performance of Hub Energy

In this section, risk-based optimal performance of hub energy system under uncertainty of upstream network price is modeled using IGDT.

3.3.5.1 Uncertainty Model

Using envelope-bound model, uncertainty of upstream network is modeled which is expressed in Eq. (3.30).

$$U\left(\alpha, \tilde{\lambda}_t^e\right) = \left\{ \lambda_t^e : \left| \frac{\lambda_t^e - \tilde{\lambda}_t^e}{\lambda_t^e} \right| \le \alpha \right\}, \alpha \ge 0 \tag{3.30}$$

3.3.5.2 Robustness Function

Robustness function of IGDT for optimal performance of hub energy system under uncertainty of upstream network price is expressed as follows:

$$\widehat{\alpha}(C_r) = \max \left\{ \alpha : \left(\max_{\lambda_t^e \in U\left(\alpha, \tilde{\lambda}_t^e\right)} Cost \le C_r \right) = (1+\omega) C_b \right\} \tag{3.31}$$

According to Eq. (3.31), maximum degree of robustness should be obtained, while total operation cost of hub energy system is less than a predefined cost, C_r. Minimum operation cost of hub energy system expected to have is C_b. Also, ω is the

cost variation factor to model the increased cost of hub energy system. Therefore, by taking a risk-averse strategy, the objective function will be maximization of α, while the required operation is satisfied:

$$\widehat{\alpha}(C_r) = \max\alpha \tag{3.32}$$

subject to:

$$\max\left\{\sum_{t}^{H}\begin{pmatrix}(1+\alpha)\widehat{\lambda}_t^e \times p_t^e + \lambda^{wi} \times p_t^{wi} + \lambda_s^e \times \left(p_t^{ch,e} + p_t^{dis,e}\right)\\ +\lambda_t^e \times \left(p_t^{ch,e} - p_t^{dis,e}\right) + \lambda^g \times g_t^B + \lambda^g \times g_t^{CHP}\\ +\lambda_s^h \times \left(p_t^{ch,h} + p_t^{dis,h}\right) + \lambda^{wa} \times wa_t\end{pmatrix}\right\} \le C_r \tag{3.33}$$

$$\text{Eqs.}(3.6) - (3.28) \tag{3.34}$$

As expressed above, maximum degree of robustness against increase of upstream network price is obtained, while total operation cost of hub energy system is less than a predefined cost.

3.3.5.3 Opportunity Function

Opportunity function of IGDT for risk-taker operation of hub energy system can be modeled using Eq. (3.35).

According to Eq. (3.35), minimum value of α should be obtained, while total operation cost of hub energy system is less than a predefined cost, C_o. Maximum operation cost of hub energy system expected to have is C_b. This means that less operation costs are possible to be obtained for hub energy system which is beneficial for hub system. Also, κ is the cost variation factor to model the decreased cost of hub energy system. Therefore, by taking risk-taking strategy, the objective function will be minimization of α, while the required operation is satisfied:

$$\widehat{\beta}(C_o) = \min\left\{\alpha: \left(\min_{\lambda_t^e \in U\left(\alpha,\tilde{\lambda}_t^e\right)} Cost \le C_o\right) = (1-\kappa)C_b\right\} \tag{3.35}$$

As expressed above, maximum possible benefits can be obtained for hub energy system, while operational requirements are satisfied.

$$\widehat{\beta}(C_o) = \min\alpha \tag{3.36}$$

subject to:

$$\min \left\{ \sum_{t}^{H} \begin{pmatrix} (1-\beta)\widehat{\lambda}_t^e \times p_t^e + \lambda^{wi} \times p_t^{wi} + \lambda_s^e \times \left(p_t^{ch,e} + p_t^{dis,e}\right) \\ +\lambda_t^e \times \left(p_t^{ch,e} - p_t^{dis,e}\right) + \lambda^g \times g_t^B + \lambda^g \times g_t^{CHP} \\ +\lambda_s^h \times \left(p_t^{ch,h} + p_t^{dis,h}\right) + \lambda^{wa} \times wa_t \end{pmatrix} \right\} \leq C_o \tag{3.37}$$

$$\text{Eqs.}(3.6) - (3.28) \tag{3.38}$$

3.4 Simulation and Results

In this section, uncertainty-based optimal operation of hub energy system is analyzed using information gap decision theory. Studied sample hub energy system is captured in Fig. 3.1.

3.4.1 Input Data

Simulations of uncertainty-based optimal performance problem of hub energy system using IGDT are based on the info and data given in the following. Electricity, gas, heating, and water demands to be supplied through hub energy system are depicted in Fig. 3.2. Hourly wind speed used by wind turbine for electric power generation is illustrated in Fig. 3.3.

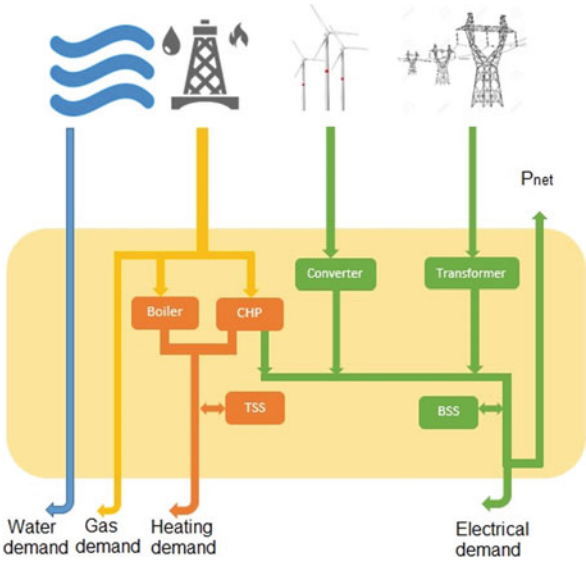

Fig. 3.1 Sample multi-carrier energy system

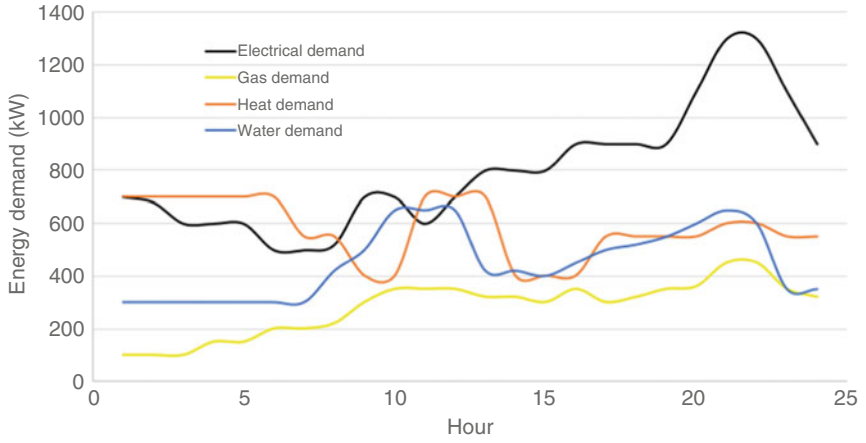

Fig. 3.2 Electricity, gas, heating, and water demands

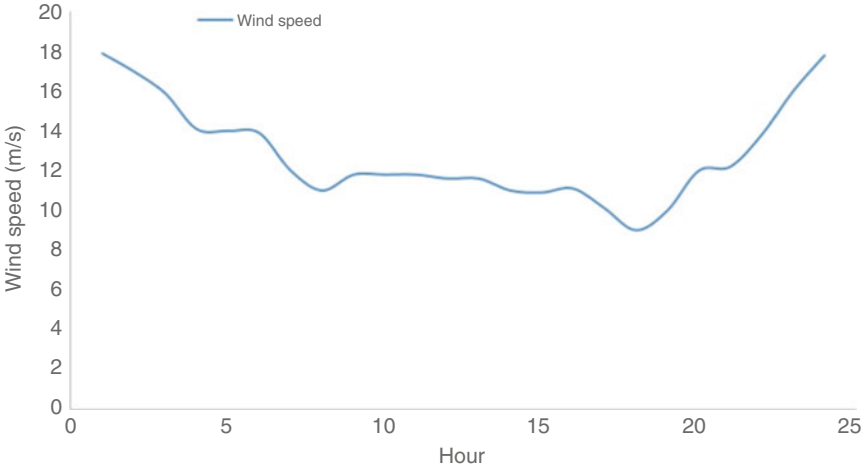

Fig. 3.3 Wind speed

Prices of imported gas and water from gas and water networks as well as operation costs of wind turbine, BSS, and TSS are presented in Table 3.1. Also, price of provided power by upstream network is illustrated in Fig. 3.4.

Technical parameters of local distribution generation units in hub system are presented in Table 3.2.

Technical data of electricity, gas, and water networks are presented in Table 3.3.

Finally, technical data of BSS and TSS are presented in Table 3.4.

Table 3.1 Prices and operation costs [22]

Parameter	Value	Unit
λ^{g}	6	Cent/kWh
λ^{wa}	4	Cent/kWh
λ^{wi}	0	Cent/kWh
λ_{s}^{e}	2	Cent/kWh
λ_{s}^{h}	2	Cent/kWh

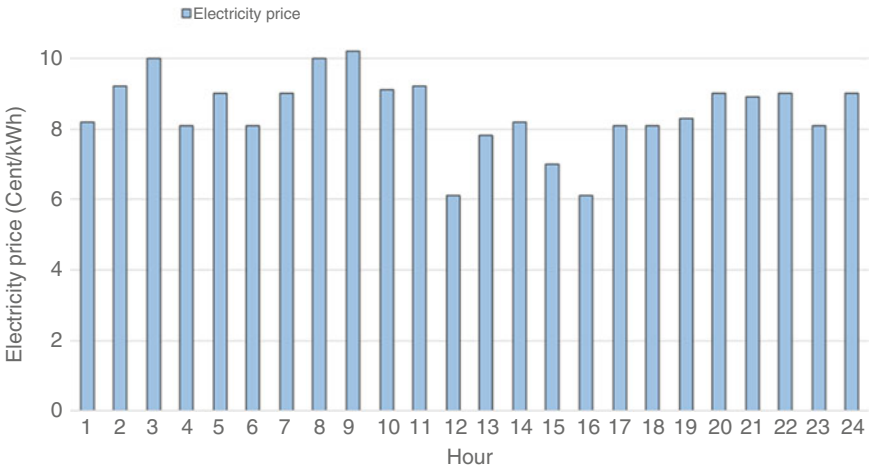

Fig. 3.4 Upstream network price

Table 3.2 Date of distribution generation units [22]

Wind turbine			CHP and boiler		
#	Unit	Value	#	Unit	Value
A^{WIND}	–	0.96	A^{CHP}	–	0.96
x, y, z	–	0.07, 0.01, 0.03	η_{ge}^{CHP}	%	40
w_{ci}	m/s	4	η_{gh}^{CHP}	%	35
w_{co}	m/s	22	p_{c}^{CHP}	kW	800
p_{r}	kW	400	η_{gh}^{B}	%	85
			p_{c}^{B}	kW	800

3.4.2 Results

In this section, by taking various types of strategies obtained through IGDT, operation of hub energy system is evaluated. It should be noted that uncertainty-based optimal operation of hub energy system is simulated under CPLEX of GAMS software [66].

Table 3.3 Date of electricity, gas, and water networks [22]

Upstream network			Gas and water network		
#	Unit	Value	#	Unit	Value
A^{NET}	–	0.99	$g^{net}_{\max}$	kW	1800
$p^{e}_{\max}$	kW	1000	$g^{net}_{\min}$	kW	0
$p^{e}_{\min}$	kW	0	$wa_{\max}$	kW	1000
p^{T}_{c}	kW	800	$wa_{\min}$	kW	0

Table 3.4 Technical data of BSS and TSS [22]

Electrical storage			Thermal storage		
#	Unit	Value	#	Unit	Value
$\alpha^{e}_{\min}$	–	0.05	$\alpha^{h}_{\min}$	–	0.05
$\alpha^{e}_{\max}$	–	0.9	$\alpha^{h}_{\max}$	–	0.9
α^{e}_{loss}	–	0.2	α^{h}_{loss}	–	0.2
η^{e}_{ch}	%	90	η^{h}_{ch}	%	90
η^{e}_{dis}	%	90	η^{h}_{dis}	%	90
$C^{st,e}_{c}$	kW	300	$C^{st,h}_{c}$	kW	200

3.4.2.1 Result of Robustness Function

Robustness of hub energy system against possible increase of price of upstream network is obtained through solving robustness function of IGDT in Eqs. (3.32, 3.33, and 3.34). Robustness of hub energy system versus total operation cost of hub energy system is illustrated in Fig. 3.5.

As shown in this figure, total operation cost of hub energy system has been increased 2.8%, while hub energy system has been robust to 24.6% possible increase of price of upstream network power. In other words, operator of hub energy system has decided to spend 2.8% more money to be resistant against maximum possible increase of upstream network price which is 24.6%.

3.4.2.2 Result of Opportunity Function

By taking risk-taking strategy, hub energy system seeks to gain economic profit due to possible reduction of upstream network price. Therefore, by solving Eqs. (3.36, 3.37, and 3.38), opportunity function of IGDT is obtained for hub energy system which is illustrated in Fig. 3.6.

According to this figure, due to reduction of upstream network price up to 10.9%, total operation cost of multi-carrier energy system is reduced 2.80%. In fact, the maximum possible benefits that could be gained by the operator of hub system are determined through this function.

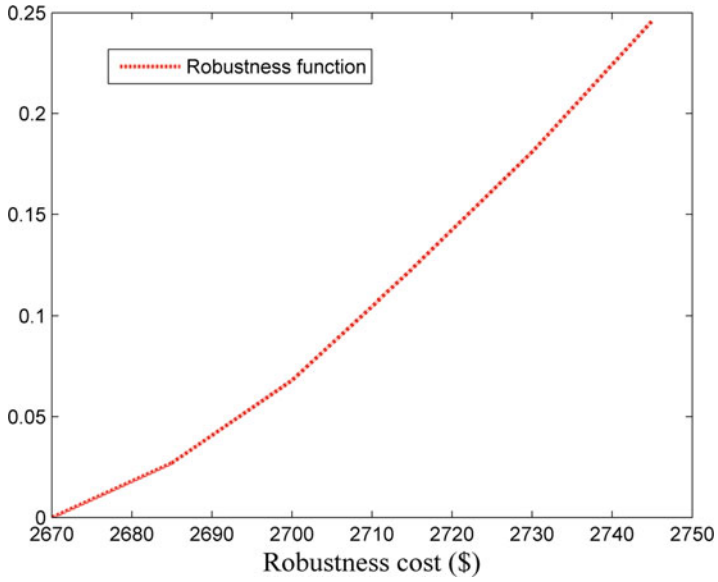

Fig. 3.5 Robustness function

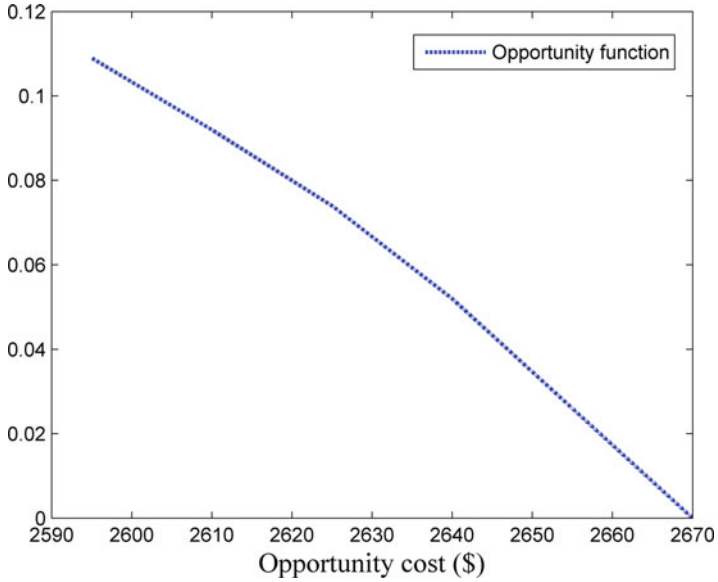

Fig. 3.6 Opportunity function

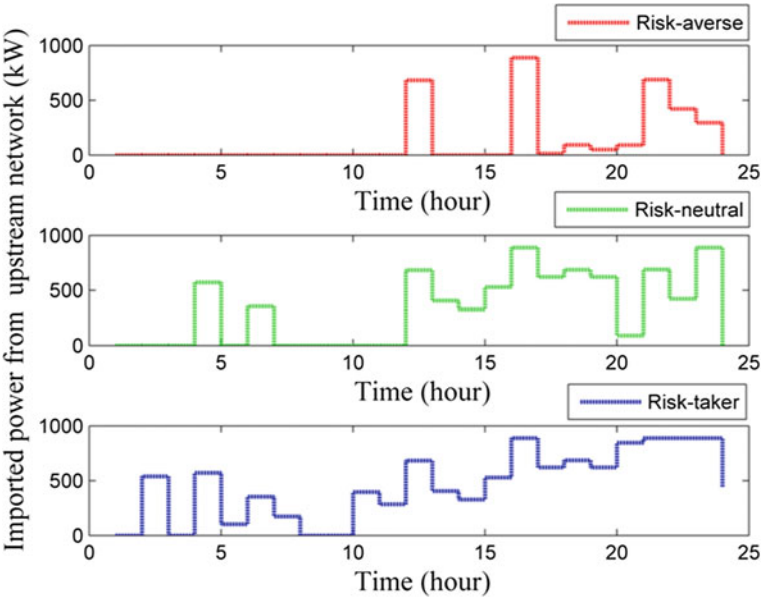

Fig. 3.7 Imported power from upstream network

3.4.2.3 Uncertainty-Based Operation of Various Sections in the Hub System

Imported power from upstream network is illustrated in risk-averse, risk-neutral, and risk-taker strategies in Fig. 3.7.

According to this Fig. 3.7, since price of purchased power from upstream network has been increased, by taking risk-averse strategy, less power has been bought from upstream network. On the other hand, due to lower values of upstream network price, more power has been bought from upstream network through taking risk-seeking strategy.

Since operation of different sections in hub energy system is dependent on the performance of other sections, therefore different sections can be influenced by uncertainty of upstream network price. Hub energy system needs to import gas for operation of some units like CHP system and boiler. Total purchased gas from gas network in risk-averse, risk-neutral, and risk-taker strategies is shown in Fig. 3.8.

As shown in Fig. 3.8, since less electric power is imported from upstream network through taking risk-averse strategy, hub system has focused more on the CHP system for electrical power generation, and then total purchased gas from network in this strategy has been increased. Also, since upstream network prices are lower in risk-taking strategies, most of the electrical demand is supplied through the purchased power from this network which means that share of CHP system in supplying electrical demand in risk-taking strategy has been reduced which consequently has led to less gas procurement in this strategy. In fact, the flexibility of hub

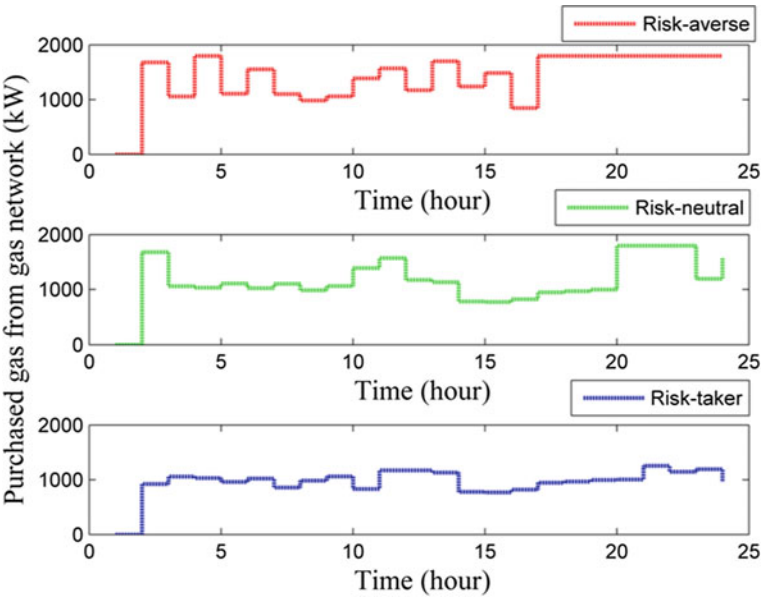

Fig. 3.8 Imported gas from gas network

systems has allowed the operator to configure the energy conversions in a way that the maximum suitable condition is reached. Gas consumption and electrical generation of CHP system is captured in Figs. 3.9 and 3.10.

It should be noted that since heat generation of CHP system is proportional with the gas consumption and electrical generation of this system, total generated heat by this system has been increased in risk-averse strategy. It fact, CHP system has used its heat generation capacity to supply heating demand which means that the share of boiler in supplying heating demand has been reduced which has led to less gas consumption of this unit. Generated heat by CHP system and boiler and gas consumption of boiler are illustrated in Figs. 3.11, 3.12, and 3.13, respectively.

3.5 Conclusions

Uncertainty of different parameters can result in positive and negative consequences in the planning and scheduling of power systems making the uncertainty modeling an essential issue. In this chapter, an uncertainty-based optimization model has been developed based on IGDT to assess risk-involved operation of hub energy system under uncertainty of upstream network price. Upstream network price showing fluctuating performance may increase or decrease from its nominal value leading to different operational conditions. In order to determine the policies and strategies to be taken against uncertainty, immunity functions of IGDT, namely, robustness and

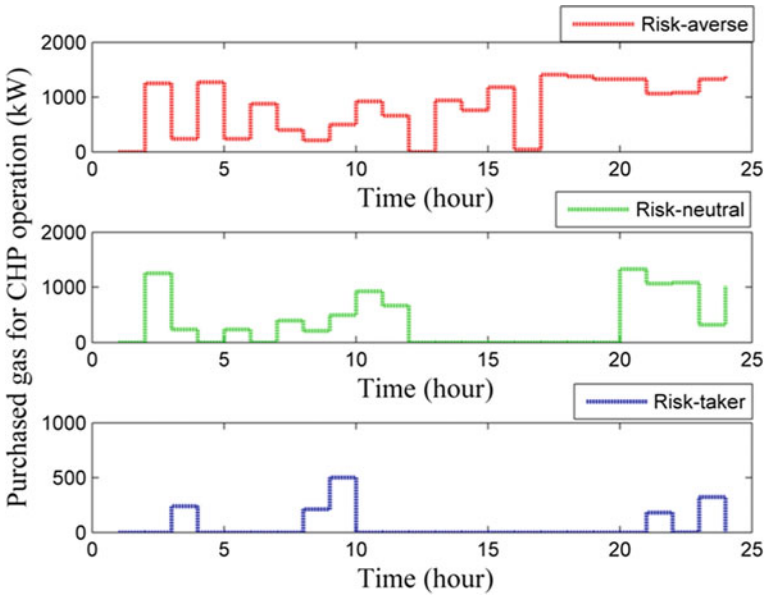

Fig. 3.9 Gas consumption of CHP system

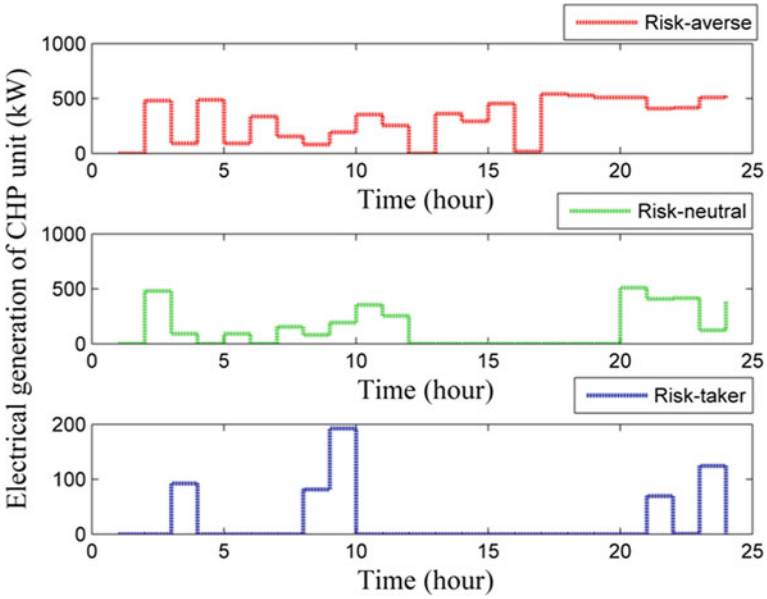

Fig. 3.10 Electric power generation of CHP system

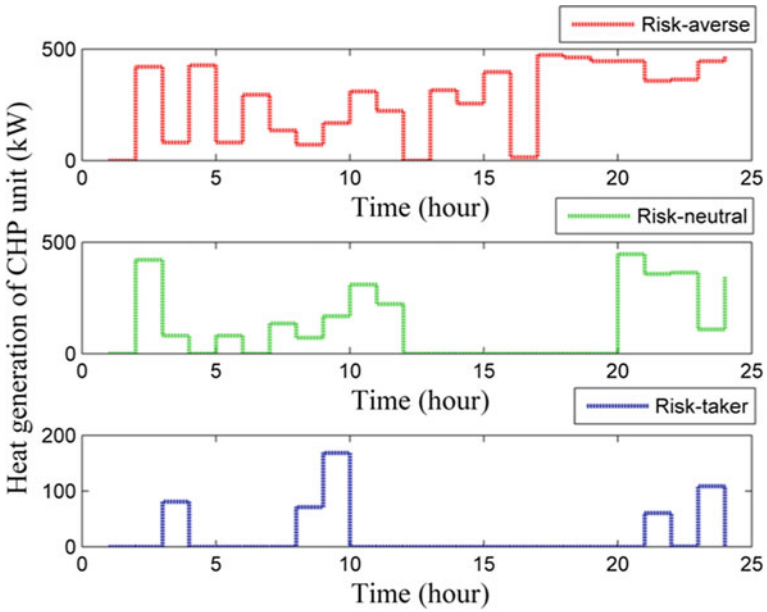

Fig. 3.11 Heat generation of CHP system

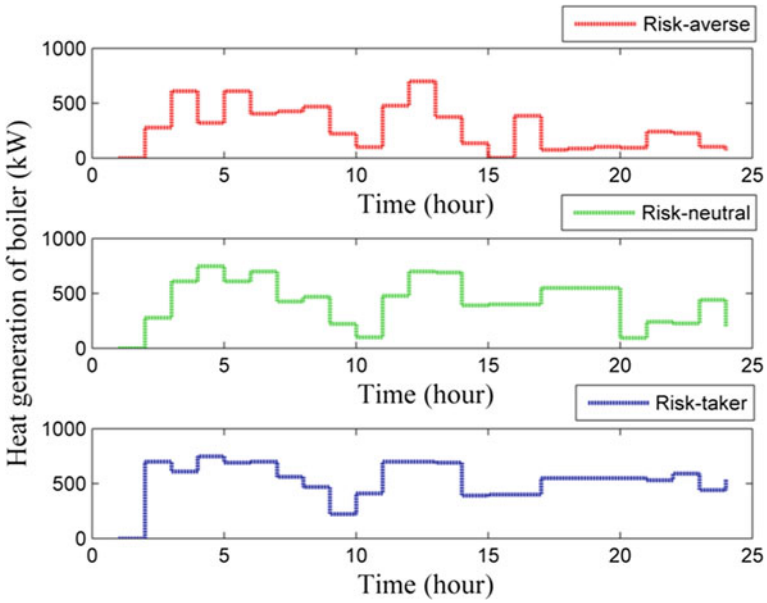

Fig. 3.12 Heat generation of boiler

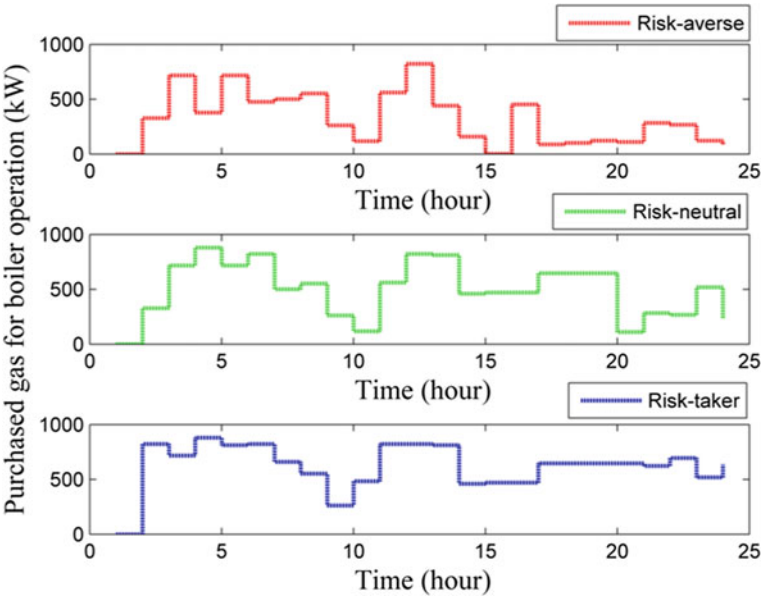

Fig. 3.13 Gas consumption of boiler

opportunity functions, are employed. Using the robustness function, maximum robustness degree of hub energy system against possible increase of upstream network price is obtained which is 24.6%. In simple words, hub energy system will proceed to experience optimal safe operation up to 24.6% more upstream network price. On the other hand, results of opportunity function revealed that by taking risk-taking strategies, hub energy system can gain 2.8% economic benefit through possible reduction of upstream network price up to 10.90%. So, different aspects of uncertainty can be taken into account through taking appropriate strategies provided by robustness and opportunity functions of IGDT.

It is noteworthy that optimal scheduling of hub energy system subject to uncertainties considering different types of demand response programs for both electrical and thermal sections as well as natural gas modeling can be considered to be studied in the future works.

References

1. Nazari-Heris, M., Mohammadi-Ivatloo, B., & Gharehpetian, G. (2017). A comprehensive review of heuristic optimization algorithms for optimal combined heat and power dispatch from economic and environmental perspectives. *Renewable and Sustainable Energy Reviews, 81*, 2128–2143.
2. Majidi, M., Nojavan, S., & Zare, K. (2017). A cost-emission framework for hub energy system under demand response program. *Energy, 134*, 157–166.

3. Nojavan, S., Majidi, M., & Zare, K. (2018). Optimal scheduling of heating and power hubs under economic and environment issues in the presence of peak load management. *Energy Conversion and Management, 156*, 34–44.
4. Nojavan, S., Majidi, M., & Zare, K. (2017). Performance improvement of a battery/PV/fuel cell/grid hybrid energy system considering load uncertainty modeling using IGDT. *Energy Conversion and Management, 147*, 29–39. https://doi.org/10.1016/j.enconman.2017.05.039.
5. Nojavan, S., Majidi, M., & Zare, K. (2017). Risk-based optimal performance of a PV/fuel cell/battery/grid hybrid energy system using information gap decision theory in the presence of demand response program. *International Journal of Hydrogen Energy, 42*(16), 11857–11867.
6. Nojavan, S., Zare, K., & Feyzi, M. R. (2013). Optimal bidding strategy of generation station in power market using information gap decision theory (IGDT). *Electric Power Systems Research, 96*, 56–63. https://doi.org/10.1016/j.epsr.2012.10.006.
7. Nojavan, S., Najafi-Ghalelou, A., Majidi, M., & Zare, K. (2018). Optimal bidding and offering strategies of merchant compressed air energy storage in deregulated electricity market using robust optimization approach. *Energy, 142*, 250–257.
8. Nazari-Heris, M., Mohammadi-Ivatloo, B., Gharehpetian, G. B., & Shahidehpour, M. (2018). Robust short-term scheduling of integrated heat and power microgrids. *IEEE Systems Journal*, (99), 1–9.
9. Nojavan, S., Majidi, M., Najafi-Ghalelou, A., & Zare, K. (2018). Supply side management in renewable energy hubs. In *Operation, planning, and analysis of energy storage systems in smart energy hubs* (pp. 163–187). Cham: Springer.
10. Majidi, M., Nojavan, S., & Zare, K. (2018). Multi-objective optimization framework for electricity and natural gas energy hubs under hydrogen storage system and demand response program. In *Operation, planning, and analysis of energy storage systems in smart energy hubs* (pp. 425–446). Cham: Springer.
11. Nojavan, S., Majidi, M., Najafi-Ghalelou, A., Ghahramani, M., & Zare, K. (2017). A cost-emission model for fuel cell/PV/battery hybrid energy system in the presence of demand response program: ε-constraint method and fuzzy satisfying approach. *Energy Conversion and Management, 138*, 383–392.
12. Majidi, M., Nojavan, S., Esfetanaj, N. N., Najafi-Ghalelou, A., & Zare, K. (2017). A multi-objective model for optimal operation of a battery/PV/fuel cell/grid hybrid energy system using weighted sum technique and fuzzy satisfying approach considering responsible load management. *Solar Energy, 144*, 79–89.
13. Najafi-Ghalelou, A., Nojavan, S., Majidi, M., Jabari, F., & Zare, K. (2018). Solar thermal energy storage for residential sector. In *Operation, planning, and analysis of energy storage systems in smart energy hubs* (pp. 79–101). Cham: Springer.
14. Nojavan, S., Majidi, M., & Esfetanaj, N. N. (2017). An efficient cost-reliability optimization model for optimal siting and sizing of energy storage system in a microgrid in the presence of responsible load management. *Energy, 139*, 89–97.
15. Majidi, M., & Nojavan, S. (2017). Optimal sizing of energy storage system in a renewable-based microgrid under flexible demand side management considering reliability and uncertainties. *Journal of Operation and Automation in Power Engineering, 5*(2), 205–214.
16. Nojavan, S., Majidi, M., & Zare, K. (2017). Stochastic multi-objective model for optimal sizing of energy storage system in a microgrid under demand response program considering reliability: A weighted sum method and fuzzy satisfying approach. *Journal of Energy Management and Technology, 1*(1), 61–70.
17. Ghalelou, A. N., Fakhri, A. P., Nojavan, S., Majidi, M., & Hatami, H. (2016). A stochastic self-scheduling program for compressed air energy storage (CAES) of renewable energy sources (RESs) based on a demand response mechanism. *Energy Conversion and Management, 120*, 388–396.
18. Majidi, M., Nojavan, S., & Zare, K. (2017). Optimal stochastic short-term thermal and electrical operation of fuel cell/photovoltaic/battery/grid hybrid energy system in the presence of demand response program. *Energy Conversion and Management, 144*, 132–142.

19. Nazari-Heris, M., Madadi, S., & Mohammadi-Ivatloo, B. (2018). Optimal management of hydrothermal-based micro-grids employing robust optimization method. In *Classical and recent aspects of power system optimization* (pp. 407–420). Elsevier.
20. Wasilewski, J. (2015). Integrated modeling of microgrid for steady-state analysis using modified concept of multi-carrier energy hub. *International Journal of Electrical Power & Energy Systems, 73*, 891–898. https://doi.org/10.1016/j.ijepes.2015.06.022.
21. Pazouki, S., & Haghifam, M.-R. (2016). Optimal planning and scheduling of energy hub in presence of wind, storage and demand response under uncertainty. *International Journal of Electrical Power & Energy Systems, 80*, 219–239. https://doi.org/10.1016/j.ijepes.2016.01.044.
22. Pazouki, S., Haghifam, M.-R., & Moser, A. (2014). Uncertainty modeling in optimal operation of energy hub in presence of wind, storage and demand response. *International Journal of Electrical Power & Energy Systems, 61*, 335–345.
23. Vahid-Pakdel, M., Nojavan, S., Mohammadi-Ivatloo, B., & Zare, K. (2017). Stochastic optimization of energy hub operation with consideration of thermal energy market and demand response. *Energy Conversion and Management, 145*, 117–128.
24. Parisio, A., Del Vecchio, C., & Vaccaro, A. (2012). A robust optimization approach to energy hub management. *International Journal of Electrical Power & Energy Systems, 42*(1), 98–104. https://doi.org/10.1016/j.ijepes.2012.03.015.
25. Orehounig, K., Evins, R., Dorer, V., & Carmeliet, J. (2014). Assessment of renewable energy integration for a village using the energy hub concept. *Energy Procedia, 57*, 940–949. https://doi.org/10.1016/j.egypro.2014.10.076.
26. Ma, T., Wu, J., & Hao, L. (2017). Energy flow modeling and optimal operation analysis of the micro energy grid based on energy hub. *Energy Conversion and Management, 133*, 292–306. https://doi.org/10.1016/j.enconman.2016.12.011.
27. Orehounig, K., Evins, R., & Dorer, V. (2015). Integration of decentralized energy systems in neighbourhoods using the energy hub approach. *Applied Energy, 154*, 277–289. https://doi.org/10.1016/j.apenergy.2015.04.114.
28. Skarvelis-Kazakos, S., Papadopoulos, P., Grau Unda, I., Gorman, T., Belaidi, A., & Zigan, S. (2016). Multiple energy carrier optimisation with intelligent agents. *Applied Energy, 167*, 323–335. https://doi.org/10.1016/j.apenergy.2015.10.130.
29. Bahrami, S., & Sheikhi, A. (2016). From demand response in smart grid toward integrated demand response in smart energy hub. *IEEE Transactions on Smart Grid, 7*(2), 650–658.
30. Gazijahani, F. S., & Salehi, J. (2018). Integrated DR and reconfiguration scheduling for optimal operation of microgrids using Hong's point estimate method. *International Journal of Electrical Power & Energy Systems, 99*, 481–492.
31. Althaher, S., Mancarella, P., & Mutale, J. (2015). Automated demand response from home energy management system under dynamic pricing and power and comfort constraints. *IEEE Transactions on Smart Grid, 6*(4), 1874–1883.
32. Bozchalui, M. C., Hashmi, S. A., Hassen, H., Cañizares, C. A., & Bhattacharya, K. (2012). Optimal operation of residential energy hubs in smart grids. *IEEE Transactions on Smart Grid, 3*(4), 1755–1766.
33. Najafi, A., Falaghi, H., Contreras, J., & Ramezani, M. (2016). Medium-term energy hub management subject to electricity price and wind uncertainty. *Applied Energy, 168*, 418–433. https://doi.org/10.1016/j.apenergy.2016.01.074.
34. Tavakoli, M., Shokridehaki, F., Akorede, M. F., Marzband, M., Vechiu, I., & Pouresmaeil, E. (2018). CVaR-based energy management scheme for optimal resilience and operational cost in commercial building microgrids. *International Journal of Electrical Power & Energy Systems, 100*, 1–9.
35. Gazijahani, F. S., Ravadanegh, S. N., & Salehi, J. (2018). Stochastic multi-objective model for optimal energy exchange optimization of networked microgrids with presence of renewable generation under risk-based strategies. *ISA Transactions, 73*, 100–111.
36. Nazari-Heris, M., Abapour, S., & Mohammadi-Ivatloo, B. (2017). Optimal economic dispatch of FC-CHP based heat and power micro-grids. *Applied Thermal Engineering, 114*, 756–769.

37. Beigvand, S. D., Abdi, H., & La Scala, M. (2017). A general model for energy hub economic dispatch. *Applied Energy, 190*, 1090–1111. https://doi.org/10.1016/j.apenergy.2016.12.126.
38. Perera, A. T. D., Nik, V. M., Mauree, D., & Scartezzini, J.-L. (2017). Electrical hubs: An effective way to integrate non-dispatchable renewable energy sources with minimum impact to the grid. *Applied Energy, 190*, 232–248. https://doi.org/10.1016/j.apenergy.2016.12.127.
39. AlRafea, K., Fowler, M., Elkamel, A., & Hajimiragha, A. (2016). Integration of renewable energy sources into combined cycle power plants through electrolysis generated hydrogen in a new designed energy hub. *International Journal of Hydrogen Energy, 41*(38), 16718–16728. https://doi.org/10.1016/j.ijhydene.2016.06.256.
40. Mancarella, P. (2014). MES (multi-energy systems): An overview of concepts and evaluation models. *Energy, 65*, 1–17. https://doi.org/10.1016/j.energy.2013.10.041.
41. Evins, R., Orehounig, K., Dorer, V., & Carmeliet, J. (2014). New formulations of the 'energy hub' model to address operational constraints. *Energy, 73*, 387–398. https://doi.org/10.1016/j.energy.2014.06.029.
42. Marzband, M., Fouladfar, M. H., Akorede, M. F., Lightbody, G., & Pouresmaeil, E. (2018). Framework for smart transactive energy in home-microgrids considering coalition formation and demand side management. *Sustainable Cities and Society, 40*, 136–154.
43. Marzband, M., Azarinejadian, F., Savaghebi, M., Pouresmaeil, E., Guerrero, J. M., & Lightbody, G. (2018). Smart transactive energy framework in grid-connected multiple home microgrids under independent and coalition operations. *Renewable Energy, 126*, 95–106.
44. Marzband, M., Javadi, M., Pourmousavi, S. A., & Lightbody, G. (2018). An advanced retail electricity market for active distribution systems and home microgrid interoperability based on game theory. *Electric Power Systems Research, 157*, 187–199.
45. Shabanpour-Haghighi, A., & Seifi, A. R. (2015). Multi-objective operation management of a multi-carrier energy system. *Energy, 88*, 430–442. https://doi.org/10.1016/j.energy.2015.05.063.
46. Maroufmashat, A., Elkamel, A., Fowler, M., Sattari, S., Roshandel, R., Hajimiragha, A., Walker, S., & Entchev, E. (2015). Modeling and optimization of a network of energy hubs to improve economic and emission considerations. *Energy, 93*, 2546–2558. https://doi.org/10.1016/j.energy.2015.10.079.
47. Sheikhi, A., Bahrami, S., & Ranjbar, A. M. (2015). An autonomous demand response program for electricity and natural gas networks in smart energy hubs. *Energy, 89*, 490–499. https://doi.org/10.1016/j.energy.2015.05.109.
48. Evins, R. (2015). Multi-level optimization of building design, energy system sizing and operation. *Energy, 90*, 1775–1789. https://doi.org/10.1016/j.energy.2015.07.007.
49. Moghaddam, I. G., Saniei, M., & Mashhour, E. (2016). A comprehensive model for self-scheduling an energy hub to supply cooling, heating and electrical demands of a building. *Energy, 94*, 157–170. https://doi.org/10.1016/j.energy.2015.10.137.
50. Kamyab, F., & Bahrami, S. (2016). Efficient operation of energy hubs in time-of-use and dynamic pricing electricity markets. *Energy, 106*, 343–355. https://doi.org/10.1016/j.energy.2016.03.074.
51. Shariatkhah, M.-H., Haghifam, M.-R., Chicco, G., & Parsa-Moghaddam, M. (2016). Adequacy modeling and evaluation of multi-carrier energy systems to supply energy services from different infrastructures. *Energy, 109*, 1095–1106. https://doi.org/10.1016/j.energy.2016.04.116.
52. Brahman, F., Honarmand, M., & Jadid, S. (2015). Optimal electrical and thermal energy management of a residential energy hub, integrating demand response and energy storage system. *Energy and Buildings, 90*, 65–75. https://doi.org/10.1016/j.enbuild.2014.12.039.
53. Rastegar, M., & Fotuhi-Firuzabad, M. (2015). Load management in a residential energy hub with renewable distributed energy resources. *Energy and Buildings, 107*, 234–242. https://doi.org/10.1016/j.enbuild.2015.07.028.
54. Shariatkhah, M.-H., Haghifam, M.-R., Parsa-Moghaddam, M., & Siano, P. (2015). Modeling the reliability of multi-carrier energy systems considering dynamic behavior of thermal loads. *Energy and Buildings, 103*, 375–383. https://doi.org/10.1016/j.enbuild.2015.06.001.

55. Koeppel, G., & Andersson, G. (2009). Reliability modeling of multi-carrier energy systems. *Energy, 34*(3), 235–244. https://doi.org/10.1016/j.energy.2008.04.012.
56. Haghrah, A., Nazari-Heris, M., & Mohammadi-Ivatloo, B. (2016). Solving combined heat and power economic dispatch problem using real coded genetic algorithm with improved Mühlenbein mutation. *Applied Thermal Engineering, 99*, 465–475.
57. Nazari-Heris, M., Mehdinejad, M., Mohammadi-Ivatloo, B., & Babamalek-Gharehpetian, G. (2017). Combined heat and power economic dispatch problem solution by implementation of whale optimization method. *Neural Computing and Applications*, 1–16.
58. Sepponen, M., & Heimonen, I. (2016). Business concepts for districts' energy hub systems with maximised share of renewable energy. *Energy and Buildings, 124*, 273–280. https://doi.org/10.1016/j.enbuild.2015.07.066.
59. Rastegar, M., Fotuhi-Firuzabad, M., & Lehtonen, M. (2015). Home load management in a residential energy hub. *Electric Power Systems Research, 119*, 322–328. https://doi.org/10.1016/j.epsr.2014.10.011.
60. Xu, X., Jia, H., Wang, D., Yu, D. C., & Chiang, H.-D. (2015). Hierarchical energy management system for multi-source multi-product microgrids. *Renewable Energy, 78*, 621–630. https://doi.org/10.1016/j.renene.2015.01.039.
61. La Scala, M., Vaccaro, A., & Zobaa, A. F. (2014). A goal programming methodology for multiobjective optimization of distributed energy hubs operation. *Applied Thermal Engineering, 71*(2), 658–666. https://doi.org/10.1016/j.applthermaleng.2013.10.031.
62. Shabanpour-Haghighi, A., & Seifi, A. R. (2016). Effects of district heating networks on optimal energy flow of multi-carrier systems. *Renewable and Sustainable Energy Reviews, 59*, 379–387. https://doi.org/10.1016/j.rser.2015.12.349.
63. Derafshi Beigvand, S., Abdi, H., & La Scala, M. (2016). Optimal operation of multicarrier energy systems using time varying acceleration coefficient gravitational search algorithm. *Energy, 114*, 253–265. https://doi.org/10.1016/j.energy.2016.07.155.
64. Nojavan, S., Zare, K., & Mohammadi-Ivatloo, B. (2017). Risk-based framework for supplying electricity from renewable generation-owning retailers to price-sensitive customers using information gap decision theory. *International Journal of Electrical Power & Energy Systems, 93*, 156–170.
65. Nojavan, S., Zare, K., & Mohammadi-Ivatloo, B. (2017). Information gap decision theory-based risk-constrained bidding strategy of price-taker GenCo in joint energy and reserve markets. *Electric Power Components and Systems, 45*(1), 49–62.
66. The GAMS Software Website. (2017). [Online]. Available: http://www.gams.com/help/index.jsp?topic=%2Fgams.doc%2Fsolvers%2Findex.html

Chapter 4
Risk-Constrained Scheduling of a Solar Ice Harvesting System Using Information Gap Decision Theory

Farkhondeh Jabari, Behnam Mohammadi-ivatloo, Hadi Ghaebi, and Mohammad-Bagher Bannae-Sharifian

Nomenclature

Variables	
$E\dot{x}_e$	Exergy transferred from warm inside air to R134a
$E\dot{x}_{D,evap}$	Exergy destructed during evaporation process
$E\dot{x}_c$	Exergy transferred from R134a to ambient air
$E\dot{x}_{D,cond}$	Exergy destructed during condensation process
$E\dot{x}_{D,cycle}$	Exergy destructed during ice-forming cycle
$E\dot{x}_{in-air}$	Exergy level of inside air
$E\dot{x}_{out-air_{cond}}$	Exergy value of supplied air
$E\dot{x}_{out-air_{evap}}$	Exergy level of cooled air
$\dot{m}_i$	Mass flow rate of R134a at state i
P_{comp}	Power consumption of compressor
P_{grid}	Electricity provided by local power network
$P_{in\ -\ fan}$	Power consumption of evaporator fan
$P_{out\ -\ fan}$	Power consumption of condenser fan
$\dot{Q}_{cond}$	Condenser output heat
$\dot{Q}_{evap}$	Inlet heat to evaporator
$T_{out-air_{cond}}$	Temperature of supplied air
$\widehat{\alpha}$	Robust factor
$\widehat{\beta}$	Opportunity factor
U	Fractional error of info-gap model

(continued)

F. Jabari (✉) · B. Mohammadi-ivatloo · M.-B. Bannae-Sharifian
Faculty of Electrical and Computer Engineering, University of Tabriz, Tabriz, Iran
e-mail: f.jabari@tabrizu.ac.ir; bmohammadi@tabrizu.ac.ir; sharifian@tabrizu.ac.ir

H. Ghaebi
Department of Mechanical Engineering, University of Mohaghegh Ardabili, Ardabil, Iran
e-mail: hghaebi@uma.ac.ir

B. Mohammadi-ivatloo, M. Nazari-Heris (eds.), *Robust Optimal Planning and Operation of Electrical Energy Systems*,
https://doi.org/10.1007/978-3-030-04296-7_4

Parameters	
λ_t	Energy price at hour t
$T_{out-air_{evap}}$	Temperature of cooled air
T_{amb}	Ambient temperature
T_C	Condensation temperature
T_e	Evaporation temperature
$T_{in\ -\ air}$	Temperature of inside air
$\dot{m}_{in-air}$	Mass flow rate of evaporator fan
$\dot{m}_{out-air}$	Mass flow rate of condenser fan
C_a	Specific heat capacity of air
$E\dot{x}_{amb}$	Exergy level of ambient air (i.e., equal to zero)
h_i	Enthalpy value of R134a at state i
F_w	Target cost of opportunity mode
F_k	Critical cost of robust mode

4.1 Introduction

In severe hot summer days, air conditioning systems consume a huge amount of electricity for space cooling, especially in afternoon hours. Therefore, annual on-peak electrical demand usually occurs in the hottest day of the year and may not only lead to load-generation imbalance, widespread outages, and catastrophic blackouts but also increases total fossil fuel consumption in thermal power plants and pollutant emissions of greenhouse gases. Therefore, use of renewable energy resources-based ice-cold thermal energy storages in building space cooling is a cost-effective strategy with zero CO_2 footprints [1].

Recently, studies on renewable energy resources-based cooling systems have attracted more attention. In [2], a solar-assisted absorption refrigeration system integrated with a liquid desiccant dehumidification cycle is proposed for cogeneration of cool and desalinated water. Energetic and economic studies demonstrated that it is suitable for application in tropical regions faced with potable water shortage because energy saving ratio and exergy efficiency are more than 25.64% and 2.97% in comparison with conventional cooling and water generation systems. Authors of [3] introduced a CO_2-driven compression-adsorption hybrid cycle for co-production of cool and desalinated water. It is proved that overall coefficient of performance is improved more than 60% by producing 12.7 m^3/day freshwater and recovering waste heat from CO_2 to drive cycle. Reference [4] combined a solar-driven gas turbine cycle with organic Rankine cycle (ORC) for electricity generation (up to 255 kW), desalination (1.5 m^3/day potable water), and air conditioning (with 8.8 kW cooling capacity) applications. Authors of [5] designed a solar-natural gas-driven cooling system and evaluated its performance from energy, exergy, and environmental viewpoints under variable solar radiations. A solar air conditioning system consisting of photovoltaic collectors and single-effect absorption chillers is investigated to satisfy 100 kW cooling capacity with 450 m^2 solar panels. Thermo-

economic analysis of a solar vapor compression refrigeration cycle is presented in [6]. Moreover, a pumped hydro storage is employed for saving energy by pumping water from lower reservoir to upper one in low-price time intervals and extracting it to generate power at high-tariff periods. In [7], a solar-geothermal air conditioning unit is developed for heating, cooling, and supplying daily electricity demand of a benchmark office building located in a tropical area. In this study, solar energy is used for water heating, and geothermal heat is employed in radiant cooling systems. Use of solar and geothermal heat reservoirs causes 44.4% annual electricity saving. In [8], a seasonal ice making system integrated with a chilled water storage is employed for storing cool as ice crystals and releases it by ice melting in summer season. In [9], short-term coordination of electric drive vehicles-ice storage-solar photovoltaic (PV) panels is optimized for supplying cooling demand of some commercial buildings in a distribution feeder. Optimization of ice making and melting decisions, load control, participation of plug-in electric vehicles in transportation, and energy procurement strategies lead to 13.4% peak load reduction and 11.6% feeder loss reduction. Authors of [10] combined ice and chilled water storage units for sizing of refrigeration capacity aiming to minimize daily operation cost. Steady-state payback period analysis is carried out to prove its economic benefit in comparison with single water-cooled chilling plant. Carbonel et al. [11] experimented an underground ice storage cavern on a pilot case with 75 m^3 chilling capacity by using heat pumps and flat-plate heat exchangers. Firstly, water is preheated by solar collectors, then enters a heat exchanger and extracts its freezing latent heat to another working fluid, changes into ice, and is stored in underground cavern. Then, heat pump-based refrigeration cycle is employed for building space cooling by absorbing heat from inside hot air and transferring it to ambient. In [12], a residential scale ice-cold thermal energy storage system is designed based on polyethylene water reservoir in a way that water-glycol mixture enters a mechanical refrigeration cycle and is frozen at off-peak hours (charging or ice making mode). In peak cooling demand periods, water-glycol mixture absorbs heat from inside air and exchanges it with ice packs (discharging or ice melting mode). In [13], a mixed-integer linear programming problem is solved for optimal participation of ice storage, thermal energy storage, and electric and absorption chillers in cooling, heating, and powering a residential tower located in Shanghai. Minimization of natural gas and electricity costs and capital investment cost of prime mover is considered as the main objective. Reference [14] proved that a biomass gasifier-solid oxide fuel cell-double effect absorption chiller hybrid industrial cooling and power system yields 49% improvement in exergy efficiency and 64% emission reduction. Jabari et al. [15] designed an air to air heat pump (AAHP)-based energy hub for cooling and power of large residential buildings located at Southern Iran. Daily charge and discharge patterns of an advanced adiabatic compressed air energy storage are optimally scheduled [16] in order to reduce total energy procured by local power network. Moreover, real-time demand-side management strategy with capability of shifting a percent of peak cooling load to low-price periods and battery energy storage for charging electricity in low-tariff hours and discharging it at peak time intervals are implemented on AAHP-based cooling and power system [17]. In

[18], artificial neural networks are used to learn and predict indoor temperature based on roof cooling techniques under various outside temperatures, relative humidity, solar intensity, and wind speed. Authors of [19] implemented artificial neural networks, adaptive neuro-fuzzy inference system (ANFIS), and fuzzy inference system (FIS) on indirect evaporative cooling system to minimize its electricity usage under variable ambient air temperature. Authors of [20] integrated an ejector refrigeration process with Kalina cycle to produce power and cooling capacity from low-temperature geothermal heat reservoirs. A feed fluid heater is installed for higher electricity generation using turbine exhaust flue gases. It is found that lower values of feed fluid heater and turbine inlet pressures and higher temperature of geothermal heat source result in more electricity production. Additionally, more refrigeration capacity is achieved if evaporation temperature and turbine inlet pressure increase and feed fluid heater pressure decreases.

As mentioned, there are some interesting works on design and performance investigation of renewable energy resources-based air conditioners. But, uncertainty of cooling demand is not considered in design and analysis of these systems. This chapter aims to study robust and opportunistic strategies for risk-assessed optimal operation of air source heat pump (ASHP)-based ice-cold thermal energy storage (ICTES) system using information gap decision theory (IGDT). In IGDT approach with robust and opportunistic operating modes, uncertainty of building cooling demand is modeled for making both risk-averse and risk-seeker decisions in energy procurement of ICTES. Two specific contributions of this chapter are stated as follows:

- Thermodynamic analysis of ASHP-based ice-cold thermal energy storage is comprehensively presented.
- Optimal scheduling of ICTES is conducted using IGDT to evaluate impact of cooling load uncertainty on energy cost minimization approach. IGDT method is employed for studying the uncertainty of the cooling demand and enables the building owner to make a risk-averse or risk-seeker decision under uncertain operating condition.

Other sections of this chapter are presented as follows: A thermodynamic analysis of ICTES is presented in Sect. 4.2. Afterward, numerical results are discussed in Sect. 4.3. Conclusion appears in Sect. 4.4.

4.2 Proposed Methodology

4.2.1 Ice Storage System

In this chapter, an air to air heat pump is employed for making ice during hot hours of summer days. As shown in Fig. 4.1, this refrigeration cycle consists of three control volumes I, II, and III. In control volume I, a heat transfer fluid such as R134a enters evaporator, absorbs heat from air entering it, and turns into a saturated vapor at

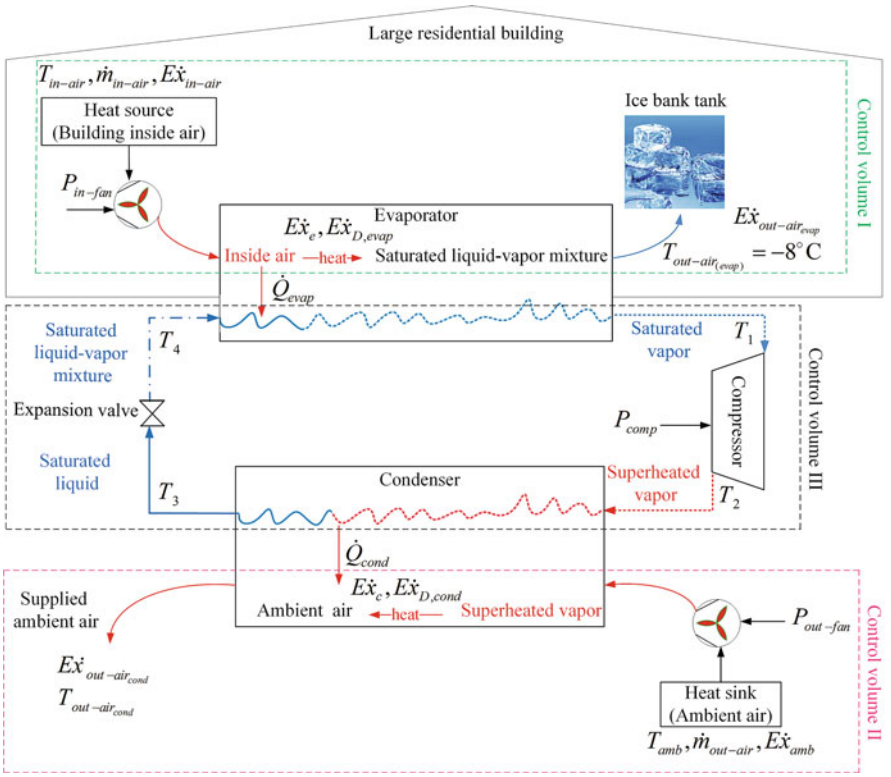

Fig. 4.1 A typical ASHP-based ice harvesting system

temperature, T_1. Electrical power consumed by inside evaporator fan, which depends on temperature difference between inlet warm and outlet cooled air and heat level of inside warm air, can be calculated from Eq. (4.1).

$$P_{in-fan} = C_a \dot{m}_{in-air} \left(T_{out-air_{evap}} - T_{in-air} \right) + \dot{Q}_{evap} \tag{4.1}$$

where

C_a: Specific heat capacity of air at constant pressure
$\dot{m}_{in-air}$: Mass flow rate of evaporator fan
$T_{out-air_{evap}}$: Temperature of cooled air
$\dot{Q}_{evap}$: Heat flow from inside air to R134a, which is calculated from Eq. (4.2).

$$\dot{Q}_{evap} = \dot{m}_4 \left(h_1 - h_4 \right) \tag{4.2}$$

in which h_i and $\dot{m}_i$ refer to enthalpy and mass flow rate of R134a at state i, respectively. The exergy destructed during the evaporation process, $\dot{E}x_{D,evap}$, and the exergy conducted from warm air to R134a, $\dot{E}x_e$, can be given by balance Eqs. (4.3, 4.4, 4.5, and 4.6).

$$\dot{S}_{gen,evap} = C_a \dot{m}_{in-air} \ln\left(\frac{T_{out-air_{evap}}}{T_{in-air}}\right) + \frac{\dot{Q}_{evap}}{T_e} \tag{4.3}$$

$$P_{in-fan} + \dot{E}x_e - \dot{E}x_{D,evap} = \dot{E}x_{out-air_{evap}} - \dot{E}x_{in-air} \tag{4.4}$$

$$\dot{E}x_e = \dot{Q}_{evap}\left(\frac{T_0 - T_e}{T_e}\right) \tag{4.5}$$

$$\dot{E}x_{D,evap} = \dot{S}_{gen,evap} T_0 \tag{4.6}$$

where

$\dot{S}_{gen,evap}$: Entropy produced during the evaporation process
T_e and T_0: Evaporation temperature and reference temperature, respectively
$\dot{E}x_{in-air}$ and $\dot{E}x_{out-air_{evap}}$: Exergy levels of input warm and output cooled air, respectively

Assuming air as an ideal gas, Eqs. (4.7) and (4.8) are used to obtain $\dot{E}x_{out-air_{evap}}$ and $\dot{E}x_{in-air}$, respectively.

$$\dot{E}x_{out-air_{evap}} = C_a \dot{m}_{in-air}\left[\left(T_{out-air_{evap}} - T_0\right) - T_0 \ln\left(\frac{T_{out-air_{evap}}}{T_0}\right)\right] \tag{4.7}$$

$$\dot{E}x_{in-air} = C_a \dot{m}_{in-air}\left[\left(T_{in-air} - T_0\right) - T_0 \ln\left(\frac{T_{in-air}}{T_0}\right)\right] \tag{4.8}$$

In control volume II, a heat flow is exchanged between superheated vapor with temperature of T_2 and ambient air with temperature of T_{amb}. As formulated by Eqs. (4.9, 4.10, 4.11, 4.12, 4.13, and 4.14), outputs of this stage are a saturated liquid with temperature of T_3 and heated ambient air at temperature $T_{out-air_{cond}}$.

$$\dot{Q}_{cond} = \dot{m}_2(h_2 - h_3) \tag{4.9}$$

$$\dot{S}_{gen,cond} = C_a \dot{m}_{out-air} \ln\left(\frac{T_{out-air_{cond}}}{T_{amb}}\right) - \frac{\dot{Q}_{cond}}{T_C} \tag{4.10}$$

$$P_{out-fan} + \dot{E}x_c - \dot{E}x_{D,cond} = \dot{E}x_{out-air_{cond}} - \dot{E}x_{amb}(=0) \tag{4.11}$$

$$\dot{E}x_c = \dot{Q}_{cond}\left(\frac{T_C - T_0}{T_C}\right) \tag{4.12}$$

$$\dot{E}x_{D,cond} = \dot{S}_{gen,cond} T_0 \tag{4.13}$$

$$\dot{E}x_{out-air_{cond}} = C_a \dot{m}_{out-air}\left[(T_{out-air_{cond}} - T_0) - T_0 \ln\left(\frac{T_{out-air_{cond}}}{T_0}\right)\right] \tag{4.14}$$

Since

$\dot{m}_{out-air}$: Mass flow rate of condenser fan
$T_{out-air_{cond}}$: Temperature of supplied air
T_C: Condensation temperature
$\dot{E}x_{D,cond}$: Exergy destructed during condensation process
$\dot{E}x_c$: Exergy transferred from R134a to ambient air
$\dot{E}x_{out-air_{cond}}$: Exergy level of supplied air

In control volume III, the saturated vapor with temperature of T_1 is pressurized by compressor and turns into the superheated vapor with high temperature of T_2. Then, it enters the condenser coil to exchange heat with ambient air, turns into the saturated liquid at temperature T_3, and heats air to temperature of $T_{out-air_{cond}}$. After passing an expansion valve, its pressure and temperature drop. Three control volumes I, II, and III are then repeated again. Hourly value of electricity consumption of compressor, P_{comp}, is computed from entropy, energy, and exergy balance relations (4.15, 4.16, and 4.17).

$$\dot{S}_{gen,cycle} = \frac{\dot{Q}_{cond}}{T_3} - \frac{\dot{Q}_{evap}}{T_1} \tag{4.15}$$

$$P_{comp} = \dot{E}x_c + \dot{E}x_e + \dot{E}x_{D,cycle} \tag{4.16}$$

$$\dot{E}x_{D,cycle} = \dot{S}_{gen,cycle} T_0 \tag{4.17}$$

while

$\dot{S}_{gen,cycle}$ and $\dot{E}x_{D,cycle}$: Entropy produced and exergy destructed in ASHP's cooling cycle, respectively

In this research, total energy procurement cost for summer ice harvesting application should be minimized as Eqs. (4.18) and (4.19):

$$P^t_{grid} = P^t_{comp} + P^t_{in-fan} + P^t_{out-fan} \tag{4.18}$$

$$\text{Objective} = \text{Min} \sum_{t=1}^{24} \lambda_t \times P^t_{grid} \tag{4.19}$$

4.2.2 Information Gap Decision Theory

As mentioned in Chap. 1, IGDT technique can be used for risk-averse and risk-seeker decision-making processes under uncertain operating conditions. It is a risk-assessed decision-making process, which makes some cost-effective and robust decisions against uncertain parameter using two robustness and opportunistic modes. The uncertain parameter of the optimization process can be adverse and causes the higher costs or lower profits or favorable with lower costs and higher profits. In this chapter, it addresses the robustness and opportunistic viewpoints of the optimization problem considering the variable nature of the cooling demand using the following requirements: objective function, performance investigation, and uncertainty analysis.

4.2.2.1 Objective Function

It is assumed that $\dot{Q}^{t}_{evap}$ is an uncertain parameter for cost minimization stated by Eq. (4.19). We consider that α refers to uncertainty variable and changes between 0 and 1 for decision variables $P^{t}_{in-fan}, P^{t}_{out-fan}, P^{t}_{comp}, P^{t}_{grid}$. Objective function, $F\left(P^{t}_{grid}, \dot{Q}^{t}_{evap}\right)$, which indicates total electricity cost in a 24-h study horizon, should be minimized. It evaluates all responses to choices of decision-maker, $P^{t}_{in-fan}, P^{t}_{out-fan}, P^{t}_{comp}, P^{t}_{grid}$, and variable parameter, $\dot{Q}^{t}_{evap}$.

4.2.2.2 Implementation Requirement

In this subsection, expectations of system operator from objective function are stated in terms of total cost and assessed by robustness and opportunity modes as Eqs. (4.20) and (4.21), respectively. According to relation (4.20), optimization problem is solved in robustness mode with maximum value of uncertainty variable, α, in a way that total cost cannot exceed from target cost, F_k. Therefore, uncertainty variable, α, should be maximized as Eq. (4.22), in which F_k refers to a predefined target cost in robustness mode. By considering $\widehat{\alpha}\left(P^{t}_{grid}, F_k\right)$, system operator makes a robust decision with less sensitivity to variations of uncertain parameter, $\dot{Q}^{t}_{evap}$, so that total cost is smaller than predefined target cost F_k.

$$\alpha = \text{Max } \alpha \text{ so that max cost is smaller than given target cost} \tag{4.20}$$

$$\beta = \text{Min } \beta \text{ so that min cost is smaller than given target cost} \tag{4.21}$$

$$\widehat{\alpha}\left(P^{t}_{grid}, F_k\right) = \text{Max } \alpha \left\{\text{Max } F\left(P^{t}_{grid}, \dot{Q}^{t}_{evap}\right) \leq F_k\right\} \tag{4.22}$$

A risk-taker decision-maker desires lower cost via implementation of opportunity function. As formulated in Eq. (4.23), variable β refers to minimum level of α aiming to pay lower cost as a result of decision variables, $P^t_{in-fan}, P^t_{out-fan}, P^t_{comp}, P^t_{grid}$. Note that F_w represents maximum cost in opportunity mode that is defined by decision-maker to pay less under favorable deviations of uncertain parameter, $\dot{Q}^{\,t}_{evap}$, and is generally smaller than F_w.

$$\widehat{\beta}\left(P^t_{grid}, F_w\right) = \text{Min}\ \alpha \left\{\text{Min}\ F\left(P^t_{grid}, \dot{Q}^t_{evap}\right) \le F_w\right\} \tag{4.23}$$

4.2.2.3 Uncertainty Formulation

For robust and opportunistic optimization processes, actual value of uncertain parameter can be calculated from fractional error information gap model as Eq. (4.24), where $\dot{Q}^{\,t}_{evap}$ and $\tilde{\dot{Q}}^{\,t}_{evap}$ refer to forecasted and actual cooling load, respectively.

$$U\left(\alpha, \tilde{\dot{Q}}^t_{evap}\right) = \left\{\frac{\dot{Q}^{\,t}_{evap} - \tilde{\dot{Q}}^{\,t}_{evap}}{\tilde{\dot{Q}}^{\,t}_{evap}} \le \alpha\right\}; \alpha \ge 0, \forall t \tag{4.24}$$

4.2.2.4 Implementing Risk-Aversion and Robust Decision-Making Strategy

The robustness variable, $\widehat{\alpha}\left(P^t_{grid}, F_k\right)$, operates as a risk-aversion tool and indicates the greatest amount of the uncertainty variable, α, while the maximum cost is lower than the target value, F_k. Hence, a high value of $\widehat{\alpha}\left(P^t_{grid}, F_k\right)$ corresponds to the higher cost, F_k, which indicates that this decision is robust. Hence, it is expected that $\widehat{\alpha}\left(P^t_{grid}, F_k\right)$ increases with the increase of F_k in cost minimization problem. The uncertain parameter can be stated as Eq. (4.25). Positive sign is used because the increasing rate of $\dot{Q}^{\,t}_{evap}$ causes the increase in cost objective function. According to Eq. (4.26), objective is maximization of α for a given maximum cost, F_k.

$$\dot{Q}^{\,t}_{evap} = \tilde{\dot{Q}}^{\,t}_{evap}(1+\alpha); \forall t = 1, 2, \ldots, T \tag{4.25}$$

$$\widehat{\alpha}\left(P^t_{in-fan}, P^t_{out-fan}, P^t_{comp}, P^t_{grid}, F_k\right) = \text{Max}\ \alpha \left\{\text{Max}\ F\left(P^t_{grid}, \dot{Q}^t_{evap}\right) \le F_k\right\} \tag{4.26}$$

4.2.2.5 Implementing Risk-Seeker and Opportunistic Design-Making Strategy

The opportunity function, $\widehat{\beta}\left(P^t_{grid}, F_w\right)$, assesses the feasibility of the low costs. Therefore, a small value of $\widehat{\beta}\left(P^t_{grid}, F_w\right)$ is desired. According to Eq. (4.27), the opportunity variable is the least amount of α for minimization of total cost as low as F_w. Therefore, it is expected that $\widehat{\beta}\left(P^t_{grid}, F_w\right)$ increases with reduction of F_w for cost minimization approach as Eqs. (4.27, 4.28, and 4.29). The decreasing rate of $\dot{Q}^{\,t}_{evap}$ causes a decrease in cost objective function. Hence, the negative sign is considered in Eq. (4.28).

$$\widehat{\beta}\left(P^t_{grid}, F_w\right) = Min\ \widehat{\alpha}\left(P^t_{grid}, F_w\right) \tag{4.27}$$

$$\dot{Q}^{\,t}_{evap} = \tilde{\dot{Q}}^{\,t}_{evap}(1-\alpha); \forall t = 1, 2, \ldots, T \tag{4.28}$$

$$\widehat{\beta}\left(P^t_{in-fan}, P^t_{out-fan}, P^t_{comp}, P^t_{grid}, F_w\right) = \mathrm{Min}\ \alpha\left\{\mathrm{Min}\, F\left(P^t_{grid}, \dot{Q}^t_{evap}\right) \le F_w\right\} \tag{4.29}$$

4.3 Simulation Result and Discussions

In this study, a benchmark residential building which comprises of 10 floors and 20 flats [21] in a tropical region such as Ahwaz, Iran, with extremely hot summer days and ambient temperature range of $26^{\circ}\mathrm{C} < T_{amb} < 43^{\circ}\mathrm{C}$ is studied. Moreover, generalized algebraic mathematical modeling system (GAMS) [22] is used to solve the optimization problem (4.1–4.29). To reveal the applicability of the IGDT-based ice harvesting strategy in making the risk-aversion and risk-taker decisions, two cases are studied as follows:

Case 1: Ice making system without IGDT
Case 2: Ice making cycle with risk-averse and risk-seeker decisions using IGDT

4.3.1 Ice Making System Without IGDT

Hourly changes of indoor and outside air temperatures, building cooling demand, and electricity tariffs [21] are considered as shown in Figs. 4.2, 4.3, and 4.4, respectively. Other technical characteristics of ice storage system [23] are given in Table 4.1. In addition, air mass flow rate and its specific heat capacity are considered 0.01 [kg/s] and 1.15 [kJ/kgK], respectively. Daily electricity cost of ICTES equals to 16.8 $. Hourly electricity requirement of compressor, fans, and ICTES for making

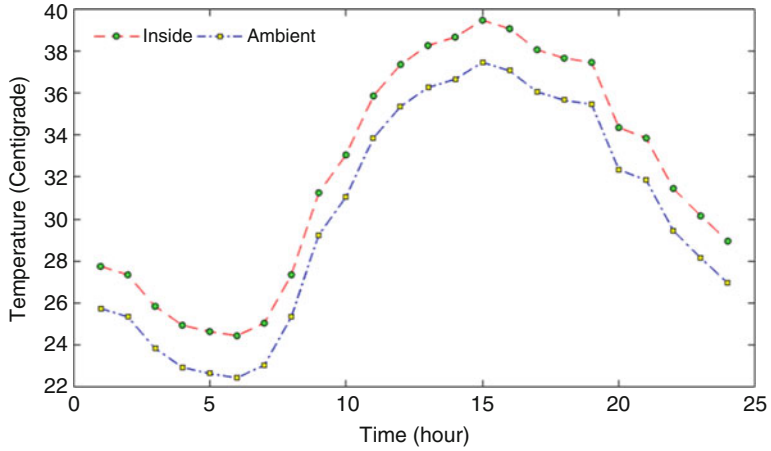

Fig. 4.2 Hourly changes of ambient and indoor air temperatures over a 24-h time horizon

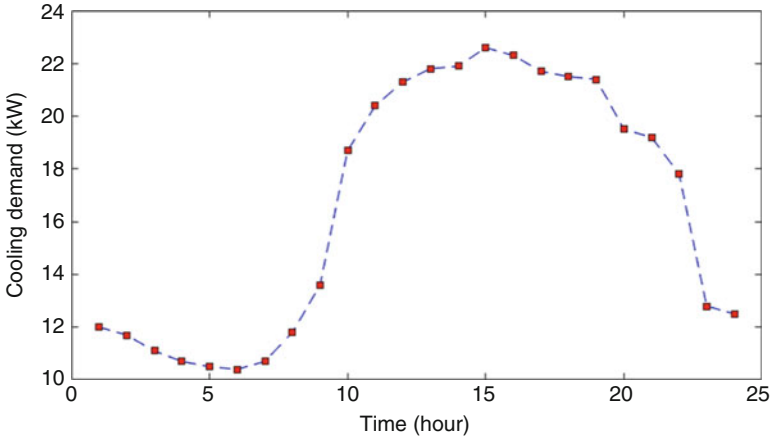

Fig. 4.3 Daily cooling demand

ice is shown in Fig. 4.5. As obvious from Figs. 4.3 and 4.5, ICTES consumes more electricity when building cooling demand increases and vice versa. In other words, with increasing rate of building space-cooling load, R134a absorbs more heating flux from indoor air and delivers it to ambient resulting in larger power consumption of ASHP. Mass flow rate of working fluid through evaporator, compressor, condenser, and expansion valve has been shown in Fig. 4.6. According to this figure, when the building cooling load, $\dot{Q}_{evap}$, increases, the quantity of the mass flow rate of refrigerant, $\dot{m}_4$, will increase, as expected from Eq. (4.2). Increasing rate of building cooling load, $\dot{Q}_{evap}$, causes an increase in electrical power consumption of inside fan, as stated in Eq. (4.1) and shown in Figs. 4.3 and 4.5. Moreover, with increment of

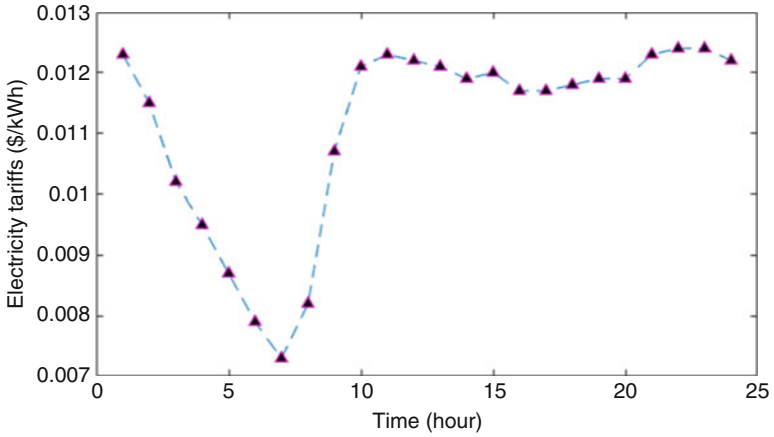

Fig. 4.4 Daily changes of energy prices

Table 4.1 Technical characteristics of ice making system

Points	Temperature (°C)	Enthalpy (kJ/kg)	Pressure (kPa)
1	10	256.2	414.9
2	115	311.9	3818.1
3	98	216.2	3818.1
4	10	216.2	414.9

cooling demand, temperature of $T_{out-air_{cond}}$ will be increased because of higher heating flow from inside air to R134a and then from superheated vapor to ambient air. Therefore, $\dot{E}x_{out-air_{cond}}$ will increase due to increasing value of heated ambient air temperature. This leads the electrical power requirement of condenser fan, $P_{out\ -\ fan}$, to increase, as expected from Eqs. (4.9, 4.10, 4.11, 4.12, 4.13, and 4.14). As formulated in Eqs. (4.5) and (4.12), $\dot{E}x_e$ and $\dot{E}x_c$ will increase after rising of cooling demand, $\dot{Q}_{evap}$, and transferred heat from superheated vapor to ambient air, $\dot{Q}_{cond}$, respectively. Hence, entropy produced, $\dot{S}_{gen,cycle}$, and exergy destructed, $\dot{E}x_{D,cycle}$, in ASHP's cooling cycle will increase based on Eqs. (4.15) and (4.17), respectively. With respect to mentioned analyses, electricity consumption of compressor, P_{comp}, will increase with increasing of $\dot{E}x_e$, $\dot{E}x_c$, and $\dot{E}x_{D,cycle}$, as indicated in Eq. (4.16).

4.3.2 Ice Making Cycle with Risk-Averse and Risk-Seeker Decisions Using IGDT

In this section, IGDT strategy is implemented on short-term scheduling of ice-cold thermal energy storage in order to model variations of building cooling demand in summer season. As mentioned, its robustness mode will be beneficial for a harmful

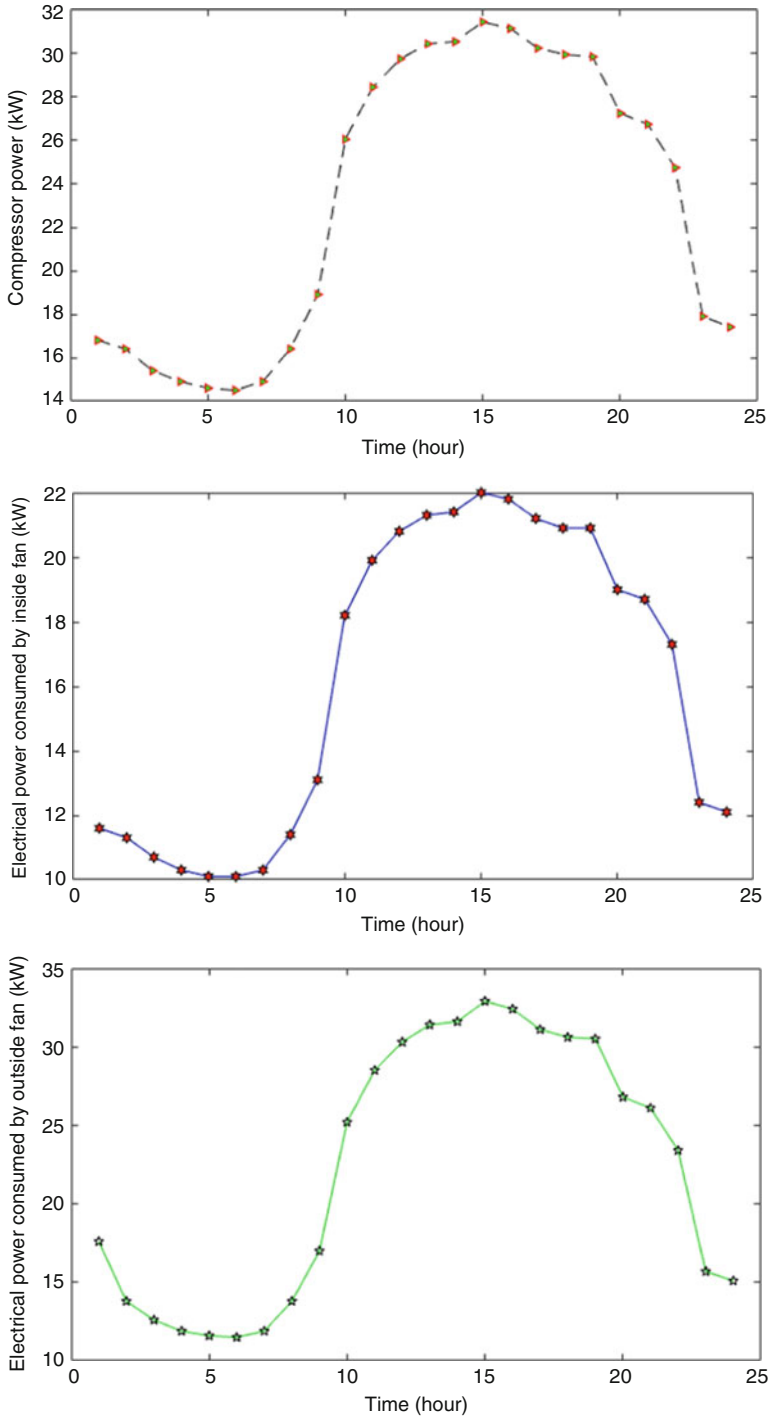

Fig. 4.5 Power consumption of air conditioning system

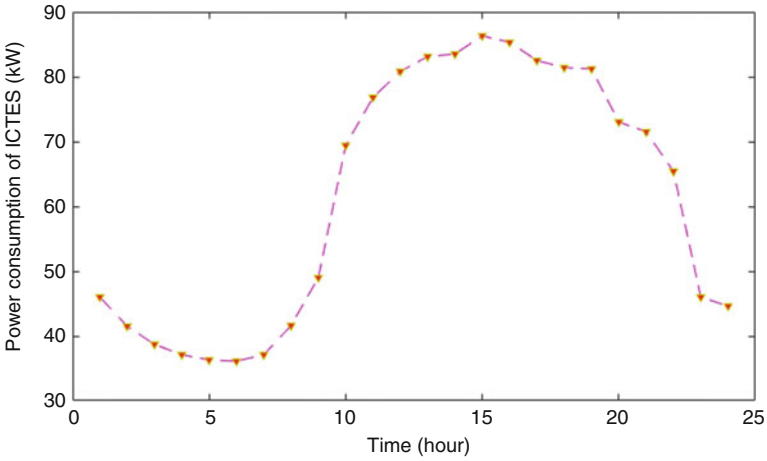

Fig. 4.5 (continued)

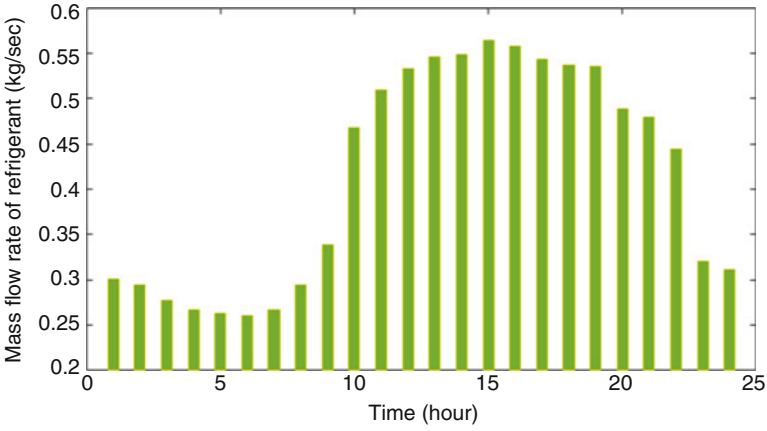

Fig. 4.6 Mass flow rate of refrigerant through evaporator, compressor, condenser, and expander

Table 4.2 Robustness function for different daily electricity costs

k	$\widehat{\alpha}\left(P^{t}_{grid}, F_k\right)$	$F_k(\$)$
1	0	16.9
2	0.09	18.5
3	0.319	22.6
4	0.565	27

Table 4.3 Opportunity function for various daily energy costs

w	$\widehat{\beta}\left(P_{grid}^{t}, F_w\right)$	$F_w(\$)$
1	0	16.9
2	0.357	10.5
3	0.464	8.6
4	0.610	6

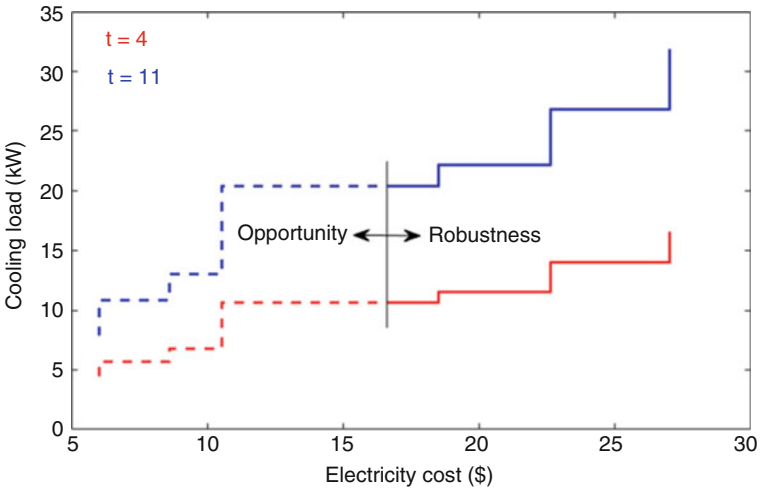

Fig. 4.7 Optimum schedules of ICTES for hours 4 and 11

face of uncertainty or risk-aversion decision-making process, which addresses the highest level of the cooling load uncertainty in a way that total energy cost will be smaller than target cost, F_k. Variations of robustness function, $\widehat{\alpha}\left(P_{grid}^{t}, F_k\right)$, in terms of various daily electricity cost, F_k, is shown in Table 4.2. As expected, it is obvious that the robustness factor, $\widehat{\alpha}\left(P_{grid}^{t}, F_k\right)$, increases as the target cost, F_k, increases. Therefore, if the building owner makes a risk-averse decision or desires the higher robustness against the cooling load uncertainty, more energy cost should be paid and vice versa; as he desires less robust cost, its decision will be less robust against the uncertainty of the cooling demand. Simulation results related to IGDT's opportunity mode are cost-effective in day-ahead scheduling of ice-cold thermal energy storage when the building owner desires to make a risk-seeker decision, which addresses the lower cooling demand values and lower electricity purchasing costs. Table 4.3 indicates the opportunity function, $\widehat{\beta}\left(P_{grid}^{t}, F_w\right)$, versus the target electricity purchasing cost, F_w. As expected, it is obvious that the opportunity factor, $\widehat{\beta}\left(P_{grid}^{t}, F_w\right)$, increases as the target cost, F_w, increases while decreasing the energy production cost. Therefore, if the building owner makes a risk-seeker decision or desires the higher opportunity against the cooling load uncertainty, less energy cost should be

Table 4.4 Calculation times with and without implementation of IGDT

Case study	Time (seconds)
Without IGDT	≈1
Robustness mode of IGDT approach with 4 iterations	1.734
Opportunistic aspect of IGDT with 4 iterations	1.651

paid and vice versa. Hourly ice-making schedules of ICTES for two operating time intervals $t = 4$ and $t = 11$ are illustrated in Fig. 4.7. The horizontal axis of this figure shows the energy purchasing cost of the proposed ice harvesting system, while the vertical one represents the value of the uncertain cooling load. The left side of each curve, which is shown with dashed line, indicates that if the building owner reduces its cooling load, the value of the electricity consumptions of compressor, inside and outside fans will be reduced causing a decrease in the energy procurement cost. The right side of this figure shows that if the cooling demand of the building increases, three components of ICTES including compressor, evaporator, and condenser fans will consume more electricity to satisfy this increased demand, and hourly energy cost of ice storage unit will then increase. In other words, Fig. 4.7 presents both robustness (risk aversion) and opportunistic (risk taker) aspects of ice making strategy.

Optimization problem is solved under GAMS software on a Lenovo with 4 GB RAM and 2.10 GHz CPU. Simulation runtime in two case studies with and without application of IGDT method in ice harvesting strategy is reported in Table 4.4. Calculation times proved that IGDT-based risk assessment ice-cold thermal energy storage methodology is a computationally friendly approach in finding its optimal operating points under different climatic condition and variable cooling demand.

4.4 Concluding Remarks

In this chapter, an air source heat pump-based ice-cold thermal energy storage was proposed and mathematically modeled for application in large-scale residential buildings located at Southern Iran. In the ice making cycle, the heating flow was absorbed by a working refrigerant such as R134a in the evaporation process and chilled the indoor air to temperature of −8 centigrade. The cooled air, which was extracted from the evaporator heat exchanger, was employed for converting water into ice. Meanwhile, the saturated vapor changed into the superheated vapor by compressor. Afterward, the superheated vapor exchanged heat with the ambient air and became the saturated liquid. After passing the saturated liquid through the expansion stage, the primary liquid refrigerant will be produced for repeating cycle. To show the robustness and applicability of the proposed system, a severe hot summer day was considered and a benchmark residential tower with 10 floors and 20 flats was used for simulations. A wide range of ambient and inside air

temperature from 22°C to 40°C were supposed for the worst-case analysis. It is obvious that when building cooling requirement increases, mass flow rate of refrigerant, compressor power, and electrical power consumptions of fans will increase and vice versa. Moreover, information gap decision theory was used to model the uncertainties associated with the building cooling demand. As discussed, IGDT approach enables the building owner to make the risk-averse and risk-seeker decisions for overestimated and underestimated cooling demand, respectively.

References

1. Jabari, F., Mohammadi-Ivatloo, B., Li, G., & Mehrjerdi, H. (2018). Design and performance investigation of a novel absorption ice-making system using waste heat recovery from flue gases of air to air heat pump. *Applied Thermal Engineering, 130*, 782–792.
2. Su, B., Han, W., & Jin, H. (2017). An innovative solar-powered absorption refrigeration system combined with liquid desiccant dehumidification for cooling and water. *Energy Conversion and Management, 153*(Supplement C), 515–525.
3. Ali, S. M., Chakraborty, A., & Leong, K. C. (2017). CO2-assisted compression-adsorption hybrid for cooling and desalination. *Energy Conversion and Management, 143*(Supplement C), 538–552.
4. Hogerwaard, J., Dincer, I., & Naterer, G. F. (2017). Solar energy based integrated system for power generation, refrigeration and desalination. *Applied Thermal Engineering, 121*(Supplement C), 1059–1069.
5. Wang, J., Lu, Y., Yang, Y., & Mao, T. (2016). Thermodynamic performance analysis and optimization of a solar-assisted combined cooling, heating and power system. *Energy, 115*(Part 1), 49–59.
6. Ozcan, H., & Akyavuz, U. D. (2017). Thermodynamic and economic assessment of off-grid portable cooling systems with energy storage for emergency areas. *Applied Thermal Engineering, 119*, 108–118.
7. Fong, K. F., Lee, C. K., & Zhao, T. F. (2017). Effective design and operation strategy of renewable cooling and heating system for building application in hot-humid climate. *Solar Energy, 143*, 1–9.
8. Yan, C., Shi, W., Li, X., & Zhao, Y. (2016). Optimal design and application of a compound cold storage system combining seasonal ice storage and chilled water storage. *Applied Energy, 171*, 1–11.
9. Sehar, F., Pipattanasomporn, M., & Rahman, S. (2018). Coordinated control of building loads, PVs and ice storage to absorb PEV penetrations. *International Journal of Electrical Power & Energy Systems, 95*, 394–404.
10. Song, X., Liu, L., Zhu, T., Chen, S., & Cao, Z. (2018). Study of economic feasibility of a compound cool thermal storage system combining chilled water storage and ice storage. *Applied Thermal Engineering, 133*, 613–621.
11. Carbonell, D., Philippen, D., Haller, M. Y., & Brunold, S. (2016). Modeling of an ice storage buried in the ground for solar heating applications. Validations with one year of monitored data from a pilot plant. *Solar Energy, 125*, 398–414.
12. Mammoli, A., & Robinson, M. (2018). Numerical analysis of heat transfer processes in a low-cost, high-performance ice storage device for residential applications. *Applied Thermal Engineering, 128*, 453–463.
13. Ruan, Y., Liu, Q., Li, Z., & Wu, J. (2016). Optimization and analysis of building combined cooling, heating and power (BCHP) plants with chilled ice thermal storage system. *Applied Energy, 179*, 738–754.

14. Gholamian, E., Zare, V., & Mousavi, S. M. (2016). Integration of biomass gasification with a solid oxide fuel cell in a combined cooling, heating and power system: A thermodynamic and environmental analysis. *International Journal of Hydrogen Energy, 41*(44), 20396–20406.
15. Jabari, F., Mohammadi-Ivatloo, B., & Rasouli, M. (2017). Optimal planning of a micro-combined cooling, heating and power system using air-source heat pumps for residential buildings. In *Energy harvesting and energy efficiency* (pp. 423–455). Cham: Springer.
16. Jabari, F., Nojavan, S., & Mohammadi-Ivatloo, B. (2016). Designing and optimizing a novel advanced adiabatic compressed air energy storage and air source heat pump based μ-combined cooling, heating and power system. *Energy, 116*, 64–77.
17. Jabari, F., Nojavan, S., Mohammadi-Ivatloo, B., & Sharifian, M. B. (2016). Optimal short-term scheduling of a novel tri-generation system in the presence of demand response programs and battery storage system. *Energy Conversion and Management, 122*, 95–108.
18. Pandey, S., Hindoliya, D. A., & Mod, R. (2012). Artificial neural networks for predicting indoor temperature using roof passive cooling techniques in buildings in different climatic conditions. *Applied Soft Computing, 12*(3), 1214–1226.
19. Kiran, T. R., & Rajput, S. P. S. (2011). An effectiveness model for an indirect evaporative cooling (IEC) system: Comparison of artificial neural networks (ANN), adaptive neuro-fuzzy inference system (ANFIS) and fuzzy inference system (FIS) approach. *Applied Soft Computing, 11*(4), 3525–3533.
20. Ghaebi, H., Parikhani, T., Rostamzadeh, H., & Farhang, B. (2018). Proposal and assessment of a novel geothermal combined cooling and power cycle based on Kalina and ejector refrigeration cycles. *Applied Thermal Engineering, 130*, 767–781.
21. Karami, R., & Sayyaadi, H. (2015). Optimal sizing of Stirling-CCHP systems for residential buildings at diverse climatic conditions. *Applied Thermal Engineering, 89*, 377–393.
22. https://www.gams.com/
23. Jiang, Q., & Wen, Z. (2011). Fundamentals of thermodynamics. In *Thermodynamics of materials* (pp. 1–35). Berlin, Heidelberg: Springer.

Chapter 5
Robust Unit Commitment Using Information Gap Decision Theory

Farkhondeh Jabari, Sayyad Nojavan, Behnam Mohammadi-ivatloo, Hadi Ghaebi, and Mohammad-Bagher Bannae-Sharifian

Nomenclature

Sets	
t	Operating time interval
i	Thermal generation unit
k	Regions in linearized fuel cost model
Variables	
λ_t	Electricity selling price
$P_{i,t}$	Output power of thermal unit i at time t
$FC_{i,t}$	Fuel cost of thermal unit i at time t
$STC_{i,t}$	Start-up cost of thermal unit i at time t
$SDC_{i,t}$	Shutdown cost of thermal unit i at time t
$u_{i,t}$	Binary variable that shows on-off status of unit i at time t
$P_i^{\max}$, $P_i^{\min}$	Maximum and minimum outputs of unit i
$\underline{P}_{i,t}$, $\bar{P}_{i,t}$	Minimum and maximum time-dependent operating limits of unit i
UT_i	Minimum uptime of thermal unit i
DT_i	Minimum downtime of unit i
$y_{i,t}$, $z_{i,t}$	Start-up and shutdown statuses of thermal unit i at time t
a_i,b_i,c_i	Fuel cost coefficients of thermal unit i
$C_{i,ini}^k$	Initial power output of unit i in region k

(continued)

F. Jabari (✉) · B. Mohammadi-ivatloo · M.-B. Bannae-Sharifian
Faculty of Electrical and Computer Engineering, University of Tabriz, Tabriz, Iran
e-mail: f.jabari@tabrizu.ac.ir; bmohammadi@tabrizu.ac.ir; sharifian@tabrizu.ac.ir

S. Nojavan
Department of Electrical Engineering, University of Bonab, Bonab, Iran
e-mail: sayyad.nojavan@bonabu.ac.ir

H. Ghaebi
Department of Mechanical Engineering, University of Mohaghegh Ardabili, Ardabil, Iran
e-mail: hghaebi@uma.ac.ir

B. Mohammadi-ivatloo, M. Nazari-Heris (eds.), *Robust Optimal Planning and Operation of Electrical Energy Systems*,
https://doi.org/10.1007/978-3-030-04296-7_5

$C^k_{i,fin}$	Final power output of unit i in region k
ΔP^k_i	Generation interval of unit i in linearized region k
n	Number of linearized regions
s^k_i	Slope of cost-generation curve for unit i in region k
SU_i, SD_i	Limits of start-up and shutdown ramp rates for unit i
$\widehat{\alpha}$	Robust factor
$\widehat{\beta}$	Opportunity factor
U	Fractional error of information gap model
F_w	Target profit of opportunity mode
F_k	Critical profit of robust mode

5.1 Introduction

In recent years, uncertainty of electricity demand and variable nature of renewable energy resources influence on stability and reliability of large-scale power systems. Moreover, air-conditioning systems consume more electricity in different residential, commercial, industrial, and administrative sectors. Hence, on-peak electricity load occurs in summer season and leads to uncertainties of energy market prices and may change optimal generation schedules of thermal power plants. Therefore, modeling of energy price uncertainty is important in economic dispatching of thermal units [1].

Recently, some scholars have focused on robust scheduling of thermal generation units. A robust security-constrained unit commitment (UC) problem is solved in [2] to evaluate impacts of wind production uncertainty in economic operation of conventional generation units. Up and down ramp rates of thermal power plants, demand response programs, energy storage units, and transmission lines switching are used for load-generation balancing in wind product shortage condition. In [3], a robust UC problem is modeled for minimization of generalized social cost in high forecast error of electrical demand and various probability distribution functions. In this study, output power of renewable energy resource-based power plants could also be considered as uncertain parameter in a way that two-stage robust UC problem should be solved using Benders' decomposition method. Three-sigma method-based stochastic UC problem is proposed in [4] to model uncertain wind products in congested transmission grids. Not-supplied electrical load of each bus and transmission line active and reactive power flows are correlated as random variables. In 3σ stochastic UC problem, some scenarios are selected within predefined circular confidence regions to guarantee a certain value of transmission line security against wind shortage. In [5], day-ahead scheduling of hydro-generation units located in a river valley is carried out. Each hydropower plant composes several turbines, and its generation efficiency nonlinearly changes with water flow [6]. In this research, half-hourly generation schedules of hydroturbines are optimally determined under uncertainties of electrical demand. In [7], a bi-level UC problem consisting of inner bilinear program and outer mixed-integer problem is presented for wind availability

analysis. In [8], optimization of hydroelectric-solar photovoltaic hybrid UC problem is developed based on cuckoo search algorithm aiming to minimize value of not-supplied demand, which resulted from insufficient solar radiations and power at cloudy sky and night. In [9], joint energy and reserve market is cleared by solving a robust unit commitment problem using information gap decision theory (IGDT). In this research, IGDT is applied on flexible loads to model their uncertain responses in offering consumption reduction capacities against hourly prices for participation in reserve markets. Soroudi et al. [10] implemented IGDT on wind-thermal UC problem in two case studies without and with application of demand-side management strategies. Authors of [11] considered dynamic line rating index in stochastic UC problem to reduce transmission overloading probability. In [12], economic and environmental benefits of demand response programs and pumped hydro-storage units, which are optimally scheduled for balancing wind power uncertainties, are proved in probabilistic UC problem. Variations of output power of renewable energy resources in economic and environmental dispatch of thermal unit plug-in electric vehicles, demand response programs, and compressed air energy storages are analyzed in [13]. Lexicographic optimization method is integrated with augmented-weighted ε-constraint algorithm to find Pareto frontiers. Availability of natural gas as uncertain parameter is considered in [14] for optimization of security-constrained UC problem using fuzzy logic. Genetic algorithm is also used for load-flow analysis in natural gas transmission system. Quantum-inspired binary gravitational search algorithm is used in [15] for probabilistic dispatch of wind-thermal units considering a chance-constrained programming model and budget of wind production uncertainty. Authors of [16] use conditional value-at-risk (CVaR) tool to model fluctuations of wind and solar generations in stochastic UC problem without and with application of demand response and energy storage. In [17], Benders' decomposition technique-based UC problem is solved to maximize social welfare under worst-case wind power scenario and demand-side management strategy. In robust model, a linearized price elastic load curve is used for modeling all possible responses of consumers to price elasticity. Nwulu and Xia [18] integrated a game theory-based demand response programming strategy with dynamic economic environmental dispatch problem to obtain optimal hourly incentives for participants in load curtailment programs. In [19], day-ahead stochastic self-scheduling of hydrothermal units is implemented to maximize daily profit in a joint energy and reserve market using a mixed-integer linear programming model. Roulette wheel mechanism combined with lattice Monte Carlo simulation is applied on energy and spinning reserve prices and forced outage rate of thermal units over a 24-h time horizon. A two-stage robust hydrothermal scheduling problem based on Benders' decomposition technique and a vector autoregressive procedure is solved by Dashti et al. [20] to consider fluctuations of water flow in electricity generation and market-clearing processes.

As reviewed, different methods have been proposed by researchers to model uncertainties associated with demand, renewables, and energy market price. But, IGDT has not been applied on electricity market price to model its fluctuations in UC problem. Therefore, this chapter solves a price-based UC problem without and with application of IGDT to prove its robustness and opportunistic capabilities in profit maximization.

Other sections of this chapter are structured as follows: In Sect. 5.2, a mathematical formulation is presented for IGDT-based UC problem. Illustrative example and discussions are presented in Sect. 5.3. Sect. 5.4 concludes this chapter.

5.2 Proposed Methodology

In this research, UC problem is solved to maximize daily profit of generation companies considering different technical constraints of thermal units such as ramp-up and ramp-down rates, minimum up- and downtimes, generation limits, and fuel cost. Moreover, hourly generation schedules of thermal power plants are optimized under uncertain electricity market prices. In addition, IGDT technique is used for finding robust and opportunistic generation schedules in a way that daily profit in case of "with application of IGDT" is higher than that of "without implementation of IGDT approach." In Sect. 5.2.1, profit-based UC problem is formulated. Then, IGDT models underestimated and overestimated market rates in Sect. 5.2.2 for making risk-averse and risk-seeker decisions via robust and opportunistic modes, respectively.

5.2.1 Unit Commitment Problem

In UC problem, total profit obtained from selling electricity is selected as objective function. According to Eq. (5.1), daily profit is defined as total revenue achieved from exchanging energy with customers minus total fuel cost of thermal power plants. Fuel cost calculations are presented in Eqs. (5.2), (5.3), (5.4), (5.5), (5.6), (5.7), (5.8), (5.9), and (5.10). Minimum and maximum power generation capacities are stated in inequality constraint (5.11). As obvious from Eqs. (5.12) and (5.13), for shutting down of unit i at hour $t+1$, $\bar{P}_{i,t} \leq SD_i z_{i,t+1}$. Since $P_{i,t-1} = 0$, so $P_{i,t} \leq SD_i$. If unit i is on at time t-1 ($u_{i,t-1} = 1$) and is going to be on at time $t+1$, $P_{i,t}$ cannot be increased more than RU_i. In other words, $\bar{P}_{i,t} \leq P_{i,t-1} + RU_i u_{i,t-1}$. If unit i is off at time t-1 ($u_{i,t-1} = 0$) and is turned on at time t ($y_{i,t} = 1$), $P_{i,t}$ cannot be more than SU_i, and we have $\bar{P}_{i,t} \leq SU_i y_{i,t}$. As stated by Eqs. (5.14) and (5.15), if unit i is on at time t, its output power will be more than $P_i^{\min} u_{i,t}$. If it is on at hours t-1 and t, output power of thermal unit i will be more than $P_{i,t-1} - RD_i u_{i,t}$. If thermal power plant i is on at hour t-1 and off at time t, its output at time t-1 will be less than $SD_i z_{i,t}$. As stated by Eqs. (5.16) and (5.17), shutdown and start-up statuses of thermal power plant i at period t are described by binary variables $y_{i,t}$ and $z_{i,t}$, respectively. Minimum uptime (UT_i) of thermal power plant i can be calculated from relations (5.18), (5.19), (5.20), and (5.21). Similarly, minimum downtime (DT_i) of unit i is formulated by Eqs. (5.22), (5.23), (5.24), and (5.25). In this study, start-up ($STC_{i,t}$) and shutdown ($SDC_{i,t}$) costs are considered to be equal to $st_i \times y_{i,t}$ and $sd_i \times z_{i,t}$, respectively.

Profit = Revenue-Cost

$$= \underset{\substack{P_{i,t}^k, u_{i,t} \\ y_{i,t}, z_{i,t}}}{\text{Max}} \sum_{i,t} \left(\underbrace{\lambda_t P_{i,t}}_{\text{Revenue}} - \underbrace{(FC_{i,t} + STC_{i,t} + SDC_{i,t})}_{\text{Cost}} \right) \tag{5.1}$$

Subjecting to:

$$0 \le P_{i,t}^k \le \Delta P_i^k u_{i,t}, \ \ \forall k = 1:n \tag{5.2}$$

$$\Delta P_i^k = \frac{P_i^{\max} - P_i^{\min}}{n} \tag{5.3}$$

$$P_{i,ini}^k = (k-1)\Delta P_i^k + P_i^{\min} \tag{5.4}$$

$$P_{i,fin}^k = \Delta P_i^k + P_{i,ini}^k \tag{5.5}$$

$$P_{i,t} = P_i^{\min} u_{i,t} + \sum_k P_{i,t}^k \tag{5.6}$$

$$C_{i,ini}^k = a_i \left(P_{i,ini}^k\right)^2 + b_i P_{i,ini}^k + c_i \tag{5.7}$$

$$C_{i,fin}^k = a_i \left(P_{i,fin}^k\right)^2 + b_i P_{i,fin}^k + c_i \tag{5.8}$$

$$s_i^k = \frac{C_{i,fin}^k - C_{i,ini}^k}{\Delta P_i^k} \tag{5.9}$$

$$FC_{i,t} = a_i \left(P_i^{\min}\right)^2 + b_i P_i^{\min} + c_i u_{i,t} + \sum_k s_i^k P_{i,t}^k \tag{5.10}$$

$$\underline{P}_{i,t} \le P_{i,t} \le \bar{P}_{i,t} \tag{5.11}$$

$$\bar{P}_{i,t} \le P_i^{\max}[u_{i,t} - z_{i,t+1}] + SD_i z_{i,t+1} \tag{5.12}$$

$$\bar{P}_{i,t} \le P_{i,t-1} + RU_i u_{i,t-1} + SU_i y_{i,t} \tag{5.13}$$

$$\underline{P}_{i,t} \ge P_i^{\min} u_{i,t} \tag{5.14}$$

$$\underline{P}_{i,t} \ge P_{i,t-1} - RD_i u_{i,t} - SD_i z_{i,t} \tag{5.15}$$

$$y_{i,t} - z_{i,t} = u_{i,t} - u_{i,t-1} \tag{5.16}$$

$$y_{i,t} + z_{i,t} \le 1 \tag{5.17}$$

$$\sum_{t=1}^{\zeta_i} 1 - u_{i,t} = 0 \tag{5.18}$$

$$\sum_{t=k}^{k+UT_i-1} u_{i,t} \geq UT_i y_{i,k} \forall k = \zeta_i + 1, \ldots, T - UT_i + 1 \tag{5.19}$$

$$\sum_{t=k}^{T} u_{i,t} - y_{i,t} \geq 0 \quad \forall k = T - UT_i + 2, \ldots, T \tag{5.20}$$

$$\zeta_i = \min\left\{T, \left(UT_i - U_i^0\right) u_{i,t=0}\right\} \tag{5.21}$$

$$\sum_{t=1}^{\xi_i} u_{i,t} = 0 \tag{5.22}$$

$$\sum_{t=k}^{k+DT_i-1} 1 - u_{i,t} \geq DT_i z_{i,k} \forall k = \xi_i + 1, \ldots, T - DT_i + 1 \tag{5.23}$$

$$\sum_{t=k}^{T} 1 - u_{i,t} - z_{i,t} \geq 0 \quad \forall k = T - DT_i + 2, \ldots, T \tag{5.24}$$

$$\xi_i = \min\left\{T, \left(DT_i - S_i^0\right)[1 - u_{i,t=0}]\right\} \tag{5.25}$$

5.2.2 Information Gap Decision Theory

As mentioned in the previous subsection, information gap decision theory is a risk-assessed decision-making process, which makes some cost-effective and robust decisions against uncertain parameter using two robustness and opportunistic modes. The uncertain parameter of the optimization process can be adverse and causes the higher costs or lower profits or favorable with lower costs and higher profits. In other words, it addresses the robustness and the opportunistic viewpoints of the optimization problem considering the variable nature of the uncertain parameter using the following requirements: objective function, performance investigation, and uncertainty analysis [21].

5.2.2.1 Objective Function

It is assumed that λ_t is an uncertain parameter for profit maximization in UC problem at operating time interval t. We consider that α refers to uncertainty variable and changes between 0 and 1 for decision variables $P_{i,t}$,$u_{i,t}$. Objective function, $F(P_{i,t}, u_{i,t}, \lambda_t)$, which indicates total profit in a T-hour study horizon, should be maximized. It evaluates all responses to choices of decision-maker, $P_{i,t}$,$u_{i,t}$, and variable parameter, λ_t.

5.2.2.2 Implementation Requirement

In this subsection, expectations of system operator from objective function are stated in terms of total profit and assessed by robustness and opportunity modes as Eqs. (5.26) and (5.27), respectively. According to relation (5.26), optimization problem is solved in robustness mode with maximum value of uncertainty variable, α, in a way that total profit cannot be lower than critical profit, F_k. Therefore, uncertainty variable, α, should be maximized as Eq. (5.28), in which F_k refers to minimum expected profit in robustness mode. By considering $\widehat{\alpha}(P_{i,t}, u_{i,t}, F_k)$, system operator makes a robust decision with less sensitivity to variations of uncertain parameter, λ_t, so that expected profit is more than critical profit F_k.

$$\alpha = \underset{\alpha}{\text{Max}} \{\text{Minimum profit is higher than given critical profit}\}\{\text{Robustness}\} \quad (5.26)$$

$$\beta = \underset{\beta}{\text{Min}} \{\text{Maximum profit is higher than given target profit}\}\{\text{Opportunity}\} \quad (5.27)$$

$$\widehat{\alpha}(P_{i,t}, u_{i,t}, F_k) = \max_{\alpha} \left\{ \alpha : \max_{P_{i,t},\, u_{i,t}} F(P_{i,t}, u_{i,t}, \lambda_t) \geq F_k \right\} \quad (5.28)$$

A risk-taker decision-maker desires higher profit via implementation of opportunity function. As formulated in Eq. (5.29), variable β refers to minimum level of α aiming to pay lower cost and obtain higher profit as a result of decision variables, $P_{i,t}$,$u_{i,t}$. Note that F_w represents minimum profit in opportunity mode that is defined by decision-maker to pay less and obtain more profit under favorable deviations of uncertain parameter, λ_t, and is generally smaller than F_k.

$$\widehat{\beta}(P_{i,t}, u_{i,t}, F_w) = \min_{\alpha} \left\{ \alpha : \min_{P_{i,t},\, u_{i,t}} F(P_{i,t}, u_{i,t}, \lambda_t) \geq F_w \right\} \quad (5.29)$$

5.2.2.3 Uncertainty Formulation

For robust and opportunistic optimization processes, actual value of uncertain parameter can be calculated from fractional error information gap models as Eq. (5.30) [22]:

$$U\left(\alpha, \tilde{\lambda}_t\right) = \left\{ \lambda_t : \left| \frac{\lambda_t - \tilde{\lambda}_t}{\tilde{\lambda}_t} \right| \leq \alpha \right\}; \quad \alpha \geq 0, \quad \forall t \quad (5.30)$$

5.2.2.4 Implementing Risk-Aversion and Robust Decision-Making Strategy

In robustness mode, $\widehat{\alpha}(P_{i,t}, u_{i,t}, F_k)$ operates as a risk-aversion tool and indicates a great amount of uncertainty variable, α, while minimum value of profit is higher than target value, F_k. Hence, a high value of $\widehat{\alpha}(P_{i,t}, u_{i,t}, F_k)$ corresponds to lower profit, F_k, indicating that this decision is robust. Hence, it is expected that $\widehat{\alpha}(P_{i,t}, u_{i,t}, F_k)$ decreases with increase of F_k for maximization of expected profit. Therefore, uncertain parameter can be stated as Eq. (5.31). Negative sign is considered because decreasing rate of λ_t leads to a decrease in profit objective function. According to Eq. (5.32), objectives are maximization of α for a minimum expected profit, F_k.

$$\lambda_t = \tilde{\lambda}_t - \alpha\tilde{\lambda}_t, \ \forall t = 1, 2, \ldots, T \tag{5.31}$$

$$\widehat{\alpha}\left(\tilde{P}_{i,t}, F_k\right) = \underset{\alpha}{\text{Max}}\left\{\alpha : \sum_{t=1}^{T}\left(\tilde{\lambda}_t(1-\alpha)\tilde{P}_{i,t} - FC_{i,t} - STC_{i,t} - SDC_{i,t}\right) \geq F_k\right\} \tag{5.32}$$

5.2.2.5 Implementing Risk-Seeker and Opportunistic Design-Making Strategy

In opportunity mode, a small value of $\widehat{\beta}(P_{i,t}, u_{i,t}, F_w)$ is desired. According to Eq. (5.33), opportunity variable is minimum amount of α for maximization of expected profit as high as target profit, F_w. Therefore, it is expected that $\widehat{\beta}(P_{i,t}, u_{i,t}, F_w)$ increases with increase of F_w for profit maximization problem as Eqs. (5.34) and (5.35). Increasing rate of λ_t leads to an increase in profit objective function. Hence, positive sign is used in Eq. (5.34).

$$\widehat{\beta}(P_{i,t}, u_{i,t}, F_w) = \underset{P_{i,t}, u_{i,t}}{\text{Min}}\ \widehat{\alpha}(P_{i,t}, u_{i,t}, F_w) \tag{5.33}$$

$$\lambda_t = \widetilde{\lambda}_t + \alpha\widetilde{\lambda}_t, \forall t = 1, 2, \ldots, T \tag{5.34}$$

$$\widehat{\beta}\left(\tilde{P}_{i,t}, F_w\right) = \underset{\alpha}{\text{Min}}\left\{\alpha : \sum_{t=1}^{T}\left(\tilde{\lambda}_t(1+\alpha)\tilde{P}_{i,t} - FC_{i,t} - STC_{i,t} - SDC_{i,t}\right) \geq F_w\right\} \tag{5.35}$$

5.3 Case Study and Discussions

In this section, a benchmark power system with ten thermal power plants [23] is studied in two cases, "Case 1: Price based UC problem without application of IGDT method" and "Case 2: Price based UC problem with implementation of IGDT strategy." All technical specifications of generation units are reported in Table 5.1.

Table 5.1 Operational characteristics of thermal units [23]

i	a_i	b_i	c_i	sd_i	st_i	RU_i	RD_i	UT_i	DT_i	SD_i	SU_i	$P_i^{\min}$	$P_i^{\max}$	U_0	U_{ini}	S_0
1	0.014	12.1	82	42.6	42.6	40	40	3	2	90	110	80	200	1	0	1
2	0.028	12.6	49	50.6	50.6	64	64	4	2	130	140	120	320	2	0	0
3	0.013	13.2	100	57.1	57.1	30	30	3	2	70	80	50	150	3	0	3
4	0.012	13.9	105	47.1	47.9	104	104	5	3	240	250	250	250	1	1	0
5	0.026	13.5	72	56.6	56.9	56	56	4	2	110	130	80	280	1	1	0
6	0.021	15.4	29	141.5	141.5	30	30	3	2	60	80	50	150	0	0	0
7	0.038	14	32	113.5	113.5	24	24	3	2	50	60	30	120	0	1	0
8	0.039	13.5	40	42.6	42.6	22	22	3	2	45	55	30	110	0	0	0
9	0.039	15	25	50.6	50.6	16	16	0	0	35	45	20	80	0	0	0
10	0.051	14.3	15	57.1	57.1	12	12	0	0	30	40	20	60	0	0	0

Table 5.2 Hourly energy market prices [23]

t	Price ($/MWh)	t	Price ($/MWh)
1	26.04	5	32.79
2	26.71	6	36.46
3	30.37	7	25.12
4	34.21	8	24.46

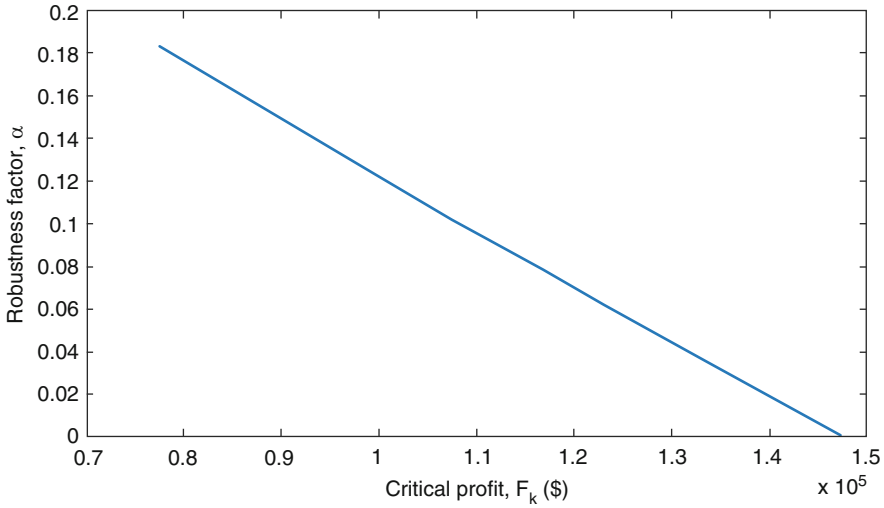

Fig. 5.1 Variations of robustness factor, $\widehat{\alpha}\left(\tilde{P}_{i,t}, F_k\right)$, versus critical profit, F_k

Moreover, hourly electricity market prices over an 8-h study horizon are shown in Table 5.2. Firstly, robustness mode of IGDT is applied on price-based UC problem as formulated in Eqs. (5.1–5.25), (5.31), and (5.32). Maximum values of robustness factor versus different critical profits are shown in Fig. 5.1. As obvious from this figure, $\widehat{\alpha}\left(\tilde{P}_{i,t}, F_k\right)$ decreases with increasing of critical profit, F_k. In robust approach, some target profits are considered to find maximum amounts of robustness factor α so that total profit for 8-h operating period is larger than given critical profit, F_k, as expected from Eq. (5.32). In other words, when hourly energy prices decrease with rate of $1 - \alpha$, total profit cannot be smaller than a given target value, and it will be guaranteed against underestimated electricity rates, $\tilde{\lambda}_t(1-\alpha)$. In addition, IGDT's capability in maximization of profit with underestimated energy prices is revealed by using optimal values of robustness factor α and calculating total profit after solving UC problem with forecasted energy prices, $\tilde{\lambda}_t$. In other words, UC problem is optimized with forecasted values of electricity prices, $\tilde{\lambda}_t$. Then, $\tilde{\lambda}_t(1-\alpha)$ $\forall t = 1, 2, \ldots, T$ is considered as energy prices and used for calculating profit based on generation schedules, $P_{i,t}$, which are obtained from UC problem before implementation of IGDT. Table 5.3 summarizes total profit obtained from solving UC problem with and without application of robust IGDT for various underestimated

Table 5.3 Profit objective function in two cases without and with implementation of robust IGDT

Robustness factor, α	Critical profit, F_k, with application of IGDT	Expected profit without implementation of IGDT
0	147,540	147,540
0.053	126,540	126,399
0.071	119,540	119,220
0.089	112,540	112,040
0.107	105,540	104,860
0.126	98,540	97,282
0.145	91,540	89,703
0.164	84,540	82,125
0.183	77,540	74,546

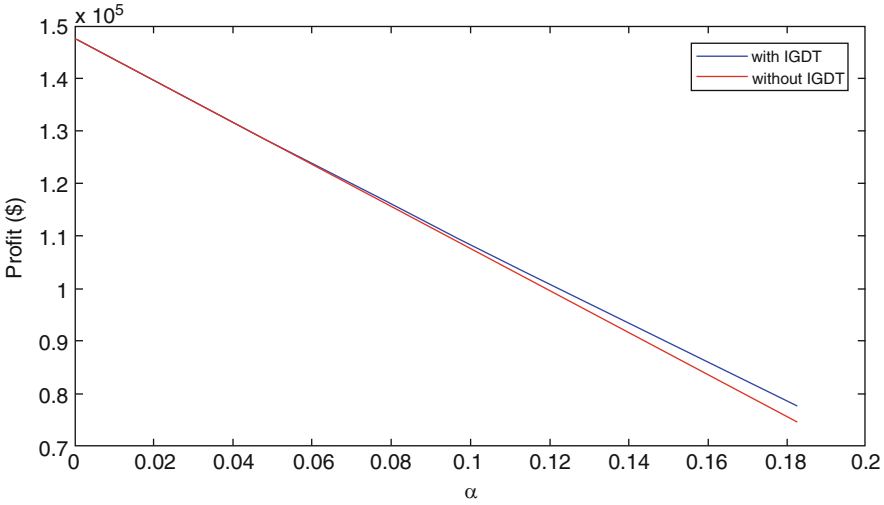

Fig. 5.2 Comparison between two cases "without IGDT" and "with IGDT" from viewpoint of profit for different robustness factor, $\widehat{\alpha}\left(\tilde{P}_{i,t}, F_k\right)$

hourly energy prices. As shown in Fig. 5.2, IGDT-based UC problem, which is shown in blue, has higher profit than that of UC without IGDT strategy, especially when energy prices reduce significantly. This means that optimization process with application of IGDT will be robust for underestimated electricity prices.

Similarly, opportunistic strategy is implemented on price-based UC problem as formulated in Eqs. (5.1–5.25), (5.34), and (5.35). Minimum values of opportunity factor versus different target profits are depicted in Fig. 5.3. As obvious from this figure, $\widehat{\beta}\left(\tilde{P}_{i,t}, F_w\right)$ increases with increasing critical profit, F_w. In opportunity mode, some target profits are considered to find minimum amounts of opportunity factor β so that total profit for 8-h operating period is larger than given target profit, F_w, as expected from Eq. (5.35). In other words, when hourly energy prices increase with

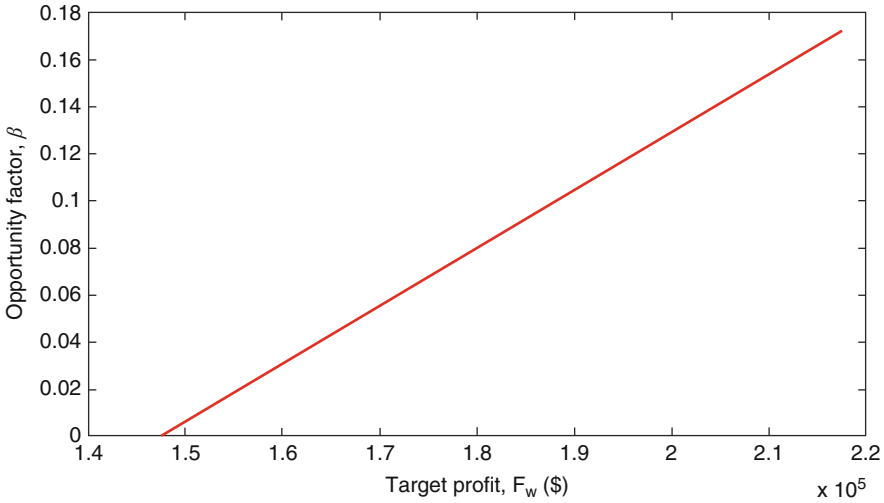

Fig. 5.3 Variations of opportunity factor, $\widehat{\beta}\left(\tilde{P}_{i,t}, F_w\right)$, versus target profit, F_w

Table 5.4 Profit objective function in two cases without and with implementation of opportunistic IGDT strategy

Opportunity factor, $\widehat{\beta}\left(\tilde{P}_{i,t}, F_w\right)$	Target profit, F_w, with application of IGDT	Expected profit without implementation of IGDT
0	147,540	147,540
0.017	154,540	154,320
0.035	161,540	161,500
0.052	168,540	168,281
0.069	175,540	175,062
0.087	182,540	182,241
0.104	189,540	189,022
0.121	196,540	195,803
0.138	203,540	202,584
0.155	210,540	209,364
0.172	217,540	216,145

rate of 1+α, total profit cannot be smaller than a given target value, and it will be maximized for overestimated electricity rates, $\tilde{\lambda}_t(1+\alpha)$, as high as possible. In addition, IGDT's capability in maximization of profit with overestimated energy prices is revealed by using optimal values of opportunity factor β and calculating total profit after solving UC problem with forecasted energy prices, $\tilde{\lambda}_t$. In other words, UC problem is optimized with forecasted values of electricity prices, $\tilde{\lambda}_t$. Then, $\tilde{\lambda}_t(1+\alpha)\forall t = 1, 2, \ldots, T$ is considered as energy prices and used for calculating profit based on generation schedules, $P_{i,t}$, which are obtained from UC problem before implementation of IGDT. Table 5.4 summarizes total profit obtained

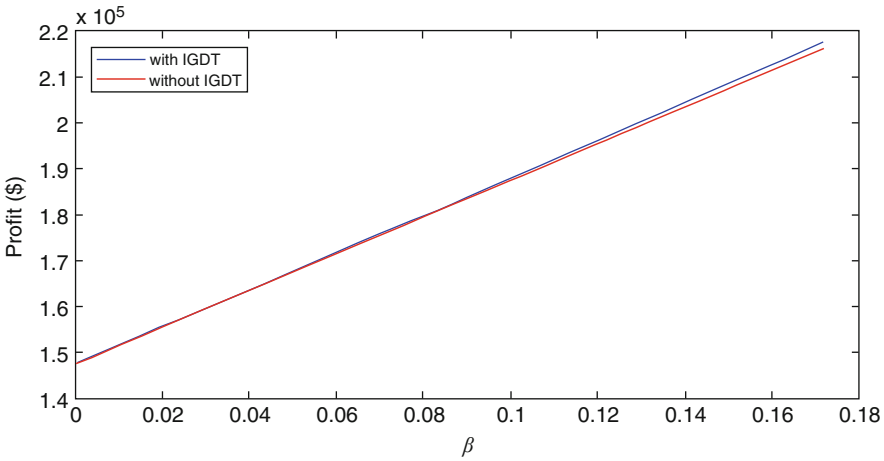

Fig. 5.4 Comparison between two cases "without IGDT" and "with IGDT" from viewpoint of profit for different opportunity factor, $\widehat{\beta}\left(\tilde{P}_{i,t}, F_w\right)$

from solving UC problem with and without application of opportunistic IGDT strategy in various overestimated hourly energy prices. As shown in Fig. 5.4, IGDT-based UC problem, which is shown in blue, has higher profit than that of UC problem without IGDT strategy, especially when energy prices increase significantly. This means that optimization process with application of IGDT is a cost-effective opportunistic strategy for overestimated electricity prices.

5.4 Conclusion and Future Trend

In this chapter, information gap decision theory was implemented on profit maximized unit commitment problem to model uncertain behavior of electricity market prices. Two cases were studied without and with implementation of IGDT. Robustness and opportunity modes of IGDT modeled underestimated and overestimated electricity rates, respectively. It is found that robust UC problem finds good operating points for thermal generation units in a way that total profit will not only be larger than a predefined critical profit but also is more than profit of UC problem, which is solved with same market prices and without application of IGDT strategy. Moreover, opportunity strategy enables market operator to make risk-seeker decisions and maximizes profit for overestimated electricity rates so that it will not only be more than a target profit but also is larger than profit of UC problem, which is solved with same prices and without implementation of IGDT. As a future trend, game theory-integrated IGDT method will be applied on UC problem without and with application of demand response programs to model uncertainties associated with renewable energy resources such as solar and wind farms, market prices, and demands.

References

1. Anand, H., Narang, N., & Dhillon, J. S. (2018). Profit based unit commitment using hybrid optimization technique. *Energy, 148*, 701–715.
2. Nikoobakht, A., & Aghaei, J. (2017). IGDT-based robust optimal utilisation of wind power generation using coordinated flexibility resources. *IET Renewable Power Generation, 11*(2), 264–277.
3. Liu, G., & Tomsovic, K. (2015). Robust unit commitment considering uncertain demand response. *Electric Power Systems Research, 119*, 126–137.
4. Kalantari, A., & Galiana, F. D. (2015). Generalized Sigma approach to unit commitment with uncertain wind power generation. *International Journal of Electrical Power & Energy Systems, 65*, 367–374.
5. Philpott, A. B., Craddock, M., & Waterer, H. (2000). Hydro-electric unit commitment subject to uncertain demand. *European Journal of Operational Research, 125*(2), 410–424.
6. Dal' Santo, T., & Costa, A. S. (2016). Hydroelectric unit commitment for power plants composed of distinct groups of generating units. *Electric Power Systems Research, 137*, 16–25.
7. Morales-España, G., Lorca, Á., & de Weerdt, M. M. (2018). Robust unit commitment with dispatchable wind power. *Electric Power Systems Research, 155*, 58–66.
8. Ming, B., et al. (2018). Robust hydroelectric unit commitment considering integration of large-scale photovoltaic power: A case study in China. *Applied Energy, 228*, 1341–1352.
9. Ghahary, K., et al. (2018). Optimal reserve market clearing considering uncertain demand response using information gap decision theory. *International Journal of Electrical Power & Energy Systems, 101*, 213–222.
10. Soroudi, A., Rabiee, A., & Keane, A. (2017). Information gap decision theory approach to deal with wind power uncertainty in unit commitment. *Electric Power Systems Research, 145*, 137–148.
11. Park, H., Jin, Y. G., & Park, J.-K. (2018). Stochastic security-constrained unit commitment with wind power generation based on dynamic line rating. *International Journal of Electrical Power & Energy Systems, 102*, 211–222.
12. Durga Hari Kiran, B., & Sailaja Kumari, M. (2016). Demand response and pumped hydro storage scheduling for balancing wind power uncertainties: A probabilistic unit commitment approach. *International Journal of Electrical Power & Energy Systems, 81*, 114–122.
13. Soltani, Z., et al. (2018). Integration of smart grid technologies in stochastic multi-objective unit commitment: An economic emission analysis. *International Journal of Electrical Power & Energy Systems, 100*, 565–590.
14. Badakhshan, S., Kazemi, M., & Ehsan, M. (2015). Security constrained unit commitment with flexibility in natural gas transmission delivery. *Journal of Natural Gas Science and Engineering, 27*, 632–640.
15. Ji, B., et al. (2014). Application of quantum-inspired binary gravitational search algorithm for thermal unit commitment with wind power integration. *Energy Conversion and Management, 87*, 589–598.
16. Huang, Y., Zheng, Q. P., & Wang, J. (2014). Two-stage stochastic unit commitment model including non-generation resources with conditional value-at-risk constraints. *Electric Power Systems Research, 116*, 427–438.
17. Zhao, C., et al. (2013). Multi-stage robust unit commitment considering wind and demand response uncertainties. *IEEE Transactions on Power Systems, 28*(3), 2708–2717.
18. Nwulu, N. I., & Xia, X. (2015). Multi-objective dynamic economic emission dispatch of electric power generation integrated with game theory based demand response programs. *Energy Conversion and Management, 89*, 963–974.
19. Esmaeily, A., et al. (2017). Evaluating the effectiveness of mixed-integer linear programming for day-ahead hydro-thermal self-scheduling considering price uncertainty and forced outage rate. *Energy, 122*, 182–193.

20. Dashti, H., et al. (2016). Weekly two-stage robust generation scheduling for hydrothermal power systems. *IEEE Transactions on Power Systems, 31*(6), 4554–4564.
21. Nojavan, S., & Zare, K. (2013). Risk-based optimal bidding strategy of generation company in day-ahead electricity market using information gap decision theory. *International Journal of Electrical Power & Energy Systems, 48*, 83–92.
22. Ben-Haim, Y. (2006). Chapter 2: Uncertainty. In Y. Ben-Haim (Ed.), *Info-gap decision theory* (2nd ed., pp. 9–36). Oxford: Academic.
23. Soroudi, A. (2017). *Power system optimization modeling in GAMS*. Springer. Cham: Switzerland.

Chapter 6
Optimal Robust Scheduling of Renewable Energy-Based Smart Homes Using Information-Gap Decision Theory (IGDT)

Morteza Nazari-Heris, Parinaz Aliasghari, Behnam Mohammadi-ivatloo, and Mehdi Abapour

6.1 Introduction

The development of smart grids in electricity networks is introduced as a novel idea for managing load demand to overcome demand increment and full load conditions, which is defined as demand side management (DSM) technology. Home energy management system (HEMS) has been presented as an inseparable part of the smart grid for application of DSM technology [1, 2]. HEMS can be introduced as one of significant techniques enabling consumers to adjust their electrical energy consumption. In fact, it is not expected from consumers to schedule their demand optimally because they are not neither an economist nor a power network operator. Accordingly, HEMS plays an important role in managing load demand of consumers from on-peak hours to off-peak hours. As a result, such technology is effective in decreasing the electricity bills of the home consumers by obtaining optimal scheduling of home appliances [3].

Recently, optimal energy management of smart homes has been studied in different frameworks, and it has absorbed remarkable attention. Optimal scheduling of apartment smart building in the presence of controllable loads considering DC buildings has been investigated in [4]. The authors have proposed an optimization model for a building in [5] to minimize the cost of natural gas and electricity consumed during a determined scheduling time interval meeting operational and electrical constraint of the building. In [6], an expert energy management system (EEMS) has been introduced for providing optimal schedule of a microgrid, where the wind power production has been estimated using artificial neural network (ANN) method. A load management system is presented in [7] for handling

M. Nazari-Heris · P. Aliasghari (✉) · B. Mohammadi-ivatloo · M. Abapour
Faculty of Electrical and Computer Engineering, University of Tabriz, Tabriz, Iran
e-mail: m.nazari@ieee.org; p.aliasghari@tabrizu.ac.ir; mohammadi@ieee.org; abapour@tabrizu.ac.ir

B. Mohammadi-ivatloo, M. Nazari-Heris (eds.), *Robust Optimal Planning and Operation of Electrical Energy Systems*,
https://doi.org/10.1007/978-3-030-04296-7_6

multi-objective scheduling of the system to attain minimum operation cost and emission of pollutant gases, which has been studied considering the system with and without renewable sources. The authors have applied a predictive controller for buildings in [8] considering hierarchical building control method. Risk-constrained scheduling of apartment smart building in the presence of market price uncertainty has been studied in [9]. Robust scheduling of apartment smart building based on the information-gap decision theory (IGDT) has been provided in [10]. In this study, the uncertainty of electricity price has been modeled by utilizing IGDT method. In [11], the scheduling of home appliances has been studied using agent-based approaches, which has limitations of appliance coordination. Point estimate method (PEM) has been implemented in [12] for dealing with the uncertainties associated with wind power output and PV system, which is optimized using particle swarm optimization (PSO) method. Risk-based scheduling of apartment smart building using information-gap decision theory considering solar thermal storage system has been presented in [13].

The uncertainties associated with electrical energy systems parameters are handled using different methods including IGDT method [14], probabilistic methods [15], possibilistic procedure [16], and robust optimization method [17, 18]. IGDT method has been vastly implemented in research works to study the uncertainties of energy systems parameters. Such uncertainty handling technique takes the advantage of employment in extreme uncertain conditions. On the other hand, this method has a high level of complexity. Uncertainty-based optimum performance of hybrid energy system has been studied in the presence of load uncertainty through IGDT approach with and without demand response services in [19, 20]. In addition, IGDT has been successfully employed to study the transmission expansion planning problem [21], operation of distribution networks [22], and planning of wind producer [23].

This chapter aims to study optimal robust scheduling of renewable energy-based smart homes considering uncertainty associated with PV system power output. Accordingly, IGDT method is implemented to handle the uncertain PV power output. The studied smart home contains PV system and energy storage system (EES) technology to cover the availability limitation of PV during the scheduling time horizon. Since, the application of PEV has significantly been increased in response to the concern of air pollution, the studied smart home is equipped with PEV. Moreover, the controllable appliances of the studied smart home include washing machine, water heater, fridge, and PEV. The proposed model has been tested, and the simulation results are reported and analyzed to evaluate the performance of the model, which verifies the practicality of the model.

This chapter is organized as follows: Sect. 6.2 proposes the problem formulation. The introduced robust scheduling scheme of smart home and the studied case are provided in Sect. 6.3. Section 6.4 provides the simulation results, and the conclusion is presented in Sect. 6.5.

6.2 Problem Formulation

The studied smart home includes smart plugs and local controller for monitoring and controlling the energy consumption of electrical appliances. The main objective is minimizing the bill through daily time scheduling, which includes purchased power from the grid while satisfying the household load and PEV mobility requirements. The objective function is obtaining the minimum electricity bill of the consumer-satisfying household load and PEV mobility constraints, which can be stated as follows:

$$\begin{aligned} &\text{Cost} = \sum_{t=1}^{T} \lambda_t . P_D(\text{t}) \\ &t \in [1 \ldots T], \nu \in [1 \ldots V], \forall n \in a, \forall p \in a, \forall h \in a \end{aligned} \tag{6.1}$$

where the electrical energy exchanged between the home and power market is defined by P_D(t). The indexes n, p, h, and ν are used to define non-shiftable, power-shiftable, and time-shiftable home appliance as well as the number of PEVs, respectively. The power-shiftable ones permit both time and power optimization parameters. Moreover, the time-shiftable ones decrease the general potential for optimizing consumption of electrical energy as they have fixed power usage scheme, so only the initial start time is an optimization parameter. Equation (6.2) defines the formulation of non-shiftable appliances and fixed hourly power consumption in working time interval. In addition, the consumption of power-shiftable appliances p with standby power $\alpha_{p,t}$ and maximum power $\beta_{p,t}$ in a possibly preferred working period are stated in (6.4) [24].

$$x_{n,t} = \delta_n \tag{6.2}$$

$$\alpha_{p,t} \leq x_{p,t} \leq \beta_{p,t} \tag{6.3}$$

$$\sum_{p \in a} x_{p,t} = l_p \tag{6.4}$$

The power consumption $r_h = [r_{h,1}, r_{h,2}, \ldots, r_{h,24}]^T$ and operation of a time-shiftable appliance can be shifted during the scheduling time interval. It should be noted that the total power consumption with and without considering DSM is the same. Accordingly, the scheduling solution $x_{h,t}$ should be equal to that of the cyclic shifts of the pattern $r_{h,t}$. Equation (6.5) defines all possible states of shiftable patterns. A controlling binary integer variable $s_h = [s_{h,1}, s_{h,2}, \ldots, s_{h,24}]^T$ is used for time-shiftable appliance h, which is used in optimization process of the home appliances, as stated in (6.6). Total power demand of non-shiftable, power-shiftable, and time-shiftable appliances are calculated in (6.7). The power balance of the smart home including power transfer between home and the main grid, PV power, charge/

discharge power of the EES unit, and the power exchanged between the PEV and home are stated in (6.8). The DSM constraints of the smart home are as follows [24]:

$$R_h = \begin{bmatrix} r_{h,1} & r_{h,24} & \cdots & r_{h,3} & r_{h,2} \\ r_{h,1} & r_{h,1} & & r_{h,4} & r_{h,3} \\ \vdots & & \ddots & & \vdots \\ r_{h,1} & r_{h,2} & & r_{h,2} & r_{h,1} \end{bmatrix} \tag{6.5}$$

$$x_h = R_h.s_h \;\; \&1^T.s_h = 1 \tag{6.6}$$

$$D_t = \sum_{n \in a} x_{n,t} + \sum_{p \in a} x_{p,t} + \sum_{h \in a} x_{h,t} \tag{6.7}$$

$$P_{buy,t} + P_{PV,t} + P_{EV,t}^{dech} + P_{ESS,t}^{dech} = D_t + P_{EV,t}^{ch} + P_{ESS,t}^{ch} \tag{6.8}$$

where the power charge and discharge of the EES unit are defined by $P_{ESS,t}^{ch}$ and $P_{ESS,t}^{dech}$, respectively. The respective indicators for the charge and discharge of the PEV are $P_{EV,t}^{ch}$ and $P_{EV,t}^{dech}$. The power purchased from the grid and the load demand at time t are defined by $P_{buy,t}$ and D_t, respectively. The equality and inequality constraints of the EES units are provided in the following. Equation (6.9) defines the energy balance of the EES unit. The energy storage in the EES unit should be limited to its lower and upper bounds as stated in (6.10). The limitation of charge/discharge rate in each time interval of the scheduling time horizon are provided in (6.11) and (6.12), respectively. Finally, the EES unit should be operated in one of the charge, discharge, and ideal modes, which is considered in (6.13) [25].

$$E_{t,b} = E_{t-1,b} + \eta_{ch} P_{t,b}^{ch} - \frac{1}{\eta_{dech}} P_{t,b}^{dech} \;, b \in EV, ESS \tag{6.9}$$

$$E_{\min,b} \le E_{t,b} \le E_{\max,b} \tag{6.10}$$

$$P_{\min,b}^{ch}.\alpha_{t,b}^{ch} \le P_{t,b}^{ch} \le P_{\max,b}^{ch}.\alpha_{t,b}^{ch} \tag{6.11}$$

$$P_{\min,b}^{dech}.\beta_{t,b}^{s,dech} \le P_{t,b}^{dech} \le P_{\max,b}^{dech}.\beta_{t,b}^{s,dech} \tag{6.12}$$

$$\alpha_{t,b}^{ch} + \beta_{t,b}^{dech} = 1 \tag{6.13}$$

The EES unit is scheduled in a way that it can only be operated in charge, discharge, or idle mode. Accordingly, binary variables $\alpha_{t,b}^{ch}$ and $\beta_{t,b}^{dech}$ are used to model such constraint. The operation of EES units in charge/discharge model is modeled as $\alpha_{t,b}^{ch} = 1/\beta_{t,b}^{dech} = 1$. The energy stored in the EES unit is defined by $E_{t,b}$. The charge and discharge efficiencies are defined by η_{ch} and η_{dech}, respectively. The minimum and maximum power charge of the EES unit are indicated by $P_{\min,b}^{ch}$ and $P_{\max,b}^{ch}$. Moreover, the respective indicators for the minimum and maximum power discharged at the EES unit are $P_{\min,b}^{dech}$ and $P_{\max,b}^{dech}$. The minimum and maximum energy storage of the EES unit are $E_{\min,b}$ and $E_{\max,b}$.

6.3 Solution Method

The solution method for the investigation of IGDT-based home energy management is proposed in this section. The robust self-scheduling of PV panel installed in the smart home can be formulated using (6.14), (6.15), (6.16), and (6.17) [26].

$$\overline{\alpha} = \max_{\alpha, P_{buy}, P_{sale}} \alpha \tag{6.14}$$

$$\text{Cost} \leq \text{Cost}_c = (1-\sigma)\,\text{Cost}_0 \tag{6.15}$$

$$\text{Cost} = \left\{ \max_{\substack{P_{PV,t}, P^{dech}_{EV,t}, P^{dech}_{ESS,t} \\ P_{sale,t}, P^{ch}_{EV,t}, P^{ch}_{ESS,t}}} \sum_{t=1}^{T} \lambda_t . P_D(\text{t}) \right\} \tag{6.16}$$

$$(1-\alpha).\hat{P}_{PV} \leq P_{PV,t} \leq (1+\alpha).\hat{P}_{PV} \quad \forall t \tag{6.17}$$

In the above equations, the robustness function is formulated as a bi-level problem. In the upper level, the greater level of uncertainty, which guarantees the cost, is lower than the critical cost, Cost_c. Critical cost Cost_c is the factor of the risk-natural cost, Cost_0, defined by σ. The defined parameter σ is utilized to change the level of risk aversion. The forecasted PV power production and the robustness region are shown in Fig. 6.1.

As Cost should be the highest cost, it is calculated by decreasing PV power generation. Thus, for a given uncertainty horizon, the maximum cost occurs at the

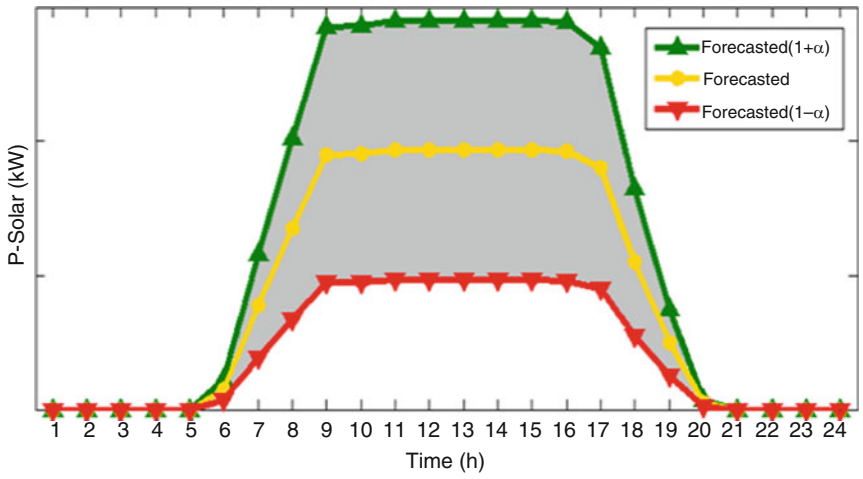

Fig. 6.1 Forecasted PV power generation and the robustness region

minimum PV generation as shown in (6.18), and the bi-level IGDT problem breaks to single-level problem [26].

$$P_{PV,t} = (1 - \alpha).\hat{P}_{PV} \tag{6.18}$$

6.4 Simulation Results

The rendered IGDT programming model is implemented to deal with optimal scheduling problem for solving the optimal scheduling problem of HEMS. Three case studies have been designed in this part. In the first case study, the role of HEMS and IGDT programing is not taken into account. In the second case, HEMS is employed during the scheduling horizon as regarding the consumer amenities. In third case, IGDT programming for both robust and opportunity functions is solved. As mentioned, home appliances can be located in three different categories based on their power consumption expect PEVs. Table 6.1 reported the name and consumption power of each appliance, which is considered in this paper. In addition, the estimated day-ahead electricity price is illustrated in Fig. 6.2.

6.4.1 Case Study 1

In this case, HEMS is not taken into account in the scheduling process. The energy consumption pattern is organized based on consumer's daily program and without

Table 6.1 Appliances and power consumption patterns

Type of appliance	Operating time	Hourly consumption (kWh)
Non-shiftable		
Fridge with freezer	24	0.12
Oven	1	0.348
Stove	2	0.8
TV	4	0.031
Entertainment system	2	0.088
Lighting	7	0.2
PV system	24	0.03
Other devices	24	0.5
Time-shiftable		
Clothes washer and dryer	2	1
Dishwasher	2	0.62
Power-shiftable		
Laptop	Daily requirement 2	0–0.075 (0.15)
Water boiler	Daily requirement 24	0–1.5 (3 kW)

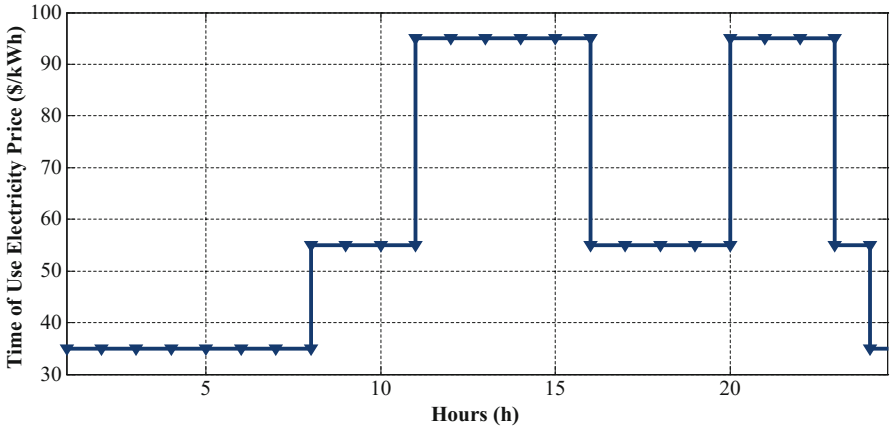

Fig. 6.2 TOU electricity price profile

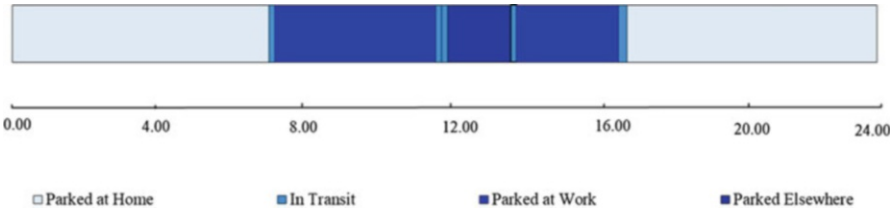

Fig. 6.3 Driving pattern of PEV during a day

considering the signals of electricity price. It is worthy to mention that electricity prices are adjusted based on the time of use program (TOU) in this chapter. The ranges of electricity price are arranged with respect to total consumption pattern prices including low-load, mid-load, and peak-load prices. The home owner could provide his demand from the PV and the grid. However, the owner cannot sell the surplus-generated power by PV system to the grid in this case.

The capacity of the PEV's battery is set to 30 kWh and the initial value of SOC is 20%. The amount of charging rate is equal to 3 kW per hour, and PEV's battery is charged as soon as it arrives at home according to the illustrated driving pattern of PEV in Fig. 6.3 [23]. According to Fig. 6.3, in this case, the role of the PEV's battery as an energy storage is ignored. The demand profile of appliances without considering their types and charging demand of PEV's battery are depicted in Fig. 6.4. The amount of generation and curtailment power of PV system with the maximum capability 2 kW as well as purchased power from the grid are illustrated in Fig. 6.5.

According to Fig. 6.4, the power consumption between 18 and 24 has high level. As result, the bought power from the grid has a significant value concurrently with high electricity prices. During the hours 6–18, the PV system can produce power because of the solar irradiation. As shown in Fig. 6.5, the PV system can provide the whole of the demand during hours 7–16. As portrayed in Fig. 6.5, PV system could

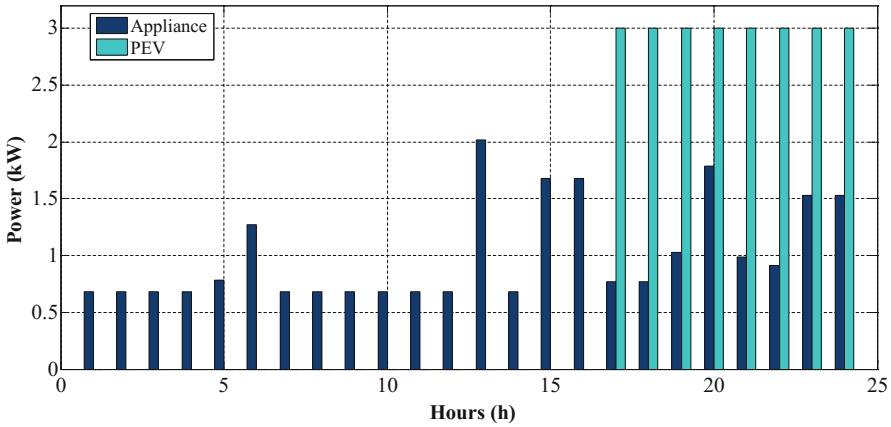

Fig. 6.4 Hourly consumption power of shiftable appliances, non-shiftable appliances, and PEV

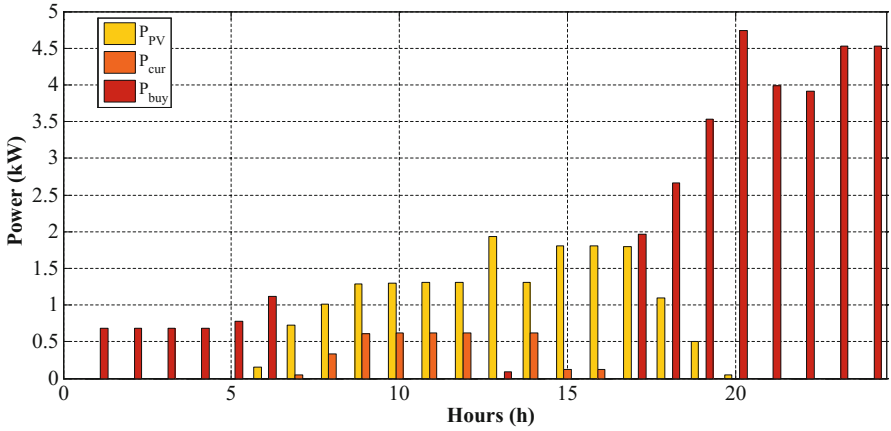

Fig. 6.5 Hourly generated and purchased power

not produce power with its maximum capacity because of the balance between supply and demand. Moreover, in this case the owner could not store or sell the surplus power to the grid. So, part of the generation power by PV system must be curtailed. The amount of cost is equal to $2.310.

6.4.2 Case Study 2

The storage technology is implemented in this case by utilizing PEV's battery. PEV's battery is used as energy storage system during the parked period at home. As explained in Sect. 6.2, the appliances can be divided into three groups: time

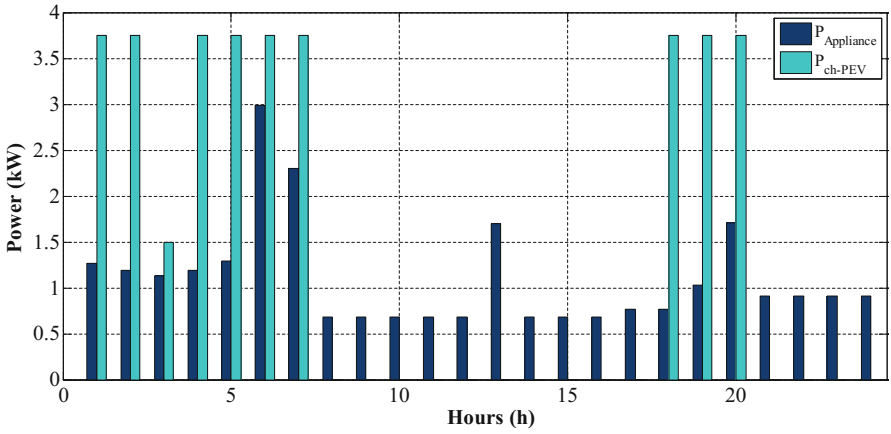

Fig. 6.6 Optimal scheduling of the power consumption of shiftable appliances, non-shiftable appliances, and PEV

shiftable, power shiftable, and non-shiftable. However, the customer's comfort and retractions of the amount of transition power are considered. The aim is to reduce the total cost by shifting power of power-shiftable appliances and delay usage of time-shiftable appliances including dish washer and clothes washer to the low price periods. Figure 6.6 shows the optimal scheduling of the hourly demand. The discharged power of the PEV's battery, the generation power of PV system, the amount of sold and purchased powers are portrayed in Fig. 6.7. The amount of total cost is equal to \$0.18.

Comparison of Figs. 6.6 and 6.4 specifies that in Case 2 a part of consuming power is transferred to low price intervals, for example, the PEV's battery is charged at hours 18, 19, and 20, due to discharging at hours 21, 22, and 23. Since PEV's battery is discharged at high electricity prices, the total cost will be decreased. Moreover, its charge process is transferred to the low price intervals. The usage time of clothes washer is transferred from hours 18 and 19 to 6 and 7. The operated time of dishwasher is changed from hours 18 and 19 to 6 and 7.

6.4.3 Case Study 3

The deterministic scheduling of smart home demand side management is solved in Cases 1 and 2 in different conditions based on the forecasted generation power of PV systems. The expected daily cost of smart home is equal to \$0.18 by considering HDSM (Case 2). The value of the robustness function related to the minimum cost of smart home scheduling would be equal to zero.

The robust scheduling is a useful strategy for risk-averse decisionmakers. Figure 6.8 portrayed the optimal value of robustness function versus critical cost.

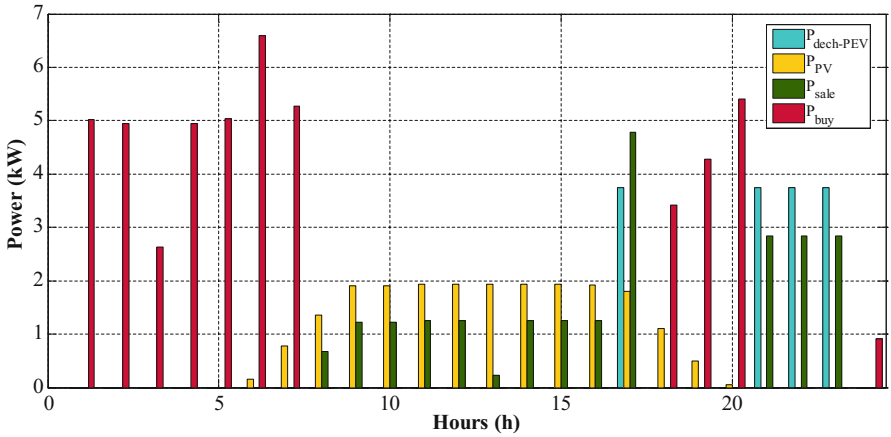

Fig. 6.7 Optimal scheduling of the hourly generated and purchased power

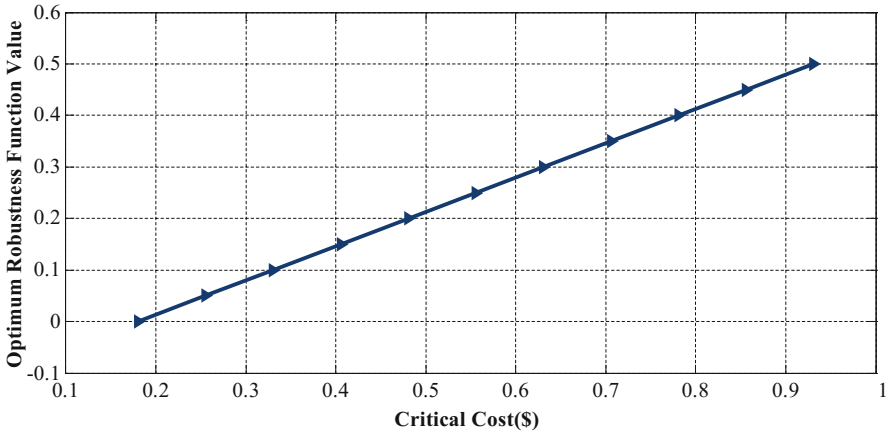

Fig. 6.8 TOU electricity price profile

As it was expected, the more resistant the program is, the more costs will be increased. Hence, if the smart home owner wants to make a risk-averse decision, more cost should be guaranteed and contrariwise; as the smart home owner wants more guaranteed cost, the decision will be more robust. Table 6.2 presents optimal robustness function value for different cost deviation factor and the related critical cost.

Table 6.2 Optimal robustness function value

Cost deviation factor (σ)	Critical cost (\$) (C_c)	Optimum robustness function value (α)
0	0.180225	0
0.05	0.255302	0.05
0.1	0.330379	0.1
0.15	0.405456	0.15
0.2	0.480533	0.2
0.25	0.55561	0.25
0.3	0.630687	0.333
0.35	0.705764	0.383
0.4	0.780841	0.433
0.45	0.855918	0.483
0.5	0.930995	0.533

6.5 Conclusions

In this paper, a robust strategy based on information-gap decision theory (IGDT) is proposed for scheduling of smart home. The IGDT method is implemented to find an interval for the PV's outputs power to study the robustness function. By the suggested model, the smart home owner can track risk-averse strategy to deal with the uncertainty of PV system. As rendered in the paper, the proposed method is able to program the household electricity demand integrating HDSM regarding three different categories of devices and utilizing the PEV's battery as an ESS. The owner could provide the household demand from the output power of PV system, the discharging power of PEV's battery, and the grid. The IGDT method is implemented to find an interval for the output power of PV to study the robustness function. Three cases have been designed to verify the usefulness of the proposed method. Two first cases have been investigated to show the impacts of the consumption pattern and how it is possible to modify it. Case 2 leads to design zero-energy house. In last case, the IGDT method has been used to mode the uncertainty of the generation power of PV. As it was expected, the cost has increased when the robust scheduling has been applied.

References

1. Nazari-Heris, M., Abapour, S., & Mohammadi-Ivatloo, B. (2017). Optimal economic dispatch of FC-CHP based heat and power micro-grids. *Applied Thermal Engineering, 114*, 756–769.
2. Shakeri, M., Shayestegan, M., Reza, S. S., Yahya, I., Bais, B., Akhtaruzzaman, M., et al. (2018). Implementation of a novel home energy management system (HEMS) architecture with solar photovoltaic system as supplementary source. *Renewable Energy, 125*, 108–120.
3. Nizami, M. S. H., & Hossain, J. (2017, November). *Optimal scheduling of electrical appliances and DER units for home energy management system*. In Universities Power Engineering Conference (AUPEC), 2017 Australasian (pp. 1–6). IEEE.

4. Shimoji, T., Tahara, H., Matayoshi, H., Yona, A., & Senjyu, T. (2015). Optimal scheduling method of controllable loads in DC smart apartment building. *International Journal of Emerging Electric Power Systems, 16*(6), 579–589.
5. Shirazi, E., & Jadid, S. (2015). Optimal residential appliance scheduling under dynamic pricing scheme via HEMDAS. *Energy and Buildings, 93*, 40–49.
6. Motevasel, M., & Seifi, A. R. (2014). Expert energy management of a micro-grid considering wind energy uncertainty. *Energy Conversion and Management, 83*, 58–72.
7. Ramchurn, S. D., Vytelingum, P., Rogers, A., & Jennings, N. R. (2011). Agent-based homeostatic control for green energy in the smart grid. *ACM Transactions on Intelligent Systems and Technology (TIST), 2*(4), 35.
8. Mayer, B., Killian, M., & Kozek, M. (2015). Management of hybrid energy supply systems in buildings using mixed-integer model predictive control. *Energy Conversion and Management, 98*, 470–483.
9. Najafi-Ghalelou, A., Nojavan, S., & Zare, K. (2018). Heating and power hub models for robust performance of smart building using information gap decision theory. *International Journal of Electrical Power & Energy Systems, 98*, 23–35.
10. Najafi-Ghalelou, A., Nojavan, S., & Zare, K. (2018). Robust thermal and electrical management of smart home using information gap decision theory. *Applied Thermal Engineering, 132*, 221–232.
11. Katipamula, S., Chassin, D. P., Hatley, D. D., Pratt, R. G., & Hammerstrom, D. J. (2006). *Transactive controls: A market-based GridWiseTM controls for building systems* (No. PNNL-15921). Pacific Northwest National Lab (PNNL), Richland, WA, USA.
12. Alavi, S. A., Ahmadian, A., & Aliakbar-Golkar, M. (2015). Optimal probabilistic energy management in a typical micro-grid based-on robust optimization and point estimate method. *Energy Conversion and Management, 95*, 314–325.
13. Najafi-Ghalelou, A., Nojavan, S., & Zare, K. (2018). Information gap decision theory-based risk-constrained scheduling of smart home energy consumption in the presence of solar thermal storage system. *Solar Energy, 163*, 271–287.
14. Mohammadi-Ivatloo, B., Zareipour, H., Amjady, N., & Ehsan, M. (2013). Application of information-gap decision theory to risk-constrained self-scheduling of GenCos. *IEEE Transactions on Power Systems, 28*(2), 1093–1102.
15. Alavi, S. A., Ahmadian, A., & Aliakbar-Golkar, M. (2015). Optimal probabilistic energy management in a typical micro-grid based-on robust optimization and point estimate method. *Energy Conversion and Management, 95*, 314–325.
16. Chen, C., Qi, M., Kong, X., Huang, G., & Li, Y. (2018). Air pollutant and CO2 emissions mitigation in urban energy systems through a fuzzy possibilistic programming method under uncertainty. *Journal of Cleaner Production, 192*, 115–137.
17. Nazari-Heris, M., Mohammadi-Ivatloo, B., & Asadi, S. (2018). Robust stochastic optimal short-term generation scheduling of hydrothermal systems in deregulated environment. *Journal of Energy Systems, 2*, 168–179.
18. Nazari-Heris, M., Mohammadi-Ivatloo, B., Gharehpetian, G. B., & Shahidehpour, M. (2018). Robust short-term scheduling of integrated heat and power microgrids. *IEEE Systems Journal, 99*, 1–9.
19. Nojavan, S., Majidi, M., & Zare, K. (2017). Performance improvement of a battery/PV/fuel cell/grid hybrid energy system considering load uncertainty modeling using IGDT. *Energy Conversion and Management, 147*, 29–39.
20. Nojavan, S., Majidi, M., Najafi-Ghalelou, A., Ghahramani, M., & Zare, K. (2017). A cost-emission model for fuel cell/PV/battery hybrid energy system in the presence of demand response program: ε-constraint method and fuzzy satisfying approach. *Energy Conversion and Management, 138*, 383–392.
21. Ranjbar, H., & Hosseini, S. H. (2016). IGDT-based robust decision making applied to merchant-based transmission expansion planning. *International Transactions on Electrical Energy Systems, 26*(12), 2713–2726.

22. Connell, A. O., Soroudi, A., & Keane, A. (2018). Distribution network operation under uncertainty using information gap decision theory. *IEEE Transactions on Smart Grid, 9*(3), 1848–1858.
23. Aghaei, J., Agelidis, V. G., Charwand, M., Raeisi, F., Ahmadi, A., Nezhad, A. E., & Heidari, A. (2017). Optimal robust unit commitment of CHP plants in electricity markets using information gap decision theory. *IEEE Transactions on Smart Grid, 8*(5), 2296–2304.
24. Mesarić, P., & Krajcar, S. (2015). Home demand side management integrated with electric vehicles and renewable energy sources. *Energy and Buildings, 108*, 1–9.
25. Aliasghari, P., Mohammadi-Ivatloo, B., Alipour, M., Abapour, M., & Zare, K. (2018). Optimal scheduling of plug-in electric vehicles and renewable micro-grid in energy and reserve markets considering demand response program. *Journal of Cleaner Production, 186*, 293–303.
26. Moradi-Dalvand, M., Mohammadi-Ivatloo, B., Amjady, N., Zareipour, H., & Mazhab-Jafari, A. (2015). Self-scheduling of a wind producer based on information gap decision theory. *Energy, 81*, 588–600.

Chapter 7
Robust Unit Commitment Applying Information Gap Decision Theory and Taguchi Orthogonal Array Technique

Hamid Reza Nikzad, Hamdi Abdi, and Shahriar Abbasi

7.1 Introduction

Generally, unit commitment problem (UCP) deals with determining operation schedule of generating units at every hour interval considering load changes and some operational and environmental constraints; in UC problem, binary decision variables determining the state of units (on/off) are produced in each hour considering demanded load and other important requirements, such as spinning reserve requirements [1]. The UCP is a large-scale non-convex complex problem, which should be solved in a reasonably small time.

A lot of research works are presented in this area, mainly focusing on fuel cost minimization. Also, other features such as calculation time, profit, security, and emission are analyzed [2]. Various classifications in this era have been presented and demonstrated. They are mainly focusing on uncertain versus deterministic, deregulated power systems versus regulated ones, multi-objective versus single objective, heuristic versus mathematical, and so on.

Deterministic UCP (DUCP) approaches are mainly focusing on the cost and executing time minimization and can be categorized as exhaustive enumeration (EE), priority list (PL), dynamic programming (DP), Lagrangian relaxation (LR), mixed integer linear programming (MILP), and decomposition approaches [1, 3]. These methods suffer from the inability to solve the large-scale problems. To overcome this challenge, meta-heuristic approaches are proposed. Genetic algorithm (GA), particle swarm optimization (PSO), simulated annealing (SA), and evolutionary programming (EP) are some examples in this regard, which have more chance to find the global optimum point, but they are usually time-consuming.

H. R. Nikzad · H. Abdi (✉) · S. Abbasi
Electrical Engineering Department, Faculty of Engineering, Razi University, Kermanshah, Iran
e-mail: hamdiabdi@razi.ac.ir

B. Mohammadi-ivatloo, M. Nazari-Heris (eds.), *Robust Optimal Planning and Operation of Electrical Energy Systems*,
https://doi.org/10.1007/978-3-030-04296-7_7

Along with increasing penetration of renewable energy sources (RESs) in the power systems, some benefits were provided. Among them, reducing amount of pollution, improving voltage profile, reducing amount of power losses and thus system cost, increasing electric power quality, and improving reliability of the system can be remarked as the most important features in this context [4]. Also, new challenges appeared in the power systems, which basically arise from uncertain behavior of these resource types. Furthermore, deregulation in power systems has resulted in some uncertain factors. The main sources of uncertainties in UCP are uncertainty on inflows for the hydro reservoirs, uncertainty on customer load, uncertainty on renewable generation, uncertainty on unit availability, and uncertainty on energy prices [3]. Solving the UCP in considering this uncertain behavior lead to uncertain UCP (UUCP). To calculate UUCP, new approaches are needed; the most proposed approaches are stochastic optimization (SO) (or scenario tree), robust optimization (RO), and chance-constrained optimization (CCO) [3].

One of the most common and basic techniques in SO is scenario representation (SR) of uncertainty. The SR is established on generating a large number of scenarios where each scenario represents a possible realization of the underlying uncertain factors [5]. This kind of simulation method is an approximation of the true distribution of the uncertainties. Depending on the number of stages in the problem, the structure of scenarios can be a number of parallel scenarios in a two-stage SO problem or a scenario tree in a multistage SO problem [5]. References [6–8] are some certified and updated examples in SUCP field in which the problem is addressed by applying topology control through transmission switching as a recourse action in the day-ahead operation of power systems with large-scale renewable generation resources, two- stage formulation based on partitioning the sample space of the uncertain factors by clustering the scenarios that approximate their probability distributions, and considering the energy storage, respectively. A stochastic real-time unit commitment dealing with the stochastic and intermittent nature of non-dispatchable renewable resources including ideal and generic energy storage devices is proposed in [9]. The impacts of integrating non-deterministic flexible ramp reserves in a multistage multi-resolution day-ahead robust unit commitment to cope with variability of renewable energy sources are analyzed in [10]. A data-driven unit commitment model with multi-objectives under wind power and load uncertainties has been presented by authors in [11]. Reference [12] addressed a new method based on information gap decision theory to evaluate a profitable operation strategy for combined heat and power units in a liberalized electricity market.

In RUCP, as it was remarked in [5], the model tries “to incorporate uncertainty without the information of underlying probability distributions, and instead with only the range of the uncertainty”. Also, RUCP minimizes the worst-case cost regarding all possible outcomes of the uncertain parameters. This type of models produces very conservative solutions, but computationally it can avoid incorporating a large number of scenarios. References [13, 14] deal with the RCUP in the presence of wind power and pumped storage hydro and wind power and demand response uncertainties, respectively.

Guarantying that the demand constraints will never be violated in UCP is very difficult. A solution is to provide answer which are "reasonably feasible" under all except the most unlikely scenarios [3]. This is therefore the main idea for applying the CCUCP, where the desired safety level can be specified under the form of a probability.

The reminder of this chapter is arranged as follow: mathematical formulation of UCP is presented in Sect. 7.2. In Sect. 7.3 the optimization method is introduced. Robust UC using IGDT and TOAT are respectively explained in Sects. 7.4 and 7.5. Examples of these methods and obtained simulation results are presented in Sect. 7.6. The concluded remarks are in Sect. 7.7.

7.2 Mathematical Formulation of UCP

7.2.1 Base Formulation of UCP

Basic model of UCP consists of solving this problem without RESs and ESSs. Minimization of total operation cost (TOC) of number of generation unit which commonly supply power demand of a network in 24-h is the target of solving of UCP. The objective function of UCP is as follows:

$$\min TOC = \sum_{t=1}^{T} \sum_{n=1}^{N} \left(u_n^t . F_n^t \left(p_n^t \right) + u_n^t . s_n^t \right) \tag{7.1}$$

Fuel cost of n-th unit at t-th hour with $p(MW)$ output power, $F_n^t\left(p_n^t\right)$, has been estimated by Quadratic Eq. (7.2) [15].

$$F_n^t\left(p_n^t\right) = a_n . \left(p_n^t\right)^2 + b_n\left(p_n^t\right) + c_n \tag{7.2}$$

On–off states of the n - th unit at t - th hour are determined by the binary variable u_n^t which has been described in (7.3):

$$u_n^t = \begin{cases} 1 & \text{unit is } on \\ 0 & \text{unit is } off \end{cases} \tag{7.3}$$

In (7.1), s_n^t is the startup cost for n - th generation unit that has been turned on at beginning of t - th hour. s_n^t depends on hours that unit is off. Finally startup cost has been calculated in (7.4) [16]:

$$s_n^t = \begin{cases} HSC_n & \text{if } T_{off,n} \le T_{cc} \\ CSC_n & \text{if } T_{off,n} \ge T_{cc} \end{cases} \tag{7.4}$$

Generally, startup cost and shutdown cost are constant and are predefined for each generation unit. Generally, the shutdown costs are assumed to be equal to zero for the sake of simplicity [17].

Decision variables in the basic form of UCP are arrays of matrix with dimension $T \times N$ in which each array shows generated power by a unit during an hour (7.5).

$$P = \begin{bmatrix} p_1^1 & \cdots & p_n^1 & \cdots & p_N^1 \\ \vdots & \ddots & \vdots & \ddots & \vdots \\ p_1^t & \cdots & p_n^t & \cdots & p_N^t \\ \vdots & \ddots & \vdots & \ddots & \vdots \\ p_1^T & \cdots & p_n^T & \cdots & p_N^T \end{bmatrix} \tag{7.5}$$

7.2.2 Formulation of UCP in Presence of RESs and ESSs

Owing to increasing of application of RESs and ESSs in the power systems, the formulation of UCP have had changed. If the investment costs of RESs and ESSs are considered zero, the following model is presented for UCP in presence of costs of RESs and ESSs. Presented model in (7.6) is consisted of cost functions of RESs and ESSs.

$$\begin{aligned} \min \ TOC = \sum_{t=1}^{T} \Bigg[\left(\sum_{n=1}^{N} \left(u_n^t . F_n^t \left(p_n^t \right) + u_n^t . s_n^t \right) \right) + \ldots \\ \left(\sum_{w=1}^{W} F_w^t \left(p_w^t \right) \right) + \left(\sum_{es=1}^{N_s} F_{es}^t \left(p_{g,es}^t + p_{s,es}^t \right) \right) \Bigg] - F(p_{res}) \end{aligned} \tag{7.6}$$

In (7.6), generation cost for RESs is considered as (7.7). Also, a cost function as (7.8) is added for each ESS. Input of these functions is sum of the stored power from the network and injected power to the network. Last cost function (7.9) is for the value of reminded energy (p_{rsp}) in ESSs at the end of study period.

$$F_w^t = a_w . \left(p_w^t \right)^2 + b_w . \left(p_w^t \right) + c_w \tag{7.7}$$

$$F_{es}^t = a_{es} . \left(p_{g,es}^t + p_{s,es}^t \right)^2 + b_{es} . \left(p_{g,es}^t + p_{s,es}^t \right) + c_{es} \tag{7.8}$$

$$F_{rsp} = a_{rsp} . \left(p_{rsp} \right)^2 + b_{rsp} . \left(p_{rsp} \right) + c_{rsp} \tag{7.9}$$

Approximately, startup costs of ESSs and RESs are equal to zero. As showed in (7.10), after adding ESSs to the system, the decision variable matrix changes to ($T \times (N + 2N_s)$); there are two decision variables for each ESS at each hour. One variable for the storage power and another for the injection power.

$$P = \begin{bmatrix} p_1^1 & \cdots & p_n^1 & \cdots & p_{N+2N_s}^1 \\ \vdots & \ddots & \vdots & \ddots & \vdots \\ p_1^t & \cdots & p_n^t & \cdots & p_{N+2N_s}^t \\ \vdots & \ddots & \vdots & \ddots & \vdots \\ p_1^T & \cdots & p_n^T & \cdots & p_{N+2N_s}^T \end{bmatrix} \tag{7.10}$$

7.2.3 Constraints of UCP

In the UCP, optimal TOC must satisfy operational conditions of generation units and conditions of system [18]. These conditions are some or all of the following conditions [18–21].

7.2.3.1 Limitations of Generation Unit

Active power output of each generation unit is within the minimum and maximum limits of that unit (7.11) [18, 22, 23].

$$p_{n,\min} \leq p_n^t \leq p_{n,\max} \tag{7.11}$$

7.2.3.2 Power Balance

The most significant constraint of UCP is balance between generated power and demanded power [18, 22]. This constraint has been presented in (7.12).

$$\sum_{n=1}^{N} p_n^t . u_n^t + \sum_{w=1}^{W} p_w^t + \sum_{es=1}^{N_s} p_{g,es}^t = d_t + \sum_{es=1}^{N_s} p_{s,es}^t \tag{7.12}$$

7.2.3.3 Minimum Uptime

When operator turns on a unit to be online, this unit cannot be turned off for number of hours which is called minimum uptime (MUT) [22, 23]. This constraint is as (7.13):

$$T_{n,on} \geq \mathrm{MUT}_n \tag{7.13}$$

7.2.3.4 Minimum Downtime

When an operator turns off a unit, for mechanical limitation, it cannot be turned on again for number of hours, i.e.:

$$T_{n,off} \geq \mathrm{MDT}_n \tag{7.14}$$

7.2.3.5 Ramp Rate Up/Down

Output power of a generation unit cannot increase or decrease as step function. Variations of output power of generation unit are limited by ramp up/down rate [18–20, 22]. These constraints are formulated:

$$p_n^t - p_n^{t-1} \leq \mathrm{RU}_n \quad \text{if generation increases} \tag{7.15}$$

$$p_n^{t-1} - p_n^t \leq \mathrm{RD}_n \quad \text{if generation decreases} \tag{7.16}$$

This should be noted that, ramp rates are not considered for RESs and ESSs.

7.2.3.6 Spinning Reserve

Spinning reserve is a percentage of power demand to satisfy demand when it changed suddenly. The related constraint is as follow:

$$\sum_{n}^{N} u_n^t p_{n,\max} \geq d_t + SR \quad 1 \leq t \leq T \tag{7.17}$$

7.3 Optimization Method (Genetic Algorithm)

So far, different methods are presented to solve UCP. Presented methods can be classified as two classic and modern types [24]. Enumeration method, priority list, dynamic programing, Lagrangian relaxation algorithm, etc. are from classical methods. Modern methods are the new algorithms that consist of neural networks, meta-heuristic algorithm (GA, PSO, etc.), etc.

Considering uncertainties of power demand, output power of RESs, etc., different methods such as Monte Carlo and stochastic programing are presented. Among these methods, RO and IGDT are more popular for their ability in solving optimization problems in uncertain environments. These methods do not need probability distribution functions (pdf) of the stochastic variables. These methods are suitable when exact data about the uncertain parameters is not available [25]. The robust UC using these methods are explained in the following sections.

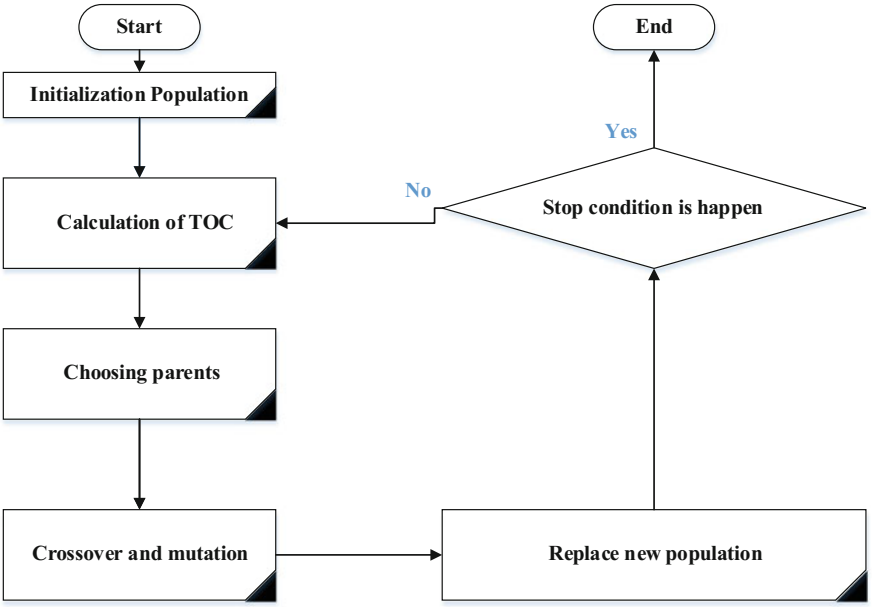

Fig. 7.1 General flowchart of GA

7.3.1 Genetic Algorithm

In this work, the GA is used to solve the UCP. So, here a summarized description regarding this algorithm is presented. GA operates based on combination of large number of solutions to achieve the best feasible ones. In each iteration, the objective function is evaluated for each probable optimal solution. Then the new solution will be resulted using the solutions of previous iteration. This process will continue until the stop criteria are achieved. These criteria can be selected as the number of iterations, running time of calculation, or a predefined accuracy of objective cost function [26]. Figure 7.1 shows the general flowchart of GA.

7.4 Robust UC Using IGDT

IGDT is a modern modeling method to solve optimization problems considering uncertainty. Here, IGDT is used for solving UCP. To solve optimization problems with IGDT, there are risk seeker and risk averse models. In UCP, the risk averse model is more suitable. Envelop-bound is one of the most appropriate methods that is commonly used in optimization problems of power system. In the continuum a brief explanation of risk averse method has been presented. Regarding UCP framework the implication of risk averse method is in this way: first, UCP has been solved

by the use of deterministic value of power demand and output power of RESs. With consideration of the legal bound for TOC by the operator, maximum legal variation for demand and output power is obtained.

$$f = \min(TOC(p,\gamma)) \tag{7.18}$$

$$\text{Subject to : constraints } (7.11) - (7.17) \tag{7.19}$$

$$\gamma \in \Omega \tag{7.20}$$

$$\Omega = \{p_w, d\} \tag{7.21}$$

In the above equations, γ is the uncertain parameter. The Ω describes the set of uncertain parameters. In Eq. (7.13), p is the set of decision variables of UCP which consist of output power of the generation units, stored power, and injected power by ESSs. The objective function in (7.18) which has been showed by $TOC(p,\gamma)$ is generally dependent on both decision variable and uncertainty parameters. Mathematical description of Ω has been brought in (7.22).

$$\Omega = \Omega(\overline{\gamma}, \alpha) = \left\{ \gamma : \left| \frac{\gamma - \overline{\gamma}}{\overline{\gamma}} \right| \leq \alpha \right\} \tag{7.22}$$

In (7.22), γ is scheduled value of uncertainty parameter. The α is the maximum possible diversion of uncertainty parameter from its scheduled value. Equations (7.18, 7.19, 7.20, and 7.21) have showed the formulation of UCP which consists of uncertainty. As it was mentioned in this method, first of all the problem is considered without the uncertainty and with scheduled values. The state which is presented in (7.23) is called base state.

$$TOC_b = \min\left(TOC\left(p,\overline{\gamma}\right)\right) \tag{7.23}$$

$$\text{Subject to : constraints } (7.11) - (7.17) \tag{7.24}$$

Risk averse strategy has been used in this problem then the target is to find maximum of α subject to that the value of TOC doesn't exceed the legal bound which is determined by the operator. Equations 7.25, 7.26, 7.27, 7.28, 7.29, and 7.30) explain this method [27].

$$R_c = \max\alpha \tag{7.25}$$

$$\text{Subject to : constraints } (7.11) - (7.17) \tag{7.26}$$

$$\text{TOC}(p,\gamma) \leq \Delta_c \tag{7.27}$$

$$\Delta_c = TOC_b\left(p,\overline{\gamma}\right) * (1+\beta) \tag{7.28}$$

$$\left| \frac{\gamma - \overline{\gamma}}{\overline{\gamma}} \right| \leq \alpha \tag{7.29}$$

$$0 \leq \beta \leq 1 \tag{7.30}$$

Δ_c is critical value of objective function that is often determined by the operator. According to Eq. (7.28), this value is determined as a function of the objective function. R_c is the radius of uncertainty that is a positive parameter. Generally, in risk averse method of IGDT, the final solution of problem is α which depends on Δ_c. In other words, the operator will make sure that for changes of uncertain parameter in the obtained uncertain bound, the TOC will not exceed from the predetermined bound which is specified by the operator.

7.5 Robust UC Using TOAT

The RO is based on the determination of variations bound for uncertain parameters subjected to TOC not exceeding legal bound determined by the operator. In fact, RO presents the worst state of the optimal response, wherein variation of uncertain variables does not exceed their legal bound. Uncertainties are controlled by a predetermined parameter which is called uncertainty budget that shows the boundaries of TOC. Different techniques have been presented for RO method. The TOAT method is used here. In this method, different levels are considered for each of the uncertainty variables. Regarding these levels, different states or experiments of the problem are considered. In general, for problems which have m parameters with uncertainty and n levels for each parameter, there are n^m different arranges of uncertain parameters. Each arrangement is an experiment problem. Solving problem for all experiments, especially in large scale, is costly and time-consuming. Dr. Taguchi presented a table as orthogonal arrays which provides problem-solving with the minimum needed experiments for finding the optimal response of the problem. The smallest presented orthogonal array is $L_4 2^3$, which provides the operation of four experiments with three uncertain parameters in which each of the parameters has two levels. This orthogonal array has been showed at Table 7.1 [28].

The features of orthogonal arrays are the following: (1) The number of parameters which has the same level in each column of the chart is equal. (2) The number of levels of one type is two.

Dr. Taguchi has presented different orthogonal arrays for different parameters and levels. Orthogonal arrays that exist for all two-level parameters are $L_4 2^3$, $L_8 2^7$, $L_{12} 2^{11}$, $L_{16} 2^{15}$, and $L_{32} 2^{31}$. For instance, if there are 25 uncertain parameters in a problem, $L_{32} 2^{31}$ should be chosen and 6-left columns are ignored. To solve UCP, regarding the number of uncertain parameters and considered levels, orthogonal

Table 7.1 Orthogonal array $L_4 2^3$ [28]

Experiments	Level of each factors		
	Factor A	Factor B	Factor C
1	1	1	1
2	1	2	2
3	2	1	2
4	2	2	1

arrays are determined for each parameter, and finally UCP formulation in the Taguchi framework is this way [28].

$$f = \min(TOC(p, \omega)) \tag{7.31}$$

$$\text{Subject to : constraints } (6-11)-(6-17) \tag{7.32}$$

$$\omega \in \Omega \tag{7.33}$$

In (7.31), ω is the uncertain parameter. The model of the problem in (7.31) and the target is to find the best arrangement for decision variables that is robust in the confrontation with the variation of uncertain parameters in the considered levels. In fact, optimal arrangement of decision variables of UCP is presented by knowing the levels of variations. Then, the objective function is as follows:

$$\begin{aligned} TOC' = \sum_{ex}^{EX}\Big[\sum_{t=1}^{T}\Big[\left(\sum_{n=1}^{N}\left(u_n^t.F_n^t\left(p_n^t\right)+u_n^t.s_n^t\right)\right)+\ldots \\ \left(\sum_{w=1}^{W}F_w^t\left(p_w^t\right)\right)+\left(\sum_{es=1}^{N_s}F_{es}^t\left(p_{g,se}^t+p_{s,es}^t\right)\right]-F(p_{res})\Big] \end{aligned} \tag{7.34}$$

$$f' = \min\ \left(\text{TOC}'\left(p\overline{\omega}\right)\right) \tag{7.35}$$

$$\text{Subject to : constraints } (7.11)-(7.17) \tag{7.36}$$

$$\overline{\omega} \in \left\{\overline{\omega}_{\min}, \overline{\omega}_{\max}\right\} \tag{7.37}$$

In (7.37), $\overline{\omega}_{\min}$ and $\overline{\omega}_{\max}$, respectively, declare the minimum and maximum levels of uncertain parameters. Orthogonal arrays are defined as:

$$\text{Level of factor} = \begin{cases} 1 & \overline{\omega}_{\min} \\ 2 & \overline{\omega}_{\max} \end{cases} \tag{7.38}$$

Finally, the output of UCP by RO is the optimal arrangement which is robust in uncertain conditions.

7.6 Examples

In this part, the presented methods for UCP are simulated on a 10-unit standard system of IEEE. At the beginning, using GA and PL, TOC_b without the regarding of the absolution of the problem has been solved. Then, the two methods IGDT and RO have been implicated on system. This case study consists of 10 thermal units. The relevant minimum and maximum output power of each unit, cost coefficients, and the other data are presented in Table 7.2. Also, the daily demanded load is specified as it is indicated in Table 7.3.

Table 7.2 The case study data [29]

Unit	p_{max}	p_{min}	MDT	MUT	c	b	a	HSC	CSC	T_{cc}	Is
Unit1	455	150	8	8	1000	16.19	0.00048	4500	9000	5	8
Unit2	455	150	8	8	970	17.26	0.00031	5000	10,000	5	8
Unit3	130	20	5	5	680	16.5	0.00211	560	1120	4	−5
Unit4	130	20	5	5	700	16.6	0.002	550	1100	4	−5
Unit5	162	25	6	6	450	19.7	0.00398	900	1800	4	−6
Unit6	80	20	3	3	370	22.26	0.00712	170	340	2	−3
Unit7	85	25	3	3	480	27.74	0.0079	260	520	2	−3
Unit8	55	10	1	1	660	25.92	0.00413	30	60	0	−1
Unit9	55	10	1	1	665	27.27	0.00222	30	60	0	−1
Unit10	55	10	1	1	670	27.97	0.00173	30	60	0	−1

Table 7.3 Hourly demanded power applied to problem (MW)

t	d_t	t	d_t	t	d_t	t	d_t
1	700	7	1150	13	1400	19	1200
2	750	8	1200	14	1300	20	1400
3	850	9	1300	15	1200	21	1300
4	950	10	1400	16	1050	22	1100
5	1000	11	1450	17	1000	23	900
6	1100	12	1500	18	1100	24	800

Table 7.4 The wind turbines data

w	p^w_{max}	p^w_{min}	MUT	MDT	a	b	c
w_1	105	5	1	1	100	6.591	0.0032
w_2	105	5	1	1	200	8.131	0.00483
w_3	30	5	1	1	181	6.299	0.00168
w_4	240	5	1	1	100	6.591	0.0032

Table 7.4 shows the wind turbines data which are used in this case. These data are consisting of the minimum and maximum output power for each turbine, cost coefficients, and other required data in the case.

7.6.1 UCP in the Base Form

At first, the UCP without the consideration of the uncertainty of problem parameters is solved. The method used in this chapter is a combination of GA and PL. The GA is a meta-heuristic algorithm that produces the stochastic responses and improves them to reach the optimal solution of the optimization problem. Some of the problem constraints have been satisfied for infeasible solutions using penalty factor strategy. By the use of PL, the generation of stochastic population has been done until all solutions satisfy constraints (7.12, 7.13, and 7.14) and constraint (7.17). Parameters

Table 7.5 Results of the case study system

Systems		TOC_b(\$)
10 units	IGDT	540,567

Table 7.6 Results of IGDT considering the wind uncertainty

Systems	β			
		$\beta = 0.01$	$\beta = 0.03$	$\beta = 0.5$
10 Units	α	0.24	0.42	0.54
	TOC	541,072	554,786	556,360

Table 7.7 Results of IGDT considering the demanded power uncertainty

System	β			
		$\beta = 0.03$	$\beta = 0.05$	$\beta = 0.07$
10 Units	α	0.974	0.973	0.971
	TOC	550,323	561,649	559,770

of GA and output power of RESs are listed in the appendices. Table 7.5 shows the results of UCP in the base form. For IGDT method wind turbines 1–3 and for RO method wind turbine number 4 are added to the system.

7.6.2 UCP Solving by IGDT

In this example, the UCP is solved by the IGDT method. The obtained results for different variation bounds in TOC_b are presented in Tables 7.6 and 7.7. Note that using the risk averse method, uncertainties that have negative effect on TOC are examined. These uncertainties are increasing demand and reduction of power output of wind turbines. As the base case, the value of TOC_b obtained by GA is as shown in Table 7.5. Now, the variable α is added as a new decision variable. In the next step, coefficients $(1 - \alpha)$ and $(1 + \alpha)$ are determined, respectively, for two uncertain parameters, output of wind turbines and demand of system. So, a new constraint as (7.39) will be added to UCP.

$$TOC - TOC_b \leq (1 + \beta) * TOC_b \tag{7.39}$$

β is the coefficient which determines the maximum legal variation of TOC from TOC_b, and β is recognized by operator. $(1 - \alpha)$ is multiplied in TOC to find the maximum bound of the variation of uncertain variables by GA. The results of UCP have been regarded for two uncertain parameters in return of the different values of β which are presented at Tables 7.6 and 7.7.

Table 7.8 Optimal output power of generation units

	Units									
Hour	1	2	3	4	5	6	7	8	9	10
1	448.2	159.5	0	0	0	0	0	0	0	0
2	451.8	249.4	0	0	0	0	0	0	0	0
3	451.1	315.7	0	0	0	0	0	0	0	0
4	454.2	447.2	0	0	0	0	0	0	0	0
5	454.5	439	61	0	0	0	0	0	0	0
6	451.2	454.9	101.3	0	0	0	35.3	0	0	0
7	447.4	434.7	97.2	107.2	0	0	26.1	0	0	0
8	452.7	419.8	105.7	96.1	30.2	0	29	0	0	0
9	454	444	116.3	122.7	114.9	0	35.9	0	0	0
10	454	453.2	80.6	117.2	152.7	0	31.7	0	0	0
11	455	442.3	129.6	116.1	134.7	0	42.2	33.9	0	0
12	447.2	444.3	121	120.7	153.7	64	56.7	14.9	0	0
13	454.2	451.2	106.5	111.7	108.1	28.7	29.6	15.8	0	0
14	454.5	418.5	86.9	112.8	108.7	21.8	0	11.7	0	0
15	450.7	432.7	95.5	121.1	0	0	0	0	0	0
16	453.5	403.8	64	56.4	0	0	0	0	0	0
17	453.5	431.4	45.3	0	0	0	0	0	0	0
18	454.8	454	123	0	0	0	0	0	0	0
19	454.9	440.1	127.6	0	0	62	0	32.1	0	0
20	455	453.5	121.2	0	0	75.6	81.6	30.1	27.1	44.8
21	454.8	454.5	116.5	0	0	54.9	58	31.2	0	19
22	449	432.2	64.8	0	31.54	21.3	25.9	10.9	0	0
23	449.9	267.3	77.9	0	33.2	0	0	11.5	0	0
24	449.3	220.3	0	0	26.8	0	0	0	0	0
TOC($)	562,330									

The results that are presented at Table 7.6 show that with increase in β, the variation bound of the output power of the wind turbines increases. Regarding the low cost of the generation of the electricity power by the use of wind turbines, the result was not far from expectation. Because TOC is a great number and the capacity of RESs is low in this system, small variation in the amount of β leads to large variation in the legal variation bound of RESs.

The obtained results at Table 7.7 show the greater sensitiveness of TOC related to variation of power demand and related to the output power of wind turbines. In other words, the smallest variations in the power demand leads to high costs. For more clarity, β is considered greater than the previous state. The arrangement of the scheduled power of the decision variables of UCP is presented only for one of the cases in Tables 7.8 and 7.9.

Table 7.9 Optimal storage power and injection power of ESSs

Hour	$p_{s,1}$	$p_{s,2}$	$p_{s,3}$	$p_{g,1}$	$p_{g,2}$	$p_{g,3}$
1	11.1	6.3	0	0	0	0
2	9.5	12.3	0.2	0.9	3.8	0
3	6	11.7	3.3	3.1	3.8	0
4	4.3	7.5	11.2	1.1	8.4	0
5	19.3	2	2.9	6.6	2.7	0
6	8.3	9	0.6	5.4	9.2	0
7	24.3	24.6	5	9.2	5	0
8	3.8	6.4	1.1	12	2.6	0
9	6.3	43.8	0.5	14.9	2.5	0
10	5.1	0.4	0.7	12.8	16.5	0.5
11	2.3	0.7	1.1	7.4	15	4.2
12	1.4	12.4	3.3	11.7	7.4	3.1
13	3.7	7.5	0.7	10.2	12	2.4
14	8.6	2.7	1.1	5	6.9	1.3
15	16.5	2.6	2.9	4.9	7.3	1.2
16	20.7	6	2.9	13.1	5.6	1.7
17	8.8	4.9	0.5	10	0.2	3.1
18	0.7	7.4	0.4	7.7	15.1	2.9
19	16.4	0.4	0.5	10.3	15.8	5.7
20	0.6	0.3	0.3	8.4	4.1	1.5
21	0.6	1.5	2.4	2	4.6	3.3
22	2.1	0.8	0.2	13.7	4.9	1.7
23	5.5	10.3	0.9	4.2	6.4	2
24	1.3	0.6	0.5	11.1	21.7	8.9
p_{rsp}(MW)	5.2					

7.6.3 UCP Solving by RO (TOAT)

In the example, the UCP is solved by TOAT as a valid RO method. Here, the uncertain variable is the output power of wind turbine. The output power of wind turbine is chosen between two levels. The number of the variables is 24 that is the output power of wind turbine during 24 h. According to the number of uncertain variables, orthogonal arrays $L_{32}2^{31}$ of Table 7.10 are considered.

Levels 1 and 2 are described at (7.40). $\overline{\omega}$ is the deterministic output power of wind turbine. The optimal *TOC* which is robust in the confrontation with worst uncertain conditions of UCP satisfies all constraints are as Tables 7.11 and 7.12.

$$\text{Level of factor}\begin{cases} 1 & 0.6^{*}\overline{\omega} \\ 2 & \min\left(1.2\overline{\omega}, p_{\max}^{w}\right) \end{cases} \tag{7.40}$$

$p_{\max}^{w}$ is maximum power of wind turbine.

Table 7.10 Orthogonal arrays for $L_{32}2^{31}$ [30]

	1	2	3	4	5	6	7	8	9	10	11	12	13	14	15	16	17	18	19	20	21	22	23	24
1	1	1	1	1	1	1	1	1	1	1	1	1	1	1	1	1	1	1	1	1	1	1	1	1
2	1	1	1	1	1	1	1	1	1	1	1	1	1	1	1	2	2	2	2	2	2	2	2	2
3	1	1	1	1	1	1	1	2	2	2	2	2	2	2	2	1	1	1	1	1	1	1	1	2
4	1	1	1	1	1	1	1	2	2	2	2	2	2	2	2	2	2	2	2	2	2	2	2	1
5	1	1	1	2	2	2	2	1	1	1	1	2	2	2	2	1	1	1	1	2	2	2	2	1
6	1	1	1	2	2	2	2	1	1	1	1	2	2	2	2	2	2	2	2	1	1	1	1	2
7	1	1	1	2	2	2	2	2	2	2	2	1	1	1	1	1	1	1	1	2	2	2	2	2
8	1	1	1	2	2	2	2	2	2	2	2	1	1	1	1	2	2	2	2	1	1	1	1	1
9	1	2	2	1	1	2	2	1	1	2	2	1	1	2	2	1	1	2	2	1	1	2	2	1
10	1	2	2	1	1	2	2	1	1	2	2	1	1	2	2	2	2	1	1	2	2	1	1	2
11	1	2	2	1	1	2	2	2	2	1	1	2	2	1	1	1	1	2	2	1	1	2	2	2
12	1	2	2	1	1	2	2	2	2	1	1	2	2	1	1	2	2	1	1	2	2	1	1	1
13	1	2	2	2	2	1	1	1	1	2	2	2	2	1	1	1	1	2	2	2	2	1	1	1
14	1	2	2	2	2	1	1	1	1	2	2	2	2	1	1	2	2	1	1	1	1	2	2	2
15	1	2	2	2	2	1	1	2	2	1	1	1	1	2	2	1	1	2	2	2	2	1	1	2
16	1	2	2	2	2	1	1	2	2	1	1	1	1	2	2	2	2	1	1	1	1	2	2	1
17	2	1	2	1	2	1	2	1	2	1	2	1	2	1	2	1	2	1	2	1	2	1	2	1
18	2	1	2	1	2	1	2	1	2	1	2	1	2	1	2	2	1	2	1	2	1	2	1	2
19	2	1	2	1	2	1	2	2	1	2	1	2	1	2	1	1	2	1	2	1	2	1	2	2
20	2	1	2	1	2	1	2	2	1	2	1	2	1	2	1	2	1	2	1	2	1	2	1	1
21	2	1	2	2	1	2	1	1	2	1	2	2	1	2	1	1	2	1	2	2	1	2	1	1
22	2	1	2	2	1	2	1	1	2	1	2	2	1	2	1	2	1	2	1	1	2	1	2	2
23	2	1	2	2	1	2	1	2	1	2	1	1	2	1	2	1	2	1	2	2	1	2	1	2
24	2	1	2	2	1	2	1	2	1	2	1	1	2	1	2	2	1	2	1	1	2	1	2	1
25	2	2	1	1	2	2	1	1	2	2	1	1	2	2	1	1	2	2	1	1	2	2	1	1

(continued)

Table 7.10 (continued)

	1	2	3	4	5	6	7	8	9	10	11	12	13	14	15	16	17	18	19	20	21	22	23	24
26	2	2	1	1	2	2	1	1	2	21	1	1	2	2	1	2	1	1	2	2	1	1	2	2
27	2	2	1	1	2	2	1	2	1	1	2	2	1	1	2	1	2	2	1	1	2	2	1	2
28	2	2	1	1	2	2	1	2	1	1	2	2	1	1	2	2	1	1	2	2	1	1	2	1
29	2	2	1	2	1	1	2	1	2	2	1	2	1	1	2	1	2	2	1	2	1	1	2	1
30	2	2	1	2	1	1	2	1	2	2	1	2	1	1	2	2	1	1	2	1	2	2	1	2
31	2	2	1	2	1	1	2	2	1	1	2	1	2	2	1	1	2	2	1	2	1	1	2	2
32	2	2	1	2	1	1	2	2	1	1	2	1	2	2	1	2	1	1	2	1	2	2	1	1

Table 7.11 Optimal output power of generation units

	Units									
Hour	1	2	3	4	5	6	7	8	9	10
1	416	150.3	0	0	0	0	0	0	0	0
2	453	188	0	0	0	0	0	0	0	0
3	454.9	276.8	0	0	0	0	0	0	0	0
4	454.2	407.7	0	0	0	0	0	0	0	0
5	454.7	387.8	55.6	0	0	0	0	0	0	0
6	454.6	413.9	103.6	0	0	0	26.1	0	0	0
7	453.4	389.6	61.4	88.3	0	0	25.3	0	0	0
8	454	423.5	61.7	112.3	0	0	25.2	0	0	0
9	455	454.5	124.3	126.2	0	39.5	25.7	0	0	0
10	451.2	454.7	97.2	122.4	60.9	23	27.4	0	0	0
11	454.8	453.9	96.7	122.9	120	20.6	25.3	0	0	0
12	454.8	453.8	122.9	123.4	136.3	23.1	25.7	0	0	0
13	454.9	453.4	75	119.7	128.1	22.4	0	0	0	0
14	454.8	438.9	81.5	117.4	26.9	20.83	0	0	0	0
15	453.9	345.1	125.8	0	52.5	0	0	0	0	0
16	454.7	315.5	112	0	27.5	0	0	0	0	0
17	454.6	356	62.8	0	0	0	0	0	0	0
18	454.7	446.8	108.4	0	0	0	0	0	0	0
19	454.7	453.3	124.1	0	0	23.75	0	0	0	0
20	453.5	444.8	109.7	127.1	0	31	0	0	0	0
21	453.6	437.7	76.2	39.3	0	21.3	0	0	0	0
22	453.3	312.6	106.1	108.3	0	20.1	0	0	0	0
23	454.6	245.8	62.1	39.3	0	0	0	0	0	0
24	454.7	151.3	0	42.4	0	0	0	0	0	0
TOC' ($)	16,322,491.3									

According to results of Tables 7.11 and 7.12, all constraints are satisfied. The combination of units shown in the two above tables is robust against variations of wind turbine output and presents the optimal combination. In Table 7.13, *TOC* of all scenarios is presented.

7.7 Conclusions

In this chapter, UCP was solved by IGDT and RO. The aim of this chapter was considering UCP in the presence of uncertainties. For this purpose TOAT and IGDT are used in order to search the optimal solution of this problem in the presence of different uncertainties. When the historical data of demanded load are needed, the TOAT and IGDT methods are the most suitable methods for UCP because these methods do not need the past data of system. Obtained results by both methods were

Table 7.12 Optimal storage power and injection power of ESSs

Hour	$p_{s,es}$	$p_{g,es}$
1	69.3	0
2	33	19.5
3	27	7.8
4	27.3	0.3
5	27.4	17.2
6	13.7	3.4
7	14.2	3.2
8	6.1	12.5
9	17.6	8.5
10	5.3	7.4
11	4.2	23
12	0.4	26.4
13	17	12.4
14	1.7	5.2
15	1.2	23
16	24.5	13.8
17	16.2	11.7
18	18.2	13.8
19	6.3	22.8
20	1.3	53.3
21	17.7	43.4
22	0.4	12.6
23	26	5.1
24	0.1	32.2
p_{rsp}(MW)	0.8	

Table 7.13 Calculated TOC ($) for all scenarios

Scenario	*TOC*	Scenario	*TOC*
1	504,330	17	506,040
2	513,340	18	513,960
3	513,090	19	513,780
4	506,740	20	506,340
5	506,000	21	506,620
6	514,030	22	514,160
7	514,260	23	513,820
8	506,930	24	506,000
9	506,690	25	506,390
10	513,380	26	513,770
11	515,060	27	513,940
12	506,390	28	505,960
13	506,380	29	506,050
14	514,540	30	513,570
15	514,130	31	513,850
16	506,930	32	506,010

presented. The results show that when IGDT is used, the planner will be sure to obtain the solutions which will not be affected by the variation of output power of wind turbines. Also by using TOAT, we can find the best TOC for variation bound of uncertainty parameter which are determined by the operator. Generally RO methods change the SUCP to DUCP, and this subject can significantly reduce the running time compared to the stochastic methods. Finally, the results confirm the capability of the suggested methods in solving the robust unit commitment in an uncertain environment.

Appendices

Table 7.14 Abbreviations and symbols

TOC	Total operation cost	T_{cc}	Cold startup time
t	Time period scheduling index	$T_{off,n}$	Total downtime
T	Time horizon of study	$T_{on,n}$	Total uptime
N	Number of generation units	$p_{s,es}^{t}$	Storage power of n-th ESS at t-th hour
n	Generation unit index	N_s	Number of ESSs
F_n	Cost function of generation unit n	$p_{n,\min}$	Minimum output power of n-th generation unit
p_n^t	Output power of generation unit n at hour t	$p_{n,\max}$	Maximum output power of n-th generation unit
u_n^t	On/off status of generating unit n in hour t	d_t	Power demand of t-th hour
s_n^t	Startup cost of n-th unit at t-th hour	MUT_n	Minimum uptime
a_n,b_n, c_n	Cost function coefficient of n-th unit	MDT_n	Minimum downtime
HSC	Hot startup cost	RU_n	Ramp up rate of n-th generation unit
CSC	Cold startup cost	RD_n	Ramp down rate of n-th generation unit
w	Wind turbine index	SR	Spinning reserve
W	Number of wind turbine	p_{rsp}	Reminded stored power
F_w	Cost function of wind turbine w	F_{es}	Cost function of energy storage system
p_w^t	Output power of wind turbine w and hour h	$p_{g,es}^{t}$	Injection power of n-th ESS at t-th hour
es	Energy storage system index		

Table 7.15 Output power of wind turbines

Hour	p_{w1}	p_{w2}	p_{w3}	p_{w4}
1	101.5	101.5	0	203
2	61.25	61.25	0	122.5
3	43.75	43.75	0	87.5
4	57.5	57.5	0	115
5	56	56	0	112
6	56	56	0	112
7	70	70	3	143
8	56	56	5	117
9	38.5	38.5	7	84
10	73.5	73.5	14	161
11	59.5	59.5	18	137
12	56	56	22	134
13	63	63	25	151
14	63	63	30	156
15	87.5	87.5	26	201
16	66.5	66.5	18	151
17	59.5	59.5	12	131
18	43.75	43.75	7	94.5
19	61.25	61.25	5	127.5
20	91	91	0	182
21	98	98	0	196
22	43.75	43.75	0	87.5
23	59.5	59.5	0	119
24	59.5	59.5	0	119

References

1. Shahbazitabar, M., & Abdi, H. (2017). A solution to the unit commitment problem applying a hierarchical combination algorithm. *Journal of Energy Management and Technology, 1*(2), 12–19.
2. Saravanan, B., et al. (2013). A solution to the unit commitment problem—A review. *Frontiers in Energy, 7*(2), 223–236.
3. Tahanan, M., et al., (2014). *Large-scale unit commitment under uncertainty: A literature survey*. Pisa, IT: Università di Pisa.
4. Abdi, H., Moradi, A., & Saleh, S. (2015). Optimal unit commitment of renewable energy sources in the micro-grids with storage devices. *Journal of Intelligent & Fuzzy Systems, 28*(2), 537–546.
5. Zheng, Q. P., Wang, J., & Liu, A. L. (2015). Stochastic optimization for unit commitment—A review. *IEEE Transactions on Power Systems, 30*(4), 1913–1924.
6. Shi, J., & Oren, S. S. (2018). Stochastic unit commitment with topology control recourse for power systems with large-scale renewable integration. *IEEE Transactions on Power Systems, 33*(3), 3315–3324.
7. Blanco, I., & Morales, J. M. (2017). An efficient robust solution to the two-stage stochastic unit commitment problem. *IEEE Transactions on Power Systems, 32*(6), 4477–4488.
8. Bakirtzis, E. A., et al. (2018). Storage management by rolling stochastic unit commitment for high renewable energy penetration. *Electric Power Systems Research, 158*, 240–249.

9. Pozo, D., Contreras, J., & Sauma, E. E. (2014). Unit commitment with ideal and generic energy storage units. *IEEE Transactions on Power Systems, 29*(6), 2974–2984.
10. Alizadeh, M. I., Moghaddam, M. P., & Amjady, N. (2018). Multistage multiresolution robust unit commitment with nondeterministic flexible ramp considering load and wind variabilities. *IEEE Transactions on Sustainable Energy, 9*(2), 872–883.
11. Zhou, M., et al. (2018). *Multi-objective unit commitment under hybrid uncertainties: A data-driven approach*. In Networking, Sensing and Control (ICNSC), 2018 IEEE 15th International Conference on, IEEE.
12. Aghaei, J., et al. (2017). Optimal robust unit commitment of CHP plants in electricity markets using information gap decision theory. *IEEE Transactions on Smart Grid, 8*(5), 2296–2304.
13. Jiang, R., Wang, J., & Guan, Y. (2012). Robust unit commitment with wind power and pumped storage hydro. *IEEE Transactions on Power Systems, 27*(2), 800.
14. Zhao, C., et al. (2013). Multi-stage robust unit commitment considering wind and demand response uncertainties. *IEEE Transactions on Power Systems, 28*(3), 2708–2717.
15. Abujarad, S. Y., Mustafa, M., & Jamian, J. (2017). Recent approaches of unit commitment in the presence of intermittent renewable energy resources: A review. *Renewable and Sustainable Energy Reviews, 70*, 215–223.
16. Hosseini, S. H., Khodaei, A., & Aminifar, F. (2007). A novel straightforward unit commitment method for large-scale power systems. *IEEE Transactions on Power Systems, 22*(4), 2134–2143.
17. Shahbazitabar, M., & Abdi, H. (2018). A novel priority-based stochastic unit commitment considering renewable energy sources and parking lot cooperation. *Energy*. https://doi.org/10.1016/j.energy.2018.07.025.
18. Othman, M., et al. (2015). Solving unit commitment problem using multi-agent evolutionary programming incorporating priority list. *Arabian Journal for Science and Engineering, 40*(11), 3247–3261.
19. Sen, S., & Kothari, D. P. (1998). Optimal thermal generating unit commitment: A review. *Electrical Power & Energy Systems, 20*(7), 443–451.
20. Sheble, G. B., & Fahd, G. N. (1994). Unit commitment literature synopsis. *IEEE Transactions on Power Systems, 9*(1), 128–135.
21. Saber, A., et al. (2007). Unit commitment computation by fuzzy adaptive particle swarm optimisation. *IET Generation, Transmission & Distribution, 1*(3), 456–465.
22. Chandrasekaran, K., et al. (2012). Thermal unit commitment using binary/real coded artificial bee colony algorithm. *Electric Power Systems Research, 84*(1), 109–119.
23. Dieu, V. N., & Ongsakul, W. (2008). Ramp rate constrained unit commitment by improved priority list and augmented Lagrange Hopfield network. *Electric Power Systems Research, 78*(3), 291–301.
24. Zhu, J. (2015). *Optimization of power system operation* (Vol. 47). New Jersey, USA: John Wiley & Sons, IEEE Press.
25. Soroudi, A., & Amraee, T. (2013). Decision making under uncertainty in energy systems: State of the art. *Renewable and Sustainable Energy Reviews, 28*, 376–384.
26. Goldberg, D. E., & Holland, J. H. (1988). Genetic algorithms and machine learning. *Machine Learning, 3*(2), 95–99.
27. Ben-Haim, Y. (2006). *Info-gap decision theory: Decisions under severe uncertainty*. Great Britain: Elsevier.
28. Hong, Y.-Y., Lin, F.-J., & Yu, T.-H. (2016). Taguchi method-based probabilistic load flow studies considering uncertain renewables and loads. *IET Renewable Power Generation, 10*(2), 221–227.
29. Kazarlis, S. A., Bakirtzis, A., & Petridis, V. (1996). A genetic algorithm solution to the unit commitment problem. *IEEE Transactions on Power Systems, 11*(1), 83–92.
30. https://www.york.ac.uk/depts/maths/tables/orthogonal.htm

Chapter 8
IGDT-Based Robust Operation of Integrated Electricity and Natural Gas Networks for Managing the Variability of Wind Power

Mohammad Amin Mirzaei, Ahmad Sadeghi-Yazdankhah, Morteza Nazari-Heris, and Behnam Mohammadi-ivatloo

Nomenclatures

Index:	
t	Time period index
i	Thermal plants index
l	Natural gas loads index
r	Wind power plant index
sp	Natural gas suppliers index
pl	Pipelines index
m,n	Nodes index in natural gas network
b,b'	Buses index
j	Loads index
L	Transmission lines index
Constants:	
NT	Total time period
NGL	Total natural gas loads
NU	Total thermal plants
NGS	Total natural gas suppliers
NR	Total wind farms
NB	Number of buses
GU	Set of natural gas-fired units

(continued)

M. A. Mirzaei · M. Nazari-Heris (✉) · B. Mohammadi-ivatloo
Faculty of Electrical and Computer Engineering, University of Tabriz, Tabriz, Iran
e-mail: ma_mirzaei@sut.ac.ir; m.nazari@ieee.org; bmohammadi@tabrizu.ac.ir

A. Sadeghi-Yazdankhah
Department of Electrical Engineering, Sahand University of Technology, Tabriz, Iran
e-mail: sadeghi@sut.ac.ir

B. Mohammadi-ivatloo, M. Nazari-Heris (eds.), *Robust Optimal Planning and Operation of Electrical Energy Systems*,
https://doi.org/10.1007/978-3-030-04296-7_8

$\alpha_i,\beta_i,\gamma_i$	Fuel function coefficient of gas-fired units
$P_i^{\max},P_i^{\min}$	Min/max capacity of thermal plant i
RU_i,RD_i	Ramp up/down limitation of thermal plant i
T_i^{On}, T_i^{Off}	Minimum up/down time of plant i
X_L	Reactance of line L
$PF_L^{\max}$	Capacity of line L
$\widehat{P_{r,\ t}}$	Forecasted wind power production at time t
$P_{r,\ t}$	Wind power production at time t
$D_{j,t}$	Expected hourly load
C_{pl}	Constant of pipeline pl
$\pi_m^{\max}, \pi_m^{\min}$	Maximum/minimum pressure
$U_{sp}^{\max}, U_{sp}^{\min}$	Maximum/minimum natural gas injection
$L_l^{\max}, L_l^{\min}$	Maximum/minimum natural gas load
Variables:	
F_i^C	Operation cost of thermal plant i
SU_i,SD_i	Start-up/shutdown cost of thermal plant i
$F_{i,t}^{\text{gas unit}}$	Fuel function of gas-fired plant i at time t
$P_{i,t}$	Production power of plant i
$I_{i,t}$	Binary on/off condition indicator of plant i
$X_{i,t-1}^{on}, X_{i,t-1}^{off}$	On/off time of plant i
$\pi_{m,t}$	Pressure of natural gas in node m at time t
$U_{sp,t}$	Gas delivery of supplier at time t
$F_{pl,t}$	Natural gas flow of pipeline pl at time t
$L_{l,t}$	Natural gas load at time t
$P_{r,t}$	Dispatched wind power
$PF_{L,t}$	Line flow at line L
$\delta_{b,t}$	Voltage angle of network buses

8.1 Introduction

Utilization of renewable sources especially wind energy because of environmental concerns is attracting more attention. To respond the uncertainties of wind power production, flexibility of power system operation should be increased. Several efficient approaches have been performed to enable the power system to increase its flexibility in operation. Operation improvement by applying algorithms and modern models to solve unit commitment and economic dispatch problems and improved wind power prediction [1, 2], utilizing flexible sources such as demand response (DR) [3], energy storage system (ESS) [4], and the use of power plants with fast starting capability such as gas turbine-based power plants [5], are some of these approaches.

Modern gas-fired power plants have start-up times of less than an hour and ramp rates more than 50 MW/min., while nuclear and coal-fueled plants have start-up times of 4–8 hours and ramp rates of megawatt per minute [6, 7]. Also, from environmental viewpoint, gas-fueled plants produce 50–60% less Co_2 [8]. Natural gas consumption for electricity generation in the USA has been increased from 34% in 2011 to 39% in 2012, while natural gas-fueled power plants have produced 40% of the total power capacity in 2012 [9]. According to Annual Outlook document 2014, estimated 16% of total electricity production in the USA at 2040 would be based on natural gas [8].

Independent system operator (ISO) performs security-constrained unit commitment (SCUC) in electricity markets to minimize system operation cost considering security constraints. Severe dependency of electric network to natural gas puts forward new issues to the ISOs. Pressure reduction at gas network nodes could cause some reduction in power generation decreasing system reliability and increasing operating cost. From the other point of view, natural gas delivery to residential and commercial loads has high priority with respect to gas-fueled plants. Therefore, increasing natural gas consumption by residential and commercial loads especially in winters reduces power generation by gas-fueled plants and increases electricity price.

In recent years, considerable research has been focused on coordinated operation of electricity and natural gas networks [10]. For example, in [11, 12], interdependency of natural gas network and power system security in solving SCUC problem has been studied, while system uncertainties are not considered. SCUC problem for coordinated electricity and natural gas infrastructures has been solved in [13], considering network load and line outage uncertainties. In [14], the authors have studied the effect of hourly price-based DR on the reduction of interdependency of natural gas network and power system, and operation cost using stochastic day-ahead scheduling of the coordinated system. In this research, uncertainties of load prediction and transmission line outage are included. In [15], coordination of interdependent electricity and natural gas networks for firming the variability of wind energy has been studied by solving stochastic day-ahead scheduling. In [16], a two-stage robust constrained operation of integrated electricity natural gas system is proposed considering possible N-k contingencies and distributed natural gas storage. A problem of robust coordination of interdependent electricity and natural gas systems in day-ahead scheduling has been investigated in [17] with combination of wind energy and power to gas technology.

The economical analysis of electrical energy systems is influenced by considering uncertainties of the system parameters. Operation of electrical energy systems is studied by approximating input data using different uncertainty handling methods. The most well-known methods implemented to study uncertain parameters include information-gap decision theory (IGDT) [18], robust optimization method [19, 20], interval-based analysis [21], two-point estimate method [22], and scenario-based modeling method [23]. The IGDT is a non-probabilistic interval optimization-based concept. Unlike Monte Carlo and scenario-based scheduling, the IGDT does not need the probabilistic distribution function of the uncertainty of wind power

production and is useful in robust decisions against severe uncertainties. The proposed method maximizes the bound of wind power generation uncertainty when setting decision variables so that the objective function lies inside the prescribed boundary. In power systems, IGDT is usually applied to bidding strategy of generation units, unit commitment, and DR scheduling [24]. In [25], IGDT is applied for self-scheduling of GenCos with the objective of maximizing the profit under electricity price uncertainty. Self-scheduling of a wind produce based on IGDT is performed in [26]. Optimal robust UC of CHP units in electricity markets is solved utilizing IGDT in [27]. In [28], the authors have solved IGDT-based robust security-constrained unit commitment using coordinated wind energy and flexible DR sources and ESS. In [29], SCUC is studied in the presence of lithium-ion battery storage units using IGDT considering load uncertainty.

Having understood all the above studies, the main features of the proposed model in this chapter are as follows:

- Considering natural gas network constraints and its impact on the participation of gas-fired units in energy market and their daily operation cost
- Using IGDT with no requirement of knowing the probabilistic distribution function (PDF) and membership of sets to model wind power uncertainty in SCUC problem of coordinated electricity and natural gas networks

The rest of the chapter is organized as follows: Sect. 8.2 presents the mathematical formulation of SCUC problem for coordinated electricity and gas networks. Section 8.3 describes IGDT technique and uncertainty modeling based on IGDT. Section 8.4 reports the obtained simulation results and discussions. Finally, Sect. 8.5 concludes the chapter.

8.2 Problem Formulation

The objective of the proposed SCUC for coordinated electricity and natural gas networks is determining the day-ahead hourly scheduling of gas-fueled power plants and network load to minimize operation cost of integrated wind power system. The objective function is provided in (8.1) determining total operation cost.

$$OF = \min \sum_{t=1}^{NT} \sum_{i=1}^{NU} \left(F_i^C(P_{i,t}) + SU_{i,t} + SD_{i,t} \right) \tag{8.1}$$

The problem constraints consist of the thermal units, power system, natural gas network, and interconnection of these two system constraints, which are discussed in the following.

8.2.1 Thermal Units and Power System Constraints

Generated power by each plant is limited to its maximum and minimum values as shown in (8.2). The ramp rates of units are dictated by (8.3) and (8.4). Minimum on/off time constraints for units are given in (8.5) and (8.6). Equation (8.7) represents power balance on each bus. Finally, transmitted power through the line and line capacity constraints are defined as (8.8) and (8.9), respectively.

$$P_i^{\min} I_{i,t} \le P_{i,t} \le P_i^{\max} I_{i,t} \tag{8.2}$$

$$P_{i,t} - P_{i,t-1} \le RU_i \tag{8.3}$$

$$P_{i,t-1} - P_{i,t} \le RD_i \tag{8.4}$$

$$\left(X_{i,t-1}^{on} - T_i^{on}\right)\ \left(I_{i,t-1} - I_{i,t}\right) \ge 0 \tag{8.5}$$

$$\left(X_{i,t-1}^{off} - T_i^{off}\right)\ \left(I_{i,t} - I_{i,t-1}\right) \ge 0 \tag{8.6}$$

$$\sum_{i=1}^{NU_b} P_{i,t} + \sum_{r=1}^{NR_b} P_{r,t} + \sum_{j=1}^{NJ_b} D_{j,t} = \sum_{l=1}^{NL_b} PF_{L,t} \tag{8.7}$$

$$PF_{L,t} = \frac{\left(\delta_{b,t} - \delta_{b',t}\right)}{X_L} \tag{8.8}$$

$$-PF_L^{\max} \le PF_{L,t} \le PF_L^{\max} \tag{8.9}$$

8.2.2 Natural Gas System Constraints

Gas transmission network transmits the natural gas from providers to natural gas consumers. Natural gas flow through the pipeline is defined as a second-order function of gas pressure at first and last end of the pipe given by (8.10) and (8.11). The value of constant pipeline factor $C_{m,n}$ depends on temperature, length, diameter, friction, and gas composition. Natural gas pressure at each node is limited to its maximum and minimum value as given in (8.12). Natural gas producers such as gas wells and/or gas storage units at the corresponding nodes have maximum and minimum values as shown in (8.13). Limit of natural gas load and natural gas balance at each node is given in (8.14) and (8.15), respectively.

$$F_{pl,t} = \mathrm{sgn}(\pi_{m,t}, \pi_{n,t})\ \ C_{m,n}\sqrt{\left|\pi_{m,t}^2 - \pi_{n,t}^2\right|} \tag{8.10}$$

$$\mathrm{sgn}(\pi_{m,t}, \pi_{n,t}) = \begin{cases} 1 & \pi_{m,t} \ge \pi_{n,t} \\ -1 & \pi_{m,t} \le \pi_{n,t} \end{cases} \tag{8.11}$$

$$\pi_m^{\min} \le \pi_{m,t} \le \pi_m^{\max} \tag{8.12}$$

$$U_{sp}^{\min} \le U_{sp,t} \le U_{sp}^{\max} \tag{8.13}$$

$$L_l^{\min} \le L_{l,t} \le L_l^{\max} \tag{8.14}$$

$$\sum_{sp=1}^{NGS_m} U_{sp,t} - \sum_{l=1}^{NGL_m} L_{l,t} = \sum_{pl=1}^{NPL_m} F_{pl,t} \tag{8.15}$$

8.2.3 *Electricity and Natural Gas Networks Coupling Constraints*

Gas-fired plants are the largest industrial users of natural gas, whose production capacity is dependent on natural gas transmission services. The value of natural gas consumed by the gas-fired units to generate electric power is reported in (8.16). Gas-fired units account as the main consumers of natural gas connected to natural gas network as (8.17). The daily consumption of natural gas by these units should not exceed the limit (8.18).

$$F_{i,t}^{\text{gas unit}} = \alpha_i + \beta_i P_{i,t} + \gamma_i P_{i,t}^2 \tag{8.16}$$

$$L_{l,t} = F_{i,t}^{\text{gas unit}} \quad i \in GU \tag{8.17}$$

$$\sum_{t=1}^{NT} F_{i,t}^{\text{gas unit}} \le \text{FU}_i^{\max} \quad i \in GU \tag{8.18}$$

8.3 IGDT-Based Uncertainty Modeling

In this chapter, wind power uncertainty is described using IGDT technique. The proposed method does not need unnecessary information such as the probabilistic distribution function of stochastic variables and fuzzy logic membership. Unlike other stochastic programming techniques which are based on scenario making, the results enhanced by IGDT technique are very precise and valuable. The following section describes the IGDT optimization technique.

$$f = \min_X \left(f(X, \Psi)\right) \tag{8.19}$$

$$H_i(X, \Psi) \le 0 \quad \forall i \in \Omega_{ineq} \tag{8.20}$$

$$G_i(X, \Psi) = 0 \quad \forall j \in \Omega_{eq} \tag{8.21}$$

$$\Psi \in U \tag{8.22}$$

where uncertain parameter Ψ is denoted as input and U describes the set of uncertainties in the behavior of uncertain input parameter. The objective function $f(X, \Psi)$ depends on decision variable X and uncertain input parameter Ψ. Mathematical description of the set of uncertainties is formulated as:

$$U = U\left(\overline{\Psi}, \alpha\right) = \left\{\Psi : \left|\frac{\Psi - \overline{\Psi}}{\overline{\Psi}}\right| \leq \alpha\right\} \tag{8.23}$$

where $\overline{\Psi}$ is the predicted value of Ψ. Also, α is defined as the maximum deviation of uncertain parameter from the predicted amount, which is denoted as unspecified radius of uncertainty for decision-making. Any strategy considering Eqs. 8.19, 8.20, 8.21, and 8.22 and assuming zero deviation is called base case (BC) and defined as:

$$f_b = \min_X \left(f\left(X, \overline{\Psi}\right)\right) \tag{8.24}$$

$$H_i\left(X, \overline{\Psi}\right) \leq 0 \quad \forall i \in \Omega_{ineq} \tag{8.25}$$

$$G_i\left(X, \overline{\Psi}\right) = 0 \quad \forall j \in \Omega_{eq} \tag{8.26}$$

Implementing the BC optimization strategy results some value for objective function which could not be reliable results, because practically α could be a different value than zero. Therefore, to respond to uncertain parameter by decision-maker, a risk-averse strategy should be performed. The following mathematical model describes the risk-averse strategy.

$$\mathfrak{R}_C = \max_X \ \alpha \tag{8.27}$$

$$H_i(X, \Psi) \leq 0 \quad \forall i \in \Omega_{ineq} \tag{8.28}$$

$$G_i(X, \Psi) = 0 \quad \forall j \in \Omega_{eq} \tag{8.29}$$

$$f(X, \Psi) \leq \Delta_C \tag{8.30}$$

$$\Delta_C = (1 + \beta_C) f_b(X, \Psi) \tag{8.31}$$

$$\left|\frac{\Psi - \overline{\Psi}}{\overline{\Psi}}\right| \leq \alpha \tag{8.32}$$

$$0 \leq \beta_C \leq 1 \tag{8.33}$$

where the critical value of objective function (Δ_C) which is system operation cost is determined by decision-maker as (8.30). $\mathfrak{R}_C$ is the uncertainty radius of Ψ. β_C is defined as the degree of robustness of operation cost increase with respect to base value and determined by decision-maker. As a result, IGDT-based robust SCUC for coordinated electricity and gas networks is represented as:

$$OF_b = \min\left\{\sum_{t=1}^{NT}\sum_{i=1}^{NU}\left(F_i^C(P_{i,t}) + SU_{i,t} + SD_{i,t}\right)\right\}_{P_{r,t}=P_{r,t}^{\wedge}} \quad \text{s.t. } 2-18 \tag{8.34}$$

where OF_b is objective function for deterministic case. In addition to (8.34), the following constraints should also be considered.

$$\mathfrak{R}_C = \max_X \alpha \quad \text{s.t. } 2-18 \tag{8.35}$$

$$OF \le (1+\beta_c)OF_b \tag{8.36}$$

$$P_{r,t} = \hat{P}_{r,t}(1-\alpha) \tag{8.37}$$

8.4 Case Study

In this chapter, a six-bus power system with a six-node gas network is used for testing the introduced model which is shown in Fig. 8.1. The proposed mixed-integer nonlinear programming (MINLP) model is applied in generalized algebraic modeling systems (GAMS) software and is solved employing DICOPT solver. The modified six-bus system consists of three gas-fired thermal units, seven transmission lines, and three loads that the specifications of units, transmission lines, and hourly load distribution are summarized in [11]. In addition, a wind power plant with maximum capacity of 20 MW is placed in bus 5. The unit start-up and shutdown costs are considered ignorable in this study [12]. The six-node system of natural gas includes five pipelines, two natural gas providers, and five natural gas. Natural gas loads include three natural gas-fired units and two residential gas loads. The specifications related to the six-node system of natural gas are provided in [12].

To have the simulation results, the following cases are considered:

Case 1: SCUC without considering natural gas network constraints
Case 2: SCUC with considering natural gas network constraints
Case 3: IGDT-SCUC with considering natural gas network constraints

Case 1 The natural gas system constraints are ignored in this case. The hourly commitment scheduling of units is shown in Fig. 8.2. The low-cost plant G1 is committed in the whole scheduling time interval. The expensive plant G2 is committed between hours 13 and 19. In addition, unit G3 is committed between 11 and 22. Daily operation cost is equal to $73,821.11 in this case.

Case 2 The natural gas network constraints are considered in this case. The scheduling of hourly commitment of plants is demonstrated in Fig. 8.3. Limitation of natural gas transmission has reduced hourly generation dispatch of unit G1 which

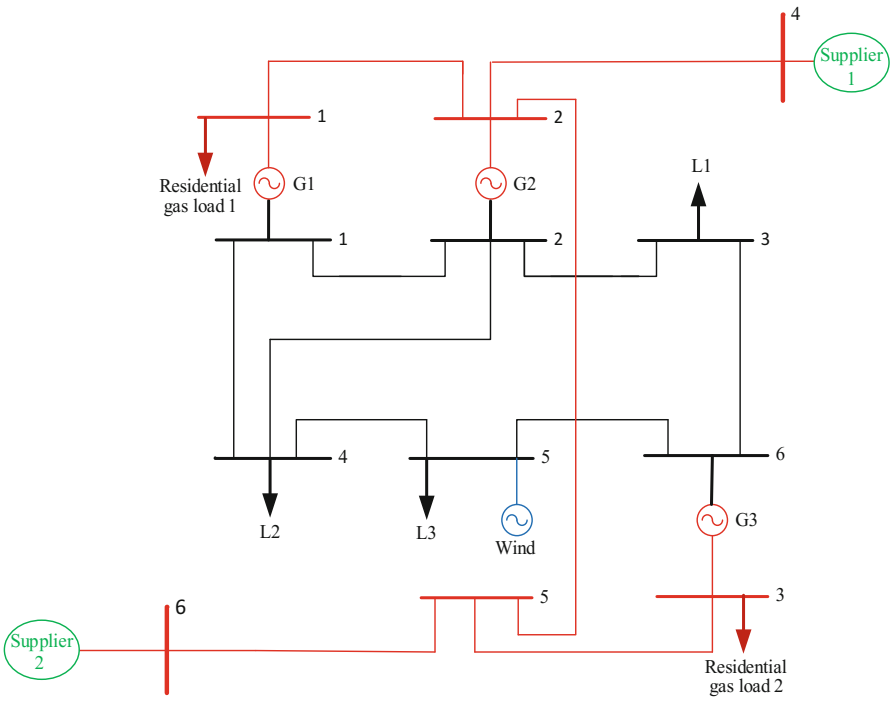

Fig. 8.1 Illustration of six-bus power system and six-node natural gas systems with wind

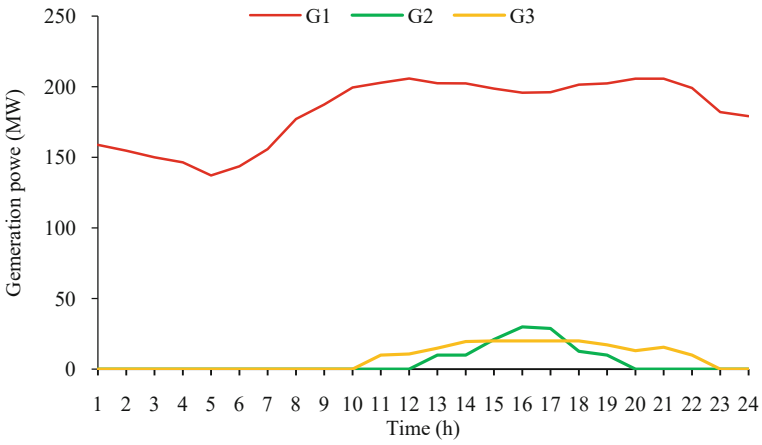

Fig. 8.2 Hourly generation dispatch of plants G1, G2, and G3 for case 1

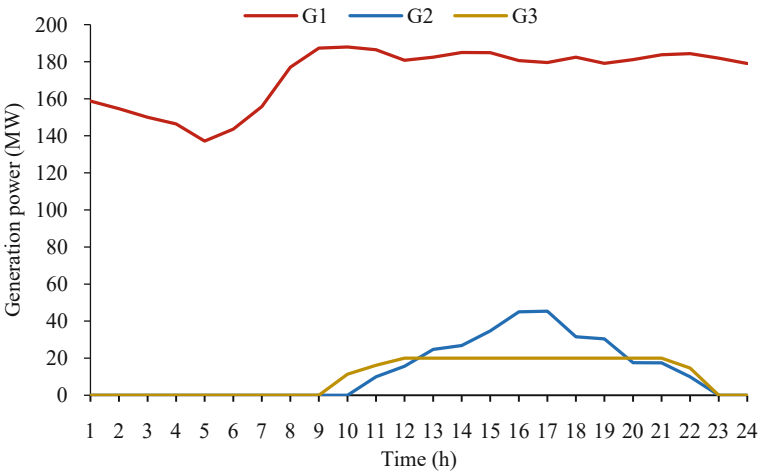

Fig. 8.3 Hourly generation dispatch of plants G1, G2, and G3 for case 2

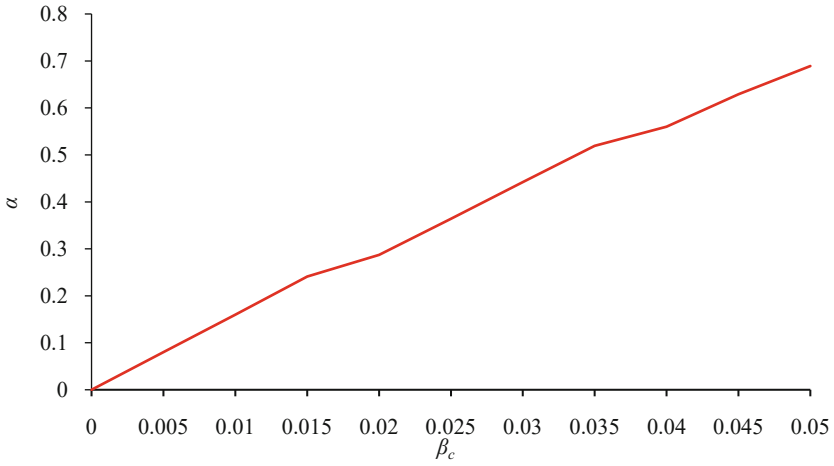

Fig. 8.4 Variation of optimal robustness function value (α) versus operation cost deviation factor (β_c)

has resulted in an increase in the hourly commitment of units G2 and G3, so that the total dispatched power by units G2 and G3 has increased from 313.46 MWh in case 1 to 551.33 MWh in this case. The daily operation cost in this case is $78,368.35, which has a dramatic increment in comparison with case 1.

Case 3 The wind power forecast uncertainty is considered in this case. We change β_c from 0 to 0.05 to investigate the impact of the critical operation cost (OF_c) on the hourly production of plants and the wind power robustness. OF_b is considered to be $78,368.35 (case 2). As shown in Fig. 8.4, by increasing β_c which has resulted in

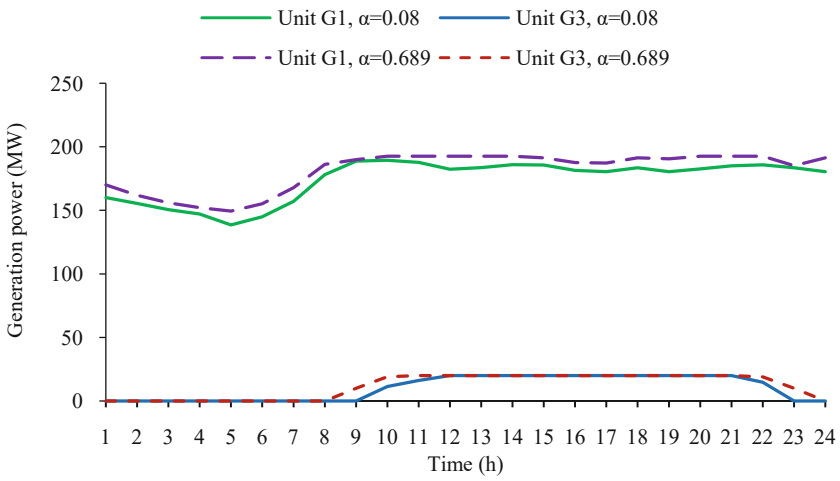

Fig. 8.5 Robust scheduling of plants G1 and G3 for two various values of α

an increase in critical operation cost, the value of α has increased. The robustness parameter also increases by increasing β_c showing a higher range of wind power forecast errors could be tolerated. As more explanation, for $\beta_c = 0.02$, $OF = (1+0.02) \times 78{,}368.35 = \$79{,}935.71$ is guaranteed if none of the hourly wind power forecast errors are more than α=0.28 or 28%. In addition, Fig. 8.5 shows the hourly generation dispatch of units G1 and G3 for two different values of α. As can be seen, by increasing the maximum radius of wind power uncertainty, hourly generation dispatch of units G1 and G3 has been increased which has resulted in an increase in the daily operation cost.

8.5 Conclusions

This chapter solved a problem of robust security-constrained unit commitment for coordinated electricity and natural gas networks with integration of wind power plant. The authors also modeled natural gas delivery to gas-fired units. Considering natural gas network model resulted in some increases in hourly participation of expensive units and also in daily operation cost. IGDT was implemented to characterize the wind power uncertainty faced by independent system operator (ISO). The introduced scheme enables ISO to adjust conservatism of the scheduling approach by changing the amount of the operation cost deviation factor. In fact, the proposed IGDT-based robust formulation determines a maximum critical operation cost if the hourly wind power fall within a robustness region.

References

1. Heydarian-Forushani, E., Golshan, M. E. H., Shafie-Khah, M., & Siano, P. (2018). Optimal operation of emerging flexible resources considering sub-hourly flexible ramp product. *IEEE Transactions on Sustainable Energy, 9*, 916–929.
2. Wang, Q., Wu, H., Florita, A. R., Martinez-Anido, C. B., & Hodge, B.-M. (2016). The value of improved wind power forecasting: Grid flexibility quantification, ramp capability analysis, and impacts of electricity market operation timescales. *Applied Energy, 184*, 696–713.
3. Wu, H., Shahidehpour, M., & Al-Abdulwahab, A. (2013). Hourly demand response in day-ahead scheduling for managing the variability of renewable energy. *IET Generation, Transmission and Distribution, 7*, 226–234.
4. Mingfei, B., Jilai, Y., Shahidehpour, M., & Yiyun, Y. (2017). Integration of power-to-hydrogen in day-ahead security-constrained unit commitment with high wind penetration. *Journal of Modern Power Systems and Clean Energy, 5*, 337–349.
5. Cui, H., Li, F., Hu, Q., Bai, L., & Fang, X. (2016). Day-ahead coordinated operation of utility-scale electricity and natural gas networks considering demand response based virtual power plants. *Applied Energy, 176*, 183–195.
6. Henderson, M. (2017). Energy system flexibility: The importance of being Nimble [from the editor]. *IEEE Power and Energy Magazine, 15*, 4–6.
7. Klimstra J., & Hotakainen, M. (2011). *Smart Power Generation*. 4th ed. Helsinki, Finland: Avain Publishers.
8. U. Energy. (2014). Information Administration, Annual Energy Outlook.
9. EIA. (2011). *Annual Energy Review* [Online], Available: http://www.eia.doe.gov/emeu/aer/
10. Khaligh, V., Oloomi-Buygi, M., Anvari-Moghaddam, A., & Guerrero, J. M. (2018, June 12–15). A leader-follower approach to gas-electricity expansion planning problem. IEEE 18th international conference on Environment and Electrical Engineering and 2nd Industrial and Commercial Power Systems Europe (EEEIC 2018), Palermo, Italy.
11. Li, T., Eremia, M., & Shahidehpour, M. (2008). Interdependency of natural gas network and power system security. *IEEE Transactions on Power Systems, 23*, 1817–1824.
12. Liu, C., Shahidehpour, M., Fu, Y., & Li, Z. (2009). Security-constrained unit commitment with natural gas transmission constraints. *IEEE Transactions on Power Systems, 24*, 1523–1536.
13. Alabdulwahab, A., Abusorrah, A., Zhang, X., & Shahidehpour, M. (2015). Stochastic security-constrained scheduling of coordinated electricity and natural gas infrastructures. *IEEE Systems Journal, 11*, 1674–1683.
14. Zhang, X., Shahidehpour, M., Alabdulwahab, A., & Abusorrah, A. (2016). Hourly electricity demand response in the stochastic day-ahead scheduling of coordinated electricity and natural gas networks. *IEEE Transactions on Power Systems, 31*, 592–601.
15. Alabdulwahab, A., Abusorrah, A., Zhang, X., & Shahidehpour, M. (2015). Coordination of interdependent natural gas and electricity infrastructures for firming the variability of wind energy in stochastic day-ahead scheduling. *IEEE Transactions on Sustainable Energy, 6*, 606–615.
16. He, Y., Shahidehpour, M., Li, Z., Guo, C., & Zhu, B. (2017). Robust constrained operation of integrated electricity-natural gas system considering distributed natural gas storage. *IEEE Transactions on Sustainable Energy, 9*, 1061–1071.
17. Chuan, H., Tianqi, L., Lei, W., & Shahidehpour, M. (2017). Robust coordination of interdependent electricity and natural gas systems in day-ahead scheduling for facilitating volatile renewable generations via power-to-gas technology. *Journal of Modern Power Systems and Clean Energy, 5*, 375–388.
18. Soroudi, A., & Keane, A. (2015). Risk averse energy hub management considering plug-in electric vehicles using information gap decision theory. In *Plug in electric vehicles in smart grids* (pp. 107–127). Singapore: Springer.

19. Nazari-Heris, M., Mohammadi-Ivatloo, B., Gharehpetian, G. B., & Shahidehpour, M. (2018). Robust short-term scheduling of integrated heat and power microgrids. *IEEE Systems Journal, 99*, 1–9.
20. Nazari-Heris, M., & Mohammadi-Ivatloo, B. (2018). Application of robust optimization method to power system problems. In *Classical and recent aspects of power system optimization* (pp. 19–32).
21. Marin, M., Milano, F., & Defour, D. (2017). Midpoint-radius interval-based method to deal with uncertainty in power flow analysis. *Electric Power Systems Research, 147*, 81–87.
22. Panigrahi, B. K., Sahu, S. K., Nandi, R., & Nayak, S. (2017, April). *Probabilistic load flow of a distributed generation connected power system by two point estimate method*. International conference on Circuit, Power and Computing Technologies (ICCPCT) (pp. 1–5), IEEE.
23. Nazari-Heris, M., Abapour, S., & Mohammadi-Ivatloo, B. (2017). Optimal economic dispatch of FC-CHP based heat and power micro-grids. *Applied Thermal Engineering, 114*, 756–769.
24. Zare, K., Moghaddam, M. P., & El Eslami, M. K. S. (2010). Demand bidding construction for a large consumer through a hybrid IGDT-probability methodology. *Energy, 35*, 2999–3007.
25. Mohammadi-Ivatloo, B., Zareipour, H., Amjady, N., & Ehsan, M. (2013). Application of information-gap decision theory to risk-constrained self-scheduling of GenCos. *IEEE Transactions on Power Systems, 28*, 1093–1102.
26. Moradi-Dalvand, M., Mohammadi-Ivatloo, B., Amjady, N., Zareipour, H., & Mazhab-Jafari, A. (2015). Self-scheduling of a wind producer based on information gap decision theory. *Energy, 81*, 588–600.
27. Aghaei, J., Agelidis, V. G., Charwand, M., Raeisi, F., Ahmadi, A., Nezhad, A. E., et al. (2017). Optimal robust unit commitment of CHP plants in electricity markets using information gap decision theory. *IEEE Transactions on Smart Grid, 8*, 2296–2304.
28. Nikoobakht, A., & Aghaei, J. (2016). IGDT-based robust optimal utilisation of wind power generation using coordinated flexibility resources. *IET Renewable Power Generation, 11*, 264–277.
29. Ahmadi, A., Nezhad, A. E., & Hredzak, B. (2018). Security-constrained unit commitment in presence of Lithium-Ion battery storage units using information-gap decision theory. *IEEE Transactions on Industrial Informatics*.

Chapter 9
Robust Short-Term Electrical Distribution Network Planning Considering Simultaneous Allocation of Renewable Energy Sources and Energy Storage Systems

Ozy D. Melgar-Dominguez, Mahdi Pourakbari-Kasmaei, and José Roberto Sanches Mantovani

Nomenclature

For quick reference, the main symbols are described in this nomenclature. Other symbols are described as needed in the main body.

A. Sets

Ω^{CB}	Set of capacities of capacitors banks
CT	Set of types of conductors
L	Set of network circuits
N	Set of network nodes
T	Set of time resolution
Y	Set of planning horizon (year)

O. D. Melgar-Dominguez (✉)
Department of Electrical Engineering, São Paulo State University-(UNESP), Ilha Solteira, São Paulo, Brazil

Department of Electrical Engineering and Automation, Aalto University, Espoo, Finland
e-mail: ozy.daniel@unesp.br

M. Pourakbari-Kasmaei
Department of Electrical Engineering and Automation, Aalto University, Espoo, Finland
e-mail: Mahdi.Pourakbari@aalto.fi

J. R. S. Mantovani
Department of Electrical Engineering, São Paulo State University-(UNESP), Ilha Solteira, São Paulo, Brazil
e-mail: mant@dee.feis.unesp.br

B. Mohammadi-ivatloo, M. Nazari-Heris (eds.), *Robust Optimal Planning and Operation of Electrical Energy Systems*,
https://doi.org/10.1007/978-3-030-04296-7_9

B. Parameters

DoD	Depth of discharging of the ESS unit
$\bar{E}^{ess}$	Maximum energy capacity defined by the ESS reservoir
$\hat{f}_t^D$	Mean value for the network demand consumption at time interval t
$\hat{f}_t^{G^{pv}}$	Mean value for the renewable output power at time interval t
$\bar{I}_a$	Maximum current flow limit for the conductor type a
l_{mn}	Length of the circuit mn
$\bar{M}^{pv}$	Maximum number of PV modules to be allocated
$P_{m,t,y}^D$	Active power demand at node m, time interval t, and year y
$\bar{P}^{pv}$	Maximum power capacity defined by each PV module
$\bar{P}^{ess}$	Allowed power rating by the ESS converting unit
$Q_{m,t,y}^D$	Reactive power demand at node m, time interval t, and year y
Q_b^{spc}	Predefined reactive power of the CB to be allocated of capacity b
$R\%$	Regulation range % of the VR to be allocated
R_a	Resistance of the conductor type a
$\bar{V}, \underline{V}$	Upper and lower limits of the voltage magnitude
X_a	Reactance of the conductor type a
Z_a	Impedance of the conductor type a
$\overline{\Phi}^S, \underline{\Phi}^S$	Upper and lower limits of the substation power factor
φ^{pv}	Predefined power factor for the PV-based DG source
$\zeta_b^{cb^{fx/sw}}$	Allocation cost of the CB fixed/switchable type of capacity b
$\zeta_{\dot{a},a}^{cr}$	Cost to replace the initial conductor $\dot{a}$ by the new type a
$\zeta_{t,y}^G$	Cost of the energy supplied by the substation at time interval t and year y
$\zeta_y^{o\&m^{ess}}$	Operating and maintenance costs of allocated of ESS at year y
$\zeta_y^{o\&m^{pv}}$	Operating and maintenance costs of allocated PV-based DG sources at year y
ζ^{pv}	Investment cost of PV-based DG sources
$\zeta^{pc^{ess}}$	Investment cost of power converter unit of the ESS
$\zeta^{rc^{ess}}$	Investment cost of energy reservoir capacity of the ESS
ζ^{vr}	Investment cost of VR allocation

C. Variables

$\bar{C}_m^{cb}$	Integer variable that defines the capacity of the installed CB at node m
$C_{m,t,y}^{cb}$	Integer variable that defines the number of modules in operation of the installed CB at node m, time t, and year y
$E_{m,t,y}^{ess}$	Stored energy of the installed ESS at node m, time t, and year y
$\tilde{E}_m^{ess}$	Energy storage capacity of the installed ESS at node m
f_t^D	Electricity demand factor at time interval t
$f_{t,y}^{G^{pv}}$	Renewable generation power factor at time interval t and year y
$\mathrm{I}_{mn,a,t,y}$	Variable that defines the square of current flow at circuit mn, cable a, time t, and year y

(continued)

M_m^{pv}	Integer variable that defines the number of installed PV modules at node m
$P_{mn,a,t,y}$	Active power flow at circuit mn, cable a, time interval t, and year y
$P_{m,t,y}^{ess^c}$	Charging active power of the installed ESS at node m, time interval t, and year y
$P_{m,t,y}^{ess^d}$	Discharging active power of the installed ESS at node m, time interval t, and year y
$\tilde{P}_m^{ess}$	Power capacity of the installed ESS in node m
$P_{m,t,y}^{pv}$	Available output power of the installed PV-based DG source at node m, time interval t, and year y
$P_{t,y}^{S}$	Active power supplied by the substation at time interval t and year y
$Q_{mn,a,t,y}$	Reactive power flow at circuit mn, cable a, time interval t, and year y
$Q_{m,t,y}^{cb}$	Reactive power supplied by the installed CB at node m, time interval t, and year y
$Q_{m,t,y}^{pv}$	Reactive power generated by the PV-based DG source at node m, time interval t, and year y
$Q_{t,y}^{S}$	Reactive power supplied by the substation at time interval t and year y
$U_{m,t,y}$	Variable that defines the square of the voltage magnitude at node m, time interval t, and year y
$\widehat{U}_{m,t,y}$	Auxiliary variable to control the square of voltage magnitude by the installed VR at node m, time interval t, and year y
$x_{mn,a}^{cr}$	Binary that defines the new conductor type a at circuit mn
x_m^{ess}	Binary variable that defines the allocation of ESS at node m
$x_{m,b}^{fx/sw}$	Binary variable that defines the type of CB (fixed or switchable) to be installed at node m of capacity b
x_m^{vr}	Binary variable that defines the VR allocation at node m

9.1 Introduction

Increasing the integration of renewable-based sources and the necessity of higher efficiency of the electrical distribution network (EDN) are the challenges that the distribution companies (DISCOs) are facing with and oblige them to improve the energy quality and obtain an efficient and low-carbon emission EDN. In technical terms, DISCOs should investigate strategies to satisfy several objectives simultaneously and ensure proper performance of the network and thus guarantee the supplied energy to end consumers. Consequently, the DISCO to fulfill the requirements and preferences of the consumers may use classical strategies such as short-term planning actions.

The short-term planning of EDN proposes investment alternatives for short horizon of 1 up to 5 years to effectively manage the voltage magnitude, network power factor, and active and reactive power flow and to reduce the energy losses of the network. To address these issues, some actions such as sizing and placement of capacitor banks (CBs), allocating of voltage regulators (VR), replacing of conductors at overloaded circuits, reconfiguration and load transfer among the feeders, and tap-changing of distribution transformers are usually applied in a

short-term plan [1–4]. On the other hand, finding a high-quality solution is another issue to be addressed. In this regard, several approaches have been proposed to solve this planning problem. These approaches can be classified by (1) the utilized solution method, (2) the objective to be optimized, and (3) the planning actions to be considered, among others [5].

In recent years, by considering the emergence of the renewable energy-based sources, the performance of the EDN has been altered mainly due to the prominent level of uncertainties associated with the intermittent operation of renewable energy-based technologies. To address this issue, sophisticated optimization techniques have been proposed to properly handle the uncertainty-based models in multiple instances. Due to the significant importance of determining an appropriate EDN expansion plan, several planning actions considering renewable energy-based sources integration have been explored [6]. To this end, the authors in [7] presented an integrated planning framework considering renewable-based dispatchable distributed generation (DG) units and reactive power support devices. To solve this problem, a hybrid approach taking the advantages of genetic algorithm (GA) and Tabu search method was used. To allocate renewable-based DG sources considering CBs, a non-dominated sorting GA was proposed in [8] while handling two criterion functions. In [9], a stochastic approach was proposed to maximize the hosting capacity of the renewable-based DG sources, without requiring a network upgrade. In this approach, the energy losses and load consumption were minimized considering the efficient energy usage. The authors in [10] proposed a two-stage stochastic mixed-integer conic programming approach to address the shortcoming of non-convex EDN planning models while taking into account renewable energy sources. Besides the conic model, a hybrid approach was also used in pre-solving stage to facilitate finding a feasible solution. However, the robust programming approach is an effective way to address the uncertainties and has been studied and applied in different fields. The electric power system, due to the huge amount of uncertainty, has dedicated plenty of attention to this paradigm [11]. A featured application was presented in [12] where a two-stage robust programming model was used for optimal placement of renewable energy-based DG sources in microgrids. In this approach, several cases were analyzed to show its applicability as a suitable planning tool. In [13], a transmission expansion planning problem was developed to address the uncertainty related to the demand growth and the availability of generation via a two-stage robust programming model. A strategic tool for energy storage placement in transmission network considering renewable energy-based sources was presented in [14]. In this proposal, the uncertainty was modeled via a discrete set, and by using two-stage robust programming, a hierarchical planning scheme was formulated. In [15], a two-stage robust optimization was developed to handle the electric distribution system planning scheme against natural disasters in which the most reliable plan under the worst-case scenario was determined. A trilevel multi-year convex planning model that identifies the timing of feeder's reinforcements and location and capacity of dispatchable/renewable wind-based DG sources was developed in [16]. To solve such complex model, a decomposition algorithm using primal and dual cutting planes was developed.

Therefore, to improve the convergence of the decomposition algorithm, the power flow equations were convexified to obtain a tractable trilevel model. Analogously, a two-stage robust programming model to solve the short-term planning problem considering renewable energy-based DG units was presented in [17]. In this proposal, an integrated planning scheme with multiple alternatives to improve the performance of an EDN was presented to duly address the uncertainties in demand and renewable energy production.

On the other hand, there is a mismatch of the time between renewable power generation and power demand. Thus, to address this mismatch, energy storage systems (ESSs) have been considered as a viable solution. These systems allow the storage of excess energy in periods with low demand to be utilized during the peak periods and, consequently, provide higher flexibility for the network. Additionally, such technology enables significant advantages such as frequency regulation, voltage control, and energy management, among others. Therefore, considering the advantages of this technology, the ESS planning problem has received compelling importance in the last decade, for which several approaches have been proposed [18]. In [19], an approach for sizing and placement of ESS problem in distribution systems was presented. The aim of this approach was reducing the voltage fluctuations as a result of high photovoltaic technology (PV) penetration, while a GA was used to solve the bi-level optimization model. A mixed-integer linear programming (MILP) model to represent the problem of siting and sizing of CBs, PV-based DG sources, and ESSs in EDN was developed in [20]. This approach was based on a deterministic environment where uncertainties relating to demand and renewable output power were considered via external indexes. A multi-objective optimization model was proposed in [21] aiming at optimal sizing and allocation of ESS taking into account minimizing the energy losses and total cost associated with the installation of renewable-based DG sources and ESS, simultaneously.

In this chapter, a reinforcement plan for electrical distribution network considering classical alternatives such as VR and CB allocation, conductor replacement, as well as sizing and placement of PV-based DG sources and ESSs is presented. These alternatives are duly represented in the optimization model where the cost of supplied energy and the total investment cost are minimized. Inherently, this optimization problem is represented by a non-convex mixed-integer nonlinear programming (MINLP) model. Although an efficient MINLP model via a resourceful recast method results in finding a proper solution, the globality of the optimal solution cannot be guaranteed [22]. Therefore, to handle such complex model and to guarantee the optimal global solution, linearization techniques are applied to obtain an approximated convex (MILP) model. To study the uncertainties related to the demand and solar irradiation of PV systems, the deterministic MILP formulation is transformed into a two-stage robust optimization model, and the problem becomes a trilevel framework. This trilevel optimization model is a tough problem which cannot be handled directly by using classical optimization techniques or commercial solvers. Consequently, the C&CG decomposition algorithm is applied in a hierarchical environment. To validate and analyze the effectiveness and potential of the proposed approach, a distribution network of 42-node is considered in detail.

Therefore, the significant contributions of this chapter can be summarized as follows:

- Proposing a suitable robust programming model for addressing the uncertainties related to the demand and renewable generation in the EDN planning problem. This approach ensures the fulfillment of technical and operational requirements against the worst realization within an uncertainty interval.
- Considering classical planning actions simultaneously with sizing and placement of PV-based DG sources and ESSs in the proposed robust decision-making tool to solve the short-term EDN planning problem. This provides a set of investment alternatives to ensure the quality and reliability of the energy provided for the end users.
- Applying an integrated hierarchical framework based on MILP models for short-term EDN planning problem that effectively guarantees the optimal global solution using available solvers.

9.2 Problem Formulation

Traditionally, planning actions such as allocating the CB and VR and replacing the conductors are performed to minimize technical energy losses and to enhance the voltage profile of the EDN. In this section, the short-term planning actions are considered with sizing and placement of ESS and renewable energy-based sources, specifically PV-based sources, simultaneously. Evidently, this problem is formulated as a non-convex MINLP model. To handle the non-convexity and nonlinearity, appropriate linearization techniques are used to obtain a mixed-integer linear programming (MILP) model in a deterministic environment. Due to the uncertainties of weather conditions and electricity demand, the solution obtained using this deterministic MILP model may not be accurate or practical if the forecasts are not precise. Hence, the uncertainties related to the renewable energy generation and demand are considered via a two-stage robust programming model.

9.2.1 EDN Steady-State Operation Constraints

The evaluation of the steady-state operating condition of an EDN is determined by using a power flow tool. This power flow provides a set of specific information of the EDN's state such as voltage magnitudes, active and reactive power flows, power losses, current flows in the branches, and phase angle for each node. Mathematically, this condition is represented by a set of nonlinear equations. To obtain its solution, iterative methods have been developed in the literature [23, 24]. This formulation can be used as a set of constraints in order to formulate a conventional optimization problem. Therefore, unlike these iterative methods, the steady-state operation point

of an EDN can be determined using classical optimization techniques. In this regard, a well-known approach to model the steady-state operation condition of an EDN is presented in this subsection. The following definitions should be declared before presenting the formulation:

(a) The EDN is represented by a monophasic equivalent system.
(b) The EDN operates with a radial topology.
(c) The EDN loads are represented by constant active and reactive power.

To formulate the power flow of an EDN, the voltage drop at the circuit mn is considered as the difference between the voltages at nodes m and n. This difference is related to the product of the current flow and the impedance of the circuit. Therefore, this expression is represented by (9.1):

$$\vec{V}_m - \vec{V}_n = \vec{I}_{mn}(R_{mn} + jX_{mn}) \tag{9.1}$$

where $mn \in L$ and L represents the set of circuits in the system and R_{mn} and X_{mn} represent the resistance and reactance at circuit mn, respectively. The current flow $\vec{I}_{mn}$ can be calculated using (9.2), which involves the active and reactive power flow P_{mn} and Q_{mn}, respectively:

$$\vec{I}_{mn} = \left(\frac{P_{mn} + jQ_{mn}}{\vec{V}_n}\right)^* \tag{9.2}$$

By substituting (9.2) in (9.1), the expression (9.3) is obtained:

$$\left(\vec{V}_m - \vec{V}_n\right)\vec{V}_n^{\,*} = (P_{mn} - Q_{mn})(R_{mn} + jX_{mn}) \tag{9.3}$$

Considering that $\vec{V} = V\angle\theta$ where V represents the voltage magnitude and θ stands for the phase angle, (9.3) can be written as (9.4):

$$V_m V_n(\cos\theta_{mn} + jsen\theta_{mn}) - V_n^2 = (P_{mn} - jQ_{mn})(R_{mn} + jX_{mn}) \tag{9.4}$$

Hence, by matching real and complex parts at both sides of (9.4), considering the square of the resulted expressions and using algebraic operations, (9.5) is obtained. It is worth noting that, in this formulation, the angle difference is not considered, and for this reason, this expression is defined by voltage magnitudes, current flow magnitudes, and active and reactive power flows:

$$V_n^2 - 2(R_{mn}P_{mn} + X_{mn}Q_{mn}) - Z_{mn}^2 I_{mn}^2 - V_m^2 = 0 \tag{9.5}$$

In order to calculate the current flow magnitude (I) at circuit mn, Equation (9.6) is used:

$$V_n^2 I_{mn}^2 = P_{mn}^2 + Q_{mn}^2 \tag{9.6}$$

Moreover, to conclude the steady-state operating representation, the balance of power flow at node m is represented by (9.7) and (9.8):

$$\sum_{nm \in L} P_{nm} - \sum_{mn \in L} \left(P_{mn} + R_{mn} I_{mn}^2\right) + P^S = P_m^D \tag{9.7}$$

$$\sum_{nm \in L} Q_{nm} - \sum_{mn \in L} \left(Q_{mn} + X_{mn} I_{mn}^2\right) + Q^S = Q_m^D \tag{9.8}$$

where P^S and Q^S are the supplied active and reactive power by the substation and P_m^D and Q_m^D are the active and reactive power demands at node m, respectively.

9.2.2 EDN Operational Constraints

To supply a high-quality service, operational limits in an EDN such as voltage magnitude, current flow magnitude, and substation power factor must be fulfilled. These constraints are shown in (9.9, 9.10, and 9.11), respectively:

$$\underline{V} \leq V_m \leq \overline{V}; \forall m \in N \tag{9.9}$$

$$0 \leq I_{mn} \leq \bar{I}_{mn}; \forall mn \in L \tag{9.10}$$

$$-P^S \tan\left(\cos^{-1}\underline{\Phi}^S\right) \leq Q^S \leq P^S \tan\left(\cos^{-1}\overline{\Phi}^S\right) \tag{9.11}$$

where in (9.9), $\underline{V}$ and $\overline{V}$ stand for the lower and upper bounds of the voltage magnitude; the current magnitude of circuit mn is bounded by the maximum current $\bar{I}_{mn}$ in (9.10); and in (9.11), the reactive power, supplied by the substation, is limited by the considering predefined lower and upper power factor bounds $\underline{\Phi}^S$ and $\overline{\Phi}^S$, respectively.

9.2.3 Planning Action Constraints

Investment alternatives such as VR allocation, replacement of overloaded circuits' conductor, and sizing and placement of CBs, PV-based DG sources, and ESSs are considered in an EDN to maximize its efficiency via a short-term plan. The planning horizon is represented by the set Y where this set contains all planning years y to be analyzed. In order to obtain an appropriate plan, a year y is represented by a time resolution T, which is divided into time intervals t that contain the information related to the demand, renewable energy output, and energy cost.

9.2.3.1 Capacitor Banks, Voltage Regulators, and Conductor Replacement

In technical terms, the CBs are classified as fixed and switchable devices. The fixed CBs provide reactive support, while the switchable brings greater flexibility to the system to avoid overvoltage in low-demand periods and undervoltage in peak-demand periods. Considering both CB types, the set Ω^{CB} contains characteristics such as the type of CB, capacity, and total investment cost associated with the type and capacity. The mathematical model of CB operation and allocation is described in (9.12, 9.13, 9.14, 9.15, 9.16, 9.17, and 9.18):

$$Q^{cb}_{m,t,y} = C^{cb}_{m,t,y} Q^{spc}_{b}; \forall m \in N, t \in T, y \in Y \tag{9.12}$$

$$0 \leq \bar{C}^{cb}_{m} \leq \sum_{b \in \Omega^{CB}} b x^{fx}_{m,b} + \sum_{b \in \Omega^{CB}} b x^{sw}_{m,b}; \forall m \in N \tag{9.13}$$

$$\bar{C}^{cb}_{m} \leq C^{cb}_{m,t,y} + \sum_{b \in \Omega^{CB}} b x^{sw}_{m,b}; \forall m \in N, t \in T, y \in Y \tag{9.14}$$

$$0 \leq C^{cb}_{m,t,y} \leq \bar{C}^{cb}_{m}; \forall m \in N, t \in T, y \in Y \tag{9.15}$$

$$\sum_{b \in \Omega^{CB}} x^{fx}_{m,b} + \sum_{b \in \Omega^{CB}} x^{sw}_{m,b} \leq 1; \forall m \in N \tag{9.16}$$

$$\sum_{b \in \Omega^{CB}} x^{fx}_{m,b} \leq 1; \sum_{b \in \Omega^{CB}} x^{sw}_{m,b} \leq 1; \forall m \in N \tag{9.17}$$

$$x^{fx}_{m,b}, x^{sw}_{m,b} \in \{0, 1\}; \forall m \in N \tag{9.18}$$

The reactive power injection $Q^{cb}_{m,t,y}$ for each installed CB in node m at time t of year y is defined by (9.12). This reactive power injection depends on the modules in operation, C^{cb}, and the specified reactive power Q^{spc}_{b} of the capacitor b. The capacity and capacitor type, fixed or switchable, to be allocated is determined by the products $b \cdot x^{fx}$ and $b \cdot x^{sw}$ in (9.13). To choose the best type of CB to be installed, constraints (9.14) and (9.15) are considered; CB is fixed if $C^{cb} = \bar{C}^{cb}$ and is switchable if $C^{cb} < \bar{C}^{cb}$. On the other hand, (9.16) is used to guarantee that only one type of CB can be installed at node m, while the capacity of the selected type of CB, fixed or switchable, is defined by (9.17). Finally, (9.18) represents that the decision variables should be binaries.

To allocate VR in an EDN, this device must operate in an appropriate regulation range to improve the voltage magnitude drop. Commercially, different regulation ranges can be found, and it is defined by $\pm R\%$; this regulation range adds more flexibility to adjust the voltage magnitude. The mathematical model of operation and allocation of VRs is represented as follows:

$$V_m = \left(1 + R\% \frac{tap_n}{Tap}\right) V_n \tag{9.19}$$

$$-x_n^{vr} Tap \leq tap_n \leq x_n^{vr} Tap \tag{9.20}$$

$$x_n^{vr} \in \{0,1\}; \forall n \in N \tag{9.21}$$

The controlled voltage magnitude at node n is represented by (9.19). The constraint (9.20) stands for the lower and upper bounds of the tap position, which should be an integer variable *tap*. The binary nature of the variable x_n^{vr} is defined by (9.21); this variable defines the location of the VR.

To obtain an economically optimal operation of EDN, the technical and financial characteristics of conductor types are prominent issues to be defined. This information is used for replacement of conductors of overloaded circuits. The optimal conductor replacement is done by choosing a type that its thermal capacity can endure peak loads considering the economic aspects. From this perspective, the set *CT* is developed, so that the conductor types, thermal capacity, and replacement cost are characterized. From the mathematical standpoint, this decision process is defined by the binary variable x_{mn}^{cr}. This variable defines that for circuit *mn*, the initial conductor $\dot{a}$ will be replaced by the new conductor type a and a replacement cost is associated.

9.2.3.2 PV-Based Sources and Energy Storage Systems

In this formulation, the PV is served for the renewable energy-based system. The PV-based DG source model, which is dependent on the cell temperature, transforms solar irradiance into the electricity. To site and size these sources in an EDN, the integer variable M_{m}^{pv} is used where m defines the location, and the value of $\bar{M}^{pv}$ defines the installed capacity. The mathematical model for sizing and placement of PV-based DG sources is represented as follows:

$$P_{m,t,y}^{pv} = M_m^{pv} \bar{P}^{pv} f_{t,y}^{G^{pv}}; \forall m \in N, t \in T, y \in Y \tag{9.22}$$

$$\left| Q_{m,t,y}^{pv} \right| \leq P_{m,t,y}^{pv} \tan\left(\cos^{-1} \varphi^{pv}\right); \forall m \in N, t \in T, y \in Y \tag{9.23}$$

$$0 \leq M_m^{pv} \leq \bar{M}^{pv}; \forall m \in N \tag{9.24}$$

The available PV output power that depends on the PV output power factor $\left(f_{t,y}^{G^{pv}}\right)$, the modules to be installed, and its maximum power capacity $\left(\bar{P}^{pv}\right)$ is represented in (9.22). To adjust reactive power injection, the injected active power and the predefined power factor (φ^{pv}) of PV-based DG sources are taken into account via (9.23). The size of each PV-based DG source is determined by (9.24) where the number of candidate modules to be installed is limited by $\bar{M}^{pv}$.

On the other hand, ESSs are categorized by the technology type, storage duration, and cost, among others. However, most of these characteristics can be defined in generic form for all types of ESSs. Generally, the operation of an ESS is modeled by

the power conversion module and the storage unit. In this work, these properties are considered in the mathematical model to optimally site and size these devices in an EDN. The mathematical model of operation and installation of an ESS is represented by (9.25, 9.26, 9.27, 9.28, 9.29, 9.30, and 9.31):

$$E^{ess}_{m,t,y} = \eta t P^{ess^c}_{m,t,y} - \frac{1}{\eta} t P^{ess^d}_{m,t,y} + E^{ess}_{m,t-1,y} - \rho E^{ess}_{m,t-1,y}; \forall m \in N, t \in T, y \in Y \quad (9.25)$$

$$\tilde{E}^{ess}_{m} DoD \leq E^{ess}_{m,t,y} \leq \tilde{E}^{ess}_{m}; \forall m \in N, t \in T, y \in Y \quad (9.26)$$

$$0 \leq P^{ess^d}_{m,t,y} \leq \tilde{P}^{ess}_{m}; \forall m \in N, t \in T, y \in Y \quad (9.27)$$

$$0 \leq P^{ess^c}_{m,t,y} \leq \tilde{P}^{ess}_{m}; \forall m \in N, t \in T, y \in Y \quad (9.28)$$

$$0 \leq \tilde{P}^{ess}_{m} \leq \bar{P}^{ess} x^{ess}_{m}; \forall m \in N \quad (9.29)$$

$$\bar{E}^{ess} x^{ess}_{m} \leq \tilde{E}^{ess}_{m} \leq \bar{E}^{ess} x^{ess}_{m}; \forall m \in N \quad (9.30)$$

$$x^{ess}_{m} \in \{0, 1\}; \forall m \in N \quad (9.31)$$

The stored energy of installed ESS at node m, time t, and year y is represented by (9.25). As can be seen from the right-hand side of (9.25), this stored energy depends on the charging and discharging energy (first and second terms, respectively), the previous state charge (third term), and also the self-discharge (fourth term). Initially, t = *1*, the state of charge is the minimum available stored energy, considering the depth of discharging (DoD). On the other hand, (9.26) defines the capacity of the ESS reservoir. The real power rating of the installed ESS is bounded by (9.27) and (9.28). It is worth mentioning that to site and size an ESS at node m, the maximum storage capacity ($\tilde{E}^{ess}_{m}$) and the allowed power rating ($\tilde{P}^{ess}_{m}$) are defined by (9.29) and (9.30). Therefore, the DISCO defines the maximum energy storage capacity and the allowed power rating, $\bar{P}^{ess}$ and $\bar{E}^{ess}$, respectively. The selected capacity depends on the EDN requirements and economic aspects. Finally, (9.31) guarantees the binary nature of the decision variable to site and size an ESS in the EDN.

9.2.4 Deterministic Optimization Model

This subsection presents the formulation of the proposed framework to obtain the most economical short-term plan of an EDN. In order to obtain a proper formulation, it is considered that the planning scheme is based on a central context, where all the alternatives are owned and operated by the DISCO. This planning model minimizes (1) energy cost supplied by the substation and (2) investment cost corresponding to the planning alternatives. Simultaneously, this model determines the (a) nominal capacity, location, and type of CBs to be installed; (b) optimal place of VRs controlling the voltage magnitude drop; (c) replacement of overloaded circuits'

conductor; (d) capacity, location, and number of PV-based DG sources to be installed; and (e) location, nominal capacity of the reservoir, nominal power rating, and number of ESSs to be installed.

The mathematical model to represent this planning problem is inherently a non-convex MINLP model. In order to remedy this issue, proper linearization methods are applied to obtain an approximated MILP model. Initially, steady-state operating constraints contain quadratic variables (V_m^2, I_{mn}^2); however, for the sake of simplicity, these quadratic variables are replaced by new variables as follows: $V_m^2 = U_m$ and $I_{mn}^2 = \mathrm{I}_{mn}$. In such a way in (9.6), the left-hand side term represents the product of new variables, $U\mathrm{I}$, and on the right-hand side are the summation of quadratic variables ($P_{mn}^2 + Q_{mn}^2$). In this regard, the right term of (9.6) is approximated using piecewise linearization, while in the left term, an estimated voltage magnitude can be used ($V_n^* = V_n^{nom}$), as can be seen in (9.37, 9.38, 9.39, 9.40, 9.41, 9.42, 9.43, 9.44, and 9.45). On the other hand, the expression (9.19) needs to be modified to consider the new variable representing the square of the voltage magnitude (U). In this regard, the left- and right-hand terms are squared, and using algebraic methods, the product of the square of the integer variable *tap* and U is obtained. Therefore, due to the complexity of this expression, an approximated model to represent the VR operation is utilized, (9.49) and (9.50). In this formulation, the tap steps are considered with continuous steps, for which the voltage magnitude at node n can vary within $\%R$.

The approximated MILP model is presented in (9.32–9.51). The objective function is presented in (9.32) and minimizes the (a) cost of the supplied energy by the substation (first term), where $\zeta_{t,y}^{G}$ stands for the cost, $\Delta P_{t,y}^{S}$ stands for the energy supplied, and Δ is the weight to convert a year to the predefined time intervals (8760/T); (b) investment cost which corresponds with the fixed and switchable CBs (second and third terms); (c) conductor replacement cost (fourth term); (d) investment cost which corresponds with the VR allocation (fifth term); (e) investment cost regarding the sizing and placement of PV-based DG sources and its corresponding operations and maintenance costs (sixth and seventh terms); and (f) investment cost of energy reservoir and power converter unit (eighth and ninth terms), where the ninth term includes the operating and maintenance costs:

$$\begin{aligned}\min & \sum_{t\in T}\sum_{y\in Y}\zeta_{t,y}^{G}\Delta P_{t,y}^{S} + \sum_{b\in\Omega^{CB}}\sum_{m\in N}\zeta_{b}^{cb^{fx}}x_{m,b}^{fx} + \sum_{b\in\Omega^{CB}}\sum_{m\in N}\zeta_{b}^{cb^{sw}}x_{m,b}^{sw} \\ & + \sum_{a\in CT}\sum_{l\in L}\zeta_{\dot{a},a}^{cr}l_{mn}x_{\mathrm{mn},a}^{cr} + \sum_{n\in N}\zeta^{vr}x_{n}^{vr} + \sum_{m\in N}\zeta^{pv}M_{m}^{pv} \\ & + \sum_{m\in N}\sum_{y\in Y}\zeta_{y}^{o\&m^{pv}}M_{m}^{pv} + \sum_{m\in N}\zeta^{rc^{ess}}\tilde{E}_{m}^{ess} + \sum_{m\in N}\left(\zeta^{pc^{ess}} + \sum_{y\in Y}\zeta_{y}^{o\&m^{ess}}\right)\tilde{P}_{m}^{ess}\end{aligned} \tag{9.32}$$

subject to (9.12, 9.13, 9.14, 9.15, 9.16, 9.17, 9.18, 9.22, 9.23, 9.24, 9.25, 9.26, 9.27, 9.28, 9.29, 9.30, and 9.31):

$$\sum_{mn\in L}\sum_{a\in CT}P_{mn,a,t,y}-\sum_{nm\in L}\sum_{a\in CT}\left(P_{nm,a,t,y}+R_a\mathrm{I}_{nm,a,t,y}\right)+P^{S}_{t,y}+P^{pv}_{m,t,y}+P^{ess^d}_{m,t,y}-P^{ess^c}_{m,t,y}=P^{D}_{m,t,y} \tag{9.33}$$

$$\sum_{mn\in L}\sum_{a\in CT}Q_{mn,a,t,y}-\sum_{nm\in L}\sum_{a\in CT}\left(Q_{nm,a,t,y}+X_a\mathrm{I}_{nm,a,t,y}\right)+Q^{S}_{t,y}+Q^{pv}_{m,t,y}+Q^{cb}_{m,t,y}=Q^{D}_{m,t,y} \tag{9.34}$$

$$U_{m,t,y}-\widehat{U}_{n,t,y}=2\sum_{a\in CT}\left[\left(R_aP_{mn,a,t,y}+X_aQ_{mn,a,t,y}\right)-\left(Z_al_{mn}\right)^2\mathrm{I}_{mn,a,t,y}\right] \tag{9.35}$$

$$-\sum_{t\in T}P^{S}_{t,y}\tan\left(\cos^{-1}\underline{\Phi}^{S}_{y}\right)\le\sum_{t\in T}Q^{S}_{t,y}\le\sum_{t\in T}P^{S}_{t,y}\tan\left(\cos^{-1}\overline{\Phi}^{S}_{y}\right) \tag{9.36}$$

$$\left(V^{*}_{n,t,y}\right)^2\mathrm{I}_{mn,a,t,y}=\sum_{r\in\kappa}m^{p}_{mn,a,r}\Delta^{P}_{mn,a,t,y,r}+\sum_{r\in\kappa}m^{q}_{mn,a,r}\Delta^{Q}_{mn,a,t,y,r} \tag{9.37}$$

$$P_{mn,a,t,y}=P^{+}_{mn,a,t,y}-P^{-}_{mn,a,t,y} \tag{9.38}$$

$$Q_{mn,a,t,y}=Q^{+}_{mn,a,t,y}-Q^{-}_{mn,a,t,y} \tag{9.39}$$

$$P^{+}_{mn,a,t,y}+P^{-}_{mn,a,t,y}=\sum_{r\in\kappa}\Delta^{P}_{mn,a,t,y,r} \tag{9.40}$$

$$Q^{+}_{mn,a,t,y}+Q^{-}_{mn,a,t,y}=\sum_{r\in\kappa}\Delta^{Q}_{mn,a,t,y,r} \tag{9.41}$$

$$0\le\Delta^{P}_{mn,a,t,y,r}\le\Delta^{S}_{mn} \tag{9.42}$$

$$0\le\Delta^{Q}_{mn,a,t,y,r}\le\Delta^{S}_{mn} \tag{9.43}$$

$$m^{p/q}_{mn,a,r}=(2r-1)\Delta^{S}_{mn} \tag{9.44}$$

$$\Delta^{S}_{mn}=\frac{V^{nom}\bar{I}}{\kappa} \tag{9.45}$$

$$\underline{V}^2\le U_{m,t,y}\le\overline{V}^2 \tag{9.46}$$

$$0\le\mathrm{I}_{mn,a,t,y}\le x^{cr}_{mn,a}\bar{I}^2_a \tag{9.47}$$

$$\sum_{a\in CT}x^{cr}_{mn,a}=1 \tag{9.48}$$

$$(1-R\%)^2\widehat{U}_{n,t,y}\le U_{n,t,y}\le(1+R\%)^2\widehat{U}_{n,t,y} \tag{9.49}$$

$$-\left(\overline{V}^2-\underline{V}^2\right)x^{vr}_{n}\le U_{n,t,y}-\widehat{U}_{n,t,y}\le\left(\overline{V}^2-\underline{V}^2\right)x^{vr}_{n} \tag{9.50}$$

$$x^{sw},x^{fx},x^{cr},x^{vr},x^{ess}\in\{0,1\} \tag{9.51}$$

where the following sets are considered for the model $m,n\in N$, $mn\in L$, $r\in\kappa$, $a\in CT$, $t\in T$, and $y\in Y$.

In this model, (9.33) and (9.34) represent the active and reactive power balance, respectively. In these equations, the integration of PV-based DG sources, ESSs, and CBs is duly represented. The voltage magnitude drop is represented by (9.35); this expression is the reformulation of (9.5) where the voltage drop is defined by the selected conductor *a* at circuit *mn*. To control the annual substation power factor, the expression (9.36) is considered. Equations (9.37, 9.38, 9.39, 9.40, 9.41, 9.42, 9.43, 9.44, and 9.45) represent the linear transformation of (9.6). In (9.37), the left-hand side terms stand for the approximations of the square values of P and Q using the variables Δ^P and Δ^Q, respectively, presented in (9.38, 9.39, 9.40, and 9.41). These variables represent blocks that denote the lengths of the discretized segments over the time. Partitions over the closed interval $\left[0, V^{nom}\bar{I}\right]$ are generated through these blocks where the summation of the discretized segments r should be equal to the sum of two nonnegative auxiliary variables presented in the left-hand side of (9.40) and (9.41). These blocks are limited by (9.42) and (9.43) where to satisfy the optimality conditions, each block should be filled sequentially in ascending order until it reaches the final point in the last segment, which is guaranteed by considering P^S in the objective function (9.32). Therefore, (9.6) can be approximated by linear expressions [25]. Finally, the parameter $m^{p/q}$ stands for the slope of the segment r in the linearization procedure, and it is defined by (9.44), where the maximum number of segments is determined by (9.45). To define the voltage magnitude and current limit expressions, (9.46) and (9.47) are considered, respectively. It is worth noting that, in (9.47), the binary variable x^{cr} was added to define the conductor type to be placed at circuit *mn*, considering the current capacity of this conductor where only one type can be selected (9.48). The mathematical model to allocate the VRs is represented by the linear expressions (9.49) and (9.50). In these constraints, it is assumed that the square of the voltage magnitude can vary due to $(1 \pm R\%)^2$; for the sake of simplicity, the tap position is considered as a continuous variable.

9.2.5 Robust Programming Approach

The deterministic model presented in the Sect. 9.2.4 requires accurate data related to output power operation of PV-based DG sources and electricity demand of an EDN. However, the error is an inseparable part of predictions, and then, a nonviable solution can be obtained from the deterministic model. Therefore, to consider the prediction errors, the deterministic model is transformed into a robust optimization model. The robust optimization determines an optimal immune solution under all the possible uncertainty realizations in a predetermined uncertainty interval [26]. Therefore, probability distribution functions are not required to represent uncertainty parameters. However, the solution obtained from this optimization method tends to be conservative where to guarantee the robustness of the solution, the objective function could be impaired. In this regard, a two-stage robust programming was

presented as an approach to address this issue in a proper way. This formulation consists in two hierarchical decision stages. The first stage determines the decisions to be applied to obtain a partial solution without the uncertainty realization, while the decision in the second stage is adjusted according to the first-stage information and the uncertainty realization [27].

9.2.5.1 Uncertainty Interval

To formulate the two-stage robust optimization short-term planning model, the uncertainty interval should be defined properly. Before introducing the uncertainty interval, the mathematical formulation of active and reactive demands $\left(P^{D}_{m,t,y}, Q^{D}_{m,t,y}\right)$ is represented by $\left(f^{D}_{t}P^{D}_{m,y}, f^{D}_{t}Q^{D}_{m,y}\right)$ to clarify its uncertainty representation. The uncertainty interval aims at capturing the prediction errors in demand factors $\left(f^{D}_{t}\right)$ and the renewable power output factors $\left(f^{G^{pv}}_{t,y}\right)$. In this regard, upper and lower limits of this interval are estimated using a certain confidence interval. To build this uncertainty interval using the historical and statistical data, it is considered that there exist k values for the demand factor $\left(f^{D^{(1)}}_{t}, f^{D^{(2)}}_{t}, \ldots, f^{D^{(k)}}_{t}\right)$ and k values for the renewable power output factor $\left(f^{G^{pv(1)}}_{t}, f^{G^{pv(2)}}_{t}, \ldots, f^{G^{pv(k)}}_{t}\right)$ in the time interval t. Using these values, mean values $\left(\hat{f}^{D}_{t}, \hat{f}^{G^{pv}}_{t}\right)$ are obtained for both uncertainty factors. In this work, for practical purposes, the uncertainty interval is built through a confidence interval of 95% where the normal probability distribution is used for the approximation. Therefore, the uncertainty interval for demand and renewable power output factors is defined by (9.52) and (9.53), respectively:

$$\hat{f}^{D}_{t} - Z_{\alpha/2}\frac{\sigma}{\sqrt{k}} \leq f^{D}_{t} \leq \hat{f}^{D}_{t} + Z_{\alpha/2}\frac{\sigma}{\sqrt{k}} \tag{9.52}$$

$$\hat{f}^{G^{pv}}_{t} - Z_{\alpha/2}\frac{\sigma}{\sqrt{k}} \leq f^{G^{pv}}_{t} \leq \hat{f}^{G^{pv}}_{t} + Z_{\alpha/2}\frac{\sigma}{\sqrt{k}} \tag{9.53}$$

These intervals are defined by the mean values plus and minus to the product of the critical value $Z_{\alpha/2}$ and the standard error $\sigma/\sqrt{k}$, where σ and k are set to 0.3 and 30, respectively. On the other hand, to control the conservatism level of the solution determined by the robust optimization model, expressions (9.54) and (9.55) are used. The parameters $\left(\underline{\Gamma}^{pv}, \overline{\Gamma}^{pv}\right)$ and $\left(\underline{\Gamma}^{D}, \overline{\Gamma}^{D}\right)$ can adjust this uncertainty budget to manage the dimension that the worst case can take [26]:

$$\underline{\Gamma}^{pv} \leq \frac{\sum\limits_{t\in T} f^{G^{pv}}_{t}}{\sum\limits_{t\in T} \hat{f}^{G^{pv}}_{t}} \leq \overline{\Gamma}^{pv} \tag{9.54}$$

$$\underline{\Gamma}^D \leq \frac{\sum_{t\in T} f_t^D}{\sum_{t\in T} \hat{f}_t^D} \leq \overline{\Gamma}^D \tag{9.55}$$

The uncertainty interval, described in (9.52) and (9.53), defines the variability range of demand and output power factors, respectively. The uncertainty budget, presented in (9.54) and (9.55), defines the relationship between output power and demand factor concerning their mean values. It is worth noting that, when these parameters $\left(\underline{\Gamma}, \overline{\Gamma}\right)$ tend to 1, the output power and demand factor tend to their mean values. In other case, when $\underline{\Gamma} < 1$ and $\overline{\Gamma} > 1$ implies that any value can be assumed by the output power and demand factor between the uncertainty interval.

9.2.5.2 Two-Stage Robust Optimization Model

The robust framework tends to be a reactionary approach to deal with uncertain data. To remedy this issue properly, a two-stage robust programming model was presented in [27]. This model is transformed into a three-level structure where the first level determines a partial solution (min-problem) via the decision variable before the uncertainty realization. Nonetheless, the middle level (max-problem) determines the uncertainty realization, while the lower level (min-problem) is the reaction of the system due to the first- and middle-level decision. The robust counterpart for the deterministic formulation presented in Sect. 9.2.4 is presented as follows:

$$\begin{aligned}
\min_{x, M^{pv}, \tilde{P}^{ess}, \tilde{E}^{ess}} & \sum_{b\in\Omega^{CB}} \sum_{m\in N} \zeta_b^{cb^{fx}} x_{m,b}^{fx} + \sum_{b\in\Omega^{CB}} \sum_{m\in N} \zeta_b^{cb^{sw}} x_{m,b}^{sw} \\
& + \sum_{a\in CT} \sum_{l\in L} \zeta_{\dot{a},a}^{cr} l_{mn} x_{\mathrm{mn},a}^{cr} + \sum_{n\in N} \zeta^{vr} x_n^{vr} + \sum_{m\in N} \zeta^{pv} M_m^{pv} \\
& + \sum_{m\in N} \sum_{y\in Y} \zeta_y^{o\&m^{pv}} M_m^{pv} + \sum_{m\in N} \zeta^{rc^{ess}} \tilde{E}_m^{ess} + \sum_{m\in N} \left(\zeta^{pc^{ess}} + \sum_{y\in Y} \zeta_y^{o\&m^{ess}} \right) \tilde{P}_m^{ess} \\
& + \max_{f^D, f^{GPV}} \left\{ \min_{\mathrm{I}, P, P^S, Q, Q^S, U} \sum_{t\in T} \sum_{y\in Y} \zeta_{t,y}^{G} \Delta P_{t,y}^{S} \right\}
\end{aligned} \tag{9.56}$$

subject to (9.12, 9.13, 9.14, 9.15, 9.16, 9.17, and 9.18), (9.22, 9.23, 9.24, 9.25, 9.26, 9.27, 9.28, 9.29, 9.30, and 9.31), and (9.33–9.55).

This optimization problem describes a decision-making process where a hierarchical structure is defined via the three-level model. In this problem, the first level determines planning actions such as the (a) sizing and placement of switchable and/or fixed CBs, (b) allocation of VRs for controlling the voltage drop, (c) replacement of the overloaded circuits' conductor, and (d) sizing and placement of PV-based DG sources and ESSs. The second level determines the uncertainty realization by considering the worst scenario within a predefined

interval. Finally, the third level corresponds to the reaction of the planning decision (first level) and uncertainty realization (second level).

9.3 Solution Scheme Method

Due to the trilevel structure, the proposed short-term EDN planning problem considering the sizing and placement of PV-based DG sources and ESSs is a complex problem to be solved directly using commercial solvers. To address such difficulties, decomposition algorithms can be used. In this work, to remedy this issue, an efficient decomposition algorithm, column-and-constraint generation (C&CG), is used [28]. This algorithm, for an uncertainty realization, dynamically generates constraints with recourse variables in the primal space. The C&CG by creating primal cuts, which are usually more powerful than Benders decomposition algorithms, requires fewer iterations to converge [28]. Consequently, in this chapter, the C&CG decomposition algorithm is applied to solve such complicated short-term planning problem.

9.3.1 Hierarchical Structure to Two-Stage Robust Programming Problem

In order to apply the C&CG algorithm, the two-stage robust formulation presented in the subsection 9.2.5 is recast into a hierarchical environment of a master problem (MP) and subproblem (SP). To demonstrate the application of the C&CG algorithm, the short-term planning problem is represented in generic form by (9.57, 9.58, 9.59, and 9.60). In this generic form, the first level is represented by (9.57) and (9.58), where (9.58) represents the investment limits and their decision variables by x in the set X. On the other hand, (9.59) stands for the middle level where the uncertainty variables are denoted by f in the set F. Finally, the variables of the lower level (9.60) are represented by z in the set $\Omega(x^*,f^*)$. This set contains the equality and inequality constraints $[\Omega(f^*,x^*) = \{G(x^*,f^*,z) = b_1; H(x^*,f^*,z) \leq b_2\}]$ and ensures the feasibility of the decision variables z. It is worth noting that this set is parametrized by the solution obtained from the first and middle levels, $x^* = x$ and $f^* = f$, respectively:

$$\min_{x \in X} c_1^T x + \psi \tag{9.57}$$

subject to:

$$c_1^T x \leq \Pi \tag{9.58}$$

$$\psi = \left\{ \max_{f \in F} \delta \right\} \tag{9.59}$$

$$\delta = \left\{ \min_{z \in \Omega(f^*, x^*)} c_2^T z \right\} \tag{9.60}$$

By using this generic form, the robust short-term planning problem is represented in an MP and SP environment. In this regard, the MP is formulated via Eqs. (9.61, 9.62, 9.63, 9.64, and 9.65). The MP is a relaxation of the original two-stage robust optimization problem, where its solution determines the lower bound (LB) of the problem. In the MP, the dimensionality of the solution space increases by introducing a set of variables (z) in each iteration due to the realization o in the set O, and iteratively this process provides tighter relaxations and stronger LBs [28]. The solution of the MP defines the appropriate planning actions x, which is fixed in the SP as x^*, while the SP defines the worst uncertainty realization f, and this information is used in the MP as f^*. Besides the planning action decisions, the MP defines the optimal operation of CBs as well as of ESSs:

$$\min_{x \in X} c_1^T x + \eta \tag{9.61}$$

subject to:

$$c_1^T x \leq \Pi \tag{9.62}$$

$$\eta \geq c_2^T z_o; \forall o \in O \tag{9.63}$$

$$G\left(x, f_o^*, z_o\right) = b_1; \forall o \in O \tag{9.64}$$

$$H\left(x, f_o^*, z_o\right) \leq b_2; \forall o \in O \tag{9.65}$$

On the other hand, the SP associated with this hierarchical structure is defined by (9.66, 9.67, 9.68, and 9.69), and its solution defines the upper bound (UB) of the problem. This SP represents a bi-level optimization problem, which cannot be solved directly using classical optimization techniques or commercial solvers:

$$\max_{f \in F} \delta \tag{9.66}$$

subject to:

$$\delta = \left\{ \min_{z \in \Omega(f, x)} c_2^T z \right\} \tag{9.67}$$

$$G(x^*, f, z) = b_1 \tag{9.68}$$

$$H(x^*, f, z) \leq b_2 \tag{9.69}$$

In order to remedy this issue, by taking into account the KKT optimality conditions, this bi-level problem is recast to a counterpart single-level MILP model with corresponding constraints (9.71, 9.72, 9.73, 9.74, and 9.75). In this regard, the KKT conditions are necessary and sufficient for optimality since the lower problem (9.67, 9.68, and 9.69) is linear and thus convex [29]:

$$\max_{f,z} c_2^T z \tag{9.70}$$

subject to:

$$G(x^*, f, z) = b_1 \tag{9.71}$$

$$f \in \left[\underline{f}, \overline{f}\right]; F\left(f, \hat{f}\right) \leq \Gamma \tag{9.72}$$

$$\frac{\partial}{\partial z}\left(c_2^T z + \lambda H(x^*, f, z) + \gamma G(x^*, f, z)\right) = 0 \tag{9.73}$$

$$0 \leq b_2 - H(x^*, f, z) \leq (1-u)\bar{M} \tag{9.74}$$

$$0 \leq \lambda \leq u\bar{M} \tag{9.75}$$

From this SP problem, λ and γ stand for the dual variables corresponding to the inequality and equality set of constraints, respectively. The uncertainty interval and budget of the variables f are represented by (9.72). Expression (9.73) defines the differentiating of the Lagrangian of the lower-level problem. Moreover, (9.74) and (9.75) present the linearized expressions which correspond to (9.76), using binary variables u and the big-M method:

$$\begin{aligned} &H(x^*, f, z) - b_2 \leq 0 \\ &\lambda(b_2 - H(x^*, f, z)) = 0 \\ &\lambda \geq 0 \end{aligned} \tag{9.76}$$

It is worth mentioning that, for this equivalent single MILP model, the linear expressions (9.37, 9.38, 9.39, 9.40, 9.41, 9.42, 9.43, 9.44, and 9.45) are not an appropriate representation of (9.6) since the performance of this linearization method is guaranteed when it is minimized in the objective function [25]. Therefore, to guarantee the optimal global solution in the SP, this piecewise approximation requires being represented by an MILP model. In other words, binary variables are necessary to guarantee that each block is filled sequentially in ascending order considering the number of segments r [30]. Considering a MILP model to represent this piecewise approximation, the KKT conditions cannot be applied to obtain an equivalent single optimization problem. To remedy this complexity, it is proposed to replace (9.37, 9.38, 9.39, 9.40, 9.41, 9.42, 9.43, 9.44, and 9.45) in the lower level by (9.77):

$$\mathrm{I}_{mn,a,t,y}\left(V^{*}_{n,t,y}\right)^{2} = \left[\left(P^{*}_{mn,t,y}\right)^{2} + 2P^{*}_{mn,t,y}\left(P_{mn,a,t,y} - P^{*}_{mn,t,y}\right) + \left(Q^{*}_{mn,t,y}\right)^{2} + 2Q^{*}_{mn,t,y}\left(Q_{mn,a,t,y} - Q^{*}_{mn,t,y}\right)\right] \tag{9.77}$$

This expression represents a linearization around an estimated operating point (V^{*},P^{*},Q^{*}) to approximate the square of the current flow magnitude. The estimated operating point can be obtained from conventional power flow or via another optimization process. This point is estimated using the solution obtained from the MP. This information is used to approximate the square of the current flow magnitude and to find the solution of the SP.

9.3.2 *The Column-and-Constraint Generation Algorithm*

In order to solve the two-stage robust optimization problem represented in an MP and SP environment, the comprehensive procedure of applying the C&CG algorithm, which is based on [28], is summarized as follows:

A. Initial step: (A.1) Set the initial value of the lower and upper bounds as $\mathrm{LB} = -\infty$ and $\mathrm{UB} = \infty$, respectively; (A.2) define the tolerance *tol* and the set $O \in \varnothing$; (A.3) define i as the iteration counter of the algorithm, and initialize this set to 1, and define $O \cup i$; (A.4) for each $o \in O$, define the initial value of $f^{(i)} \in \left[\underline{f}, \bar{f}\right]$ and $f^{(i)} = f^{(o)^{*}}$.
B. MP step: In this step, solve $\mathrm{MP}^{(i)}\left(f^{(o)^{*}}\right)$, and then update the lower by the obtained solution (x,η), $\mathrm{LB} = \eta$, and submit $x = x^{*}$ to the subproblem.
C. SP step: For this step, solve the $\mathrm{SP}^{(i)}(x^{*})$, denote the solution z and f, and update the $\mathrm{LB} = \min\left\{UB, c_2^{T} z\right\}$.
D. Last step: If $\left(gap = \frac{(UB-LB)}{LB}^{*} 100\right) \leq tol$, then terminate the process; otherwise update $i = i$+1,$O \cup i$ and $f^{(i)} = f^{(i-1)}$, and go to the MP step.

To solve this optimization problem, in the initial step, the MP considers (9.63, 9.64, and 9.65) where the values of uncertain data within the interval are used as initial data of the C&CG algorithm, and for the following iterations, the results of the SP is used. This technique, by initiating from a feasible point, helps in reducing the number of iterations in the C&CG.

9.4 Case Studies and Numerical Results

The two-stage robust formulation presented in this chapter is tested on an adapted 42-node real distribution network [31]. This section provides case studies applied to this network under different conditions.

9.4.1 Case Studies and Assumptions

In order to provide a proper analysis of the proposed planning framework, information related to technical and financial terms, assumptions, and cases under different conditions are presented in this subsection. A 42-node distribution system is used for numerical analysis, as illustrated in Fig. 9.1. This distribution system contains 1 substation, 41 load nodes, and 41 circuits with different conductor types. The conventional active and reactive demands are 1873 MW and 3.898 MVAr, respectively. The voltage magnitude can vary between 0.95 p.u. and 05 p.u., while the nominal medium voltage level is 13.8 kV [31]. The lower and upper limits of the annual power are 0.95 and 1.00, respectively, where the delivered active power will mainly define the reactive power supply by the substation. The VRs with a regulation range of 10% and investment cost of $16.5 k are assumed. Switchable and fixed CBs are considered with different capacities and installation cost in Table 9.1. In this study, four different conductor types are considered to replace the conductors of the system, the technical and financial characteristic of conductor types are presented in Table 9.2, and this data information related with the classical short-term planning actions was based on [2].

In this planning problem, PV-based DG sources are considered. The maximum output of each PV module is 40 kW with a power factor of 0.99. The maximum

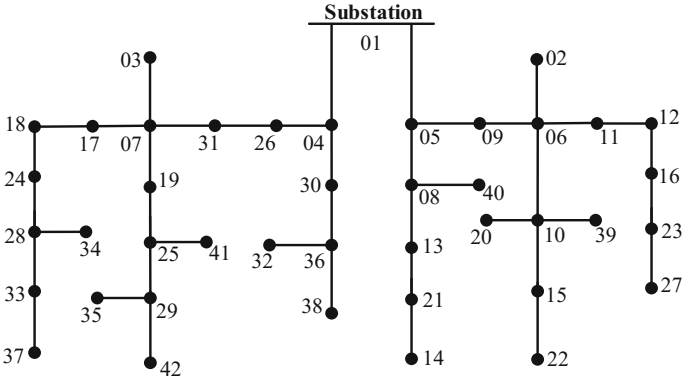

Fig. 9.1 42-node distribution network

Table 9.1 Technical and economic information of CBs

CB installation cost		
Q^{spc} (kVAr)	Fixed ($)	Switchable ($)
300	4950.00	7450.00
600	5150.00	7650.00
900	6550.00	9550.00
1200	7500.00	10,150.00
1500	8075.00	10,950.00

Table 9.2 Data and replacement cost of conductor types

Data of conductors			Conductor (a)–$\zeta^{cr}_{\acute{a},a}$ (103 $/km)		
Type ($\acute{a}$)	R + jX (Ω/km)	$\bar{I}$	AA2	AA3	AA4
AA1	0.762 + j0.708	300	14.00	22.00	29.00
AA2	0.599 + j0.661	350	–	17.50	25.00
AA3	0.369 + j0.415	450	–	–	20.50
AA4	0.321 + j0.355	600	–	–	–

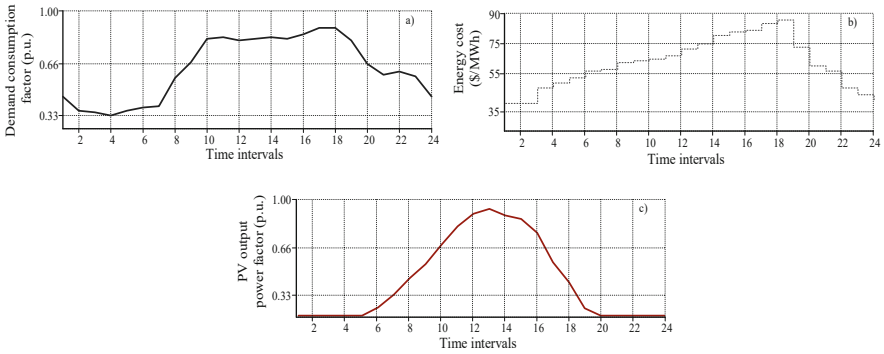

Fig. 9.2 Expected profile of demand consumption factor (**a**), energy cost (**b**), and PV output power factor (**c**)

number of PV modules that can be installed at node m is set to 10 with an investment cost of $30 k for each module; the operation and maintenance cost of each module is $150; this cost increases annually by 5% [20]. Technical information of the ESS are as follows: the maximum power rating is 300 kW; minimum/maximum energy reservoir capacities are 1300 kWh and 4500 kWh, respectively; charging and discharging efficiency is 90% with *DoD* of 0.3; and for the sake of simplicity, the self-discharging in the ESS is disregarded. The capital costs of energy and power are $90 per kWh and $300 per kW [32], respectively, while the operation and maintenance costs are $50 per kW that increases annually by 5%.

In this analysis, a planning horizon of 3 years is considered with an annual demand growth rate of 10%, while the energy cost increases in 2%. Each year is divided into 24 time intervals; each time interval is represented by 1 h, thus $\Delta = 365$. In summary, as can be seen in Fig. 9.2, each time interval involves expected energy cost, demand consumption factor, and PV output power factor. Accordingly, the uncertainty intervals for PV output power factor and electricity demand factor are built using the procedure explained in subsection 9.2.5. To adjust the conservatism level, parameters $\underline{\Gamma}$ and $\overline{\Gamma}$ are set to 0.90 and 1.05, respectively. It is worth mentioning that these parameters can be defined considering the decision-maker's criterion. Finally, the optimality gap of the C&CG algorithm is set to 0.5%.

To validate the proposed planning model, three different cases are studied. However, before starting the planning process, a conventional power flow is used

to perform a pre-analysis to learn the initial condition of the 42-node distribution network in the first year. For this analysis, the uncertainty in demand is disregarded, and the mean values are considered. Under the initial conditions, the distribution network reveals several violations in aspects such as substation power factor, with a power factor of 0.9448, and voltage magnitude limits, as can be seen in Fig. 9.3. Under this infeasible operation, the cost of the supplied energy by the substation was $4,401.68 k.

To improve the performance of this network, several planning alternatives are considered. The following cases represent these alternatives:

Case I: Considering the classical short-term planning actions such as conductor replacement and CB and VR allocation
Case II: Considering VR and CB allocation and siting and sizing of PV-based DG sources
Case III: Considering siting and sizing of CBs, PV-based DG sources, and ESSs

9.4.2 Numerical Results and Analysis

This subsection presents numerical results obtained by the proposed robust planning model. The proposed model is developed in the mathematical language AMPL, and to obtain the solution of the problem, commercial solver CPLEX is used.

9.4.2.1 Case I: Classical Short-Term Planning Alternatives

This case aims to evaluate the proposed EDN planning framework considering uncertainty in electricity demand using classical investment alternatives such as allocation of the CBs and VRs and replacement of the conductors. The obtained solution for this case shows a total investment cost of $57.25 k that is summarized as follows: (a) allocation of a switchable CB with $10.95 k investment cost; (b) allocation of a VR with $16.50 k total investment cost; and (c) conductor replacement of 3 circuits with $29.80 k total cost.

This planning scheme demonstrates that using classical planning alternatives, the operation of an initially violated 42-node distribution network can be improved. For comparative purposes, the same conditions of this case were considered in a deterministic environment where the mean value of electricity demand considering 24 time intervals was used. Under this condition, the objective function was $14,866.04 k, which shows about 7.67% lower outcome than the robust solution (considering investment cost and LB value in Table 9.3). Comparing the cost of the supplied energy of the substation obtained by the robust and deterministic model in Table 9.3 shows that the robust solution was 7.77% greater than the deterministic solution. This higher cost of the supplied energy by the substation using the robust framework is a result of considering the uncertainty realization.

Table 9.3 Optimal UB and LB values, gaps, and deterministic value of the cost of energy supplied

Case	Iteration	UB (10^3\$)	LB (10^3\$)	Gap (%)	Deterministic (10^3\$)
I	1	15,956.70	14,804.85	7.78	14,799.18
	2	15,956.70	15,949.50	0.04	
II	1	15,844.74	14,639.01	8.24	14,636.70
	2	15,663.78	15,649.17	0.09	
III	1	15,266.94	13,817.40	10.49	13,820.43
	2	15,258.51	15,183.57	0.49	

9.4.2.2 Case II: VR and CB Allocation and Siting and Sizing of PV-Based DG Sources and ESSs

In this case, allocation of devices to control the voltage magnitude and reactive power flow is considered with siting and sizing of PV-based DG sources and ESSs. The solution obtained from this analysis has a total cost of \$476.46 k. The planning actions are summarized as follows: (a) allocation of two fixed CBs with total investment cost of \$16.85 k; (b) allocation of two VRs with a total cost of \$33.00 k; and (c) installation of 14 PV modules in the network, where these PV modules have been distributed in two PV-based DG sources. This planning action has a total cost (including maintenance and operation cost) of \$426.61 k.

This solution shows that by considering CB and VR allocation and siting and sizing of PV-based DG sources, the performance of an initially violated 42-node distribution network can be improved in technical, operational, and economic aspects. Comparing the cost of the supplied energy in cases I and II (see Table 9.3), this value is 92% smaller; this benefit was obtained via allocation of PV-based DG sources. Similar to case I, the same conditions of this case were considered via a deterministic approach. The deterministic objective function was \$14,959.40 k, which is 7.80% lower than the robust solution. The robust solution determines a higher cost of the energy supplied by the substation, compared with the deterministic solution (see Table 9.3), to attend the uncertainty realization.

9.4.2.3 Case III: Considering Siting and Sizing of CBs, PV-Based DG Sources, and ESSs

In this case, ESS allocation is considered with reactive support devices and renewable energy-based sources. The solution of this case shows a short-term plan with total investment cost of \$1876.54 k, which corresponds to planning actions such as (a) allocation of two fixed CBs with investment cost of \$13.225 k and switchable CBs with investment cost of \$10.95 k; (b) installing 37 PV modules distributed in 5 PV sources with total investment cost of \$1127.46 k including maintenance and operation cost; and (c) siting three ESSs dimensioned in the 42-node distribution network with an energy reservoir cost of \$364.50 k, where the investment cost of the

power unit conversion was $360.40 k (containing the maintenance and operation cost).

The planning scheme, presented in this case, represents the greater investment cost comparing with the cases I and II. However, considering these alternatives, the energy cost was 5.04% and 3.07% lower than the cases I and II, respectively. On the other hand, a deterministic solution was obtained under the same conditions as case III. Similar in previous cases, the deterministic objective function for this with total cost $15,607.96 k represents 9.30% lower value than the robust solution.

In summary, the proposed EDN planning model delivers appropriate solutions for cases I–III under different circumstances within few iterations. The maximum gap for the solutions was less than 0.49%. Some useful information such as UB and LB values and the gap in each case and iteration are presented in Table 9.3. Additionally, this table contains deterministic values of energy cost by the substation. In this regard, both values obtained from the robust and deterministic approaches can be compared. It can be observed that the deterministic solutions propose investment plans with lower costs than the robust formulation, however under risky conditions.

To satisfy the technical and operational conditions of the 42-node distribution network, which was initially violated, a set of planning actions has been identified in each case. These sets are summarized by the information presented in Fig. 9.3 and Table 9.4. Figure 9.3 illustrates the planning actions for each case, where the location of switchable and/or fixed CBs and VRs and conductor replacement of overloaded circuits, PV-based DG sources, and ESSs are duly identified. On the other hand, Table 9.4 presents the detail information related to each case. This table contains the location of VRs controlling the voltage magnitude at node *m*, the conductor type to be replaced by the new one, the location and type and capacity of CBs, the location and capacity of PV-based DG sources, and location and energy and power capacity of ESSs.

Table 9.4 Information related to the proposed planning alternatives for each case

	Planning alternatives					
			Conductor replacement			
Case	VR (*#m*)	CB type *#m*: (capacity kVAr)	Circuit *#m-#n*: (type)	New type	PV sources *#m*: (capacity KW)	ESSs *#m*: (energy capacity kWh; power capacity kW)
I	05	Switchable: 42: (1500)	01–04: (AA1) 01–05: (AA1) 04–26: (AA1)	AA4 AA2 AA3	–	–
II	06, 07	Fixed: 24: (600) 25: (900) 33: (300)	–		25: (200) 42: (500)	–
III	–	Fixed: 33: (600) 42: (1500) Switchable: 39: (1500)	–		2: (250) 25: (300) 33: (300) 39: (500) 42: (500)	02: (1350; 288) 39: (1350; 300) 42: (1350; 290)

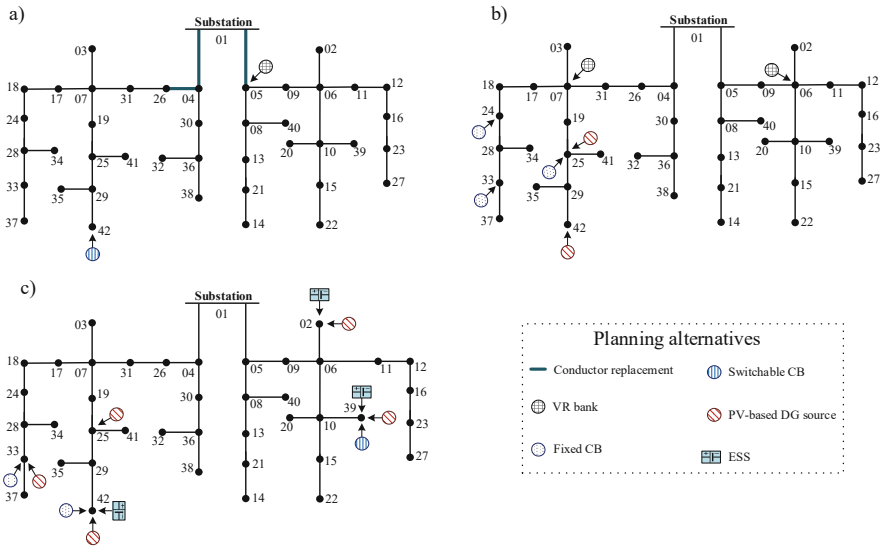

Fig. 9.3 Proposed planning actions for the 42-node distribution system for (**a**) case I, (**b**) case II, and (**c**) case III

9.4.2.4 Robust Solution Validation

The proposed approach guarantees feasible solutions against the worst realization within the uncertainty interval. Accordingly, the solutions obtained by the two-stage robust programming model for each case are validated by using random annual profiles in electricity demand and PV-based output power. In this regard, the obtained solution of each case is fixed, and by using a conventional optimal power flow (OPF) tool, the operating conditions for the 42-node distribution network, under these random profiles, are determined. This OPF tool reveals the feasibility of the results for each case. In the following, the validation of the robust model for different cases is considered in detail using Figs. 9.4 and 9.5. Figure 9.4 presents the comparisons of the minimum voltage profiles of before planning (red profile) and for the validation of each case. Figure 9.5 presents the active power profile for each case in the last planning year of the 42-node distribution network containing the power injected by the substation and PV-based DG sources and the active power injected and demanded by the ESSs. The positive values in this figure stand for the active power injected into the EDN, while the negative values show the active power demanded by ESSs.

For the first case, the conventional OPF tool determines that the costs of supplied energy by the substation for each year are \$4749.88 k, \$5345.14 k, and \$6016.88 k corresponding with the power factors 0.967, 0.966, and 0.969, respectively. Comparing these results with the initial condition of the network before planning, it can

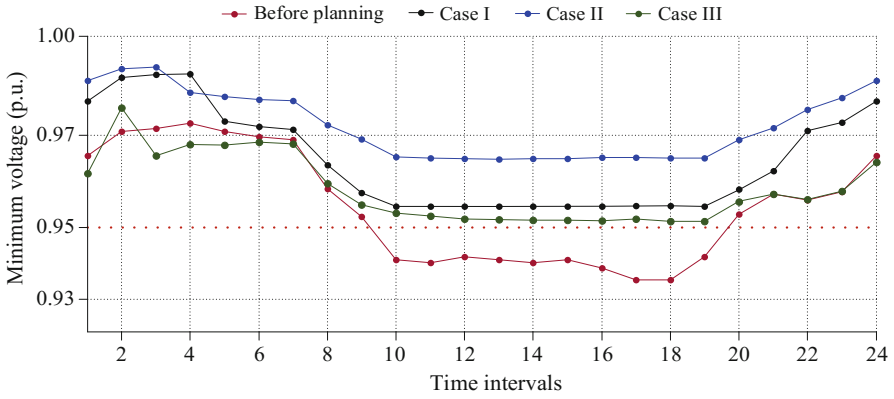

Fig. 9.4 Minimum voltage magnitude of the 42-node distribution network for (**a**) before planning and (**b**) validation of the robust solution of cases I–III in the last year

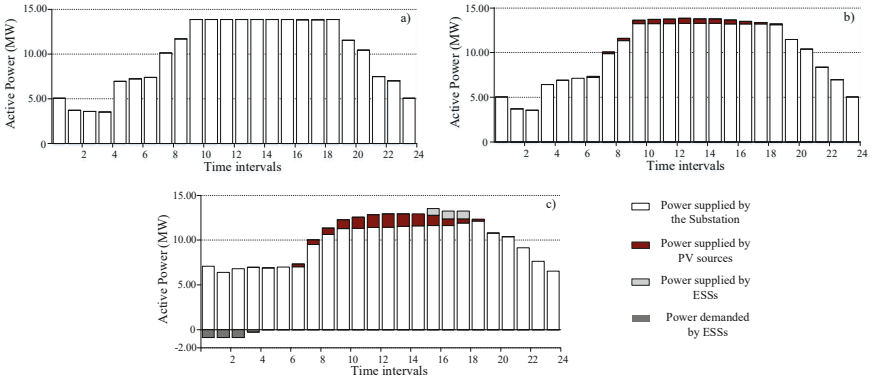

Fig. 9.5 Active power injected into the network for validation of robust solution in the last planning year of (**a**) case I, (**b**) case II, and (**c**) case III

be concluded that via this set of planning actions, the technical aspects such as voltage magnitude (see Fig. 9.4) and power factor were improved to attend the quality requirements. This case presents an economic investment plan in which classical planning actions such as CB and VR allocation and conductor replacement of overloaded circuits improve the technical and operational conditions.

For the second case, the costs of the energy supplied by the substation for each year are \$4618.17 k, \$5211.87 k, and \$5882.97 k, respectively. Comparing this result with the first case reveals a reduction in the energy costs by about 2.85%, 2.56%, and 2.28% for each year. This benefit has been obtained by considering the allocation of PV-based DG sources. It is worth mentioning that the proposed set of planning actions found in this case approved an appropriate short-term plan where the technical and operational aspects are fulfilled considering a random profile in

demand and renewable output power. This fact can be observed in aspects such as annual power factors of 0.990, 0.988, and 0.985 and voltage magnitude profile as shown in Fig. 9.4, which presents the fulfillment of the voltage profile of the EDN in the last year (considered as the peak load year).

The yearly planning outcome for case III shows a cost of the supplied energy by the substation of $4413.37 k, $5003.04 k, and $5670.10 k, respectively, while the power factors in each planning year are 0.998, 0.998, and 0.990, respectively. Comparing these costs with the costs of the first case reveals that reductions of 7.62%, 6.84%, and 6.12% have been obtained for each year of the planning horizon, while, compared to case II, the reductions are 4.64%, 4.17%, and 3.75%, respectively. It is worth mentioning that these cost reductions were obtained due to PV-based DG sources and ESS allocation. As can be seen in Fig. 9.5, this technology presents a good flexibility for storing electrical energy at intervals with low cost and then providing it at peak time intervals.

Therefore, the results of the conventional OPF tool considering the outcomes of the robust model prove the feasibility of solutions. From Fig. 9.4, it can be observed that the initial condition of the 42-node distribution network presents technical violations. Therefore, to remedy this initially violated condition, the proposed two-stage robust planning framework found several appropriate short-term plans. Results of validation of the first case show that the voltage magnitude limits (black profile) for the last year of the planning horizon were satisfied. In the same way, the validation of cases II and III shows compliance with this limit for the last year (blue and green profile, respectively). Moreover, as can be seen in Fig. 9.5c, the proposed approach determines an optimal schedule for the operation of PV-based DG sources and ESSs, mainly to reduce the energy costs provided by the substation.

In this subsection, the planning actions obtained by the proposed approach have been validated for all the case studies. In the first case, via classical short-term planning actions, the technical operation was improved, while two other cases by taking advantage of renewable-based DG sources and ESSs have maximized the efficiency of the initially violated 42-node distribution network. This validation demonstrates the effectiveness of a useful decision-making process tool where the planner can define the most suitable short-term plan to satisfy financial, technical, quality, and operational conditions to an EDN.

9.5 Conclusions

A robust strategic framework for the short-term electrical distribution network planning was presented in this chapter. The proposed approach defines reinforcement plans such as voltage regulator allocation, replacement of overloaded circuits' conductor, sizing and placement of capacitor banks, renewable-based distributed generation sources, and energy storage systems. To consider uncertainties in demand and renewable-based generation, a two-stage robust programming model was developed, which represents a hierarchical decision-making process where the

master problem defines the investment decisions and the subproblem determines the operating reaction of the network. Consequently, this robust programming formulation guarantees the fulfillment of the technical and operational requirements against the worst realization of uncertainties within a specified confidence interval.

The effectiveness and robustness of the proposed planning framework were revealed by illustrative examples. Three different cases were analyzed with several planning alternatives, for which, the robust model determined appropriate planning actions to enhance the efficiency of an initially violated EDN and to fulfill the technical issues and standards. Although the obtained solution for these cases via a deterministic approach provides the most economical option for the substation supplied energy, under uncertainty conditions, this deterministic approach could present technically and operationally infeasible conditions. In contrast, the robust programming approach presents larger total costs, which is dealt with the demand and renewable generation uncertainties.

Therefore, the proposed model, which is a two-stage robust programming approach, is an efficient tool to solve the complex short-term EDN planning problem. This strategy can be useful for the EDN planner as a suitable alternative in the decision-making process to choose the most appropriate short-term plan to attend the EDN necessities and to manage the risk levels associated with the uncertainty. For practical and exploratory purposes, an adapted medium scale 42-node distribution network was analyzed in this chapter. In the presented analysis, different planning actions were found as a result of the proposed approach. To validate these robust solutions, a random profile in demand and renewable output power was considered, for which, feasible solutions for each short-term investment plan were determined.

The prospects of further research works can be considering the uncertainty in the energy price that is subject to variability in the real electricity market, adopting different planning strategies to enrich the applicability of the proposed decision-making tool in addressing the existing concerns related to low-emission power systems, and consequently, demonstrating the applicability of the resulted model in a very large-scale system.

Acknowledgments The authors would like to thank the Brazilian institutions CAPES (Finance code 001), CNPq (Grant NO. 305318/2016-0), and FAPESP (Grant NO. 2015/21972-6) for the financial support.

References

1. Szuvovivski, I., Fernandes, T. S. P., & Aoki, A. R. (2012). Simultaneous allocation of capacitors and voltage regulators at distribution networks using genetic algorithms and optimal power flow. *International Journal of Electrical Power and Energy Systems, 40*, 62–69.
2. Pereira Junior, B. R., Cossi, A. M., & Mantovani, J. R. S. (2013). Multiobjective short-term planning of electric power distribution systems using NSGA-II. *Journal of Control Automation and Electrical Systems, 24*, 286–299.

3. Asrari, A., Lotfifard, S., & Ansari, M. (2016). Reconfiguration of smart distribution systems with time varying loads using parallel computing. *IEEE Transaction on Smart Grid, 7*, 2713–2723.
4. Rupolo, D., Pereira, B. R., Contreras, J., et al. (2017). Medium- and low-voltage planning of radial electric power distribution systems considering reliability. *IET Generation Transmission and Distribution, 11*, 2212–2221.
5. Resener, M., Haffner, S., Pereira, L. A., et al. (2018). Optimization techniques applied to planning of electric power distribution systems: A bibliographic survey. *Energy System, 9*(3), 473–509.
6. Adefarati, T., & Bansal, R. C. (2016). Integration of renewable distributed generators into the distribution system: A review. *IET Renewable Power Generation, 10*, 873–884.
7. Pereira, B. R., Martins Da Costa, G. R. M., Contreras, J., et al. (2016). Optimal distributed generation and reactive power allocation in electrical distribution systems. *IEEE Transactions on Sustainable Energy, 7*, 975–984.
8. Jannat, M. B., & Savić, A. S. (2016). Optimal capacitor placement in distribution networks regarding uncertainty in active power load and distributed generation units production. *IET Generation Transmission and Distribution, 10*, 3060–3067.
9. Quijano, D. A., Wang, J., Sarker, M. R., et al. (2017). Stochastic assessment of distributed generation hosting capacity and energy efficiency in active distribution networks. *IET Generation Transmission and Distribution, 11*, 4617–4625.
10. Ortiz, J. M. H., Pourakbari-Kasmaei, M., López, J., et al. (2018). A stochastic mixed-integer conic programming model for distribution system expansion planning considering wind generation. *Energy System, 9*, 551–571.
11. Nazari-Heris, M., & Mohammadi-Ivatloo, B. (2018). Application of robust optimization method to power system problems. In *Classical and recent aspects of power system optimization* (pp. 19–32). Imprint: Academic Press: Elsevier. https://doi.org/10.1016/C2016-0-03379-X.
12. Wang, Z., Chen, B., Wang, J., et al. (2014). Robust optimization based optimal DG placement in microgrids. *IEEE Transactions on Smart Grid, 5*, 2173–2182.
13. Ruiz, C., & Conejo, A. J. (2015). Robust transmission expansion planning. *European Journal of Operational Research, 242*, 390–401.
14. Jabr, R. A., Dzafic, I., & Pal, B. C. (2015). Robust optimization of storage investment on transmission networks. *IEEE Transactions on Power Systems, 30*, 531–539.
15. Yuan, W., Wang, J., Qiu, F., et al. (2016). Robust optimization-based resilient distribution network planning against natural disasters. *IEEE Transactions on Smart Grid, 7*, 2817–2826.
16. Amjady, N., Attarha, A., Dehghan, S., et al. (2018). Adaptive robust expansion planning for a distribution network with DERs. *IEEE Transactions on Power Systems, 33*, 1698–1715.
17. Melgar Dominguez, O. D., Pourakbari Kasmaei, M., & Mantovani, J. R. S. (2018). Adaptive robust short-term planning of electrical distribution systems considering siting and sizing of renewable energy-based DG units. *IEEE Transactions on Sustainable Energy*, 1.
18. Saboori, H., Hemmati, R., Ghiasi, S. M. S., et al. (2017). Energy storage planning in electric power distribution networks – A state-of-the-art review. *Renewable and Sustainable Energy Reviews, 79*, 1108–1121.
19. Babacan, O., Torre, W., & Kleissl, J. (2017). Siting and sizing of distributed energy storage to mitigate voltage impact by solar PV in distribution systems. *Solar Energy, 146*, 199–208.
20. Melgar Dominguez, O. D., Pourakbari Kasmaei, M., Lavorato, M., et al. (2018). Optimal siting and sizing of renewable energy sources, storage devices, and reactive support devices to obtain a sustainable electrical distribution systems. *Energy Systems, 9*, 529–550.
21. Khalid Mehmood, K., Khan, S. U., Lee, S.-J., et al. (2017). Optimal sizing and allocation of battery energy storage systems with wind and solar power DGs in a distribution network for voltage regulation considering the lifespan of batteries. *IET Renewable Power Generation, 11*, 1305–1315.

22. Pourakbari-Kasmaei, M., & Sanches Mantovani, J. R. (2018). Logically constrained optimal power flow: Solver-based mixed-integer nonlinear programming model. *International Journal Electrical Power and Energy Systems, 97*, 240–249.
23. Shirmohammadi, D., Hong, H. W., Semlyen, A., et al. (1988). A compensation-based power flow method for weakly meshed distribution and transmission networks. *IEEE Transactions on Power Systems, 3*, 753–762.
24. Cespedes, R. G. (1990). New method for the analysis of distribution networks. *IEEE Transactions on Power Delivery, 5*, 391–396.
25. Alguacil, N., Motto, A. L., & Conejo, A. J. (2003). Transmission expansion planning: A mixed-integer LP approach. *IEEE Transaction on Power Systems, 18*, 1070–1077.
26. Bertsimas, D., & Sim, M. (2003). Robust discrete optimization and network flows. *Mathematical Programming, 98*, 49–71.
27. Ben-Tal, A., Goryashko, A., Guslitzer, E., et al. (2004). Adjustable robust solutions of uncertain linear programs. *Mathematical Programming, 99*, 351–376.
28. Zeng, B., & Zhao, L. (2013). Solving two-stage robust optimization problems using a column-and-constraint generation method. *Operations Research Letters, 41*, 457–461.
29. Stephen Boyd, L. V. (2004). *Convex optimization*. Cambridge: Cambridge University Press.
30. Rebennack, S. (2016). Computing tight bounds via piecewise linear functions through the example of circle cutting problems. *Mathematical Methods of Operations Research, 84*, 3–57.
31. LaPSEE Power System Test Cases Repository, [Online]. Available: http://www.feis.unesp.br/#!/lapsee
32. Masteri, K., Venkatesh, B., & Freitas, W. (2018). A fuzzy optimization model for distribution system asset planning with energy storage. *IEEE Transactions on Power Systems, 33*(5), 5114–5123.

Chapter 10
Optimal Robust Microgrid Expansion Planning Considering Intermittent Power Generation and Contingency Uncertainties

Mehrdad Setayesh Nazar and Alireza Heidari

Nomenclature

Λ_{DG}	DG allocation alternatives costs
Λ_{RL}	RL alternatives costs
Λ_{ESS}	ESS allocation alternatives costs
Λ_{IPG}	IPG alternatives costs
Λ_{Trans}	New substation transformer costs
Λ_{Feed}	New feeder costs
Energy _ Purchased	Energy purchased from upward utility
Energy _ Sold	Energy sold to upward utility
ENSC	Energy not supplied costs
TR	Number of transformer allocation alternatives
DGC	Number of DG allocation alternatives
FR	Number of feeder allocation alternatives
IPGC	Number of IPG allocation alternatives
RLC	Number of RL contribution scenarios
ESSC	Number of ESS allocation alternatives
NY	Number of planning years
NP	Number of periods
NDASC	Number of DA market scenarios
NRTSC	Number of RT market scenarios
NH	Number of DA market hours

(continued)

M. S. Nazar (✉)
Faculty of Electrical Engineering, Shahid Beheshti University, A.C., Tehran, Iran
e-mail: m_setayesh@sbu.ac.ir

A. Heidari
School of Electrical Engineering and Telecommunication, University of New South Wales, Sydney, NSW, Australia
e-mail: Alireza.heidari@unsw.edu.au

B. Mohammadi-ivatloo, M. Nazari-Heris (eds.), *Robust Optimal Planning and Operation of Electrical Energy Systems*,
https://doi.org/10.1007/978-3-030-04296-7_10

NRT	Number of RT market settlement steps
φ_{Trans}	Decision variable for new transformer installation
φ_{Feed}	Decision variable for feeder installation
φ_{RL}	Decision variable for RL contribution
φ_{IPG}	Decision variable for IPG installation
φ_{DG}	Decision variable for DG installation
λ	Probability of scenario
β^{DA}	Energy price of DA market
E^{DA}	Energy purchased from upward network in DA market
γ^{RT}	Marginal cost of DG
PG^{RT}	Power generated by DG in RT market
ξ^{RT}	Marginal cost of RL
PRL^{RT}	Power consumption reduced by RL in RT market
ς^{RT}	Cost of ESS contribution in RT market
$PBAT^{RT}$	Power delivered by ESS in RT market
σ^{RT}	Energy price of RT market
E^{RT}	Energy purchased from upward network in RT market
$\overline{\sigma}^{RT}$	Expected value of RT market price
Ξ	Dual variable of inner-step optimization
Ψ	Robustness level parameter

10.1 Introduction

A microgrid can be introduced as a system, which includes distributed generations (DGs), electrical storage systems (ESSs), and RLs, in a way that it has at least one controllable energy source. The microgrid operator (MGO) can utilize its microgrid separately or connected to the main upward network [1]. From the point of view of the distribution system operator (DSO), an active microgrid can be considered as a controllable element that is connected to its network [2]. The MGO should perform the optimal planning and scheduling of microgrid by considering the uncertainties of IPGs and RLs [3, 4]. Figure 10.1 depicts the microgrid configuration that consists of IPGs, RLs, and ESSs [4].

The RMEP problem consists of optimizing of the decision variables of system device installation based on reliability criteria and RL and IPG power generation scenarios.

Over the recent years, different aspects of optimal planning and scheduling of the microgrid problem have been studied.

Reference [5] presents an algorithm for planning and design of IPGs for microgrids, and the performance of the system is evaluated using optimization analyses. Reference [6] introduces a bi-level planning algorithm that the upper-level problem minimizes planning and operational cost and the lower-level problem optimizes reliable power supply. These references do not consider uncertainties of contingencies.

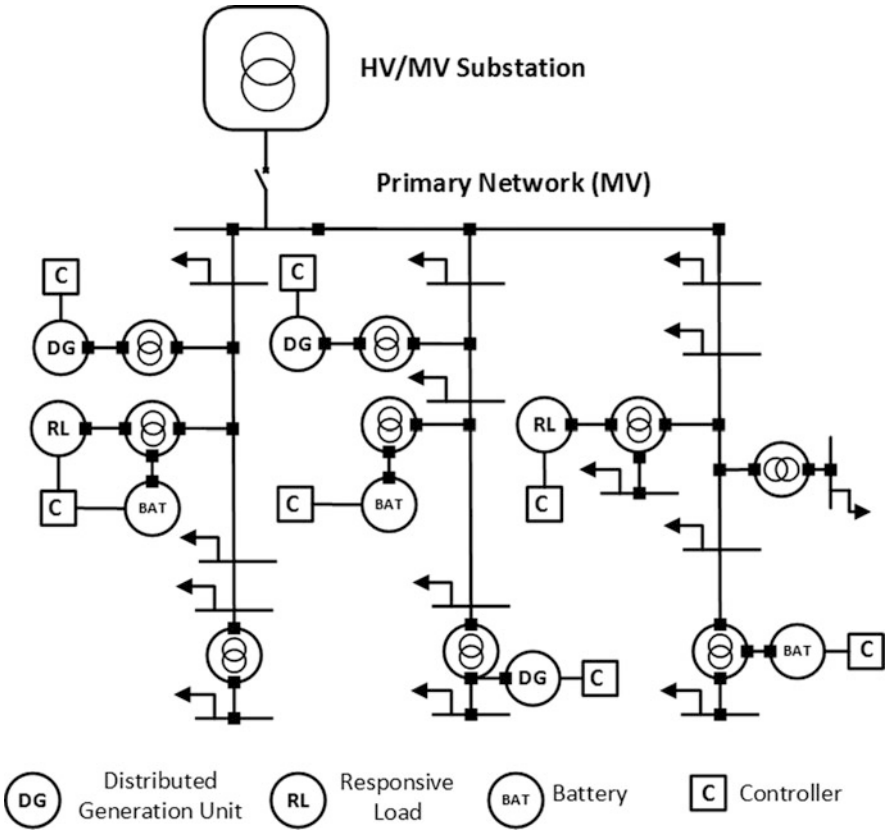

Fig. 10.1 Schematic diagram of an electric distribution microgrid

Reference [7] presents an optimal microgrid scheduling method in connection to the main grid modes. The uncertainty of IPGs with demand response is investigated in five scenarios for DG sources; however, the AC load flow constraints are not considered. The optimal microgrid scheduling is performed using the robust scheduling method. Reference [8] presents a stochastic bidding strategy for the participation of microgrid in the day-ahead (DA) market of energy and spinning reserve services by taking into account the uncertainty of IPGs and electrical load demand. In Ref. [9], optimal power scheduling of microgrid for DA is investigated. In Ref. [10], a balance between the profit maximization of a microgrid in the power market and the operation cost minimization of a microgrid is reviewed. Refs. [8–10] do not consider microgrid configuration and its topological limitations. In Ref. [11], an optimal bidding in the DA market model is presented for a virtual power plant that includes a set of microgrids. The microgrids include IPGs, ESSs, and DGs. The bidding model is formulated as a two-stage stochastic mixed-integer nonlinear programming, which maximizes the profit of the virtual power plant by trading the electricity in the DA and real-time (RT) markets. The uncertain data are modelled by

scenarios, but the risk of the microgrid expected profit is not considered. In Ref. [12], a stochastic linear programming model is presented with the DA and RT market price scenario and load forecast error. In Ref. [13], the optimal islanded microgrid scheduling with robust optimization is studied, while the AC power flow constraints are not considered. In Ref. [14], a method for optimal bidding of a microgrid, which purchases electricity in the wholesale market, is introduced by using the genetic algorithm (GA). In Ref. [15], a robust multi-objective optimization for microgrid operation is investigated in the presence of intermittent sources. The multiple objective functions are optimized by using the Pareto front concept, but the microgrid AC power flow constraints are not modelled. These references do not consider uncertainties of contingencies.

In Ref. [16], a stochastic algorithm is presented for expansion planning of microgrid considering IPG uncertainties. The proposed algorithm maximizes profit and reliability, while it minimizes investment and operation costs.

In Ref. [17], a two-level stochastic planning algorithm is introduced. The algorithm determines the optimal location and size of devices, and it considers DGs and ESSs. These references do not consider uncertainties of contingencies.

This book chapter is about the RMEP algorithm that considers the DG/RL contribution uncertainty and contingency scenarios.

10.2 Problem Modelling and Formulation

The RMEP criteria can be summarized as:

1. Minimizing the microgrid investment and operation costs consisting of energy purchased from the upward network
2. Maximizing the microgrid reliability
3. Maximizing the expected profit of MGO in the DA/RT markets

The second planning criteria are maximized through minimization of interruption cost by the MGO [18, 19]. The MGO should optimize its expected profit in the DA/RT markets based on the fact that the purchasing price of power for compensating the generation deficit in the RT market is usually more than the DA market. The MGO should maximize its expected profit in the DA market and reduce the electricity trading in the RT market as much as possible. In addition, the RT market price is assumed to depend on unpredictable market conditions, which makes it extremely difficult to investigate the problem by considering the stochastic parameters. Therefore, in this book chapter, the uncertainty of the DG outputs and the DA market price is modelled with the scenario, and the robust optimization covers the uncertainty of RT price for the worst-case planning scenarios.

An IPG can be classified as dispatchable and non-dispatchable distributed generation (DG). The MGO can utilize dispatchable IPGs/RLs to optimize its benefits and mitigate the impacts of contingencies. Figure 10.2 shows the MGO interactions with upward network and its IPGs/RLs, ESSs, and nonresponsive loads.

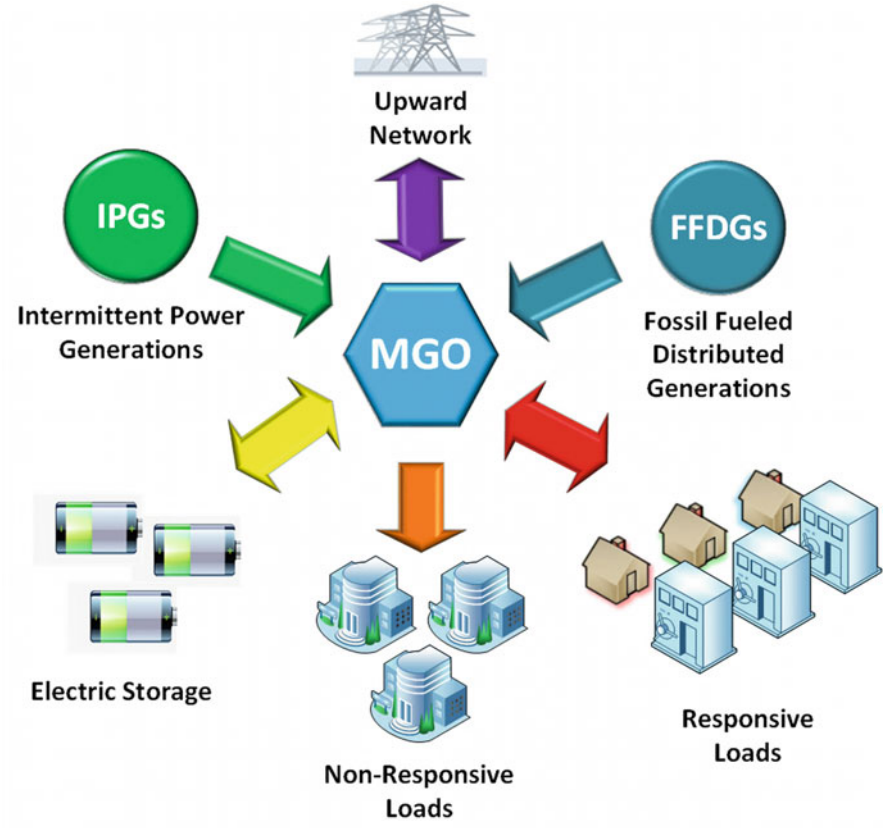

Fig. 10.2 The schematic diagram of MGO interactions

The RMEP problem is subject to the two sources of uncertainty: IPG/RL power generation scenarios and system contingencies. Thus, the uncertainty can be modelled as a scenario-driven model. Hence, the MGO must make optimal decisions throughout planning horizon with incomplete information, and it must determine the optimal values of problem decision variables that consist of the location, the capacity, and the time of installation of system devices. The RMEP takes into account the optimal coordination of control variables such as DGs, ESSs, dispatchable IPGs, and RLs.

Based on the described planning criteria, the RMEP decision variables can be summarized as:

1. Location, capacity, and type of energy resources
2. The volume of energy purchased from the upward network

The system costs and benefits can be categorized as:

1. Investment costs of resources
2. Operation costs of system resources
3. Energy purchased costs
4. The expected profit of energy sold to upward network in the DA/RT markets

The reliability of the system can be considered as objective functions and constraints. The energy not supplied cost (ENSC) can be considered as an objective function in RMEP [18].

10.2.1 First-Level Problem Formulation

The MGO determines the number of upward network electricity price and its system's contingencies, and it estimates the IPG/RL power generation scenarios for each contingency.

The stochastic single-order independent failures are considered as contingencies in this book chapter. The reliability data which is used in the book chapter can be categorized as:

- Single independent device failure in scenarios, in which their failure rates are extracted from the database
- The line to ground faults for cables

For each contingency and IPG and RL power generation scenario, the problem optimizes cost allocation. The objective function of the first-level problem is as follows:

$$\begin{aligned}\text{Min}\quad C_1 = \sum_{i=1}^{NY}\sum_{j=1}^{NP}\Bigg[&\sum_{k\in FR}\Lambda_{Feed\,ijk}{}^{*}\varphi_{Feed\,ijk} + \sum_{k\in TR}\Lambda_{Trans\,ijk}{}^{*}\varphi_{Trans\,ijk} \\ &+ \sum_{k\in DGC}\Lambda_{DG\,ijk}{}^{*}\varphi_{DG\,ijk} + \sum_{k\in IPGC}\Lambda_{IPG\,ijk}{}^{*}\varphi_{IPG\,ijk} \\ &+ \sum_{k\in RLC}\Lambda_{RL\,ijk}{}^{*}\varphi_{RL\,ijk} + \sum_{k\in ESSC}\Lambda_{ESS\,ijk}{}^{*}\varphi_{ESS\,ijk} \\ &+ Energy\_Purchased_{ij} - Energy\_Sold_{ij} + \sum_{k=1}^{Contingency} ENSC_{ijk}\Bigg]\end{aligned} \tag{10.1}$$

The objective function is decomposed into the following groups: (1) microgrid feeder, transformers, DGs, IPGs, RLs, and ESSs operation and investment costs; (2) the costs of purchased energy from the upward network; (3) the benefits of energy sold to the upward network; and (4) ENSCs.

The constraints of first-level optimization can be summarized as device loading and DC load flow constraints.

The worst-case planning scenarios are determined by the calculation of first-level optimization objective function components. The first-level objective

functions that their ENSCs are more than a predefined threshold will be considered as the worst-case planning scenarios.

The second-level problem deals with optimal MGO estimated profits in DA and RT markets for the worst-case planning scenarios.

10.2.2 Second-Level Problem Formulation

The active MGO should implement the stochastic optimization process in order to maximize his/her expected profit and minimize his/her operation costs. The MGO determines the optimal schedule of ESSs, DGs, RLs, and the energy transacted in the DA market for the worst-case planning scenarios. The DA and RT market prices and output of IPGs are modelled by scenarios.

This level of optimization problem can be modelled as a three-step stochastic problem for the worst-case planning scenarios. In the first step, the MGO provides its bidding curve scenarios, before the DA and RT market prices, and the output of IPGs becomes known. In the second step, it is assumed that the DA market is settled and the DA market price is determined. In this step, the MGO schedules the dispatchable IPGs, DGs, and RLs as well as ESSs to ensure the realization of each scenario. This step occurs before the RT market settlement. In the third step, the RT market price is realized, and the unbalanced power is supplied through the RT market [20].

The objective function minimizes the difference between the costs and expected profits. The formulation of the objective function is as follows:

$$\begin{aligned}\text{Min}\quad & \sum_{l=1}^{NDASC}\lambda_l\left(\sum_{m=1}^{NH}\beta_{lm}^{DA}*E_{lm}^{DA}+\sum_{m=1}^{NRTSC}\lambda_m\sum_{n=1}^{NRT}\left[\gamma_{lmn}^{RT}*PG_{lmn}^{RT}\right]\right.\\ & -\sum_{m=1}^{NRTSC}\lambda_m\sum_{n=1}^{NRT}\left[\xi_{lmn}^{RT}*PRL_{lmn}^{RT}\right]+\sum_{m=1}^{NRTSC}\lambda_m\sum_{n=1}^{NRT}\left[\varsigma_{lmn}^{RT}*PBAT_{lmn}^{RT}\right]\\ & \left.+\sum_{m=1}^{NRTSC}\lambda_m\sum_{n=1}^{NRT}\left[\sigma_{lmn}^{RT}*E_{lmn}^{RT}\right]\right)\end{aligned}\tag{10.2}$$

The components of Eq. 10.1 are the purchasing electricity in the DA market (first sentence), the DG costs (second sentence), the profit from the presence of RLs (third sentence), the ESS cost (fourth sentence), and the purchasing electricity cost in the RT market (fifth sentence).

The objective function is restricted to the following constraints: the maximum and minimum power generations of microgrid energy resources, ramp-up and ramp down, minimum uptime and downtime, AC power flow, state of charge, and upper and lower limits of ESSs.

10.3 Solution Algorithm

The described RMEP problem has a large state space that involves thousands of variables in the expansion planning horizon. The uncertainties of the problem highly increase the state space of the RMEP problem. Further, the subproblems are nonlinear and non-convex.

For the first-level optimization problem, the particle swarm optimization (PSO) algorithm is used. Figure 10.3 depicts the flowchart of the optimization algorithm. At first, the upper-level problem is optimized for estimated scenarios by the PSO. Then, the second-level problem is solved by hybrid stochastic-robust optimization procedure to minimize the total cost of microgrid while limiting the unbalanced power in the RT market and considering the uncertainty in RT market price for the worst-case planning scenarios. The introduced hybrid decomposed model is preferable to pure stochastic optimization for two reasons: First, it gives the MGO an opportunity to decide at different risk levels according to their system resources. Second, due to the instability of the RT market price, the profitability and competitiveness of a microgrid may reduce greatly by relying on the RT market price. Through the robust control parameter Ψ, the extent of uncertainty in RT market prices can be controlled, and the level of risk associated with the bidding is determined.

The first stage considers the uncertainty of day-ahead market price. The uncertainty of IPGs is introduced in the second stage. The variables in this stage include the unit status and output of dispatchable units, RLs, and scheduling of ESSs. The third stage ensures the result is robust to uncertain real-time price for each scenario.

Thus, the formulation of the objective function can be rewritten as follows [21]:

$$\begin{aligned}\text{Min}\quad & \sum_{l=1}^{NDASC}\lambda_l\left(\sum_{m=1}^{NH}\beta_{lm}^{DA}*E_{lm}^{DA}+\sum_{m=1}^{NRTSC}\lambda_m\sum_{n=1}^{NRT}\left[\gamma_{lmn}^{RT}*PG_{lmn}^{RT}\right]\right.\\ & -\sum_{m=1}^{NRTSC}\lambda_m\sum_{n=1}^{NRT}\left[\xi_{lmn}^{RT}*PRL_{lmn}^{RT}\right]+\sum_{m=1}^{NRTSC}\lambda_m\sum_{n=1}^{NRT}\left[\varsigma_{lmn}^{RT}*PBAT_{lmn}^{RT}\right]\\ & \left.+\sum_{m=1}^{NRTSC}\bar{\sigma}_{lm}^{RT}*E_{lm}^{RT}+\Xi_{lm}{}^{*}\Psi_{lm}\right)\end{aligned}\tag{10.3}$$

The MATLAB software is used to generate random numbers, and LHS method is used for scenario generation. Then, by connecting the MATLAB to GAMS, the generated scenarios are inserted into GAMS, and scenario reduction is implemented by a forward method in the GAMS/SCENRED library. Next, for each of the scenarios, the introduced decomposition method is applied. The scenario generation and reduction procedure are shown in Fig. 10.4.

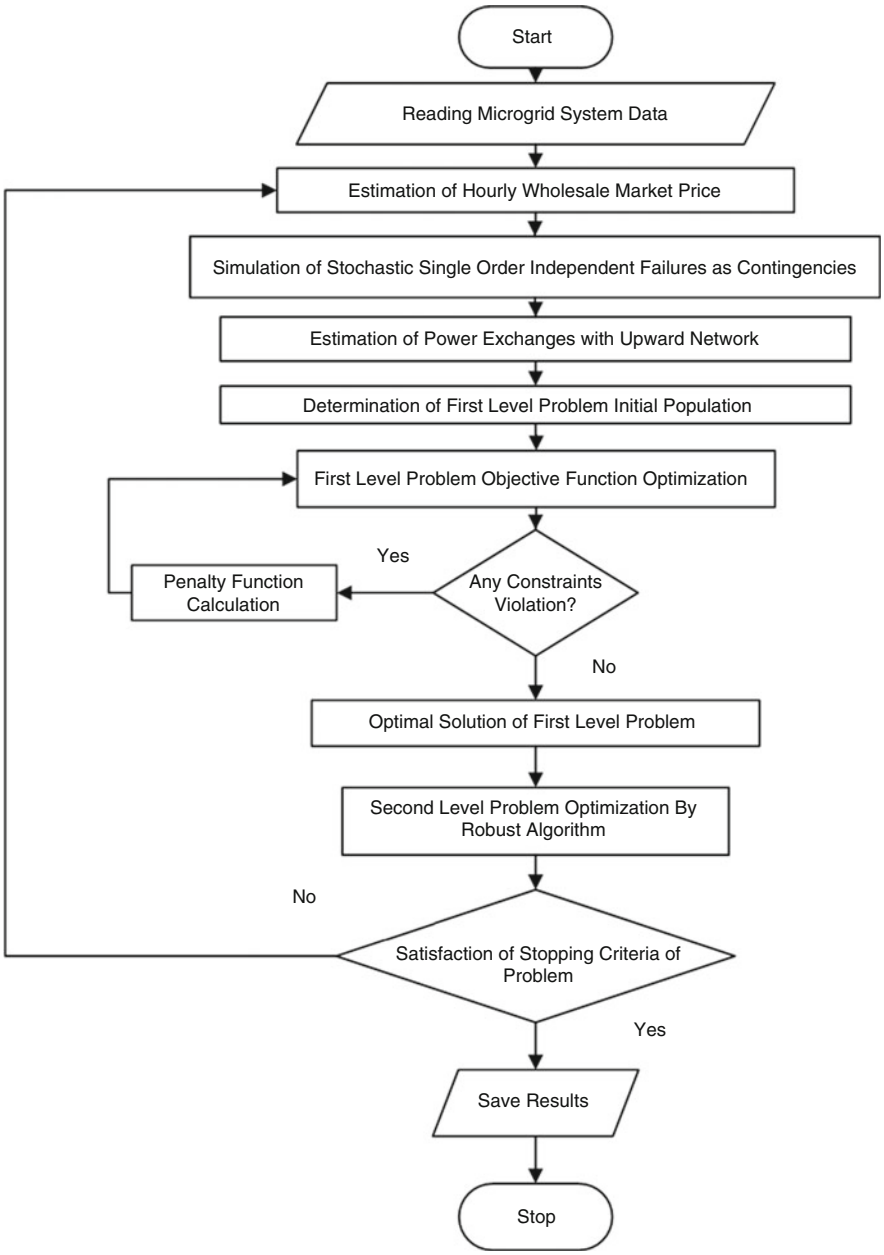

Fig. 10.3 The flowchart of the two-level optimization introduced algorithm

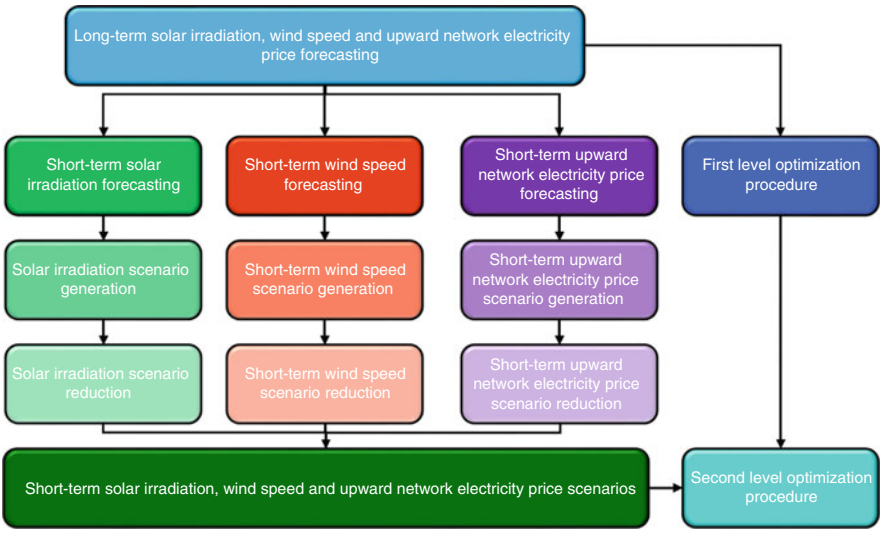

Fig. 10.4 The scenario generation and reduction procedure

10.4 Numerical Results

The introduced model is implemented on the 9-bus and 33-bus test systems. The wind turbine and solar panel data are available at [22]. Figures 10.5 and 10.6 depict the 9-bus and 33-bus microgrids, respectively. The 9-bus and 33-bus test system data are presented at [23–25] and [26], respectively.

10.4.1 The Nine-Bus Test System

Figures 10.7 and 10.8 depict the base load and upward network electricity price of the nine-bus microgrid, respectively.

Table 10.1 shows the DG installation alternatives technical characteristics and fixed and variable costs in monetary units (MUs).

The feeders' conductor data and ESSs data are presented in Tables 10.2 and 10.3, respectively. Table 10.4 presents the optimization input data for the nine-bus test system.

The optimal system topologies of the nine-bus test system for different years of expansion planning horizon are depicted in Fig. 10.9.

Table 10.5 depicts the optimal aggregated investment and operational costs of the nine-bus test system.

Table 10.6 presents the optimal operational costs of the nine-bus test system for different planning years.

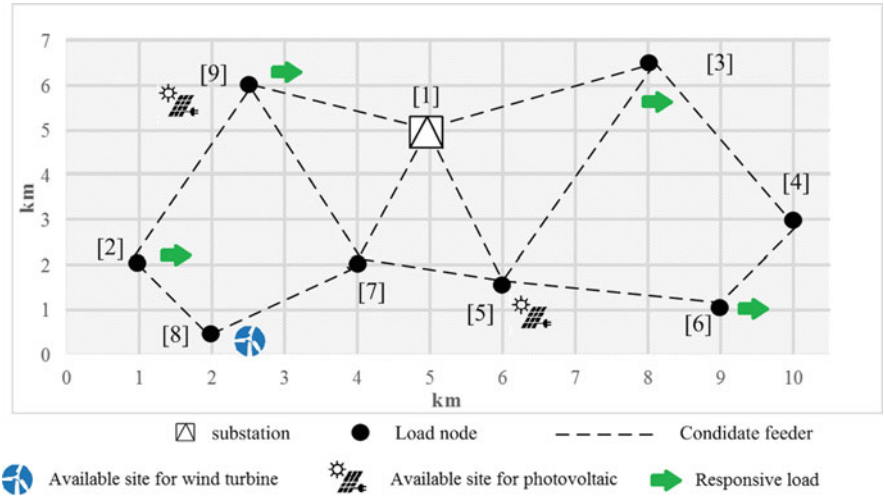

Fig. 10.5 The nine-bus microgrid

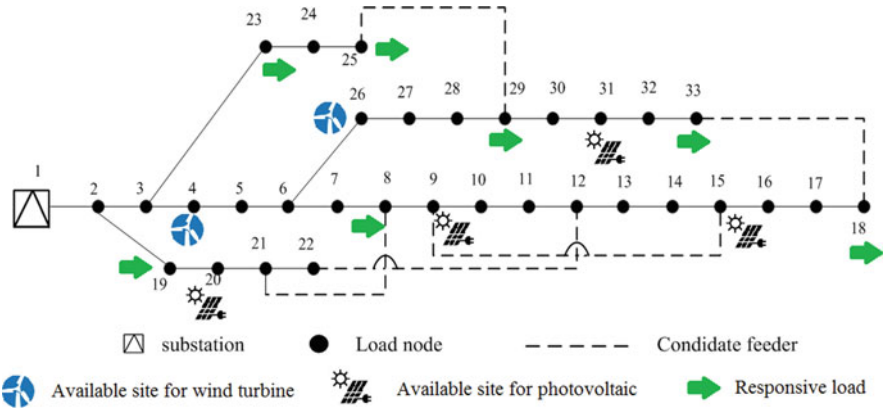

Fig. 10.6 The 33-bus microgrid

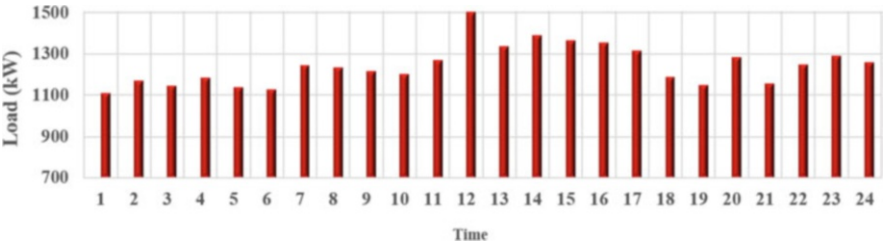

Fig. 10.7 The base electric load of the nine-bus test system

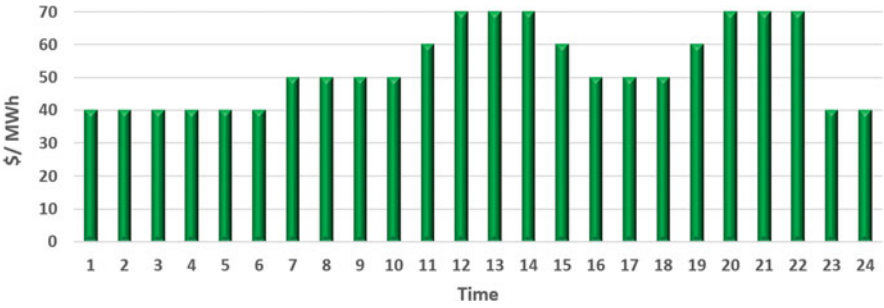

Fig. 10.8 The base electricity price of upward network of the nine-bus test system

Table 10.1 The DG installation alternatives technical characteristics and fixed and variable costs

DG type	Maximum output power P_{max}(kW)	Installation fixed cost (MUs)	Installation variable cost (MUs/kVA)	Operation fixed cost (MUs/kW)	Operation variable cost (MUs/kWh)
1	330	63,283.5	350	0.2588	1.0853
2	540	111,510	450	0.2692	1.3011
3	844	166,584.5	550	0.2373	1.0569

Table 10.2 Feeder's conductor data

Type	Resistance (Ω/km)	Reactance (Ω/km)	Capacity (MVA)	Cost (MMUs/km)
1	0.1738	0.2819	12	0.1
2	0.0695	0.2349	18	0.15

Table 10.3 ESS data

Type	Capacity (kW)	Rated output (kW)	Efficiency (%)
1	500	200	0.75

Table 10.4 The optimization input data for the nine-bus test system

Parameter	Value
Planning horizon year	5
Discount rate (%)	12.5
Load power factor	0.85
Load growth rate of (%)	3
Number of solar irradiation scenarios	4500
Number of wind turbine power generation scenarios	5000
Number of upward market price scenarios	500
Number of solar irradiation reduced scenarios	40
Number of wind turbine power generation reduced scenarios	45
Number of upward market price reduced scenarios	5

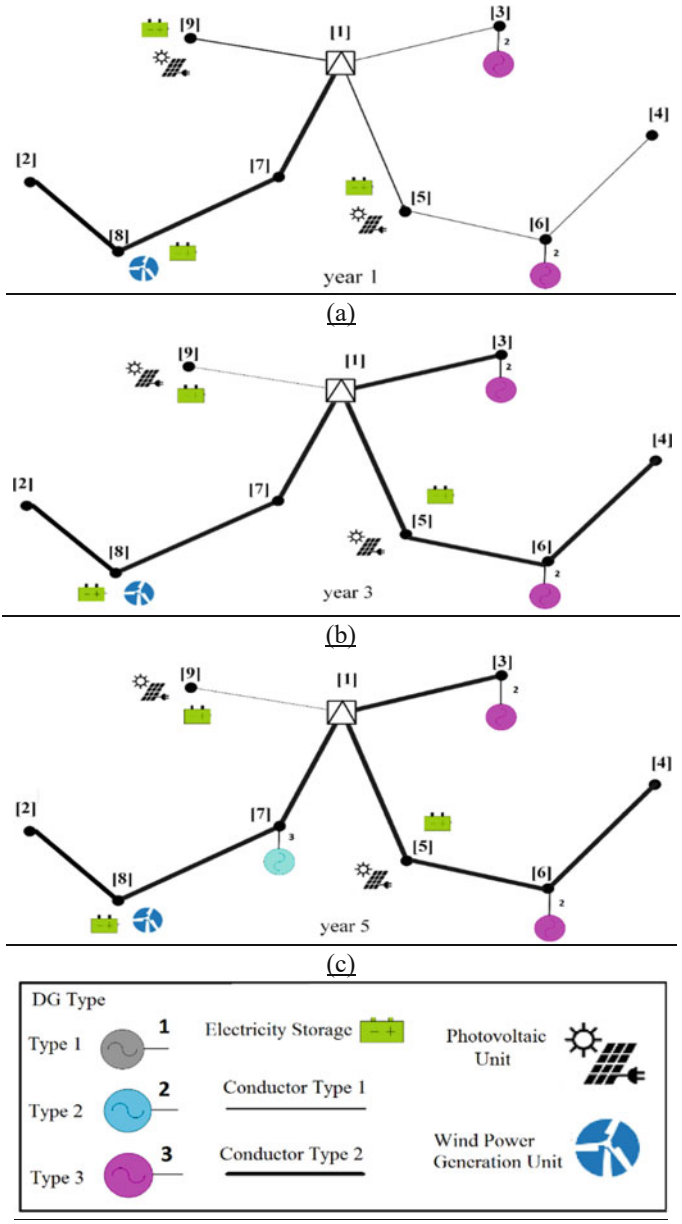

Fig. 10.9 (**a**) The optimal system topology of the nine-bus test system for the first year of expansion planning horizon, (**b**) the optimal system topology of the nine-bus test system for the third year of expansion planning horizon, (**c**) the optimal system topology of the nine-bus test system for the fifth year of expansion planning horizon

Table 10.5 The optimal aggregated investment and operational costs of the nine-bus test system

Costs (MMUs)			
Feeder installation costs	4.1514	Transformer and feeder operation costs	4.215
Transformer and ESS installation costs	9.2102	DG installation and operation costs	26.8213
ENSCs	0.39265	Energy loss costs	0.7214

Table 10.6 The optimal operational costs of the nine-bus test system for different planning years

	Year				
Costs	1	2	3	4	5
DG operation costs (MMUs)	2.760744	2.917854	3.026737	3.250342	3.369455
Energy loss costs (MMUs)	0.149915	0.154201	0.142806	0.133136	0.141342
Energy purchased from upward network costs (MMUs)	0.2125	0.2118	0.1842	0.1522	0.1421
Transformer operation costs (MMUs)	0.648962	0.790089	0.829612	0.969424	0.976913
RL costs (MMUs)	0.8213	0.8254	0.8421	0.8697	0.8924

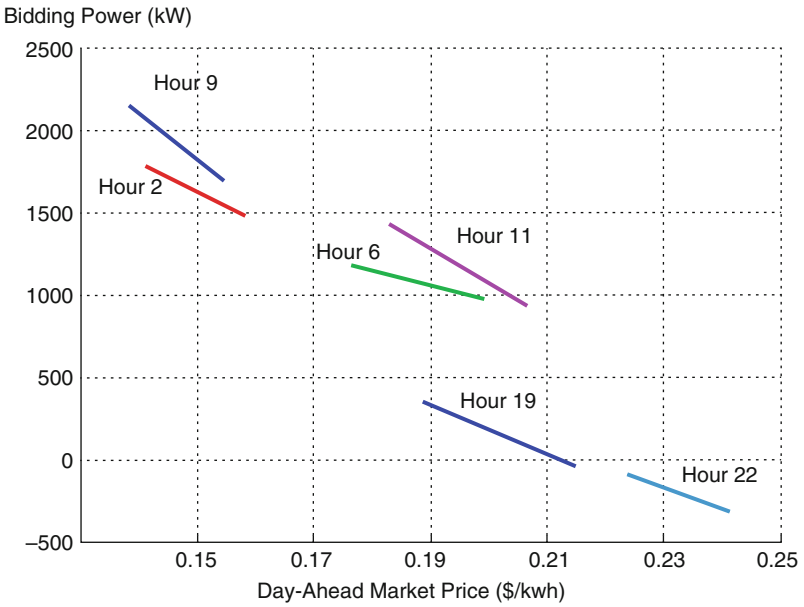

Fig. 10.10 The nine-bus MGO price-power bidding curves in the DA market

The bidding curves of the nine-bus system in the DA market for selected hours of the worst-case planning scenarios are shown in Fig. 10.10. The purchase bidding quantity decreases as the market price increases for all hours. The microgrid increases the output power of dispatchable units and discharges power from the ESSs, while during low price hours, the microgrid reduces its output and charges the ESSs.

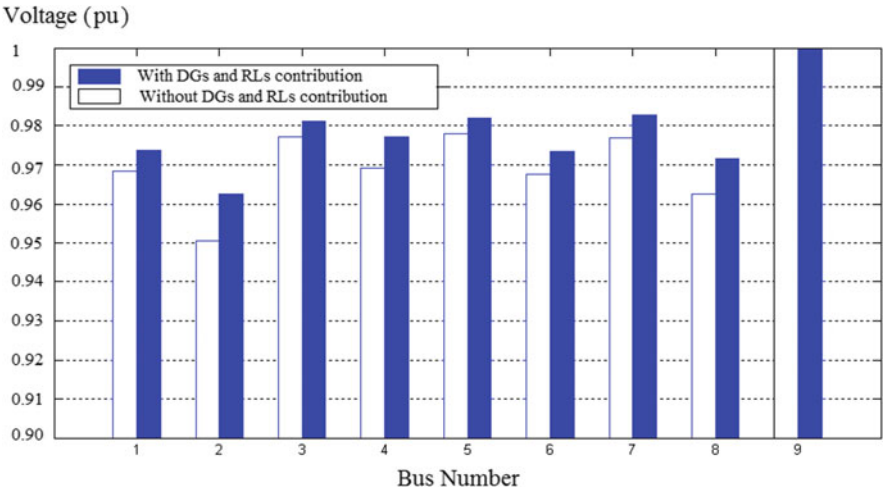

Fig. 10.11 The voltage of the nine-bus test system for one of the worst-case planning scenarios and different conditions of DG/RL contribution

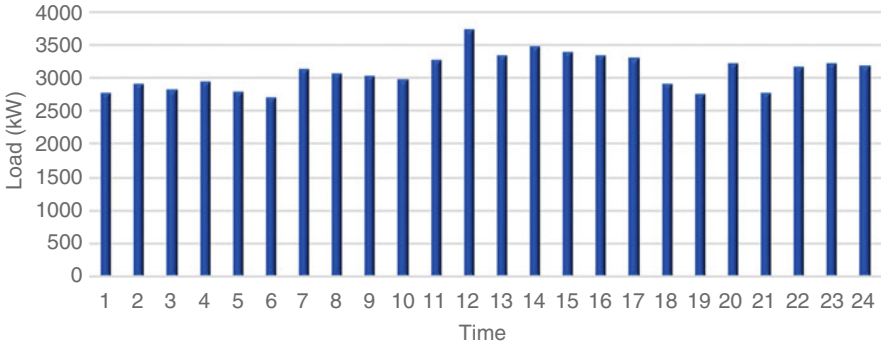

Fig. 10.12 The base electric load of the 33-bus test system

Figure 10.11 displays the voltage of the nine-bus test system for one of the worst-case planning scenarios and different conditions of DG/RL contribution.

10.4.2 The 33-Bus Test System

Figures 10.12 and 10.13 depict the base load and upward network electricity price of the 33-bus microgrid, respectively.

The optimal system topologies of the 33-bus test system for the first, third, and fifth years of expansion planning horizon are depicted in Fig. 10.14a, b, and c, respectively.

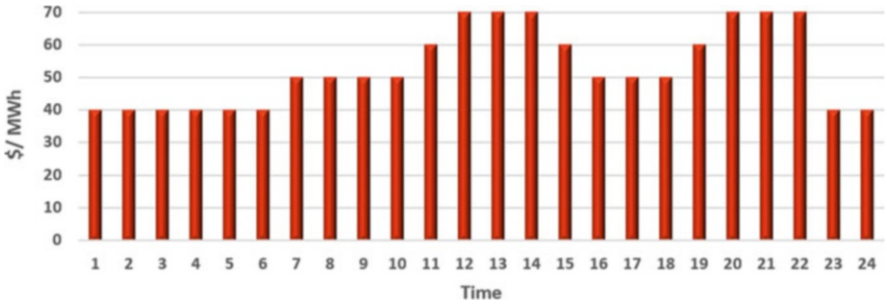

Fig. 10.13 The base electricity price of upward network of the 33-bus test system

Table 10.7 depicts the optimal aggregated investment and operational costs of the 33-bus test system.

Table 10.8 presents the optimal operational costs of the 33-bus test system for different planning years.

The bidding curves of the 33-bus system in the DA market for selected hours of the worst-case planning scenarios are shown in Fig. 10.15. The purchase bidding quantity decreases as the market price increases for all hours. This process continues to the point where the purchase bid is offered by the microgrid to the market. Figure 10.16 displays the voltage of the 33-bus test system for one of the worst-case planning scenarios and different conditions of DG/RL contribution.

The robust optimization limits the unbalanced power of the RT market. The expected microgrid operation cost for different values of Ψ for the 9-bus and the 33-bus systems is shown in Figs. 10.17 and 10.18, respectively.

As illustrated in Figs. 10.17 and 10.18, while Ψ increases, the expectation increases, indicating the trade-off between risk and benefit.

The value of stochastic solution (VSS) index shows the economic advantage of using the stochastic scheduling into the deterministic scheduling under uncertainty. To calculate this index, the optimal solutions of deterministic and stochastic optimizations are obtained, and the difference between these two solutions is the VSS index. The obtained results for $\Psi = 0$ and $\Psi = 24$ modes are presented in Tables 10.9 and 10.10 for the 9-bus and the 33-bus test systems, respectively. The computation time for the 9-bus and the 33-bus test systems is 629 and 1564 s, respectively. The simulation was carried out on a PC (Intel Core 2, 2.93 GHz, 4 GB RAM). With considering the randomness of the day-ahead market price, as well as the wind and solar powers, the operation cost is improved in the stochastic optimization compared to the deterministic case. The VSS index is calculated for the two cases of deterministic generation power of IPGs and deterministic market price for the worst-case planning scenarios.

According to the results, an accurate problem-solving structure is introduced that is appropriate for optimal microgrid planning and scheduling for the worst-case planning scenarios.

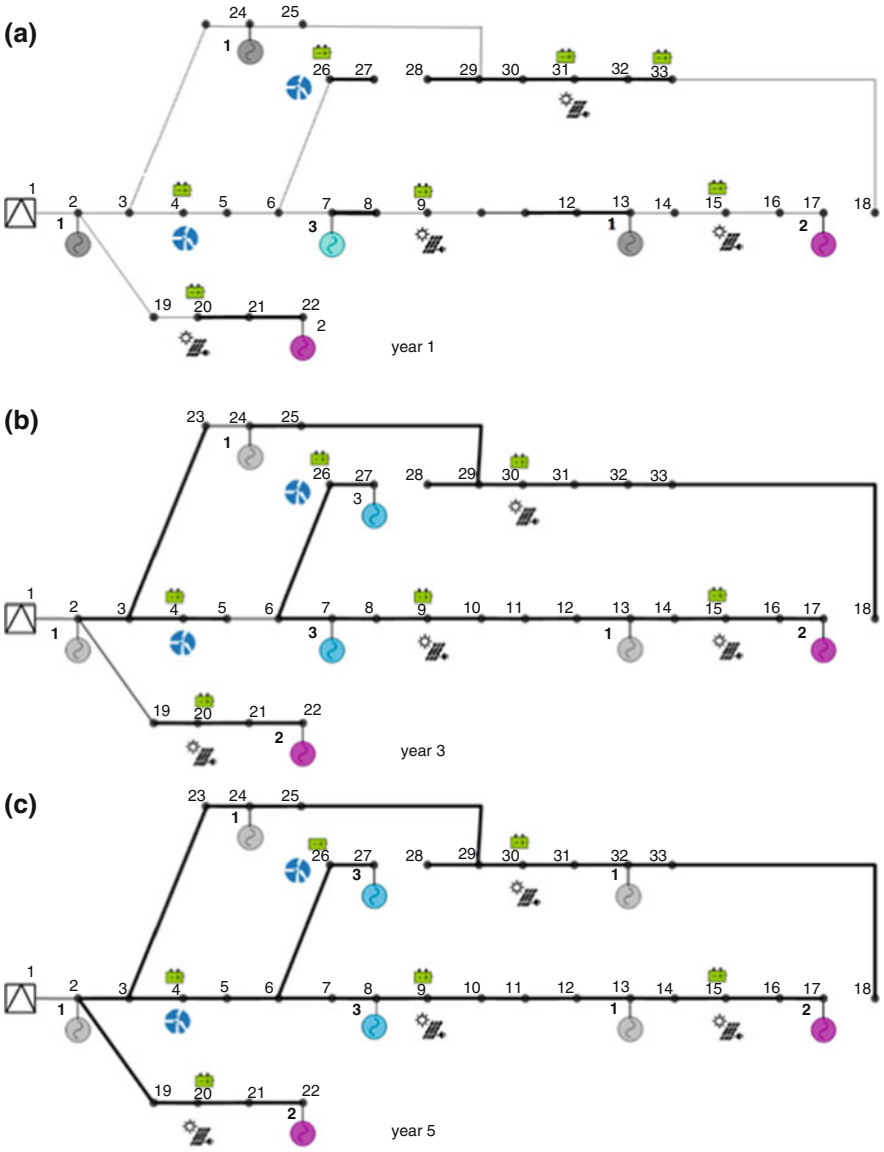

Fig. 10.14 (**a**) The optimal system topology of the 33-bus test system for the 1st year of expansion planning horizon, (**b**) the optimal system topology of the 33-bus test system for the 3rd year of expansion planning horizon, (**c**) the optimal system topology of the 33-bus test system for the 5th year of expansion planning horizon

Table 10.7 The optimal aggregated investment and operational costs of the 33-bus test system

Costs (MMUs)			
Feeder installation costs	17.2891	Transformer and feeder operation costs	19.6214
Transformer and ESS installation costs	38.7412	DG installation and operation costs	82.1451
ENSCs	2.3518	Energy loss costs	2.1162

Table 10.8 The optimal operational costs of the 33-bus test system for different planning years

	Year				
Costs	1	2	3	4	5
DG operation costs (MMUs)	11.2784	11.00639	11.45726	11.85176	12.63635
Energy loss costs (MMUs)	0.342408	0.419038	0.446115	0.461738	0.446901
Energy purchased from upward network costs (MMUs)	0.280421	0.5621	0.6814	0.7321	0.7692
Transformer operation costs (MMUs)	2.384952	2.658685	3.112461	2.762407	2.606095
RL costs (MMUs)	4.2681	4.6214	4.6325	4.8971	5.0125

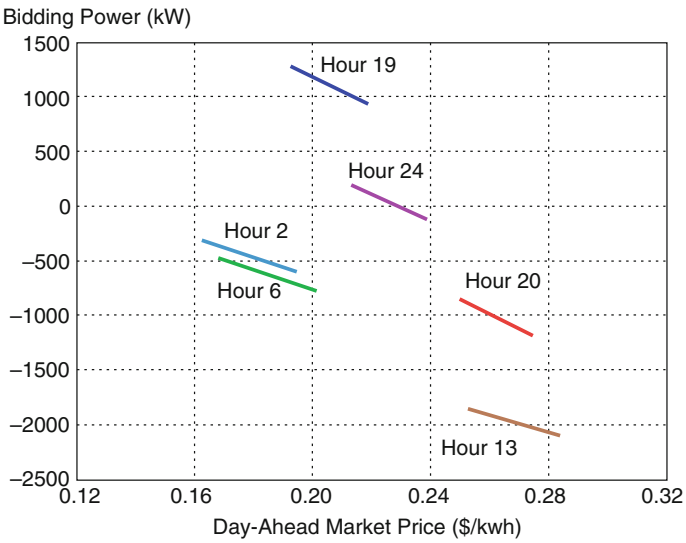

Fig. 10.15 The 33-bus MGO price-power bidding curves in the DA market

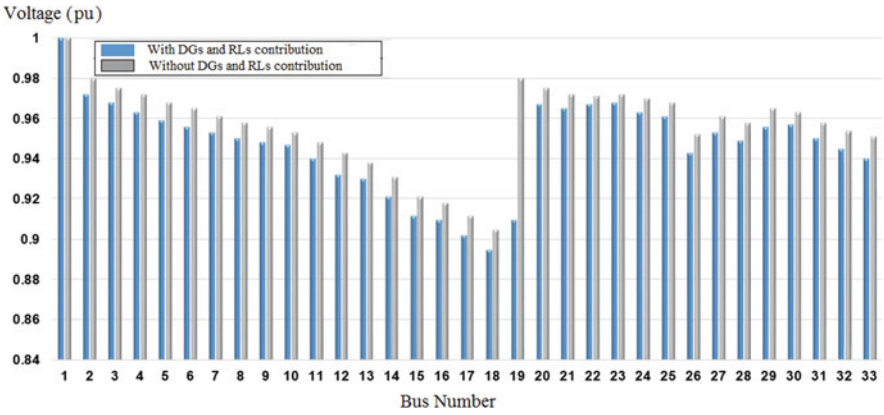

Fig. 10.16 The voltage of the 33-bus test system for one of the worst-case planning scenarios and different conditions of DG/RL contribution

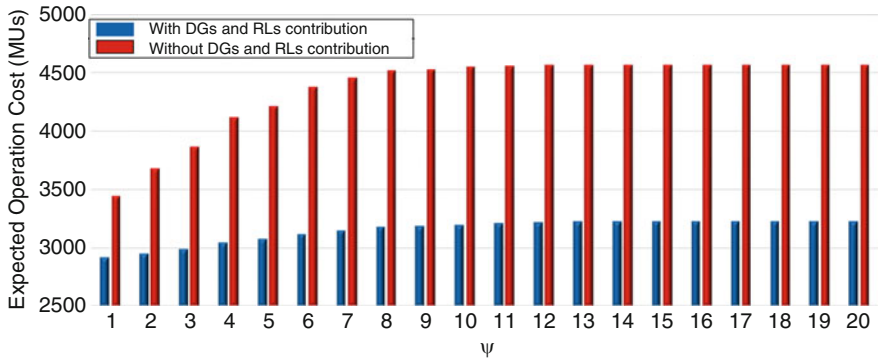

Fig. 10.17 The expected microgrid operation cost for different values of Ψ for the nine-bus system

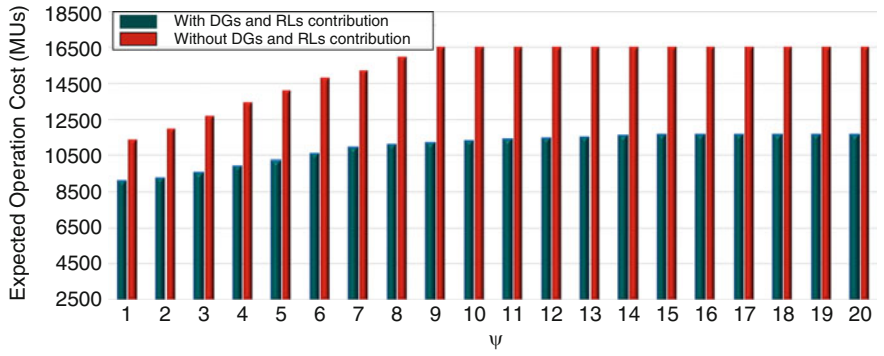

Fig. 10.18 The expected microgrid operation cost for different values of Ψ for the 33-bus system

Table 10.9 VSS index for the nine-bus system

$\Psi = 0$		
Stochastic solution (MUs)	Expected cost using deterministic IPG power generation solution (MUs)	VSS using deterministic IPG power generation solution (MUs)
2984.2	2984.7	0.5 (0.016574%)
Stochastic solution (MUs)	Expected cost using deterministic upward network electricity price solution (MUs)	VSS using deterministic upward network electricity price solution (MUs)
2984.2	2993.1	8.9 (0.2982%)
$\Psi = 24$		
Stochastic solution (MUs)	Expected cost using deterministic IPG power generation solution (MUs)	VSS using deterministic IPG power generation solution (MUs)
2998.7	3005.3	6.6 (0.22%)
Stochastic solution (MUs)	Expected cost using deterministic upward network electricity price solution (MUs)	VSS using deterministic upward network electricity price solution (MUs)
2998.7	3008.1	9.4 (0.3134%)

Table 10.10 VSS index for the 33-bus system

$\Psi = 0$		
Stochastic solution (MUs)	Expected cost using deterministic IPG power generation solution (MUs)	VSS using deterministic IPG power generation solution (MUs)
9258.6	9271.2	12.6 (0.1360%)
Stochastic solution (MUs)	Expected cost using deterministic upward network electricity price solution (MUs)	VSS using deterministic upward network electricity price solution (MUs)
9258.6	9272.3	13.7 (0.1479%)
$\Psi = 24$		
Stochastic solution (MUs)	Expected cost using deterministic IPG power generation solution (MUs)	VSS using deterministic IPG power generation solution (MUs)
9347.2	9352.1	4.9 (0.05242%)
Stochastic solution (MUs)	Expected cost using deterministic upward network electricity price solution (MUs)	VSS using deterministic upward network electricity price solution (MUs)
9347.2	9361.8	14.6 (0.15619%)

10.5 Conclusions

A microgrid expansion planning procedure was reviewed in the present chapter. The introduced method used a model to investigate the IPG/RL impacts on RMEP. The RMEP formulation found the optimum usage of IPG/RL power generation scenarios, and it considered the impact of robust optimization on the RMEP.

This algorithm decomposed the RMEP problem into two-level subproblems. The model of RMEP was a MINLP problem, and the PSO algorithm was used. The bidding strategy in the DA market is introduced based on hybrid stochastic-robust optimization for the worst-case planning scenarios and considering the AC model and the configuration of the microgrid.

The proposed hybrid model is preferable to pure stochastic optimization for two reasons: First, it gives the MGO an opportunity to decide at different risk levels according to his/her system configuration. Second, due to the instability of the real-time market price, the profitability and competitiveness of a microgrid may reduce greatly by relying on the real-time market price for the worst-case planning scenario.

The algorithm was assessed for the 9-bus and the 33-bus test systems with quite acceptable results.

References

1. Chowdhury, S., Chowdhury, S. P., & Crossley, P. (2009). *Microgrids and active distribution networks* (Renewable energy series). Stevenage: IET.
2. Tsikalakis, A. G., & Hatziargyriou, N. D. (2008). Centralized control for optimizing microgrids operation. *IEEE Transactions on Energy Conversion, 23*(1), 241–248.
3. Nwulu, N. I., & Xia, X. (2017). Optimal dispatch for a microgrid incorporating renewables and demand response. *Renewable Energy, 101*, 16–28.
4. Gu, W., Wu, Z., Bo, R., Liu, W., Zhou, G., Chen, W., & Wu, Z. (2014). Modeling, planning and optimal energy management of combined cooling, heating and power microgrid: A review. *International Journal of Electrical Power & Energy Systems, 54*, 26–37.
5. Junga, J., & Villaranb, M. (2017). Optimal planning and design of hybrid renewable energy systems for microgrids. *Renewable and Sustainable Energy Reviews, 75*, 180–191.
6. Quashie, M., Marnay, C., Bouffard, F., & Joós, G. (2018). Optimal planning of microgrid power and operating reserve capacity. *Applied Energy, 210*, 1229–1236.
7. Mehdizadeh, A., & Taghizadegan, N. (2017). Robust optimisation approach for bidding strategy of intermittent generation-based microgrid under demand side management. *IET Generation, Transmission and Distribution, 11*, 1446–1455.
8. Shi, L., Luo, Y., & Tu, G. Y. (2014). Bidding strategy of microgrid with consideration of uncertainty for participating in power market. *International Journal of Electrical Power & Energy Systems, 59*, 1–13.
9. Liu, G., Xu, Y., & Tomsovic, K. (2016). Bidding strategy for microgrid in day-ahead market based on hybrid stochastic/robust optimization. *IEEE Transactions on Smart Grid, 7*(1), 227–237.
10. Nguyen, D. T., & Le, L. B. (2014). Optimal bidding strategy for microgrids considering intermittent energy and building thermal dynamics. *IEEE Transactions on Smart Grid, 5*(4), 1608–1620.
11. Pandžić, H., Morales, J. M., Conejo, A. J., & Kuzle, I. (2013). Offering model for a virtual power plant based on stochastic programming. *Applied Energy, 105*, 282–292.
12. Fleten, S. E., & Pettersen, E. (2005). Constructing bidding curves for a price-taking retailer in the norwegian electricity market. *IEEE Transactions on Power Systems, 20*(2), 701–708.
13. Liu, G., Starke, M., Xiao, B., & Tomsovic, K. (2017). Robust optimisation-based microgrid scheduling with islanding constraints. *IET Generation, Transmission, and Distribution, 11*, 1820–1828.

14. Herranz, R., Roque, A. M. S., Villar, J., & Campos, F. A. (2012). Optimal demand-side bidding strategies in electricity spot markets. *IEEE Transactions on Power Systems, 27*(3), 1204–1213.
15. Wang, L., Li, Q., Ding, R., Sun, M., & Wang, G. (2017). Integrated scheduling of energy supply and demand in microgrids under uncertainty: A robust multi-objective optimization approach. *Energy, 130*, 1–14.
16. Shaban Boloukat, M. H., & Foroud, A. A. (2016). Stochastic-based resource expansion planning for a grid-connected microgrid using interval linear programming. *Energy, 113*, 776–787.
17. Hemmati, R., Saboori, H., & Siano, P. (2017). Coordinated short-term scheduling and long-term expansion planning in microgrids incorporating renewable energy resources and energy storage systems. *Energy, 134*, 699–708.
18. Nazar, M. S., Haghifam, M. R., & Nazar, M. (2012). A scenario driven multiobjective primary–secondary microgrid Expansion Planning algorithm in the presence of wholesale–retail market. *International Journal of Electrical Power & Energy Systems, 40*, 29–45.
19. Shahnia, F., Arefi, A., & Ledwich, G. (2018). *Electric distribution network planning*. Singapore: Springer.
20. Liu, G., & Tomsovic, K. (2014). A full demand response model in co-optimized energy and reserve market. *Electric Power Systems Research, 111*, 62–70.
21. Bertsimas, D., & Sim, M. (2003). Robust discrete optimization and network flows. *Mathematical Programming B, 98*, 49–71.
22. Derakhshandeh, S. Y., Masoum, A. S., Deilami, S., Masoum, M. A. S., & Golshan, M. E. H. (2013). Coordination of generation scheduling with PEVs charging in industrial microgrids. *IEEE Transactions on Power Systems, 28*(3), 3451–3461.
23. El-Khattam, W., Bhattacharya, K., Hegazy, Y., & Salama, M. M. A. (2004). Optimal investment planning for distributed generation in a competitive electricity market. *IEEE Transactions on Power Systems, 19*(3), 1674–1684.
24. El-Khattam, W., Hegazy, Y. G., & Salama, M. M. A. (2005). An integrated distributed generation optimization model for distributed system planning. *IEEE Transactions on Power Systems, 20*(2), 1158–1165.
25. Falaghi, H., & Haghifam, M. R. (2007). ACO based algorithm for distributed generation sources allocation and sizing in distribution systems, power tech. *IEEE power tech conference*, 555–560.
26. Kia, M., Nazar, M. S., Sepasian, M. S., Heidari, A., & Siano, P. (2017). An efficient linear model for optimal day ahead scheduling of CHP units in active distribution networks considering load commitment programs. *Energy, 139*, 798–817.

Chapter 11
Robust Transmission Network Expansion Planning (IGDT, TOAT, Scenario Technique Criteria)

Shahriar Abbasi and Hamdi Abdi

Nomenclature

B	Set of load buses
B_{ij}	Susceptance of a single line in corridor (i,j)
c_{ij}	Cost of an added line to corridor (i,j) ($)
$\boldsymbol{f}$	Vector of power flows in corridors (MW)
f_b	Basic value of objective function
f_{ij}	Power flow in corridor (i,j) (MW)
$\bar{f}_{ij}$	Power flow limit of a single line in corridor (i,j) (MW)
n_{ij}	Number of added lines to corridor (i,j)
$\bar{n}_{ij}$	Maximum number of lines that can be added to corridor (i,j)
n_{ij}^0	Number of existing lines in corridor (i,j)
p_f	Penalty factor for load and wind power generation curtailment ($/MW)
$\boldsymbol{P}_d$	Vector of loads (MW)
$\boldsymbol{P}_g$	Vector of generated powers (MW)
$\underline{\boldsymbol{P}}_g/\bar{\boldsymbol{P}}_g$	Vector of lower/upper generation limits (MW)
$\boldsymbol{P}_w$	Vector of wind power generations (MW)
$\boldsymbol{r}$	Vector of curtailed loads (MW)
r_i	Curtailed load at bus i (MW)
$\boldsymbol{S}$	Node-branch incidence matrix
v	Wind speed (m/sec)
v_{ci}	Cut-in speed of wind turbine (m/sec)
v_{co}	Cutout speed of wind turbine (m/sec)
v_r	Rated speed of wind turbine (m/sec)
$\boldsymbol{w}$	Vector of curtailed wind power generations (MW)

(continued)

S. Abbasi · H. Abdi (✉)
Electrical Engineering Department, Faculty of Engineering, Razi University, Kermanshah, Iran
e-mail: hamdiabdi@razi.ac.ir

B. Mohammadi-ivatloo, M. Nazari-Heris (eds.), *Robust Optimal Planning and Operation of Electrical Energy Systems*,
https://doi.org/10.1007/978-3-030-04296-7_11

w_i	Curtailed wind power generation at bus i (MW)
$\boldsymbol{X}$	Set of decision variables
α	Scale parameter
β	Shape parameter
$\boldsymbol{\Gamma}$	Uncertainty set
$\boldsymbol{\gamma}$	Set of input uncertain variables
$\overline{\gamma}$	Predicted (expected) value of uncertain variable γ
ζ	Radius of uncertainty
$\hat{\zeta}$	Maximum radius of uncertainty
θ_i/θ_j	Voltage angle at bus i/j
Λ_C	Critical value of objective function
ς_C	Degree of acceptable tolerance on increasing f_b
Ψ	Set of wind farms
Ψ_{eq}	Set of equality and inequality constraints
Ψ_{ineq}	Set of inequality constraints
Ω	Set of available corridors

11.1 Introduction

The aim of transmission network expansion planning (TNEP) is providing enough capacity to transfer power from generation section to load centers in a reliable and economically efficient manner. Generally, the TNEP is a mixed integer optimization problem with the aim of identifying where, when, and what type of new transmission lines should be installed in the transmission network.

However, the power system uncertainties can affect the expansion plan of a transmission network. Therefore, these uncertainties should be considered in TNEP calculations. In the previous works, different uncertainty modeling methods are presented to investigate the impact of power system uncertainties on TNEP. In Ref. [1], the point estimation method (PEM) is used to study the impact of conventional generation replacement with wind power generation on TNEP. In Ref. [2], TNEP with correlation among load uncertainties is considered; to model load correlation, the unscented transformation (UC) is used. References [3–5] implemented numerical methods to consider uncertain behavior of power system uncertainties (load, wind power generation, etc.) in TNEP. In Refs. [6, 7], the effect of large-scale distant wind farms on TNEP applying the two-point estimation method (2-PEM) is studied.

In general, different uncertainties must be addressed in TNEP. The TNEP calculation must be so that the obtained expansion plan withstands effects of these uncertainties. Among these uncertainties, the uncertainties of demanded load and wind power generation are more discussed in the literature. This is mainly because

the demanded load is significantly uncertain and the aim of each power system is supplying loads in a reliable manner [2]. Also, in most power systems, the renewable generations, especially wind power generation, have notable share in total generation capacity. But the renewable generations are changeable and uncontrollable in nature. The generated power by a wind farm depends on wind speed at its location that changes intermittently [1]. For these reasons, in this chapter work, these two major sources of uncertainty are addressed in TNEP calculation.

In this chapter, the robust TNEP (RTNEP) in the presence of uncertainties of loads and wind power generation is studied. A transmission network is robust against a set of uncertainties if withstand their variations and transfer power from generation section to load centers in a reliable manner. The robust methods of (a) information-gap decision theory (IGDT), (b) Taguchi's orthogonal array testing (TOAT), and (c) scenario technique criteria (min-max regret criterion) are proposed and simulated here. Applying each of these methods, the robust expansion plan for the transmission network of the considered case study is calculated on the modified 6-bus Garver test system [8]. The obtained results verify the capability of the mentioned methods in RTNEP. These methods can easily be implemented on any large- and real-scale power system. Also, different uncertainty types can be inserted in these methods.

The rest of this chapter is organized as follows: In Sect. 11.2, the optimization problem of conventional deterministic TNEP is formulated, wherein the persuaded objective function is minimizing sum of investment cost and costs of load and wind power generation curtailment. In Sect. 11.3, the modeling of uncertainties of load and wind power generation is presented. The robust methods of IGDT, TOAT, and min-max regret criterion are, respectively, explained and simulated in Sects. 11.4, 11.5, and 11.6. Finally, the concluding remarks from this chapter are drawn in Sect. 11.7.

11.2 Conventional Deterministic TNEP

In a power system represented by the DC power flow model, the conventional deterministic TNEP is a mixed integer nonlinear optimization problem as follows [4, 9, 10]:

$$f = \underset{n_{ij},\, r_i,\, w_i}{\text{minimize}} \left\{ \sum_{(i,j)\in\Omega} c_{ij} n_{ij} + p_f \sum_{i\in B} r_i + p_f \sum_{i\in\Psi} w_i \right\} \tag{11.1}$$

subject to

$$\boldsymbol{S}^T\boldsymbol{f} + \boldsymbol{P}_g + (\boldsymbol{P}_w - \boldsymbol{w}) = (\boldsymbol{P}_d - \boldsymbol{r}) \tag{11.2}$$

$$f_{ij} - B_{ij}\left(n_{ij}^0 + n_{ij}\right)\left(\theta_i - \theta_j\right) = 0 \tag{11.3}$$

$$\left|f_{ij}\right| \le \left(n_{ij}^0 + n_{ij}\right)\bar{f}_{ij} \tag{11.4}$$

$$\underline{\boldsymbol{P}}_g \le \boldsymbol{P}_g \le \bar{\boldsymbol{P}}_g \tag{11.5}$$

$$0 \le \boldsymbol{r} \le \boldsymbol{P}_d \tag{11.6}$$

$$0 \le \boldsymbol{w} \le \boldsymbol{P}_w \tag{11.7}$$

$$0 \le n_{ij} \le \bar{n}_{ij},\ \forall (i,j) \in \Omega \tag{11.8}$$

The objective of formulation (11.1) is minimizing investment cost (total cost of new transmission lines) and costs of load and wind power generation curtailments. The decision variables are n_{ij}, r_i, and w_i. After minimizing (11.1), the transmission network must satisfy all constraints (11.2)–(11.8). Equality constraint (11.2) is the nodal active power balances. Equality constraint (11.3) is the equation of lines power flow. Inequality constraints (11.4) and (11.5) are physical limits which confine lines power flow and generators output, respectively. Operational limits of loss of load and wind power generation curtailment are, respectively, as inequality constraints (11.6) and (11.7). Inequality constraint (11.8) limits maximum number of new lines added to corridors.

11.3 Load and Wind Power Generation Uncertainties

In power systems, future loads are not certain; loads change stochastically around their expected values. Therefore one of the main uncertainty sources in power systems is related to the demanded loads. Probabilistic distribution functions (pdfs) are appropriate tools for modeling stochastic variations of power systems loads. Usually, the normal pdf is used in literatures for modeling the load uncertainty [11–13]. For the uncertain variable x, with mean (expected) value μ and standard deviation σ, the normal pdf is as follows:

$$f(x) = \frac{1}{\sigma\sqrt{2\pi}} e^{\frac{-(x-\mu)^2}{2\sigma^2}} \tag{11.9}$$

where parameters μ and σ of loads are calculated using the historical data of loads [11–13]. For a typical uncertain variable with the mean value of 100 and standard deviation of 10, the normal pdf is as follows (Fig. 11.1):

Another considered uncertainty is wind power generation. Generated power by a wind power unit depends on wind speed at generator location. On the one hand, wind speed is not fixed, and on the other hand, in most today's power systems, wind

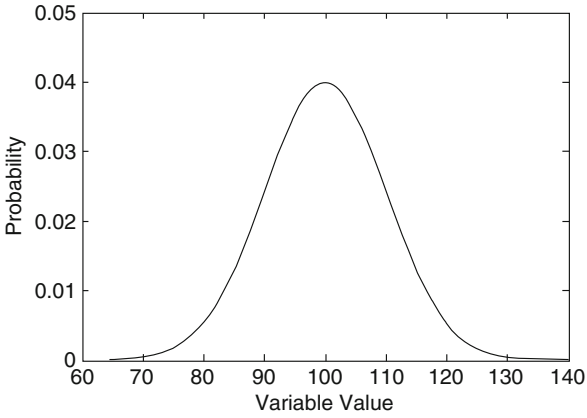

Fig. 11.1 A typical normal pdf

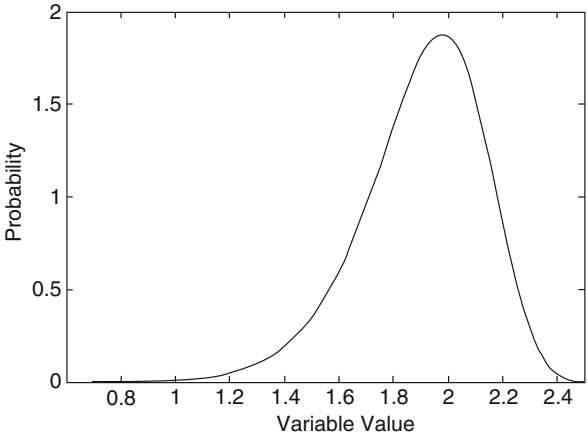

Fig. 11.2 A typical Weibull pdf

power generation has a notable share in total generation capacity. So, wind power generation is a major source of uncertainty in these power systems and should be modeled appropriately.

Commonly, the Weibull pdf is used for modeling the stochastic variations of wind speed [1, 4, 6]. For uncertain variable x, this pdf is formulated as follows:

$$f(x) = \frac{\beta}{\alpha^{\beta}} x^{\beta-1} e^{-\left(\frac{x}{\alpha}\right)^{\beta}} \tag{11.10}$$

where α and β are the scale and shape parameters.

For a typical uncertain variable with the scale parameter equals to 2 and shape parameter equals to 10, the Weibull pdf is as follows (Fig. 11.2):

The scale and shape parameters of Weibull pdf are calculated using the historical data of the wind speed at wind generator location, using Justus formulas as follows:

$$\beta = \left(\frac{\sigma^2}{\mu}\right)^{-1.086} \tag{11.11}$$

$$\alpha = \frac{\mu \times \beta^{2.6674}}{0.184 + 0.816\beta^{2.73855}} \tag{11.12}$$

The generated power by a wind power generator (P_w) is nonlinearly related to the wind speed at the wind turbine location. This relation is as follows:

$$P_w = \begin{cases} 0 & 0 \le v \le v_{ci} \\ P_r(v - v_{ci})/(v_r - v_{ci}) & v_{ci} \le v \le v_r \\ P_r & v_r \le v \le v_{co} \\ 0 & v_{co} \le v \end{cases} \tag{11.13}$$

where P_r is the rated power of generator in MW and v is the wind speed in m/sec. v_{ci}, v_{co}, and v_r are, respectively, the cut-in speed, cutout speed, and rated speed of wind turbine [4].

Above pdfs of uncertain input variables are needed in probabilistic solution methods. In robust optimization, these pdfs are not needed; in fact, robust strategies are appropriate when historical data of input variables are limited or unavailable.

11.4 RTNEP Applying Information-Gap Decision Theory (IGDT)

In IGDT uncertainty modeling methods, the pdfs of uncertainties are not needed. In these methods, for a predetermined range of objective function of optimization problem, the problem will be solved to find a definite uncertainty budget (UB) of input uncertain variables. IGDT is useful when uncertainties are severe and the relevant historical data are not accessible [14].

Here, a risk-averse IGDT-based strategy is implemented to solve RTNEP problem with load and wind power generation uncertainties. The TNEP formulation (11.1)–(11.8) can be written as the following compact form:

$$\underset{\boldsymbol{X}}{\text{minimize}}\, f(\boldsymbol{X}, \boldsymbol{\gamma}) \tag{11.14}$$

subject to

$$\boldsymbol{H_i}(\boldsymbol{X}, \boldsymbol{\gamma}) = 0,\ i \in \Psi_{eq} \tag{11.15}$$

$$\boldsymbol{G_j}(\boldsymbol{X}, \boldsymbol{\gamma}) \le 0,\ j \in \Psi_{ineq} \tag{11.16}$$

$$\boldsymbol{\gamma} \in \boldsymbol{\Gamma} \tag{11.17}$$

where f is the objective function (1) that its value depends to the set of decision variables $\boldsymbol{X}$ and the set of input uncertain variables $\boldsymbol{\gamma}$; $\boldsymbol{X}$ includes n_{ij}, r_i, and w_i; and $\boldsymbol{\gamma}$ consists of $\boldsymbol{P}_d$ and $\boldsymbol{P}_w$. $\boldsymbol{\Gamma}$ is the uncertainty set describing behavior of uncertain input variables. $\boldsymbol{H_i}$ and $\boldsymbol{G_j}$ are ith equality and jth inequality constraints, respectively, and Ψ_{eq} and Ψ_{ineq} are the sets of equality and inequality constraints. The set $\boldsymbol{\Gamma}$ can be written as follows:

$$\forall \gamma \in \boldsymbol{\Gamma}\left(\overline{\gamma}, \zeta\right) = \left\{\gamma : \left|\frac{\gamma - \overline{\gamma}}{\overline{\gamma}}\right| \leq \zeta\right\} \tag{11.18}$$

where $\overline{\gamma}$ is the predicted (expected) value of variable γ. ζ is the maximum variation of γ from its expected value called "radius of uncertainty." This radius is uncertain, and finding its value is the aim of IGDT.

Initially, the TNEP optimization problem (11.1)–(11.8) will be solved supposing all uncertain input variables at their predicted values, as follows:

$$\underset{\boldsymbol{X}}{\text{minimize}}\, f_b = f\left(\boldsymbol{X}, \overline{\boldsymbol{\gamma}}\right) \tag{11.19}$$

subject to

$$\boldsymbol{H_i}\left(\boldsymbol{X}, \overline{\boldsymbol{\gamma}}\right) \leq 0,\ i \in \Psi_{eq} \tag{11.20}$$

$$\boldsymbol{G_j}\left(\boldsymbol{X}, \overline{\boldsymbol{\gamma}}\right) = 0,\ j \in \Psi_{ineq} \tag{11.21}$$

Above formulation is the conventional deterministic TNEP, known as the "base case." The value of function f for this case is called the basic value of objective function (f_b).

The aim of IGDT is making f_b robust against variations of uncertain input variables. Mathematically speaking, the decision variables $\boldsymbol{X}$ must be optimally selected so that the objective function f remain immune against the deviations of uncertain input variables $\boldsymbol{\gamma}$ from their expected values $\overline{\boldsymbol{\gamma}}$. This conservative IGDT-based strategy is called "risk-averse strategy," wherein the maximum radius of uncertainty ($\hat{\zeta}$) will be found by solving the following optimization problem:

$$\underset{\boldsymbol{X}, \zeta}{\text{maximize}}\, \hat{\zeta} \tag{11.22}$$

subject to

$$\boldsymbol{H_i}(\boldsymbol{X}, \boldsymbol{\gamma}) \leq 0,\ i \in \Psi_{eq} \tag{11.23}$$

$$\boldsymbol{G_j}(\boldsymbol{X}, \boldsymbol{\gamma}) = 0,\ j \in \Psi_{ineq} \tag{11.24}$$

$$\left\{\begin{array}{l} \hat{\zeta} = \text{maximum}_{\zeta}\, \zeta \\ f(\boldsymbol{X}, \boldsymbol{\gamma}) \leq \Lambda_C \\ \Lambda_C = f_b(\boldsymbol{X}, \boldsymbol{\gamma}) \times (1 + \varsigma_C),\ \boldsymbol{\gamma} \in \boldsymbol{\Gamma} \end{array}\right\} \tag{11.25}$$

Λ_C is the critical (maximum allowed) value of objective function to immunize it; this objective function should not surpass the critical value. This value can be determined based on planner's knowledge and requirements of power system decision-maker. Usually, it is determined per the basic value f_b. Here, the positive parameter ς_C determined by decision-maker is used to define Λ_C. ς_C is the degree of acceptable tolerance on increasing f_b owing to the possible variations of uncertainties.

The proposed structure in (11.22)–(11.25) is a bi-level optimization problem. In the lower level (11.25), the maximum radius of uncertainty ($\hat{\zeta}$) for a given value of decision variables ($\boldsymbol{X}$) is determined. Then, $\hat{\zeta}$ is passed to the upper level (11.22)–(11.24). In this level, the decision-maker sets the decision variables $\boldsymbol{X}$ to increase $\hat{\zeta}$. But the objective function f should not increase more than its critical value (Λ_C) [14–17].

For RTNEP optimization problem described in (11.1)–(11.8), the above risk-averse IGDT-based strategy is mentioned as follows:

$$f_b = \underset{n_{ij},\, r_i,\, w_i}{\text{minimize}} \left\{ \sum_{(i,j)\in\Omega} c_{ij} n_{ij} + p_f \sum_{i\in B} r_i + p_f \sum_{i\in\Psi} w_i \right\} \tag{11.26}$$

subject to

$$\boldsymbol{S}^T \boldsymbol{f} + \boldsymbol{P}_g + (\boldsymbol{P}_w - \boldsymbol{w}) = (\boldsymbol{P}_d - \boldsymbol{r}) \tag{11.27}$$

$$f_{ij} - B_{ij}\left(n_{ij}^0 + n_{ij}\right)\left(\theta_i - \theta_j\right) = 0 \tag{11.28}$$

$$\left|f_{ij}\right| \le \left(n_{ij}^0 + n_{ij}\right)\bar{f}_{ij} \tag{11.29}$$

$$\underline{\boldsymbol{P}}_g \le \boldsymbol{P}_g \le \bar{\boldsymbol{P}}_g \tag{11.30}$$

$$0 \le \boldsymbol{r} \le \boldsymbol{P}_d \tag{11.31}$$

$$0 \le \boldsymbol{w} \le \boldsymbol{P}_w \tag{11.32}$$

$$0 \le n_{ij} \le \bar{n}_{ij},\ \ \forall (i,j) \in \Omega \tag{11.33}$$

The basic value f_b is the sum of investment cost and costs of load and wind power generation curtailments for the base case, wherein loads ($\boldsymbol{P}_d$) and wind power generations ($\boldsymbol{P}_w$) are fixed at their predicted values with no prediction error.

In the next step, loads and wind power generations take their actual values. In this step, the bi-level optimization problem should be solved to maximize radius of uncertainty (ζ), as follows:

$$\underset{n_{ij},\, r_i,\, w_i,\, \zeta}{\text{maximize}}\ \zeta \tag{11.34}$$

subject to

$$\boldsymbol{S}^T\boldsymbol{f} + \boldsymbol{P}_g + \left(\boldsymbol{P}_w^{av} - \boldsymbol{w}\right) = \left(\boldsymbol{P}_d^{av} - \boldsymbol{r}\right) \tag{11.35}$$

$$f_{ij} - B_{ij}\left(n_{ij}^0 + n_{ij}\right)\left(\theta_i - \theta_j\right) = 0 \tag{11.36}$$

$$\left|f_{ij}\right| \le \left(n_{ij}^0 + n_{ij}\right)\bar{f}_{ij} \tag{11.37}$$

$$\underline{\boldsymbol{P}}_g \le \boldsymbol{P}_g \le \bar{\boldsymbol{P}}_g \tag{11.38}$$

$$0 \le \boldsymbol{r} \le \boldsymbol{P}_d^{av} \tag{11.39}$$

$$0 \le \boldsymbol{w} \le \boldsymbol{P}_w^{av} \tag{11.40}$$

$$0 \le n_{ij} \le \bar{n}_{ij},\ \forall (i,j) \in \Omega \tag{11.41}$$

$$\left\{\sum_{(i,j)\in\Omega} c_{ij}n_{ij} + p_f\sum_{i\in B} r_i + p_f\sum_{i\in\Psi} w_i\right\} \le f_b \times (1+\varsigma_C) \tag{11.42}$$

$$\boldsymbol{P}_d^{av} = \boldsymbol{P_d} \times (1+\zeta) \tag{11.43}$$

$$\boldsymbol{P}_w^{av} = \boldsymbol{P}_w \times (1+\zeta) \tag{11.44}$$

where n_{ij}, r_i, w_i, and ζ are decision variables. In above optimization problem, three more constraints (11.42)–(11.44) are added. Inequality constraint (11.42) keeps the objective function below the predetermined critical value. Equality constraints (11.43) and (11.44) are required to address the actual values of loads ($\boldsymbol{P}_d^{av}$) and wind power generations ($\boldsymbol{P}_w^{av}$) in the problem. In the risk-averse strategy, the actual values of loads and wind power generations are more than their predicted values. Because there is positive correlation between the TNEP objective function and these parameters, in other words, the objective function increases (decreases) as loads and wind power generations increase (decrease). In this strategy, the objective function remains immune against the maximum radius of uncertainty $\hat{\zeta}$ of the loads and wind power generation uncertainties.

The above IGDT-TNEP model is tested on the modified Garver 6-bus test system [8]. The single-line diagram of the system is shown in Fig. 11.3. It includes three generation buses and eight transmission lines. Load and generation relevant data is presented in Table 11.1. The number of existing transmission lines is 8 (Table 11.2), and there are 15 corridors to install new transmission lines (Table 11.3). The maximum capacity of each corridor is limited to three lines. Initial load and generation (without wind capacity of bus 2) capacity of system are assumed to be 760 MW and 1110 MW, respectively. The aim of TNEP is expanding transmission network for the next 5 years with incremental rate 10% for both load and generation capacity. As shown in Fig. 11.3, wind power generation is injected to bus 2. The capacity of this generation type is 100 MW. The penalty factor p_f for load and wind power generation curtailment is assumed to be 5270 $/MW.

There are six uncertain input variables, five loads, and a single wind power generation unit. For the base case, loads are fixed at their predicted (mean) values,

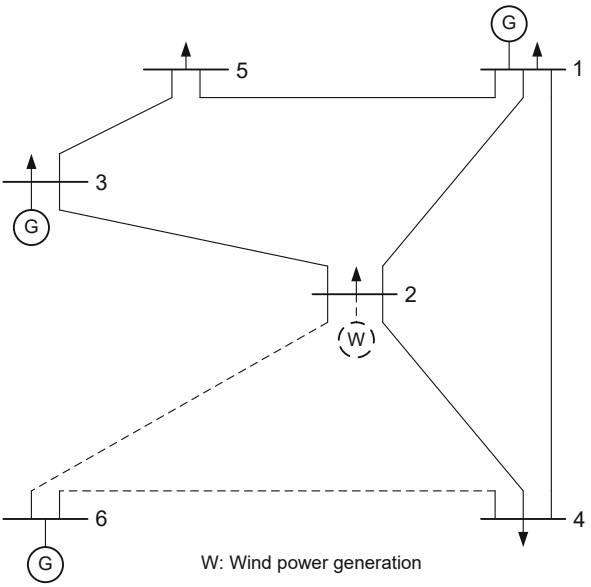

Fig. 11.3 Single-line diagram of modified Garver 6-bus test system

Table 11.1 Load and generation data for modified Garver 6-bus test system

Bus No.	1	2	3	4	5	6
Load (MW)	80	240	40	160	240	0
Generation (MW)	150	100	360	0	0	600

Table 11.2 Data of existing transmission lines for modified Garver 6-bus test system

From bus	To bus	Reactance (p.u.)	Capacity (MW)
1	2	0.4	100
1	4	0.6	80
1	5	0.2	100
2	3	0.2	100
2	4	0.4	100
2	6	0.3	100
3	5	0.2	100
4	6	0.3	100

and wind power generation at bus 2 is supposed to be equal to 50% of its rated capacity. Based on the abovementioned uncertain input variables, the TNEP problem is solved, and the value of base objective function is 139 M$; the optimal expansion plans for the base case are 2–6, 2 × (3–5), and 2 × (4–6). The problem is solved in MATLAB platform using CPLEX solver.

Assuming the degree of acceptable tolerance on increasing the value of base objective function (ς_C) is equal to 30%, the optimization problem (11.34)–(11.44) is calculated. Considering this value of ς_C, the optimal expansion plans are 1–5, 2 × (2–6), 2 × (3–5), and 2 × (4–6), with required investment cost equals to 180 M$. The maximum radius of uncertainties ($\hat{\zeta}$) that objective function remains immune against it will be equal to 7%.

Table 11.3 Data of candidate transmission lines for modified Garver 6-bus test system

From bus	To bus	Reactance (p.u.)	Capacity (MW)	Capital cost (M$)
1	2	0.4	2 × 100	40
1	3	0.38	3 × 100	38
1	4	0.6	2 × 80	60
1	5	0.2	2 × 100	20
1	6	0.68	3 × 70	68
2	3	0.2	2 × 100	20
2	4	0.4	2 × 100	40
2	5	0.31	3 × 100	31
2	6	0.3	2 × 100	30
3	4	0.59	3 × 100	59
3	5	0.2	2 × 100	20
3	6	0.48	3 × 100	48
4	5	0.63	3 × 75	63
4	6	0.3	2 × 100	30
5	6	0.61	3 × 78	61

11.5 RTNEP with Taguchi's Orthogonal Array Testing (TOAT)

Taguchi's orthogonal array testing (TOAT) method was presented in [18] to find robust solutions for manufacturing problems. The method provides much smaller testing scenarios of uncertain input variables and needs less computational burden than Monte Carlo simulation (MCS). In TOAT method, appropriate scenarios of uncertain input variables are provided to cover all possible scenarios. To explain this method, assume a system Y, which can be represented by a function $y = Y(x_1, \ldots, x_F)$, where $x_1, \ldots, x_F$ are F uncertain input variables. If each of these variables had B levels in its variation range, the number of full possible combination of system states will be B^F. Thereupon, testing all these states needs large computational burden, especially when F is large. TOAT reduces the number of testing states and computational burden by selecting the optimal number of testing scenarios. In TOAT, the scenarios are generated according to orthogonal arrays (OAs). An OA for F variables with B levels for each one is shown by $L_H(B^F)$. H is the number of combinations of variable levels. $L_H(B^F)$ is shown as a matrix with H rows and F columns, and values of matrix elements are indicated using variable levels. For instance, an OA $L_4(2^3)$ is as follows:

$$L_4\left(2^3\right) = \begin{bmatrix} 1 & 1 & 1 \\ 1 & 2 & 2 \\ 2 & 1 & 2 \\ 2 & 2 & 1 \end{bmatrix}$$

Table 11.4 Four testing scenarios obtained by OA $L_4(2^3)$

	Variable levels		
No. of testing scenarios	Variable 1	Variable 1	Variable 1
Scenario 1	1	1	1
Scenario 2	1	2	2
Scenario 3	2	1	2
Scenario 4	2	2	1

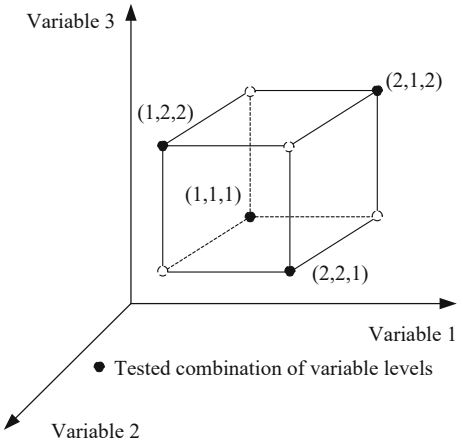

Fig. 11.4 Orthogonal array $L_4(2^3)$

where there are three variables with two levels for each of them and four scenarios in $L_4(2^3)$. Let us assume, "1" and "2" denote low and high levels of variables, respectively. The scenarios obtained by $L_4(2^3)$ are represented in Table 11.4.

So, H is so smaller than B^F. In the considered system with three uncertain variables and each shown by two levels, the number of full scenarios is equal to 2^3. As shown, using $L_4(2^3)$, just four scenarios are tested. Therefore, the number of testing scenarios is reduced notably.

Features of an OA are as follows:

(a) Each level of an uncertain variable occurs H/B times in each column.
(b) In each two columns, the numbers of occurrences of two variable levels are the same. For instance, in any two columns of $L_4(2^3)$, "11", "12", "21", and "22" occur one time.
(c) The scenarios obtained by OA are uniformly distributed over the space of all possible scenarios. This feature is illustrated in Fig. 11.4 for the combinations of $L_4(2^3)$.
(d) If each two columns of an OA are exchanged or some columns are ignored, the new array still satisfies the abovementioned features.

OAs can be determined by various ways. A simple way to determine an OA is to select a suitable OA from OA libraries [19].

Maybe, for a given system, there is no OA in the OA libraries whose number of column is equal to the number of system uncertain variables. In such a case, an OA whose number of columns is a few more than the number of system uncertain variables must be selected. So, based on the feature (d), the redundant column can be ignored.

Suppose, in the TNEP problem, loads and wind power generations are uncertain input variables. Orthogonal arrays of these uncertain variables should be defined. Assuming a load with the normal distribution, $\mu - \sigma$ and $\mu + \sigma$ are chosen as representatives of load values, where μ and σ are, respectively, expected and standard deviations. The output of a wind power generator changes between zero and its rated capacity. These limit values are chosen as representatives to define the uncertain wind power generation. Therefore, here the OAs with two levels are used in robust TNEP. The operating testing scenarios for TNEP are defined as follows:

(a) Counting the number of uncertain loads n_d and the number of uncertain wind power generations n_w.
(b) Defining an OA $L_H(B^F)$ for above uncertain variables, wherein $F \geq n_d + n_w$. Suppose, "1" and "2" in an OA column are, respectively, low and high representative values of variables (or vice versa); here, each uncertain variable has two levels low and high.
(c) If the number of columns in OA is more than the number of uncertain variables, ignore redundant columns, and suppose the first $n_d + n_w$ column of $L_H(B^F)$ are variables of load and wind power generation. Then, select H rows of $L_H(B^F)$ as operating scenarios.

The selected scenarios are implemented in TNEP optimization problem. The TNEP formulation with TOAT with these scenarios is as follows:

$$f = \underset{n_{ij},\, r_{i,h},\, w_{i,h}}{\text{minimize}} \left\{ \sum_{(i,j)\in\Omega} c_{ij} n_{ij} + p_f \sum_h \sum_{i\in B} r_{i,h} + p_f \sum_h \sum_{i\in\Psi} w_{i,h} \right\} \tag{11.45}$$

subject to

$$\boldsymbol{S}^T \boldsymbol{f}_h + \boldsymbol{P}_{g,h} + (\boldsymbol{P}_{w,h} - \boldsymbol{w}_h) = (\boldsymbol{P}_{d,h} - \boldsymbol{r}_h) \tag{11.46}$$

$$f_{ij,h} - B_{ij}\left(n_{ij}^0 + n_{ij}\right)\left(\theta_{i,h} - \theta_{j,h}\right) = 0 \tag{11.47}$$

$$\left|f_{ij,h}\right| \leq \left(n_{ij}^0 + n_{ij}\right)\bar{f}_{ij} \tag{11.48}$$

$$\underline{\boldsymbol{P}}_g \leq \boldsymbol{P}_{g,h} \leq \bar{\boldsymbol{P}}_g \tag{11.49}$$

$$0 \leq \boldsymbol{r}_h \leq \boldsymbol{P}_d \tag{11.50}$$

$$0 \leq \boldsymbol{w}_h \leq \boldsymbol{P}_w \tag{11.51}$$

$$0 \leq n_{ij} \leq \bar{n}_{ij},\ \forall (i,j) \in \Omega \tag{11.52}$$

All above variables have been previously introduced in Sect. 11.2. Here, the subscript h denotes the serial number of implemented scenario and $h = 1,2,3,\ldots,H$. The objective of formulation (11.45) is to minimize the sum of investment cost and costs of load and wind power generation curtailments for H implemented testing scenarios.

The generated scenarios by TOAT do not cover all possible scenarios regarding the uncertain input variables. Thereupon, this is needed to check the robustness of the obtained solution for TNEP from the above formulation. To this end, K scenarios are generated by MCS using the pdfs of the uncertain variables, where K is much more than H. Supposing k is the serial number of scenario and $k = 1,2,3,\ldots,K$, the testing formula is as follows:

$$\underset{r_{i,k},\, w_{i,k}}{\text{minimize}} \left\{ \sum_{i \in \mathcal{B}} r_{i,k} + \sum_{i \in \Psi} w_{i,k} \right\} \tag{11.53}$$

subject to

$$\boldsymbol{S}^T \boldsymbol{f}_k + \boldsymbol{P}_{g,k} + (\boldsymbol{P}_{w,k} - \boldsymbol{w}_k) = (\boldsymbol{P}_{d,k} - \boldsymbol{r}_k) \tag{11.54}$$

$$f_{ij,k} - B_{ij}\left(n_{ij}^0 + n_{ij}\right)\left(\theta_{i,k} - \theta_{j,k}\right) = 0 \tag{11.55}$$

$$\left|f_{ij,k}\right| \le \left(n_{ij}^0 + n_{ij}\right)\bar{f}_{ij} \tag{11.56}$$

$$\underline{\boldsymbol{P}}_g \le \boldsymbol{P}_{g,k} \le \bar{\boldsymbol{P}}_g \tag{11.57}$$

$$0 \le \boldsymbol{r}_k \le \boldsymbol{P}_d \tag{11.58}$$

$$0 \le \boldsymbol{w}_k \le \boldsymbol{P}_w \tag{11.59}$$

When objective function (11.53) is zero, the calculated planning scheme satisfies testing scenario k. The robustness degree of the planning scheme in percent is calculated as follows:

$$\beta = \frac{K_1}{K} \times 100\% \tag{11.60}$$

where K_1 is the number testing scenarios whose objective function (11.53) becomes zero.

The above TOAT-based TNEP is implemented on the modified Garver 6-bus test system. As mentioned in Sect. 11.4, the number of uncertain input variables is supposed to be six (five loads and one wind power generation). Assuming a load has normal distribution, $\mu - \sigma$ and $\mu+\sigma$ are selected as low and high levels of load. Standard deviation (σ) of each uncertain load is supposed to be 10% of its expected value (μ). Let us assume that the expected value of wind power generation at bus 2 is

Table 11.5 Eight testing scenarios obtained by OA $L_8(2^7)$ for modified Garver 6-bus test system

No. of testing scenarios	Variable levels						
	P_{d1}	P_{d2}	P_{d3}	P_{d4}	P_{d5}	P_{w2}	Ignored column
1	187	560	93	374	560	0	1
2	187	560	93	456	684	161	2
3	187	684	114	374	560	161	2
4	187	684	114	456	684	0	1
5	229	560	114	374	684	0	2
6	229	560	114	456	560	161	1
7	229	684	93	374	684	161	1
8	229	684	93	456	560	0	2

50% of its rated capacity. The expected values of loads at buses 1–5 are, respectively, 80, 240, 40, 160, and 240 MW, and the rated capacity of wind power generation at bus 2 is 100 MW. So, an orthogonal array with six uncertain two-level variables is needed. From the OA libraries [19], the OA $L_8(2^7)$ is proper for this set of uncertainties. This OA is as follows:

$$L_8\left(2^7\right) = \begin{bmatrix} 1 & 1 & 1 & 1 & 1 & 1 & 1 \\ 1 & 1 & 1 & 2 & 2 & 2 & 2 \\ 1 & 2 & 2 & 1 & 1 & 2 & 2 \\ 1 & 2 & 2 & 2 & 2 & 1 & 1 \\ 2 & 1 & 2 & 1 & 2 & 1 & 2 \\ 2 & 1 & 2 & 2 & 1 & 2 & 1 \\ 2 & 2 & 1 & 1 & 2 & 2 & 1 \\ 2 & 2 & 1 & 2 & 1 & 1 & 2 \end{bmatrix}$$

However, the number of column in this OA is more than the number of uncertain variables that is six. So, the first six columns of this OA are selected, and the final redundant column is ignored. Assuming "1" and "2," respectively, indicate low and high levels of uncertainties, the testing scenarios obtained by $L_8(2^7)$ for modified Garver 6-bus test system are shown in Table 11.5. Note that the low and high values of loads in this table are calculated based on load values at the end of time horizon, i.e., in the 5th year, with the annual incremental rate of 10%.

With the above chosen scenarios, the TOAT-based TNEP problem (11.45)–(11.52) is solved, and the obtained solution is 2 × (1–5), 2–3, 2 × (2–6), 2 × (3–5), and 2 × (4–6), with the required investment cost 220 M$. The problem is solved in MATLAB platform using CPLEX solver.

Now, the robustness of above planning scheme should be checked. To do this, these new transmission lines are added to the system, and the optimization problem (11.53)–(11.59) is solved for 1000 scenarios generated by MCS. In 944 scenarios, the objective function (11.53) becomes zero. Therefore, the robustness degree of the obtained planning scheme is 94.4%.

11.6 RTNEP Using Scenario Technique Criteria (Min-Max Regret Criterion)

This robust optimization method is a risk analysis technique that is proposed in [20] for robust unit commitment problem. The method aims to minimize the maximum regret of planning schemes (TNEP solutions) under all possible scenarios [21]; regret of scheme X in scenario s is the difference among cost of scheme X in scenario s and cost of optimum scheme $\bar{X}$ in scenario s, i.e.:

$$regret(X,s) = f(X,s) - f\left(\bar{X},s\right) \tag{11.61}$$

where $regret(X,s)$ is the regret of scheme X in scenario s. $f(X,s)$ and $f\left(\bar{X},s\right)$ are the costs (objective function values) of scheme X and optimal scheme $\bar{X}$ in scenario s, respectively. The optimal scheme $\bar{X}$ can be calculated by solving the TNEP optimization problem only applying the scenario s.

In this method, the scheme which minimizes the maximum regret over all scenarios is chosen as the final optimal plan, i.e., [21, 22]:

$$\underset{X}{\text{minimize}} \quad \underset{s}{\text{maximum}} \quad (regret\,(X,s)) \tag{11.62}$$

To explain the min-max regret criterion, a simple example is presented. Let us assume, a planning problem is optimized for three scenarios. The optimal scheme of each scenario is bolded in Table 11.6. Table 11.7 shows the regrets of expansion schemes in different scenarios. Also, the maximum regret of each scheme is determined in this table. Scheme 2 with the minimum-maximum regret is selected as the final optimal scheme.

The mathematical formulation of min-max regret criterion for TNEP optimization problem is explained below.

Initially for each single scenario s, the optimal cost $f\left(\bar{X},s\right)$ should be calculated as:

Table 11.6 Optimal scheme of each scenario

Schemes	Scenario A	Scenario B	Scenario C
Scheme 1	**150**	166	194
Scheme 2	170	168	174
Scheme 3	178	**154**	**170**

Table 11.7 Regrets of expansion schemes in different scenarios

Schemes	Scenario A	Scenario B	Scenario C	Maximum regret
Scheme 1	0	12	24	24
Scheme 2	20	14	4	**20**
Scheme 3	28	0	0	28

$$f\left(\bar{X},s\right)=\underset{n_{ij},r_{i,s},w_{i,s}}{\text{minimize}}\left\{\sum_{(i,j)\in\Omega}c_{ij}n_{ij}+p_f\sum_{i\in B}r_{i,s}+p_f\sum_{i\in\Psi}w_{i,s}\right\} \tag{11.63}$$

subject to

$$\boldsymbol{S}^T\boldsymbol{f}_s+\boldsymbol{P}_{g,s}+\left(\boldsymbol{P}_{w,s}-\boldsymbol{w}_s\right)=\left(\boldsymbol{P}_{d,s}-\boldsymbol{r}_s\right) \tag{11.64}$$

$$f_{ij,s}-B_{ij}\left(n_{ij}^0+n_{ij}\right)\left(\theta_{i,s}-\theta_{j,s}\right)=0 \tag{11.65}$$

$$\left|f_{ij,s}\right|\le\left(n_{ij}^0+n_{ij}\right)\bar{f}_{ij} \tag{11.66}$$

$$\underline{\boldsymbol{P}}_g\le\boldsymbol{P}_{g,s}\le\bar{\boldsymbol{P}}_g \tag{11.67}$$

$$0\le\boldsymbol{r}_s\le\boldsymbol{P}_d \tag{11.68}$$

$$0\le\boldsymbol{w}_s\le\boldsymbol{P}_w \tag{11.69}$$

$$0\le n_{ij}\le\bar{n}_{ij},\ \forall(i,j)\in\Omega \tag{11.70}$$

So, a bi-level optimization problem should be calculated to obtain final optimal scheme to minimize the maximum regret, as follows:

(*Master problem*)

$$\underset{X}{\text{minimize}}\ \underset{s}{\text{maximum}}\ \left(f(X,s)-f\left(\bar{X},s\right)\right) \tag{11.71}$$

where in each scenario, the cost $f(X, s)$ is calculated as:

(*Slave problem*)

$$f(X,s)=\underset{r_{i,s},w_{i,s}}{\text{minimize}}\left\{\sum_{(i,j)\in\Omega}c_{ij}n_{ij}+p_f\sum_{i\in B}r_{i,s}+p_f\sum_{i\in\Psi}w_{i,s}\right\} \tag{11.72}$$

subject to

$$\boldsymbol{S}^T\boldsymbol{f}_s+\boldsymbol{P}_{g,s}+\left(\boldsymbol{P}_{w,s}-\boldsymbol{w}_s\right)=\left(\boldsymbol{P}_{d,s}-\boldsymbol{r}_s\right) \tag{11.73}$$

$$f_{ij,s}-B_{ij}\left(n_{ij}^0+n_{ij}\right)\left(\theta_{i,s}-\theta_{j,s}\right)=0 \tag{11.74}$$

$$\left|f_{ij,s}\right|\le\left(n_{ij}^0+n_{ij}\right)\bar{f}_{ij} \tag{11.75}$$

$$\underline{\boldsymbol{P}}_g\le\boldsymbol{P}_{g,s}\le\bar{\boldsymbol{P}}_g \tag{11.76}$$

Table 11.8 Optimal scheme of each scenario, in modified Garver 6-bus test system

Schemes	Scen.[a]1	Scen.2	Scen.3	Scen.4	Scen.5	Scen.6	Scen.7	Scen.8
Sch.[b]1	**110**	437	110	1157	619	197	477	820
Sch.2	161	**145**	140	826	469	180	382	661
Sch.3	197	491	**98**	1183	646	203	530	943
Sch.4	220	220	220	**220**	220	220	220	220
Sch.5	220	220	220	220	**220**	220	220	220
Sch.6	585	412	464	1345	983	**166**	862	1099
Sch.7	181	181	181	431	335	181	**190**	181
Sch.8	160	292	160	412	329	177	292	**160**

[a]Scenario
[b]Scheme

Table 11.9 Regrets of expansion schemes in different scenarios, in modified Garver 6-bus test system

Schemes	Scen.1	Scen.2	Scen.3	Scen.4	Scen.5	Scen.6	Scen.7	Scen.8	MR[a]
Sch.1	0	292	12	937	399	31	287	660	937
Sch.2	51	0	42	606	249	14	192	501	606
Sch.3	87	346	0	963	426	37	340	783	963
Sch.4	110	75	122	0	0	54	30	60	**122**
Sch.5	110	75	122	0	0	54	30	60	**122**
Sch.6	475	267	366	1125	763	0	672	939	1125
Sch.7	71	36	83	211	115	15	0	21	211
Sch.8	50	147	62	192	109	11	102	0	192

[a]Maximum regret

$$0 \leq \boldsymbol{r}_s \leq \boldsymbol{P}_d \tag{11.77}$$

$$0 \leq \boldsymbol{w}_s \leq \boldsymbol{P}_w \tag{11.78}$$

The set of scenarios are generated from uncertain input variables, i.e., loads and wind power generations. These scenarios can be defined by different methods such as Taguchi orthogonal arrays method.

This scenario-based RTNEP is performed on the modified Garver 6-bus test system. The scenarios determined by Taguchi method (Table 11.5) are used as the set of possible scenarios. In each scenario, the optimal scheme is found using CPLEX solver. Values of objective function (11.63) for the optimal schemes are presented in Table 11.8. Regrets of these schemes in other scenarios are as Table 11.9. The final column of this table indicates the maximum regret of each scheme in the set of scenarios. Therefore, scheme 4 (or 5) with the minimum-maximum regret equals to 122 is the final optimal scheme. This expansion scheme needs 220 M$ to install new lines 2 × (1–5), 2–3, 2 × (2–6), 2 × (3–5), and 2 × (4–6).

11.7 Conclusions

The robust TNEP considering uncertainties of load and wind power generation was considered in this chapter. The three common robust methods, IGDT, TOAT, and min-max regret criterion, were explained, and their mathematical formulations for TNEP problem were presented. The methods were successfully implemented on the modified Garver 6-bus test system. Demanded loads and output of wind power generator were supposed in an uncertain manner to provide an uncertain power system in the test system. The obtained simulation results verify the capability of the mentioned methods in planning a robust transmission network. A risk-averse IGDT-based strategy to solve the robust TNEP problem was implemented. By doing so, the problem objective function (capital cost) remained immune against deviations of uncertain input variables of loads and wind power generation. In the modified Garver 6-bus test system, the maximum radius of uncertainties that objective function remained immune against it was equal to 7%. Wherein, the degree of acceptable tolerance on increasing the value of base objective function was 30%. Also, the TOAT was implemented on the considered system to solve RTNEP. An OA with six columns for six uncertain input variables (five load and one wind power generation) was selected. The robustness degree of the obtained planning scheme by this method was 94.4%. Also, for the case study system, the RTNEP was solved based on the min-max regret criterion. Eight scenarios of demanded loads and wind power generation were considered in this method. An expansion plan with 122 M$ regret was selected as optimal plan. The needed capital cost for this plan was 220 M $. In each of the abovementioned methods, an acceptable solution for RTNEP with uncertainties of load and wind power generation was calculated. These methods can easily be implemented on any larger- and real-scale power system to expand its transmission network in a robust manner. Also, other uncertainties can be considered in these methods.

References

1. Abbasi, S., & Abdi, H. (2016). Multiobjective transmission expansion planning problem based on ACOPF considering load and wind power generation uncertainties. *International Transactions on Electrical Energy Systems, 27*(6), 1–15.
2. Abbasi, S., Abdi, H., Bruno, S., & La, M. (2018). Transmission network expansion planning considering load correlation using unscented transformation. *International Journal of Electrical Power and Energy Systems, 103*, 12–20.
3. Buygi, M. O., Balzer, G., Shanechi, H. M., & Shahidehpour, M. (2004). Market-based transmission expansion planning. *IEEE Transactions on Power Apparatus and Systems, 19* (4), 2060–2067.
4. Orfanos, G. A., Georgilakis, P. S., & Hatziargyriou, N. D. (2013). Transmission expansion planning of systems with increasing wind power integration. *IEEE Transactions on Power Apparatus and Systems, 28*(2), 1355–1362.

5. Hemmati, R., Hooshmand, R. A., & Khodabakhshian, A. (2014). Market based transmission expansion and reactive power planning with consideration of wind and load uncertainties. *Renewable and Sustainable Energy Reviews, 29*, 1–10.
6. Moeini-Aghtaie, M., Abbaspour, A., & Fotuhi-Firuzabad, M. (2012). Incorporating large-scale distant wind farms in probabilistic transmission expansion planning; part I: Theory and algorithm. *IEEE Transactions on Power Apparatus and Systems, 27*(3), 1594–1601.
7. Moeini-Aghtaie, M., Abbaspour, A., & Fotuhi-Firuzabad, M. (2012). Incorporating large-scale distant wind farms in probabilistic transmission expansion planning; part II: Case studies. *IEEE Transactions on Power Apparatus and Systems, 27*(3), 1585–1593.
8. Garver, L. L. (1970). Transmission network estimation using linear programming. *IEEE Transactions on Power Apparatus and Systems, 7*, 1688–1697.
9. Fang, R., & Hill, D. J. (2003). A new strategy for transmission expansion in competitive electricity markets. *IEEE Transactions on Power Apparatus and Systems, 18*(1), 374–380.
10. Maghouli, P., Hosseini, S. H., Buygi, M. O., & Shahidehpour, M. (2009). A multi-objective framework for transmission expansion planning in deregulated environments. *IEEE Transactions on Power Apparatus and Systems, 24*(2), 1051–1061.
11. Aien, M., Fotuhi-Firuzabad, M., Member, S., & Aminifar, F. (2012). Probabilistic load flow in correlated uncertain environment using unscented transformation. *IEEE Transactions on Power Apparatus and Systems, 27*(4), 2233–2241.
12. Verbic, G., Claudio, A., & Canizares, A. (2006). Probabilistic optimal power flow in electricity markets based on a two point estimate method. *IEEE Transactions on Power Apparatus and Systems, 21*(4), 1883–1894.
13. Papaefthymiou, G., & Kurowicka, D. (2009). Using copulas for modeling stochastic dependence in power system uncertainty analysis. *IEEE Transactions on Power Apparatus and Systems, 24*(1), 40–49.
14. Rabiee, A., Soroudi, A., & Keane, A. (2014). Information gap decision theory based OPF with HVDC connected wind farms. *IEEE Transactions on Power Apparatus and Systems, 30*(6), 3396–3406.
15. Dehghan, S., Kazemi, A., & Amjady, N. (2014). Multi-objective robust transmission expansion planning using information-gap decision theory and augmented ?-constraint method. *IET Generation Transmission and Distribution, 8*(5), 828–840.
16. Taherkhani, M., & Hosseini, S. H. (2015). IGDT-based multi-stage transmission expansion planning model incorporating optimal wind farm integration. *International Transactions on Electrical Energy Systems, 25*(10), 2340–2358.
17. Alseddiqui, J., & Thomas, R. J. (2006). *Transmission expansion planning using multi-objective optimization*. Power and Energy Society General Meeting (pp. 1–8). IEEE.
18. Tsui, K. (1992). An overview of Taguchi method and newly developed statistical methods for robust design. *IIE Transactions, 24*(5), 44–57.
19. "Orthogonal Arrays (Taguchi Designs)." [Online]. Available: http://www.york.ac.uk/depts/maths/tables/orthogonal.htm.
20. Jiang, R., Wang, J., & Zhang, M. (2013). Two-stage minimax regret robust unit commitment. *IEEE Transactions on Power Apparatus and Systems, 28*(3), 2271–2282.
21. Maghouli, P., Hosseini, S. H., Oloomi Buygi, M., & Shahidehpour, M. (2011). A scenario-based multi-objective model for multi-stage transmission expansion planning. *IEEE Transactions on Power Apparatus and Systems, 26*(1), 470–478.
22. Chen, B., et al. (2014). Robust optimization for transmission expansion planning: Minimax cost vs. minimax regret. *IEEE Transactions on Power Apparatus and Systems, 29*(6), 3069–3077.

Chapter 12
A Robust-Stochastic Approach for Energy Transaction in Energy Hub Under Uncertainty

Khezr Sanjani, Neda Vahabzad, Morteza Nazari-Heris, and Behnam Mohammadi-ivatloo

Nomenclature

$P_{s,g,t}$	Generation power during time interval t
RU_g	Ramp-up rates of thermal unit g
RD_g	Ramp-down rates of thermal unit g
$f_{s,m,n,t}$	A gas flow from n to m
$Sg_{s,n,t}$	Gas supply at node n
$Sg_n^{\min}$	Minimum of gas supply at node n
$Sg_n^{\max}$	Maximum of gas supply at node n
Sd_n	Gas load of node n
$C_{m,n}$	Constant of pipe
$\mathrm{Pr}_{s,n,t}$	Pressure of gas node n
$\mathrm{Pr}_n^{\max}$	Maximum pressure gas at node n
$\mathrm{Pr}_n^{\min}$	Minimum pressure gas at node n
a_g	First coefficient for the power sector
$P_{s,ij,t}$	Electrical power transmitted from bus i to j
OF	Objective function
EC	Electrical system cost
GC	Natural gas system cost
$\delta_{s,i,t}$	Voltage angle of bus i
V_u^{CO}	Cutout speed of the u_{th} wind turbine
$load(t)$	Load after implementation of DRPs
$load_0(t)$	Initial load at time period t
$DR(t)$	Percentage of load participation in DRPs
$ldr(t)$	Shifted load using DRPs at time t
$DR_{\max}$	Maximum percentage of load in DRPs

(continued)

K. Sanjani (✉) · N. Vahabzad · M. Nazari-Heris · B. Mohammadi-ivatloo
Faculty of Electrical and Computer Engineering, University of Tabriz, Tabriz, Iran
e-mail: sanjani96@ms.tabrizu.ac.ir; n.vahabzad96@ms.tabrizu.ac.ir; mnazari@tabrizu.ac.ir; bmohammadi@tabrizu.ac.ir

B. Mohammadi-ivatloo, M. Nazari-Heris (eds.), *Robust Optimal Planning and Operation of Electrical Energy Systems*,
https://doi.org/10.1007/978-3-030-04296-7_12

$V_{u,t}^{w}$	The u_{th} wind turbine speed at time t
V_{u}^{CI}	Cut-in speed of the u_{th} wind turbine
V_{u}^{R}	Rated wind speed of the u_{th} wind turbine
$P_{u,t}^{w}$	Power generated by the u_{th} wind turbine
$P_{u}^{\max}$	Rated power of the u_{th} wind turbine
π_s	Probability assigned to each scenario
P_{buy}	Purchase power from market
$\lambda_{s,i,t}$	Robust market price

12.1 Introduction

The use of distribution energy networks and the concept of energy hub have been presented in the last decade to inquire optimal scheduling of new incorporated multi-carrier energy systems [1, 2]. Operational flexibility of energy services increases by these hybrid inputs and outputs of energy carriers. In addition, it gives the operator an alternative in providing the energy demands at different time intervals [3, 4].

12.1.1 Co-generation

A novel linear model formulation of integrated power and gas systems is presented in [5] in order to minimize total operation cost of the short-term scheduling while considering the natural gas grid dynamics. A dynamic optimal energy flow in coordinated natural gas and electricity systems is formulated as a single-stage linear optimization model in [6] taking into account an incorporated natural gas and electricity transmission systems with DC power flow constraints. A new multi-objective methodology is introduced in [7] in order to coordinate the natural gas and electricity networks. The presented goal is to minimize operation cost and maximize the safety margins of the natural gas and electricity networks. A risk-averse stochastic optimal energy management of energy hub algorithm is proposed in [8]. Several energy producers are considered in [9] who trade their resources systematically in the integrated natural gas and electricity markets. The traditional producers give a price offer and quantity of products to the energy market, where they are willing to maximize their own profit.

Addressing how synergistic operation of electricity and natural gas networks can be gained is proposed in [10] by a distributed path utilizing alternating direction method of multipliers. A reliability-based optimal planning model is proposed in [11] for coordination of multiple energy hubs. A least-cost selection of grid components (i.e., transmission lines and natural gas pipelines) for interconnecting multi-carrier energy systems, which can assure the stated probabilistic reliability criteria,

is considered in planning stage of the problem. An examination of the effect of curtailments by altering natural gas pressure in order to measure how ramp rates of gas-fired plants change is presented in [12].

12.1.2 Uncertain Models

Due to the significant uncertainty impact of energy demand and market price in power systems, such parameters have important contribution in increasing volume of computation in scenario-based stochastic programming approach. Accordingly, the stochastic and robust optimization methods have been studied as the subject of recent works, which can handle the forecast errors of uncertainties related to energy systems scheduling. Dolatabadi et al. presented a solution model in [13], where the global optimal solution is found and also level of calculations is lightened. So, a hybrid stochastic/IGDT optimization method is considered for the optimal scheduling of wind integrated energy hub, where wind turbine uncertainty is considered including energy prices and energy demands. The uncertainties related to wind power generation and SEH electricity and thermal demand in the operation issues are formulated in [14] in various scenarios. Moreover, scenario reduction method is utilized to decline the calculation role of the scenario-based operation issue.

A new stochastic planning formulation for multi-carrier energy systems is studied considering the uncertainty of wind turbine, amount of demand, and visibility of components in [15]. In this reference, scenario-based model is engaged to handle these uncertainties perfectly, in order to gain an extensive multi-carrier energy planning formulation. The planning stage of new gas-fired units and power-to-gas (P2G) facilities and modifying wind power resource cost to decline wind spillage are investigated under uncertainties. Furthermore, incorporation of both $N - 1$ and probabilistic reliability criteria are considered in the co-optimization framework, so that low-probability/high-impact events are adequately addressed while overall reliability is also ensured [16]. A robust co-optimization operation formulation is proposed in [17], in order to analyze the coordinated optimal operation of multi-carrier energy systems. The aim of introduced model is to minimize total costs of the multi-carrier energy system, by applying power system key uncertainties and natural gas system dynamics.

A robust optimization model is proposed in [18] to specify how uncertainties associated with wind speed forecasts modify the economic and secure operation of a multi-energy system. The studied system in this reference is constructed of natural gas, coal, and electricity infrastructures interconnected in some common nodes. Addressing the percent of the demand that can be supplied by various types of carriers is proposed in [19], where its effects on multi-energy system modeling and the utilization of this type of demand within DR programs are discussed. A control approach using robust optimization (RO) technique is proposed in [20], where the input of multi-carrier energy system, their distribution among converters, and their

storage are determined in order to satisfy the energy hub output time-varying requests while minimizing the energy expenses. Risk-averse energy hub management by applying plug-in electric vehicles utilizing information gap decision theory is analyzed in [21]. The thermal demand response program (TDRP) besides the electrical demand response program (EDRP) was investigated in [22].

An identification method and protection path of sensitive components of combined gas and electric infrastructures from malicious attacks, deployment of valid corrective actions to guarantee a resilient operation, while considering the interdependency of gas pipeline network and power transmission network [23]. A consideration of detailed demand response program in the stochastic scheduling model as cost-effective function for optimizing the day-ahead scheduling of coupled electricity and natural gas transmission networks (referred to as EGT ran) is presented in [24]. An optimal probabilistic scheduling model of energy hubs exploitation is presented in [25]. A determination of energy carriers to be purchased as input and converted or stored in energy hub schedule in order to minimize the total hub's cost by proper meeting of energy demands.

12.1.3 Market

Economically, electricity is a commodity capable of bilateral bidding transactions. Electricity market systematically enables purchasing power through bids to buy; sales, through offers to sell and hourly transactions. Systematically, bids and offers use equality of supply and demand principles to set the value price. The real-time operation issue of multi-carriers is modeled in a dynamic pricing market in [26]. The multi-carriers interaction is formulated as an accurate potential of game to optimize each energy hub's payment to the electricity and gas utilities, as well as the users' satisfaction for energy commitment [26]. The uncertainty of energy market prices, auxiliary service market prices, wind power, and photovoltaic power are taken into account to propose a day-ahead scheduling strategy for the integrated community energy system in a joint energy and auxiliary service markets [27]. In this chapter, a definition of hybrid robust-stochastic approach is presented, in which this methodology focuses on optimal scheduling of natural gas and electricity co-generation. An evaluation of market bidding price contingencies by RO is presented. Both electrical and natural gas demand uncertainties were considered in stochastic programming term. Also, a time-amount DR program is applied on coordinated grids in order to reduce total fuel cost by shifting a part of electrical loads from on-peak or high-price periods to off-peak or low-price hours.

The reminder of the paper is organized as follows: Sect. 12.2 presented the model of problem formulation, which consists of stochastic and robust programming for uncertainty model of demands and prices. The case study and numerical results are considered in Sect. 12.3. Finally, Sect. 12.4 described the conclusion of the paper.

12.2 Problem Formulation

Nowadays, hybrid co-generation systems are interesting topics all around the world, where the system operators try to make the systems more reliable and cost-effective. Hence, this work proposes a hybrid robust-stochastic optimization approach which focuses on coordinated hybrid co-generation of natural gas and electricity. The proposed model aims to minimize the total operation costs of the hybrid system simultaneously, where robust optimization method handles market price uncertainties, and both electrical and natural gas demand uncertainties are considered in stochastic programming part. On the other hand, a real-time demand response to shift load demands from high-price periods to low-price periods is considered [28].

12.2.1 Hybrid Robust-Stochastic Model

This work proposes a novel hybrid robust-stochastic optimization approach which revolves around demand uncertainty in both electrical and natural gas networks and power market price.

12.2.1.1 Stochastic Optimization

The stochastic programming is a suitable approach to opt intentions under probabilistic and uncertain conditions. In this study, the stochastic optimization is applied to specify the optimal production of generators in each scenario. Stochastic uncertainties are considered in both load demand of electricity and natural gas networks.

As the nature of uncertainty in electrical and natural load demands, the values of demands are considered to be uncertain. The uncertain parameter is obtained using probability distribution function (PDF). In Fig. 12.1, the forecast error distribution curves are divided into five intervals with the width of one standard deviation [29, 30].

A part of uncertain load demands of electricity network at time interval 10 (t_{10}) are described in Table 12.1. It should be noted that whole demands at uncertain program are vast, and the authors just bring a part of them to show the adoption in demands by applying the stochastic programming. Demand response with maximum value of 15% is considered for the forecasted demands ($DR_{\max} = 0.15$).

12.2.1.2 Robust Optimization

Robust optimization is one of the high-performance optimization fields which handles the optimization issues with uncertain parameters and gives an apparent robustness versus uncertainty that can be represented as deterministic mutability in the amount of the parameters of the problem itself and/or its solution.

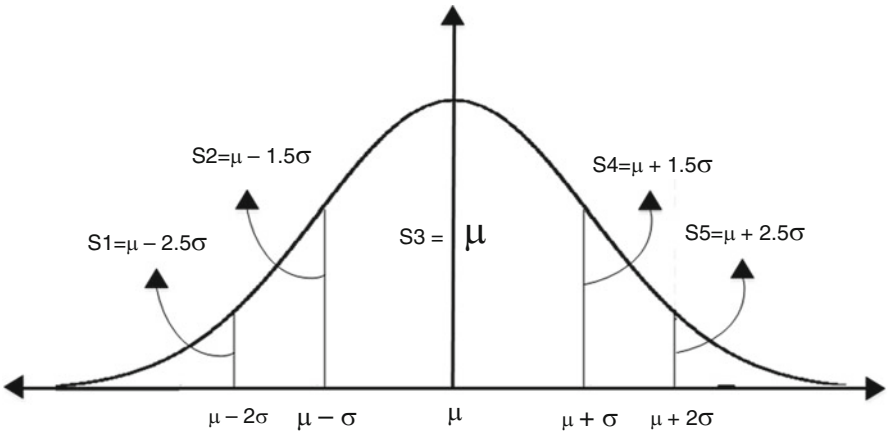

Fig. 12.1 Probability distribution function

Table 12.1 Part of demands in five scenarios

Demand	S1	S2	S3	S4	S5
D5	0.9153	0.7744	0.8128	0.8425	0.8767
D13	2.7952	2.8914	3.0337	3.1767	3.2722
D18	3.1153	4.1730	3.8121	3.9920	4.1118

In the proposed method, upstream grid has been considered as a power source which is only able to gain power from electricity market. There is a limitation in the amount of purchase power; it means the system cannot buy the whole of demand from market, which is presented in (12.3) and (12.4) in the following.

12.2.2 Objective Function

The objective of the proposed hybrid model is to minimize the total operation cost of natural gas and electricity co-generation, simultaneously as provided in (12.1). In this cost-effective optimization method, uncertainties in demand and price are considered as well as uncertainty of power market price. The proposed objective function consists of two parts, which is written as follows:

$$\min OF = EC + GC \tag{12.1}$$

$$EC = \sum_{s=1}^{5} \sum_{i,t} \pi_s \left\{ a_g \left(P_{s,g,t}\right)^2 + \text{VOLL} \times \text{LS}_{s,i,t} + \text{VWC} \times P_{s,i,t}^{WC} \right\} + \sum_{t=2}^{24} \xi_t + \Gamma\beta \tag{12.2}$$

$$GC = \sum_{s=1}^{5} \sum_{i,t} \pi_s \times \left\{ c_n \times Sg_{s,n,t} \right\} \tag{12.3}$$

The worst-case electricity price is proposed by robust optimization for power market price and various electric/gas demand scenarios handled by stochastic programming. The electricity cost terms are the generation cost of units (i.e., thermal units, common units, and wind turbines), the cost of the purchasing electricity from power market, unsupplied demand penalty cost, and value of wind curtailment penalty factor (12.2). The natural gas cost term is the amount of supply gas cost (12.3).

12.2.3 The Natural Gas Network Constraints

The technical characteristic of natural gas network is provided in [31]. Natural gas network constraints of the proposed model are described as follows: Also, Eq. (12.4) is for the natural gas network equality constraint. Equations (12.5) and (12.6) are the active and passive arcs. Finally, the last two Eqs. (12.7) and (12.8) are employed for gas flow and pressure limitations.

$$\sum_{m} f_{s,m,n,t} = \sum_{m} f_{s,m,n,t} + Sg_{s,n,t} - \xi_{g,t} Sd_n - Se_{n,t} \tag{12.4}$$

$$f_{s,m,n,t} = C_{m,n} \sqrt{\mathrm{Pr}_{s,m,t}^2 - \mathrm{Pr}_{s,n,t}^2} \text{ passive arc} \tag{12.5}$$

$$f_{s,m,n,t} \geq C_{m,n} \sqrt{\mathrm{Pr}_{s,m,t}^2 - \mathrm{Pr}_{s,n,t}^2} \text{ active arc} \tag{12.6}$$

$$Sg_n^{\min} \leq Sg_{s,n,t} \leq Sg_n^{\max} \tag{12.7}$$

$$\mathrm{Pr}_n^{\min} \leq \mathrm{Pr}_{s,n,t} \leq \mathrm{Pr}_n^{\max} \tag{12.8}$$

12.2.4 Electricity Network Constraints

In the main equality constraint, the sum of generated power from thermal power generators and wind turbines and the sum of bidding from power market and load shedding subtracted to demand after applying demand response program should be equal to transmitted power from node i to node j (12.9) and (12.10). Ramp-up and ramp-down of generators have a limitation provided in (12.11) and (12.12). The amount of power transmitted between two nodes is described in (12.13). Also, the amount of load shedding has a maximum curtailed (12.14). Moreover, maximum value of power purchased from market is unfolded in (12.15), and finally the robust optimization constraint is demonstrated in (12.19).

$$\sum_{g\in\Omega_G^i}\left\{P_{s,g,t}+LS_{s,i,t}+P_{s,i,t}^{w}-L_{s,i,t}+Pbuy_{i,t}\right\}=\sum_{g\in\Omega_G^i}P_{s,ij,t}:\lambda_{i,t} \tag{12.9}$$

$$P_{s,ij,t}=\frac{\theta_{s,i,t}-\theta_{s,j,t}}{X_{ij}} \tag{12.10}$$

$$P_{s,g,t}-P_{s,g,t-1}\le RU_g \tag{12.11}$$

$$P_{s,g,t-1}-P_{s,g,t}\le RD_g \tag{12.12}$$

$$-P_g^{\max}\le P_{ij,t}\le P_g^{\max} \tag{12.13}$$

$$0\le LS_{i,t}\le L_{i,t} \tag{12.14}$$

$$0\le Pbuy_{i,t}\le Pbuy_{i,t}^{\max} \tag{12.15}$$

$$\xi_{i,t}+\beta_i\times\Gamma\ge\lambda_{i,t}^{R}Pbuy_{i,t} \tag{12.16}$$

12.2.5 Wind Power Generation

The amount of power generated by wind unit generally has a nonlinear relationship with the wind speed value and the other turbine factors. In the proposed method, a simplified linear formula is considered in which the amount of power generated from wind turbine is related to variation of wind speed value (12.17), which can be described as follows:

$$P_{s,i,t}^{W}=\begin{cases}0 & V_{\mathrm{u,t}}^{W}>V_{\mathrm{u}}^{CO},V_{\mathrm{u,t}}^{W}<V_{\mathrm{u}}^{CI}\\ P_{\mathrm{u}}^{\max}\times\left(\dfrac{V_{\mathrm{u,t}}^{W}-V_{\mathrm{u}}^{CI}}{V_{\mathrm{u}}^{R}-V_{\mathrm{u}}^{CI}}\right) & V_{\mathrm{u}}^{CI}<V_{\mathrm{u,t}}^{W}<V_{\mathrm{u}}^{R}\\ P_{\mathrm{u}}^{\max} & V_{\mathrm{u}}^{R}<V_{\mathrm{u,t}}^{W}<V_{\mathrm{u}}^{CO}\end{cases} \tag{12.17}$$

12.2.6 Real-Time Demand Response

By implementing DR program, electricity consumers adopt changeable part of their loads from high-price time intervals to inexpensive periods in order to reduce total fuel cost and their own revenues. At first, (12.18) shows the load after applying demand response program which is constructed from two parts, one is the normal load and the other is the demand response term. Moreover, (12.19) is demand response term which consists of two parts including the demand response percent which is crossed to the normal demand and adds to the normal demand to construct the final demand after applying demand response. Equation (12.20) means that in each demand response program, the sum of the demand response terms

should be equal to zero. Finally, the curtailment for percent of demand response is shown in (12.21).

$$load(t) = load_0(t) + ldr(t) \tag{12.18}$$

$$ldr(t) = DR(t).load_0(t) \tag{12.19}$$

$$\sum_{t=1}^{24} ldr(t) = 0 \tag{12.20}$$

$$DR(t) \leq DR_{\max} \tag{12.21}$$

12.3 Case Study and Simulation Results

12.3.1 Case Study

At this part, the proposed method in this chapter is applied on IEEE-RES 24-bus combined with 20 nodes and 24 pipeline natural gas network, to define the effectiveness of the proposed method. The study considered the value of lost load (VOLL) and value of lost wind (VOLW) to be 180 $/MW h and 1000 $/MW h, respectively [32]. The maximum purchase power is considered to be 5 p.u ($Pbuy = 5$).

The effect of hybrid robust-stochastic optimization on natural gas and electricity integration in the presence of DRPs is unfolded by solving a nonlinear programming problem using general algebraic modeling system (GAMS) optimization software [33].

12.3.2 Numerical Results

In this case, the results of co-generation scheduling problem are compared to show the differences between the cases of studies.

It should be remarked that there are several worst-case realizations of the price sequence for the same optimal consumption schedule. Figure 12.2 only shows the worst price with robust budget is equal to 7.5 in comparison with the upper bound and lower bound of the nominal price with a considered deviation equal to 15% [34].

Figure 12.3 shows electrical demand in two visions including nominal demand and demand after applying DR programs.

A comparison between the hourly schedules of generated power in three types of robust budget (i.e., RB = 7.5, 15, and 22.5) for generator 7 is unfolded in Fig. 12.4. As it is clear from Fig. 12.4, the amount of generated power from generators increases close to maximum value by increasing the amount of robust budget. The

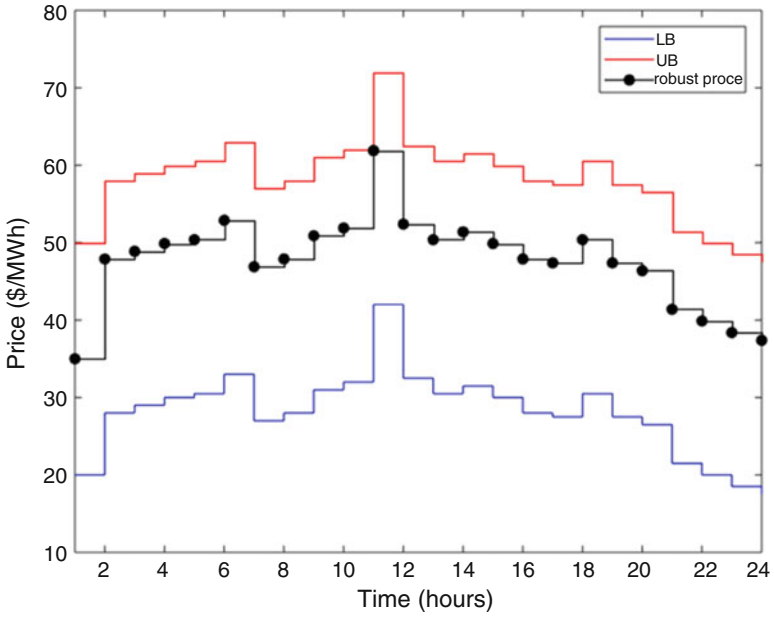

Fig. 12.2 Price range in robust optimization

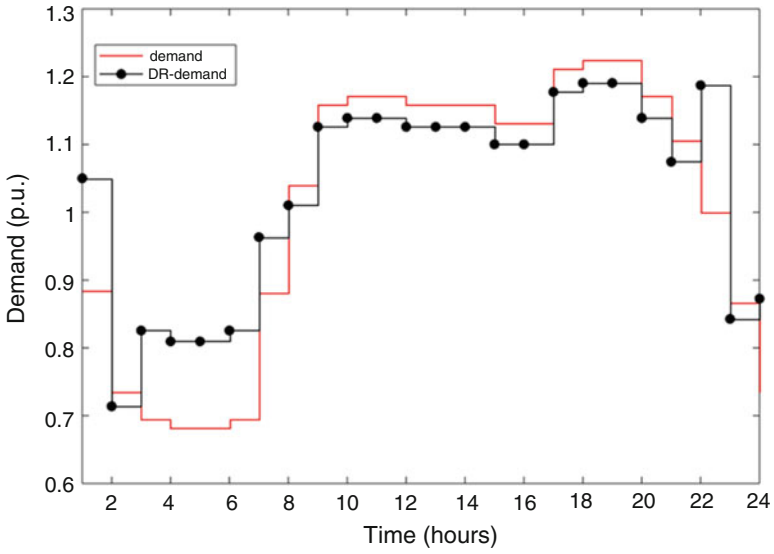

Fig. 12.3 The electrical load demand before/after applying DR program

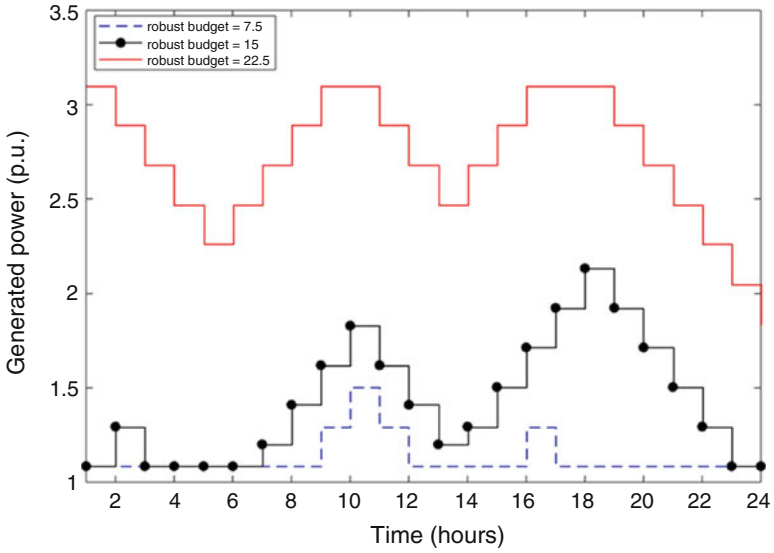

Fig. 12.4 Hourly generation schedule of generator 4 in scenario 4

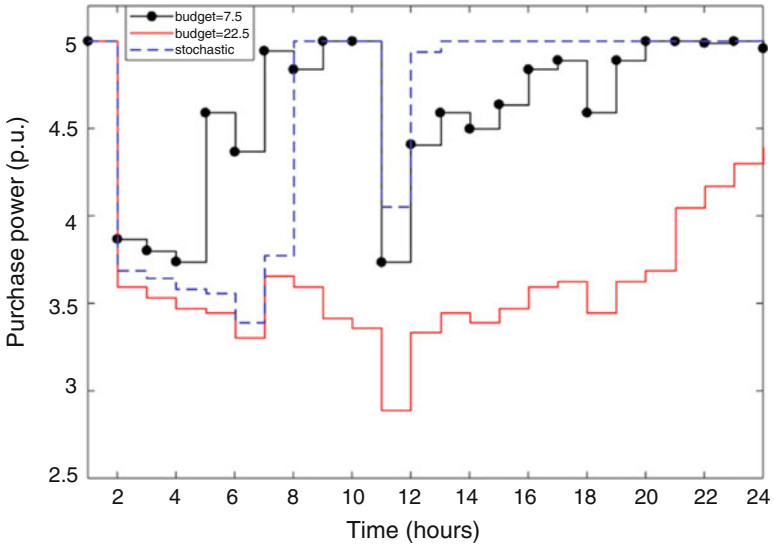

Fig. 12.5 Purchase power comparison RO-level = 1/stochastic

generated power of the generator in robust budgets 7.5, 15, and 22.5 is illustrated in this figure.

As in the base of the RO programming, the grid trend for power absorption in the market became lower by increasing price value to worst case. Figure 12.5 shows a

Table 12.2 The objective values in three different cases (stochastic, RO-stochastic with RO levels of 7.5, 15, and 22.5)

Mode	Cost
Stochastic	3.9534e + 5
RO-Stochastic (RO-Level = 7.5)	4.6118e + 5
RO-Stochastic (RO-Level = 15)	5.3554e + 5
RO-Stochastic (RO-Level = 22.5)	6.0647e + 5

part of purchase power from grid in three case studies, stochastic, RO-level = 7.5, and RO-level = 22.5 which proves that by increasing the robust budget, the grid trend for purchase power became lower.

Table 12.2 allows a comparison between the three case studies, a stochastic one and hybrid stochastic-RO with two kinds of robust level (7.5, 15, and 22.5).

12.4 Conclusion

An illustration of a hybrid robust-stochastic approach is the main objective of the presented work, which focused on coordinated optimal scheduling of natural gas and electricity co-generation. In this case, the authors utilized RO for considering power market price uncertainty. In addition, both electrical and natural gas demand uncertainties were considered in stochastic programming term. On the other hand, a real-time demand response (DR) was also considered in order to make load profile so smoother. In addition, the presented method is applied on a case study; IEEE RTS 24-bus combined with natural gas network was the test system. The results show that considering hybrid robust-stochastic model has more economic efficiency and benefits of gas-electric coordinated schedule. The obtained results show that the operation cost of the studied system increases by increasing the robust level of the system.

References

1. Colson, C. M., Nehrir, H., & Nehrir, M. H. (2011). Evaluating the benefits of a hybrid solid oxide fuel cell combined heat and power plant for energy sustainability and emissions avoidance. *IEEE Transactions on Energy Conversion, 26*(1), 140–148.
2. Geidl, M., Koeppel, G., & Favre-Perrod, P. (2007, March). *The energy hub–A powerful concept for future energy systems*. Third annual Carnegie mellon conference on the electricity industry, pp. 13–14.
3. Hashemi, R. (2009). A developed offline model for optimal operation of combined heating and cooling and power systems. *IEEE Transactions on Energy Conversion, 24*(1), 222–229.
4. Hemmes, K., Zachariah-Wolf, J. L., Geidl, M., & Andersson, G. (2007). Towards multi-source multi-product energy systems. *International Journal of Hydrogen Energy, 32*(10–11), 1332–1338.

5. Correa-Posada, C. M., & Sanchez-Martin, P. (2015). Integrated power and natural gas model for energy adequacy in short-term operation. *IEEE Transactions on Power Apparatus and Systems, 30*(6), 3347–3355.
6. Fang, J., Zeng, Q., Ai, X., Chen, Z., & Wen, J. (2018). Dynamic optimal energy flow in the integrated natural gas and electrical power systems. *IEEE Transactions on Sustainable Energy, 9*(1), 188–198.
7. Sardou, I. G., Khodayar, M. E., & Taghi Ameli, M. (2018). Coordinated operation of natural gas and electricity networks with microgrid aggregators. *IEEE Transactions on Smart Grid, 9*(1), 199–210.
8. Soroudi, A., Mohammadi-Ivatloo, B., & Rabiee, A. (2014). Energy hub management with intermittent wind power (pp. 413–438). https://doi.org/10.1007/978-981-4585-30-9_16.
9. Wang, C., Wei, W., Wang, J., Liu, F., & Mei, S. (2017). Strategic offering and equilibrium in coupled gas and electricity markets. *IEEE Transactions on Power Apparatus and Systems, 33*(1), 1–1.
10. Wen, Y., Qu, X., Li, W., Liu, X., & Ye, X. (2017). Synergistic operation of electricity and natural gas networks via ADMM. *IEEE Transactions on Smart Grid*, 1–1.
11. Zhang, X., Che, L., Shahidehpour, M., Alabdulwahab, A. S., & Abusorrah, A. (2015). Reliability-based optimal planning of electricity and natural gas interconnections for multiple energy hubs. *IEEE Transactions on Smart Grid, 99*, 1–10.
12. Zhou, Y., Gu, C., Wu, H., & Song, Y. (2017). An equivalent model of gas networks for dynamic analysis of gas-electricity systems. *IEEE Transactions on Power Apparatus and Systems, 32*(6), 4255–4264.
13. Dolatabadi, A., Jadidbonab, M., & Mohammadi-Ivatloo, B. (2017). Short-term scheduling strategy for wind-based energy hub: A hybrid stochastic/IGDT approach. *IEEE Transactions on Sustainable Energy, 99*, 1.
14. Dolatabadi, A., & Mohammadi-Ivatloo, B. (2017). Stochastic risk-constrained scheduling of smart energy hub in the presence of wind power and demand response. *Applied Thermal Engineering, 123*, 40–49.
15. Dolatabadi, A., Mohammadi-Ivatloo, B., Abapour, M., & Tohidi, S. (2017). Optimal stochastic design of wind integrated energy hub. *IEEE Transactions on Industrial Informatics, 13*(5), 2379–2388.
16. He, C., Wu, L., Liu, T., & Bie, Z. (2018). Robust co-optimization planning of interdependent electricity and natural gas systems with a joint N-1 and probabilistic reliability criterion. *IEEE Transactions on Power Apparatus and Systems, 33*(2), 2140–2154.
17. He, C., Wu, L., Liu, T., & Shahidehpour, M. (2017). Robust co-optimization scheduling of electricity and natural gas systems via ADMM. *IEEE Transactions on Sustainable Energy, 8*(2), 658–670.
18. Martinez-Mares, A., & Fuerte-Esquivel, C. R. (2013). A robust optimization approach for the interdependency analysis of integrated energy systems considering wind power uncertainty. *IEEE Transactions on Power Apparatus and Systems, 28*(4), 3964–3976.
19. Neyestani, N., Yazdani-Damavandi, M., Shafie-Khah, M., Chicco, G., & Catalao, J. P. S. (2015). Stochastic modeling of multi-energy carrier dependencies in smart local networks with distributed energy resources. *IEEE Transactions on Smart Grid, 6*(4), 1748–1762.
20. Parisio, A., Del Vecchio, C., & Vaccaro, A. (2012). A robust optimization approach to energy hub management. *International Journal of Electrical Power & Energy Systems, 42*(1), 98–104.
21. Soroudi, A., & Keane, A. (2015). Risk averse energy hub management considering plug-in electric vehicles using information gap decision theory. In *Power systems* (Vol. 89, pp. 107–127). Singapore: Springer.
22. Vahid-Pakdel, M. J., Nojavan, S., Mohammadi-Ivatloo, B., & Zare, K. (2017). Stochastic optimization of energy hub operation with consideration of thermal energy market and demand response. *Energy Conversion and Management, 145*, 117–128.
23. Wang, C., et al. (2017). Robust defense strategy for gas-electric systems against malicious attacks. *IEEE Transactions on Power Apparatus and Systems, 32*(4), 2953–2965.

24. Zhang, X., Shahidehpour, M., Alabdulwahab, A., & Abusorrah, A. (2016). Hourly electricity demand response in the stochastic day-ahead scheduling of coordinated electricity and natural gas networks. *IEEE Transactions on Power Apparatus and Systems, 31*(1), 592–601.
25. Alipour, M., Zare, K., & Abapour, M. (2017). MINLP probabilistic scheduling model for demand response programs integrated energy hubs. *IEEE Transactions on Industrial Informatics, 14*(1), 1–1.
26. Bahrami, S., Toulabi, M., Ranjbar, S., Moeini-Aghtaie, M., & Ranjbar, A. M., (2017). A decentralized energy management framework for energy hubs in dynamic pricing markets. Ieeexplore.Ieee.Org
27. Zhou, Y., Wei, Z., Sun, G., Cheung, K. W., Zang, H., & Chen, S. (2018). A robust optimization approach for integrated community energy system in energy and ancillary service markets. *Energy, 148*, 1–15.
28. Nazari-Heris, M., Mohammadi-Ivatloo, B., Gharehpetian, G. B., & Shahidehpour, M. (2018). Robust short-term scheduling of integrated heat and power microgrid. *IEEE Systems Journal, 99*, 1–9.
29. Majidi, M., Nojavan, S., & Zare, K. (2017). Optimal stochastic short-term thermal and electrical operation of fuel cell/photovoltaic/battery/grid hybrid energy system in the presence of demand response program. *Energy Conversion and Management, 144*, 132–142.
30. Nazari-Heris, M., Abapour, S., & Mohammadi-Ivatloo, B. (2018). Optimal economic dispatch of FC-CHP based heat and power micro-grids. *Applied Thermal Engineering, 114*, 756–769.
31. Soroudi, A. (2017). Energy storage systems. In *Power system optimization modeling in GAMS* (pp. 175–201). Cham: Springer.
32. Wu, J., Zhang, B., Deng, W., & Zhang, K. (2015). Application of Cost-CVaR model in determining optimal spinning reserve for wind power penetrated system. *International Journal of Electrical Power & Energy Systems, 66*, 110–115.
33. CONOPT. [Online]. Available: https://www.gams.com/latest/docs/S_CONOPT.html. Accessed 20 May 2018.
34. Nazari-Heris, M., Madadi, S., & Mohammadi-Ivatloo, B. (2018). Optimal management of hydrothermal-based micro-grids employing robust optimization method. In *Classical and recent aspects of power system optimization*. (pp. 407–420). London, United Kingdom: Elsevier.

Chapter 13
Robust Optimal Multi-agent-Based Distributed Control Scheme for Distributed Energy Storage System

Desh Deepak Sharma and Jeremy Lin

13.1 Introduction

Worldwide, there is a rapid growth of renewable power generations, especially wind and solar PV, which have made inroads into the existing electricity grids. According to the International Energy Agency Photovoltaic Power Systems Programme (IEA-PVPS), this growth rate in installed capacity is ranging from 35% to 85% in Organisation for Economic Co-operation and Development (OECD) countries. The IEA-PVPS has shown that 40 GW of solar capacity has already been installed around the world. The energy from installed solar PV would increase to 600 GW in 2035 due to decrease in expenses and government aids. In 2035, the expected solar capacity would reach 113 GW in China, 85 GW in India, and 54 GW in Japan [1].

Furthermore, IEA-PVPS has analyzed that hybrid PV system configuration such as PV and BESS are economical and clean [2]. The hybrid PV system is basically a microgrid in which DC link can be shared between PV system and BESS [3]. During recent years, installed price of solar PV system has decreased due to decrement in the hardware cost. Expected financial returns and concerns about operations and maintenance are the major other determining factors in the adoption of solar PV system [4]. The storage systems paired with solar plants can overcome the risks, faced by the solar power producer, due to uncertain production of solar plant [5]. The variability and uncertainty feature in solar PV power and wind power generation must be analyzed in order to develop a mechanism for evaluating both the economic and

D. D. Sharma (✉)
Electrical Engineering Department, M.J.P. Rohilkhand University, Bareilly, India
e-mail: ddsharma@mjpru.ac.in

J. Lin
Transmission Analytics, Austin, TX, USA
e-mail: Jeremylin@transmissionanalytics.net

B. Mohammadi-ivatloo, M. Nazari-Heris (eds.), *Robust Optimal Planning and Operation of Electrical Energy Systems*,
https://doi.org/10.1007/978-3-030-04296-7_13

reliability impacts of solar PV and wind power variability and uncertainty at multiple scales [6].

Possibilities of uncertainty in forecasting may be due to different factors. In various literatures, different models are developed for forecasting, but these methods are based on a number of assumptions of the future. Forecasting may not be accurate due to collection of bad input data found from either measurement or estimation. It is impossible to perfectly develop the relationships among all possible factors and output of a system. Reliability and security will be the new challenges in the development of a smart grid with the penetration of more and more renewable sources which are uncertain in nature in terms of power generation. In the presence of uncertainties, the grid can be made more secure and reliable by deploying energy storage devices as new technology in the system. With both grid-connected and islanded operations, intelligent energy management schemes are developed while deciding the capacity and charging rate of storage devices, residential load variations, and distribution network electricity price [7, 8].

A solar photovoltaic (PV) unit consists of a number of solar cells. In solar power generation of each cell, modeling has been done for two parts such as the solar irradiation function and the power generation function in which solar irradiation is linked to the power output of the solar PV generator. In different literatures, it is found that, generally, the beta PDF is being used in the modeling of the random behavior of the solar irradiation for each day. The parameters beta PDF can be inferred from the estimates of mean and variance values of historical irradiance data [9–11]. Based on the model of irradiation distribution, the output of a solar generator is decided by the function of power generation [12]. Similarly, in wind turbine generation modeling, two parts are considered as wind speed modeling and the turbine generation function. For modeling of wind speed randomness, the Weibull distribution is generally used. Forecast values and associated uncertainties of wind power are important to the utilities. These information help in optimal scheduling of energy storage and distributed generations [13]. At substations, load patterns are uncertain as compared to that at large system. Several qualitative and quantitative variables influence the electrical load demand. Some of these variables are random in nature, and, hence, the load demand is uncertain. The shape of curve representing the typical load pattern can be expressed in a group of deterministic variables which show the qualitative characteristic of the load pattern. Some groups of load patterns may be based on weekdays, weekends, or holidays. Others may consider the seasons such as autumn, winter, spring, and summer [14, 15]. A new empirical method is developed to model the prediction uncertainty of the solar irradiance forecast on numerical weather prediction. The predicted and measured solar irradiances are transformed into Gaussian random variables with past observed data, and a multivariate normal joint distribution model is estimated using this data [16]. A periodic optimization method is developed that determines an optimum periodic solution for any load profile over a 24-h period. The cyclic solution for the battery state of charge is represented by Fourier coefficients. The optimization process is embedded in a receding horizon battery control system [17].

In smart grid infrastructure, the distributed multi-step optimal scheduling is introduced for energy storage devices and distributed generation. This algorithm is

based on the local communications with neighbors [18]. In order to reduce generation cost, in microgrid, the distributed optimal strategy is proposed for the resource management [19]. The computationally tractable distributed optimal control strategy, which includes AC optimal power flow, for batteries is proposed in a microgrid [20]. Multi-agent-based optimal distributed charging rate scheme is proposed for numerous plug-in electric vehicle (PEV). In this scheme, an agent for a PEV decides optimal charging rate based on remaining charging time and state of charge along with other battery parameters [21]. In smart grid, an adjustment cost is considered for dynamic adjustment of distributed generations and loads. In distributed control algorithm, this cost is minimized to achieve generation-demand balance [22]. A multi-agent-based dynamic optimal power flow is suggested for microgrid with energy storage devices and distributed generations [23].

13.2 Multi-agent System

A multi-agent system is a group of interacting agents that acts in a concurrent way existing in the distributed environment. They have cooperation as well as competition among themselves, and they are conjunct in some common infrastructure. In MAS local goals of individual agents are more important to be accomplished as compared to the overall system goal [24–28].

13.2.1 MAS for Power System: An Overview

The penetration of various distributed generations into the electric network and liberalization of electricity markets with new business models pose the new challenges to the power industries such as enhancement of complexity in distribution network, problems in power system management, disturbance of power system protection, and frequency stability [26, 29]. Present power system equipped with old legacy SCADA system does not suffice to cater aforementioned challenges in highly decentralized system [26, 30]. Market-based MAS is proposed in [31] for reconfiguration of radial shipboard power system, developed with Java Agent Development Framework (JADE) which conforms to FIPA standards for intelligent agents. MASCEM, a multi-agent simulator system, is a framework which deals with new rules, new behavior, and also new actors involved in various electricity markets within liberalized and competitive environment [32]. ABMS, agent-based modeling and simulation system, based on traditional game theory, is able to perceive and analyze the complexities of power market (e.g., repeated auctions, fluctuating supply and demand, non-storability of electricity, etc.) and interactions among all entities involved [33]. In multi-agent approach to power system, each bus agent (BAG), which possesses local information, tends to restore load after fault occurrence, directly connected to its associated bus interacting with other numerous BAGs,

and a single facilitator agent (FAG) acts as a manager for the negotiation process [34].

Multi-agent system is developed for monitoring of transformer condition [35] and industrial gas turbine start-up sequence [36]. An agent-based automation system is developed for substation, while the information is gathered by control/monitoring agents over Ethernet network [37]. A multi-agent system is also capable in efficient operation of microgrids with minimum operation cost [24, 38]. PEDA (Protection Engineering Diagnostic Agents), a multi-agent system, which complies FIPA standards, integrates legacy intelligent systems SCADA and digital fault recorder data and can interpret intelligently and manage data online [30, 39]. As virtual power plant (VPP) is scattered in a decentralized system, multi-agent system facilitates virtual power point to take decisions at local level so that the main goal is achieved [24, 25].

13.2.2 Preliminaries

Let $V = \{1,\ldots,n\}$ be a set of nodes and $E \subseteq V \times V$ be a set of edges of a weighted digraph (or directed graph) $G = \{V,E,A\}$. $\boldsymbol{A} = [a_{ij}]$ be the adjacency matrix with non-negative adjacency elements a_{ij} and $a_{ii} = 0$ for $i = 1, 2, \ldots, n$. The ed_{ij} is the directed edge, from node i to node j, of digraph G. The adjacency elements of an edge ed_{ji} are positive, i.e., $a_{ij} > 0$ if and only if $ed_{ji} \in E$. A digraph is undirected if $a_{ij} = a_{ji}$ for $\forall i,j \in \{1,2,\ldots,n\}$.

A group of agents represents the nodes in a digraph G and unidirectional information exchange links among agents correspond to edges of the graph. An interaction topology among the battery agents shows the communication pattern at some particular time and is designed by using the digraph G. In adjacency matrix $\boldsymbol{A}$, an element a_{ij} is greater than zero, if and only if node i gets information from node j. A directed tree is defined as a directed graph in which every node except the root has exactly one parent. A directed (rooted) spanning tree of the digraph G is a subgraph such that this subgraph is a directed tree and consists of all the nodes of G. A spanning tree of G consists of n nodes and $n - 1$ edges and a path exists from root node to every other node. Thus, root node can send information to every other node.

The $n \times n$ Laplacian matrix $\boldsymbol{L_n} = (l_{ij})$, associated with the adjacency matrix $\boldsymbol{A}$ of a digraph G, is defined as given below:

$$l_{ij} = -a_{ij}, i \neq j \quad \text{and} \quad l_{ii} = \sum\nolimits_{j=1,j\neq i}^{n} a_{ij}$$

According to the definition of $\boldsymbol{L_n}$, it is ensured that in any row, $\sum_{j=1}^{n} l_{ij} = 0$, and it is the asymmetric matrix of a digraph. There is an aim to control all the nodes such that information state of all agents of a group converges to one single state [40–42].

In the uncertain power distribution system, the objectives are to develop a robust optimal distributed control protocol such that the battery agents of respective BESSs

should communicate to achieve the consensus for abovementioned goals during charging and discharging cycles and, furthermore, find global stability in the overall dynamic system. The control objective is to cater the imbalance in active power and uncertainty in the power distribution system with different BESSs and transforms this imbalance into the design of distributed control scheme. Two leader-follower pinning control schemes are designed for distributed control of the BESS to achieve their fair participations. These battery agents decide and control the power exchange to and from the respective BESSs. These agents exist at the BESS installation. These agents can receive information from the virtual leader to be pinned and to start distributed consensus control while communicating with neighboring battery agents, locally.

13.3 Robust Optimal Control

Briefly, the basics of robust optimal control are given as follows. Let the linear uncertain system be

$$x(k+1) = Ax(k) + Bu(k) + Ew(k) \tag{13.1}$$

where $x(k) \in R^n$ and $u(k) \in R^m$ are the state and input vectors, respectively. The sets X and U are polytopes, and $w(k)$ is the additive uncertainty present in the system. The Eq. (13.1) may be subject to constraints

$$x(k) \in X, \quad u(k) \in U \tag{13.2}$$

Now define the cost function for the given uncertainty $w \in W$ and the $u(k) \in U$.

$$J_w(k) = q(x(k), u(k)) \tag{13.3}$$

$$q(x(k), u(k)) = x^T Q x + u^T R u \tag{13.4}$$

The cost $J_w(k)$ is evaluated for the given uncertainty $w(k)$ and input $u(k)$ and with Eq. (13.1).

In case the probability density function is considered for the uncertainty $w(k)$ then

$$\text{Probability}\,[w(k) \in W] = 1 = \int_{w \in W} f(w)dw \tag{13.5}$$

The expected value of a function $g(w)$ of the uncertainty is defined as

$$E_w[g(w)] = \int_{w \in W} g(w)f(w)dw \tag{13.6}$$

The expected cost with admissible uncertainty is given as

$$J_w = E_w\left[x^T Q x + u^T R u\right] \tag{13.7}$$

$$\text{where} \begin{cases} x(k+1) = Ax(k) + Bu(k) + Ew(k) \\ x(k) \in X, \quad u(k) \in U \end{cases} \tag{13.8}$$

Now, the worst-case cost is defined as given below:

$$J_w = \max_w\left[x^T Q x + u^T R u\right] \tag{13.9}$$

$$\text{where} \begin{cases} x(k+1) = Ax(k) + Bu(k) + Ew(k) \\ x(k) \in X, \quad u(k) \in U \end{cases} \tag{13.10}$$

In all cases, the robust optimal control is given below while minimizing the cost function:

$$J_w^* = \min_u J_w \tag{13.11}$$

$$\text{where} \begin{cases} x(k+1) = Ax(k) + Bu(k) + Ew(k) \\ x(k) \in X, \quad u(k) \in U \end{cases} \tag{13.12}$$

13.4 BES System Modeling

The different scattered battery energy storage (BES) systems are considered to be connected to an AC system using bidirectional AC/DC converters. In this power distribution system, the BES systems are assumed to achieve reliable operation, in real time, at the distribution substation [15]. As the demand changes, the BES systems come into action. During off-peak hours, these systems can be charged, and in peak hours, these can be discharged. Therefore, the BES system can operate as a load during charging and as generator during discharging. Controlling and managing scattered BES systems with different ratings is a challenging task. The charging and discharging of a BES unit can be expressed as follows:

$$E_{es}(k+1) = E_{es}(k) - \frac{P_{es}(k)}{\eta_d}\Delta t, \text{ for } P_{es} > 0 \tag{13.13}$$

$$E_{es}(k+1) = E_{es}(k) - \eta_c P_{es}(k)\Delta t, \text{ for } P_{es} < 0 \tag{13.14}$$

where E_{es} is the stored energy in BES system, P_{es} is the power to be exchanged by BES system during charging and discharging, Δt is the time duration of k. η_d, and η_c are the discharging and charging efficiencies of BES system, respectively. The upper and lower limits of stored energy are as given below:

$$E_{es}^{\min} < E_{es}(k) < E_{es}^{\max} \tag{13.15}$$

where $E_{es}^{\max}$ and $E_{es}^{\min}$ are, respectively, the maximum and minimum bounds of the energy in the BES system.

The Eqs. (13.13) and (13.14) for BES system are modified as below:

$$\frac{E_{es}(k+1)}{E_{mm}} = \frac{E_{es}(k)}{E_{mm}} - \frac{P_{es}(k)}{E_{mm} \cdot \eta_d} \Delta t, \text{ for } P_{es} > 0 \tag{13.16}$$

$$\frac{E_{es}(k+1)}{E_{mm}} = \frac{E_{es}(k)}{E_{mm}} - \eta_c \frac{P_{es}(k)}{E_{mm}} \Delta t, \text{ for } P_{es} < 0 \tag{13.17}$$

where $E_{mm} = E_{es}^{\max} - E_{es}^{\min}$.

The power balance equation in an AC system at a time instant k

$$P_{grid}(k) + P_{ren}(k) + P_{es}(k) = P_{dem}(k) \tag{13.18}$$

where P_{grid} is grid supply, P_{ren} is the renewable power generation, P_{es} is power exchange by BES unit, and P_{dem} is the electrical demand.

The power balance equation incorporating uncertainties present in renewable power generation and electrical demand while dropping k for simplicity.

$$P_{grid} + (P_{ren} + \Delta P_{ren}) + (P_{es} + \Delta P_{es}) = (P_{dem} + \Delta P_{dem}) \tag{13.19}$$

where ΔP_{ren} and ΔP_{dem} represent uncertain parts of renewable power generation and electrical demand, respectively. The ΔP_{es} is the power exchange by BES unit to cater the uncertainties in an AC power distribution system.

On considering uncertainties in the system, the Eqs. (13.13) and (13.14) are modified as given below:

$$\begin{aligned} &\frac{E_{es}(k+1) + \Delta E_{es}(k+1)}{E_{mm}} = \frac{E_{es}(k) + \Delta E_{es}(k)}{E_{mm}} \\ &- \frac{P_{es}(k) + \Delta P_{es}(k)}{E_{mm} \cdot \eta_d} \Delta t, \text{ for } P_{es} > 0 \end{aligned} \tag{13.20}$$

$$\begin{aligned} &\frac{E_{es}(k+1) + \Delta E_{es}(k+1)}{E_{mm}} = \frac{E_{es}(k) + \Delta E_{es}(k)}{E_{mm}} \\ &- \eta_c \frac{P_{es}(k) + \Delta P_{es}(k)}{E_{mm}} \Delta t, \text{ for } P_{es} < 0 \end{aligned} \tag{13.21}$$

where ΔE_{es} represents the uncertain part of E_{es} .

For expected uncertainty, the (13.20) and (13.21) are modified as

$$\frac{E_{es}(k+1)+E\Delta E_{es}(k+1)}{E_{mm}}=\frac{E_{es}(k)+E\Delta E_{es}(k)}{E_{mm}} -\frac{P_{es}(k)+E\Delta P_{es}(k)}{E_{mm}\cdot\eta_d}\Delta t,\ \text{for } P_{es}>0 \tag{13.22a}$$

$$\frac{E_{es}(k+1)+E\Delta E_{es}(k+1)}{E_{mm}}=\frac{E_{es}(k)+E\Delta E_{es}(k)}{E_{mm}} -\eta_c\frac{P_{es}(k)+E\Delta P_{es}(k)}{E_{mm}}\Delta t,\ \text{for } P_{es}<0 \tag{13.23a}$$

For worst-case uncertainty, the (13.20) and (13.21) are modified as

$$\frac{E_{es}(k+1)+\max\limits_{\Delta E_{es}(k+1)}f(\Delta E_{es}(k+1))}{E_{mm}}=\frac{E_{es}(k)+\max\limits_{\Delta E_{es}(k)}f(\Delta E_{es}(k))}{E_{mm}} -\frac{P_{es}(k)+\max\limits_{\Delta P_{es}(k)}f(\Delta P_{es}(k))}{E_{mm}\cdot\eta_d}\Delta t,\ \text{for } P_{es}>0 \tag{13.22b}$$

$$\frac{E_{es}(k+1)+\max\limits_{\Delta E_{es}(k+1)}f(\Delta E_{es}(k+1))}{E_{mm}}=\frac{E_{es}(k)+\max\limits_{\Delta E_{es}(k)}f(\Delta E_{es}(k))}{E_{mm}} -\eta_c\frac{P_{es}(k)+\max\limits_{\Delta P_{es}(k)}f(\Delta P_{es}(k))}{E_{mm}}\Delta t,\ \text{for } P_{es}<0 \tag{13.23b}$$

On consideration of many BES systems, the aforementioned equations are generalized and used for *i*th BES system. Hence, the simplified model of *i*th BES system is

$$\begin{aligned}&x_i(k+1)=A_{x,i}x_i(k)+B_{x,i}u_i \text{ where } x_i=E_{i,es}/E_{i,mm},\\&u_i=P_{i,es}, A_{x,i}=1, B_{x,i}=\Delta t/\left(E_{i,mm}\cdot\eta_{i,d}\right) \text{ for } P_{i,es}>0,\\&B_{x,i}=\left(\eta_{i,c}\cdot\Delta t\right)/E_{i,mm} \text{ for } P_{i,es}<0\end{aligned} \tag{13.24}$$

The model pertaining to uncertainty

$$\begin{aligned}&y_i(k+1)=A_{y,i}y_i(k)+B_{y,i}v_i \text{where } y_i=\Delta E_{i,es}/E_{i,mm},\\&v_i=\Delta P_{i,es}, A_{y,i}=1, B_{y,i}=\Delta t/\left(E_{i,mm}\cdot\eta_{i,d}\right)\\&\text{for } P_{i,es}>0, B_{y,i}=\left(\eta_{i,c}\cdot\Delta t\right)/E_{i,mm} \text{for } P_{i,es}<0\end{aligned} \tag{13.25}$$

The abovementioned Eqs. (13.24) and (13.25) form the basis for development of the multi-agent system.

13.5 Agent-Based Robust Optimal Control Scheme

The multi-agent-based system deals with two control schemes which are optimal and incorporate uncertainties. Two leader-follower control schemes are given below.

$$x_i(k+1) = A_{x,i}x_i(k) + B_{x,i}u_i(k) \tag{13.26}$$

And

$$y_i(k+1) = A_{y,i}y_i(k) + B_{y,i}v_i(k) \tag{13.27}$$

$i = 1,\ldots,n$ where n is number of agents. The x_0,y_0 are the variables associated with leader agents. The abovementioned leader-follower schemes get consensus on following conditions:

$$x_i \to x_0 \text{ and } y_i \to y_0 \tag{13.28}$$

The linear consensus protocols are defined as given below:

$$u_i(k) = \sum_{j=1, j\neq i}^{n} a_{ij}\left[x_j(k) - x_i(k)\right] - b_i[x_i(k) - x_0] \tag{13.29}$$

And

$$v_i(k) = \sum_{j=1, j\neq i}^{n} w_{ij}\left[y_j(k) - y_i(k)\right] - d_i[y_i(k) - y_0] \tag{13.30}$$

The optimal control problem for the system (13.26)

$$\begin{aligned} &\min_{U(k)} J_x(U(k), X(0)) \\ &\text{subject to (13.26) and (13.28)} \end{aligned} \tag{13.31}$$

where

$$J_x(U(k), X(0)) = \sum_{k=0}^{\infty}\sum_{i=1}^{n} q_{x,i}(x_i - x_0)^2 + r_{x,i}u^2 \tag{13.32}$$

Similarly, the robust optimal control problem for the system (13.26) with expected cost function

$$\begin{aligned} &\min_{V(k)} \; EJ_y(V(k), Y(0)) \\ &\text{subject to (13.27) and (13.28)} \end{aligned} \tag{13.33}$$

where

$$E_{\Delta E(k)} J_y(V(k), Y(0)) = \sum_{k=0}^{\infty} \sum_{i=1}^{n} q_{y,i}(y_i - Ey_0)^2 + r_{y,i} v^2 \tag{13.34}$$

where $q_x > 0$, $q_y > 0$, $r_x > 0$, $r_y > 0$ and Ey_0 is the expected value of y_0.

Similarly, the robust optimal control problem for the system (13.26) with worst-case cost function

$$\begin{aligned} &\min_{V(k)} \; J_y(V(k), Y(0)) \text{ where} \\ &\text{subject to (13.27) and (13.28)} \end{aligned} \tag{13.35}$$

where

$$J_y(V(k), Y(0)) = \max_{\Delta E(k)} \sum_{k=0}^{\infty} \sum_{i=1}^{n} q_{y,i}(y_i - wy_0)^2 + r_{y,i} v^2 \tag{13.36}$$

where $q_x > 0$, $q_y > 0$, $r_x > 0$, $r_y > 0$, and wy_0 is the worst-case value of y_0.

Theorem For the joint optimal control problem, the optimal topology is star topology in which the follower i is only connected to the leader with the control gains $d_{x,i} = \frac{B_{x,0}}{2}\left(\frac{q_i}{r_i}\right)$ and $d_{y,i} = \frac{B_{y,0}}{2}\left(\frac{q_i}{r_i}\right)$ with the following assumptions:

Assumption 1:

$B_{x,1} = B_{x,2} = \ldots = B_{x,n} = B_{x,0}$ and $B_{y,1} = B_{y,2} = \ldots = B_{y,n} = B_{y,0}$

Assumption 2:

Let $B_{x,0} = \frac{2}{\sqrt{3}}\sqrt{\frac{r_i}{q_i}}$ and $B_{y,0} = \frac{2}{\sqrt{3}}\sqrt{\frac{r_i}{q_i}}$

The proof of this theorem is given in appendix.

13.5.1 Generation of x_0 and y_0

The x_0 is the desired value for all x_i and this value is provided to all agents from the leader agent. The leader agent knows the expected and worst case that may be associated with y_i, $i = 1,\ldots,n$, and y_0 is set to this expected and worst case. In

consensus-based robust optimal control scheme, all y_i track to this Ey_0 and wy_0, which are set to expected or worst-case value, respectively, as given below.

For expected value,

$$Ey_0 = f_e(\Delta E) \tag{13.37}$$

where f_e is the probability density function (pdf). Let, for any pdf,

$$Ey_0 = f_e(\Delta E) = \mathrm{G}_E g_E \leq p_E \tag{13.38}$$

where $\mathrm{G_E}$ and $\mathrm{g_E}$ are two different values which satisfy (13.37), and $\mathrm{p_E}$ is fixed constant value.

In worst case

$$wy_0 = \max_{\Delta E} y_i, \quad \forall i \in [1, \ldots, n] \tag{13.39}$$

Let, on maximizing the worst case

$$wy_0 = \max_{\Delta E} y_i = G_w g_w \leq p_w, \quad \forall i \in [1, \ldots, n] \tag{13.40}$$

Similar to (13.37), $\mathrm{G_w}$ and $\mathrm{g_w}$ are two different values which satisfy (13.39), and $\mathrm{p_w}$ is fixed constant value. The ($\mathrm{p_E}$,$\mathrm{G_E}$, $\mathrm{g_E}$) and ($\mathrm{p_w}$,$\mathrm{G_w}$, $\mathrm{g_w}$) are identified and set to the values based on past data.

With the allowed uncertainty in the system, the Eq. (13.34) is rewritten as

$$E_{\Delta E(k)} J_y(V(k), Y(0)) = \sum_{k=0}^{\infty} \sum_{i=1}^{n} q_{y,i} (y_i - p_E)^2 + r_{y,i} v^2 \tag{13.41}$$

$$E_{\Delta E(k)} J_y(V(k), Y(0)) = \sum_{k=0}^{\infty} \sum_{i=1}^{n} q_{y,i} (e_E)^2 + r_{y,i} v^2 \tag{13.42}$$

where $e_E = (y_i - p_E)$.

Similarly, on maximizing the worst case in the uncertainty, the equation is modified as

$$J_y(V(k), Y(0)) = \sum_{k=0}^{\infty} \sum_{i=1}^{n} q_{y,i} (y_i - p_w)^2 + r_{y,i} v^2 \tag{13.43}$$

$$J_y(V(k), Y(0)) = \sum_{k=0}^{\infty} \sum_{i=1}^{n} q_{y,i} (e_w)^2 + r_{y,i} v^2 \tag{13.44}$$

where $e_w = (y_i - p_w)$.

13.6 Results and Discussions

The test microgrid is shown in the Fig. 13.1. The sizes of the battery energy storage devices are 0.2 MW/0.8MWh, 0.15 MW/0.75MWh, 0.1 MW/0.4MWh, 0.15 MW/0.45MWh, and 0.4 MW/1.6MWh with charging and discharging efficiencies $\eta_c = \eta_d = 80\%$, and the size of solar PV system is 1MWp. The maximum and minimum allowed energy on energy storage devices are $Emax_1 = 0.8MWh$ and $Emin_1 = 0.35MWh$, $Emax_2 = 0.75MWh$ and $Emin_2 = 0.40MWh$, $Emax_3 = 0.4MWh$ and $Emin_3 = 0.1MWh$, $Emax_4 = 0.45MWh$ and $Emin_4 = 0.1MWh$, and $Emax_5 = 1.6MWh$ and $Emin_5 = 1.25MWh$, respectively. In order to satisfy assumptions 1 and 2, the discharging efficiencies of these energy storage devices are assumed as 0.70, 0.85, 0.95, 0.82, and 0.85, and charging efficiencies are assumed as 0.86, 0.89, 0.91, 0.89, and 0.89, respectively.

The considered load profile of electrical demand and solar PV generation profile with added uncertainty are shown in Figs. 13.2 and 13.3, respectively. The included uncertainty remains within the permissible range as per Eqs. (13.38) and (13.40). The optimal energy and power are shared based on given power generation and electrical demand as shown in Figs. 13.4, 13.5, and shared optimal uncertain energy and power are shown in 13.6, and 13.7, respectively. Assume $q_i = r_i = 1$ for $i = 1,...,5$ then $d_{x,i} = d_{y,i} = 1.73$.

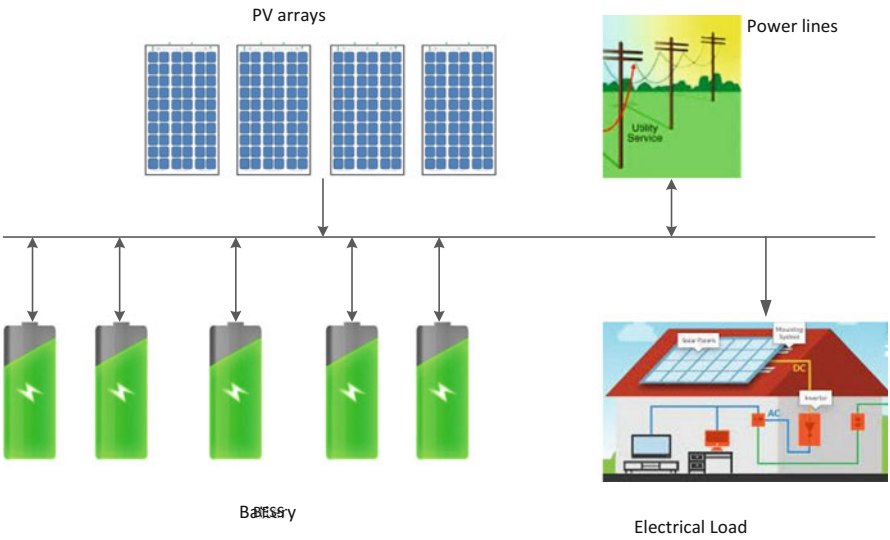

Fig. 13.1 Test microgrid

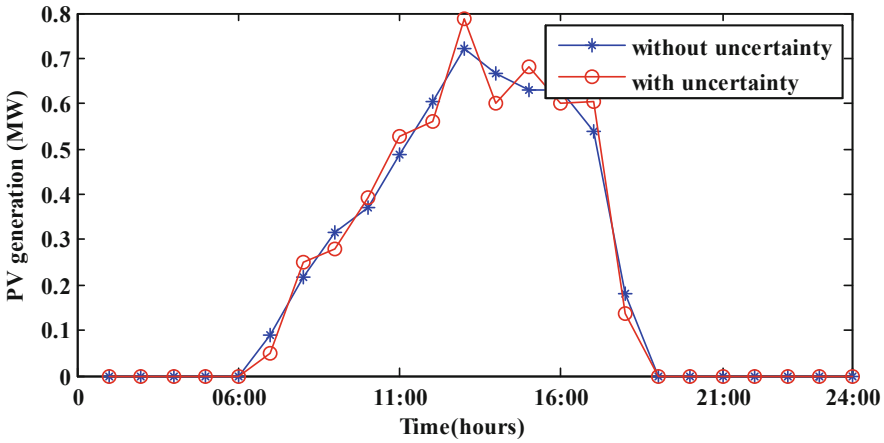

Fig. 13.2 Forecasted PV generation (blue) and PV generation with uncertainty (red)

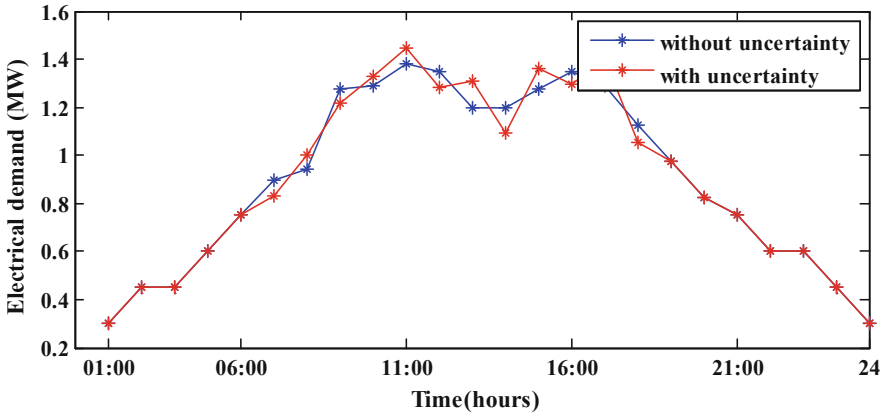

Fig. 13.3 Electrical demand

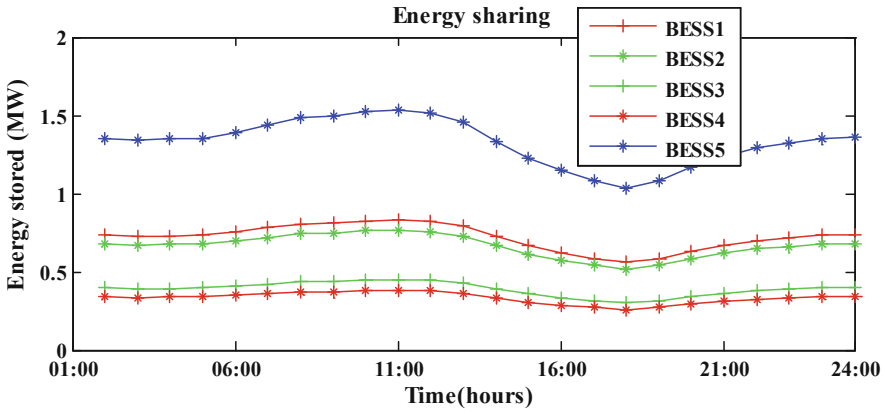

Fig. 13.4 Energy stored shared by different BESSs

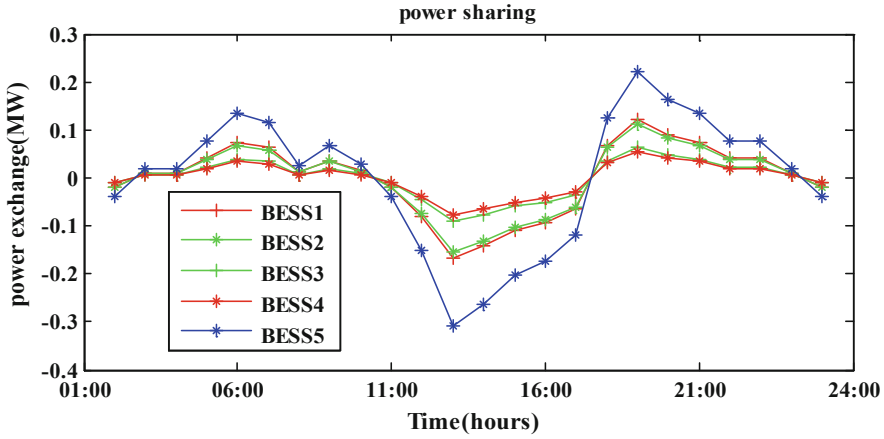

Fig. 13.5 Power exchange shared by different BESSs

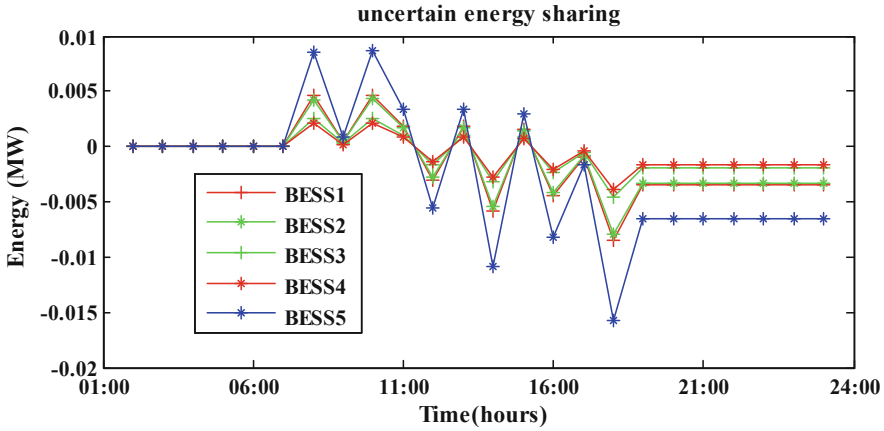

Fig. 13.6 Uncertain energy shared by different BESSs

13.7 Conclusions

This chapter has discussed agent-based distributed robust optimal control scheme. This scheme considers two objective functions out of which second objective function pertains to the uncertainties which are present in the power distribution system integrated with renewable power generation along with energy storage devices. Distributed multi-agent system works for deciding the charging and discharging of the batteries in the presence of uncertainties. In two expected and worst cases, all the agents get consensus and be driven to the values decided by the leader agent. In this distributed robust optimal control scheme, the optimal topology for communication is the star topology as proved in the theorem.

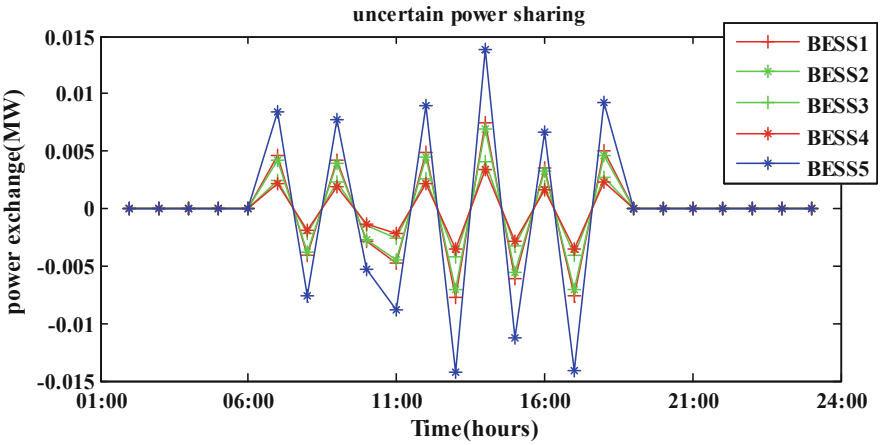

Fig. 13.7 Uncertain power exchange shared by different BESSs

Appendix

Proof of theorem

Let the error system for (13.26) be

$$\begin{aligned} e(k+1) &= A_x e(k) + B_x U(k), \\ U(k) &= -L_x e(k) \end{aligned} \tag{13.45}$$

where $A_x = \ diag\ (A_{x,1}, A_{x,2}, \ldots, A_{x,n})$ and $B_x = \ diag\ (B_{x,1}, B_{x,2}, \ldots, B_{x,n})$ and

$$e(k) = X(k) - 1_n \otimes U(k) \tag{13.46}$$

The modified LQR-based optimal control problem is

$$\min_{U(k)} \sum_{k=0}^{\infty} e(k)^T Q e(k) + U(k)^T R U(k) \tag{13.47}$$

For the system $X(k+1) = AX(k)+BU(k)$, the discrete time ARE is

$$A^T PA - P + Q - A^T PB\left(R + B^T PB\right)^{-1} B^T PA = 0 \tag{13.48}$$

For the system (13.45), the ARE is

$$Q = PB_x\left(R + B_x^2 P\right)^{-1} B_x P \tag{13.49}$$

where $A = A_x = 1$ and $B = B_x$.

Let $B_{x,1} = B_{x,2} = \ldots = B_{x,n} = B_{x,0}$

Then matrix $B_x = B_{x,0} I_n$

The optimal feedback gain matrix is

$$L_x = \left(R + B_{x,0}^2 I_n P\right)^{-1} B_{x,0} I_n P \tag{13.50}$$

Multiply R^{-1} both sides of (13.49) then

$$R^{-1}Q = R^{-1} P B_{x,0} I_n \left(R + B_{x,0}^2 I_n P\right)^{-1} B_{x,0} I_n P \tag{13.51}$$

$$R^{-1}Q = R^{-1} P B_{x,0} \left(I_n + B_{x,0}^2 R^{-1} P\right)^{-1} B_{x,0} R^{-1} P \tag{13.52}$$

Since it is known that

$$\left(I_n + B_{x,0}^2 R^{-1} P\right)^{-1} = I_n - B_{x,0}^2 R^{-1} P \left(I_n + B_{x,0}^2 R^{-1} P\right)^{-1} \tag{13.53}$$

We now get

$$\begin{aligned} &R^{-1} P B_{x,0} \left(I_n + B_{x,0}^2 R^{-1} P\right) B_{x,0} R^{-1} P = \left[B_{x,0} R^{-1} P\right]^2 - B_{x,0}^2 R^{-1} P \\ &\times \left[R^{-1} P B_{x,0} \left(I_n + B_{x,0}^2 R^{-1} P\right)^{-1} B_{x,0} R^{-1} P\right] \end{aligned} \tag{13.54}$$

$$R^{-1}Q = B_{x,0}^2 \left(R^{-1} P\right)^2 - B_{x,0}^2 R^{-1} P R^{-1} Q \tag{13.55}$$

On simplification it is obtained that

$$R^{-1}P = \frac{1}{2}\left[R^{-1}Q + \sqrt{\left(R^{-1}Q\right)^2 + \frac{4R^{-1}Q}{B_x^2}}\right] \tag{13.56}$$

Hence, the optimal feedback gain matrix is

$$L_x^* = \frac{B_{x,0}}{2}\left[\sqrt{\left(R^{-1}Q\right)^2 + \frac{4R^{-1}Q}{B_{x,0}^2}} - R^{-1}Q\right] \tag{13.57}$$

Let

$$L_x^* = diag(d_{x,1}, d_{x,2} \ldots, d_{x,n}) \tag{13.58}$$

Then, for *i*th agent the feedback gain is

$$d_{x,\mathrm{i}} = \frac{B_{x,0}}{2}\left[\sqrt{\left(\frac{q_i}{r_i}\right)^2 + \frac{4q_i}{B_{x,0}^2 r_i}} - \frac{q_i}{r_i}\right] \tag{13.59}$$

Similarly, it can be proved that

$$d_{y,\mathrm{i}} = \frac{B_{y,0}}{2}\left[\sqrt{\left(\frac{q_i}{r_i}\right)^2 + \frac{4q_i}{B_{y,0}^2 r_i}} - \frac{q_i}{r_i}\right] \tag{13.60}$$

Let

$$B_{x,0}^2 = \frac{4}{3}\frac{r_i}{q_i} \tag{13.61}$$

Then from (13.59)

$$d_{x,\mathrm{i}} = \frac{B_{x,0}}{2}\left[\sqrt{\left(\frac{q_i}{r_i}\right)^2 + 3\left(\frac{q_i}{r_i}\right)^2} - \frac{q_i}{r_i}\right] \tag{13.62}$$

$$d_{x,\mathrm{i}} = \frac{B_{x,0}}{2}\frac{q_i}{r_i} \tag{13.63}$$

Similarly, we can obtain

$$d_{y,\mathrm{i}} = \frac{B_{y,0}}{2}\frac{q_i}{r_i} \tag{13.64}$$

While

$$B_{y,0}^2 = \frac{4}{3}\frac{r_i}{q_i} \tag{13.65}$$

References

1. Sumathi, S., Kumar, L. A., & Surekha, P. (2015). *Solar PV and wind energy conversion systems an introduction to theory, modeling with MATLAB/SIMULINK, and the role of soft computing techniques*. Cham: Springer.
2. Song, S., Ko, B., Suh, J., Han, C., & Jang, G. (2017). Operation algorithm of PV/BESS application considering demand response uncertainty in an independent microgrid system. *Journal of International Council on Electrical Engineering, 7*(1), 242–248.
3. Prusty, B., Ali, S., & Sahoo, D. (2012). Modeling and control of grid connected hybrid photo voltaic/battery distributed generation system. *International Journal of Engineering Research and Technology, 24*(1), 125–132.
4. Rai, V., Reeves, C., & Margolis, R. (2016). Overcoming barriers and uncertainties in the adoption of residential solar PV. *Renewable Energy, 89*, 498–505.
5. Attarha, A., Amjady, N., & Dehghan, S. (2018). Affinely adjustable robust bidding strategy for a solar plant paired with a battery storage. *IEEE Transactions on Smart Grid, PP*(99), 1. https://doi.org/10.1109/TSG.2018.2806403.
6. Ela, E., Diakov, V., Ibanez, E., & Heaney, M. (2013). Impacts of variability and uncertainty in solar photovoltaic generation at multiple timescales. *National Renewable Energy Laboratory, 1*, 41.
7. de la Fuente, D. V., Rodriguez, C. L. T., Garcera, G., Figueres, E., & Gonzalez, R. O. (2013). Photovoltaic power system with battery backup with grid-connection and islanded operation capabilities. *IEEE Transactions on Industrial Electronics, 60*(4), 1571–1581.
8. Kim, S.-T., Bae, S., Kang, Y. C., & Park, J.-W. (2015). Energy management based on the photovoltaic hpcs with an energy storage device. *IEEE Transactions on Industrial Electronics, 62*(7), 4608–4617.
9. Atwa, Y. M., El-Saadany, E. F., Salama, M. M. A., & Seethapathy, R. (2010). Optimal renewable resources mix for distribution system energy loss minimization. *IEEE Transactions on Power Systems, 25*(1), 360–370.
10. Zeng, J., Liu, J. F., Wu, J., & Ngan, H. W. (2011). A multi-agent solution to energy management in hybrid renewable energy generation system. *Renewable Energy, 36*(5), 1352–1363.
11. Conti, S., & Raiti, S. (2007). Probabilistic load flow using Monte Carlo techniques for distribution networks with photovoltaic generators. *Solar Energy, 81*, 1473–1481.
12. Paparoditis, E., & Sapatinas, T. (2013). Short-term load forecasting: the similar shape functional time-series predictor. *IEEE Transactions on Power Systems, 28*(4), 3818–3825.
13. Xydas, E., Qadrdan, M., Marmaras, C., Cipcigan, L., Jenkins, N., & Ameli, H. (2017). Probabilistic wind power forecasting and its application in the scheduling of gas-fired generators. *Applied Energy, 192*, 382–394.
14. Sun, X., Luh, P. B., Michel, L. D., Corbo, S., Cheung, K. W., Guan, W., & Chung, K. (2013). An efficient approach for short-term substation load forecasting. *IEEE Power & Energy Society General Meeting*. https://doi.org/10.1109/PESMG.2013.6673009.
15. Hung, D. Q., Mithulananthan, N., & Bansal, R. C. (2014). Integration of PV and BES units in commercial distribution systems considering energy loss and voltage stability. *Applied Energy, 113*, 1162–1170.
16. Murata, A., Ohtake, H., & Oozeki, T. (2018). Modeling of uncertainty of solar irradiance forecasts on numerical weather predictions with the estimation of multiple confidence intervals. *Renewable Energy, 117*, 193–201.
17. Wolfs, P., Emami, K., Lin, Y., & Palmer, E. (2018). Load forecasting for diurnal management of community battery systems. *Journal of Modern Power System and Clean Energy, 6*(2), 215–222.
18. Rahbari-Asr, N., Zhang, Y., & Mo-Yuen, C. (2015). Consensus-based distributed scheduling for cooperative operation of distributed energy resources and storage devices in smart grids. *IET Generation, Transmission and Distribution, 10*(5), 1268–1277.

19. Zhao, T., & Ding, Z. (2018). Distributed agent consensus-based optimal resource management for microgrids. *IEEE Transactions on Sustainable Energy, 9*(1), 443–452.
20. Fortenbacher, P., Mathieu, J. L., & Andersson, G. (2017). Modeling and optimal operation of distributed battery storage in low voltage grids. *IEEE Transactions on Power Systems, 32*(6), 4340–4350.
21. Xu, Y. (2015). Optimal distributed charging rate control of plug-in electric vehicles for demand management. *IEEE Transactions on Power Systems, 30*(3), 1536–1545.
22. Xu, Y., Yang, Z., Gu, W., Li, M., & Deng, Z. (2017). Robust real-time distributed optimal control based energy management in a smart grid. *IEEE Transactions on Smart Grid, 8*(4), 1568–1579.
23. Morstyn, T., Hredzak, B., & Agelidis, V. G. (2018). Network topology independent multi-agent dynamic optimal power flow for microgrids with distributed energy storage systems. *IEEE Transactions on Smart Grid, 9*(4), 3419–3429.
24. Dimeas, A. L., & Hatziargyrious, N. D. (2005). Operation of multi agent system for micro grid control. *IEEE Transaction Power System, 20*(3), 1447–1445.
25. Dimeas, A. L., & Hatziargyriou, N. D. (2007, November). *Agent based control of virtual power plants*. Interference conference on intelligent systems applications to power systems. ISAP 2007, Toki Messe, Niigata.
26. McArthur, S. D. J., Davidson, E. M., Catterson, M. V., Dimeas, A. L., Ponci, F., Hatziargyriou, N. D., & Funabashi, T. (2007). Multi agent systems for power engineering applications –part I: Concepts, approaches and technical challenges. *IEEE Transaction on Power Systems, 22*(4), 1743–1752.
27. McArthur, S. D. J., Davidson, E. M., Catterson, V. M., Dimeas, A. L., Ponci, F., Hatziargyriou, N. D., & Funabashi, T. (2007). Multi agent systems for power engineering applications –part II: Technologies, standards and tools for building multi agent systems. *IEEE Transaction on Power Systems, 22*(4), 1753–1759.
28. Colson, C. M., Nehrir, M. H., & Gunderson, R. W. (2011, August–September). *Multi agent microgrid power management*. 18th IFAC World Congress, Milano.
29. Fakham, H., Doniec, A., Colas, F., & Guillaud, X. (2010). *A multi-agent system for a distributed power management of micro turbine generators connected to grid*. *IFAC Proceedings. 43*(1), 175–180.
30. Davidson, E. M., McArthur, S. D. J., McDonald, J. R., Cumming, T., & Watt, I. (2006). Applying multi-agent system technology in practice: Automated management and analysis of SCADA and digital fault recorder data. *IEEE Transaction on Power Systems, 21*(2), 559–566.
31. Huang, K., Srivastava, S. K., Cartes, D. A., & Sun, L. (2009). Market based multi-agent system for reconfiguration of shipboard power systems. *Electric Power Systems, 79*, 550–556.
32. Praca, I., Ramos, C., Vale, Z., & Corderio, M. (2003). MASCEM: A multi agent system that simulates competitive electricity markets. *IEEE Intelligent System, 18*(6), 54–60.
33. Karitov, V. S. (2004). Real-world market representation with agents. *IEEE Power Energy Magazine, 2*(4), 39–46.
34. Nagata, T., & Sasaki, H. (2002). A multi-agent approach to power system restoration. *IEEE Transaction Power System, 17*(2), 457–462.
35. McArthur, S. D. J., Strachan, S. M., & Jahn, G. (2004). The design of a multi-agent transformer condition monitoring system. *IEEE Transaction Power System, 19*(4), 1845–1852.
36. Mangina, E. E., McArthur, S. D. J., McDonald, J. R., & Moyes, A. (2001). A multi agent system for monitoring industrial gas turbine start-up sequences. *IEEE Transaction Power System, 16* (3), 396–401.
37. Buse, D. P., Sun, P., Wu, Q. H., & Fitch, J. (2003, March–April). Agent – Based substation automation. *IEEE Power Energy Magazine, 1*(2), 50–55.
38. Logenthiran, T., Srinivasan, D., & Khambadkone, A. M. (2011). Multi-agent system for energy resource scheduling of integrated microgrids in a distributed system. *Electrical Power System Research, 81*, 138–148.

39. Hossack, J., Menal, A. J., McArthur, S. D. J., & McDonald, J. R. (2003). A multi-agent architecture for protection engineering diagnostic assistance. *IEEE Transaction on Power System, 18*(2), 639–647.
40. Fax, J. A., & Murray, R. M. (2004). Information flow and cooperative control of vehicle formations. *IEEE Transactions Automatic Control, 49*, 1464–1476.
41. Reza, O.-S., Fax, J. A., & Murray, R. M. (2007). Consensus and cooperation in networked multi-agent systems. *Proceedings of the IEEE, 95*(1), 215–233.
42. Ren, W., & Beard, R. W. (2008). *Distributed consensus in multi-vehicle cooperative control: Theory and applications*. London: Springer.

Chapter 14
Robust Short-Term Scheduling of Smart Distribution Systems Considering Renewable Sources and Demand Response Programs

Mehrdad Ghahramani, Morteza Nazari-Heris, Kazem Zare, and Behnam Mohammadi-ivatloo

14.1 Introduction

The increasing growth in global energy consumption and environmental problems due to increased fossil fuel consumption has led to more interest in clean sources of energy [1]. On the other hand, the advancement of technology and reduction in the cost of carbon-free resources have accelerated the move toward usage of these technologies [2]. Among RESs, WT and solar energy have attracted more attention than other types of energy due to the uncertain nature and uncontrollability [3–5]. In addition, the potential and participation of consumers in DR programs are more advanced due to the movement of power networks to smart grids especially at the distribution level [6].

14.1.1 Problem Definition

The uncertain and uncontrollable nature of power system parameters increases the complexity and challenges of operation of SDSs and DSO such as loss of power balance, loss of reliability, and increase in operational costs. ODAS of SDSs is normally studied in short-term scheduling category. In this scheduling, 24-h prior to the implementation of the program, the production levels of different units, including WTs, DGs, and BESSs, and purchasing power from the upstream network should be

M. Ghahramani (✉) · M. Nazari-Heris · K. Zare · B. Mohammadi-ivatloo
Faculty of Electrical and Computer Engineering, University of Tabriz, Tabriz, Iran
e-mail: m.ghahramani94@ms.tabrizu.ac.ir; m.nazari@ieee.org; Kazem.zare@tabrizu.ac.ir; mohammadi@ieee.org

B. Mohammadi-ivatloo, M. Nazari-Heris (eds.), *Robust Optimal Planning and Operation of Electrical Energy Systems*,
https://doi.org/10.1007/978-3-030-04296-7_14

determined. Correct and continuous operation of these networks considering RESs requires optimal scheduling. This scheduling scheme should reduce operating costs and handles the uncertainty of input parameters such as the power price of upstream grid simultaneously.

14.1.2 Literature Review

Recently, remarkable efforts have been made in the area of proposing new and realistic models for optimal scheduling of distribution networks. In [7], a two-level optimization framework for SDS scheduling has been proposed that firstly focuses on purchasing power from market, while unit commitment of DGs and interactions with the real-time market are taken in the second phase of the proposed framework. The authors in [8] used an optimal power flow algorithm to minimize the overall cost of a SDS's performance. A fuzzy-based method is proposed to plan a SDS in [9], which aims to minimize operation costs on the one hand and minimize environmental pollution on the other. Although these studies help decision-makers to gain a general view of optimization issues, they cannot show the uncertainty in real-world strategic decisions. Also, considering the absence of precise forecasting methods, a deterministic optimization method is not appropriate for the ODAS of the SDSs. Time-of-use DRPs have been investigated in optimal bidding strategy of electrical energy retailers in [10]. The authors in this study have studied the impact of system flexibility in improving the generation dispatch and reducing electricity bills for the supply and demand sections, respectively. Various modeling approaches with different strategies for fixed and flexible loads in obtaining optimal dispatch of power networks have been compared in [11]. In addition, the utilization of energy storage units and their advantages in ancillary services have been discussed in the area of improving system reliability indexes and modifying the load profile [12].

Studies in ODAS of SDSs are mainly divided into two categories including deterministic studies and stochastic studies. In the field of deterministic studies, all the inputs of the problem are entered as known values, and the outputs are determined for a given time period. For example, in the deterministic scheduling of the SDS, regardless of the probabilistic nature of the predicted variables, the reservation required by the SDS is determined prior to the planning of energy. On the other hand, in stochastic studies, non-deterministic parameters can be estimated by specific probabilistic distribution functions (PDFs), and their general purpose is to optimize the expected value of an objective function. In [13], uncertain variables related to SDS operation are modeled by PDF, and the operation is accomplished based on probabilistic scenarios. In [14], the model presented in [7] has been developed so that the expected cost of network performance is minimized and the risk associated with the uncertainties in the problem is considered in this study. However, the stochastic model presented in this reference investigates energy planning without paying attention on RESs and the risk associated with their uncertainties. The authors in [15] presented a two-level stochastic optimization model for energy

and reserve planning of SDSs with the goal of minimizing the expected operating cost of the network. In [16], a two-level risk-based optimization model for SDS planning has been proposed that aims to minimize cost. The authors in [17] utilized a stochastic method for multi-objective ODAS, which aims to minimize the cost of performance and environmental pollution. In this study, consumer responsiveness is also considered as one of the sources of energy supply. The accuracy and optimality of random methods depend on the accuracy of the PDF of uncertain variables and the number of utilized scenarios in the optimization problem. The absence of proper historical data will result in an uncertain PDF of random variables and false results. In addition, with increasing in number of scenarios, the computational complexity of the optimization problem will greatly increase.

14.1.3 Novelties and Contributions

This chapter presents an optimization framework based on the concepts of robust optimization that can address the problems of both deterministic and stochastic methods. This method models random variables with uncertain PDFs and frees up the constraints. The solutions obtained from this method are safe against the worst conditions of uncertainty associated with power market price. Compared with stochastic optimization, the proposed method has several advantages. First, this method only requires the predicted values of the upper limit and the lower limit of random variables that are easier to obtain from historical data. Second, unlike stochastic methods that use probabilistic guarantees to satisfy constraints, the proposed method is followed by optimal solutions that are safe against all changes in random variables [18]. In this chapter, the SDS scheduling considering RESs is based on a mixed integer optimization. The proposed model defines the short-term operation of the network, including the amount of exchange with the upstream network and the generation of distributed resources including WTs, BESSs, and DGs. In addition through this chapter, the participation of responsive loads in network operation and their effects in minimizing the cost of network operation are studied. In addition, in order to provide a model for SDSs, the presence of DGs and RESs including WTs and BESSs, as well as DR programs, are provided in the 33-bus network. The purpose of the proposed method is to minimize the operational cost of the SDS with respect to the predicted values of upstream grid power cost. The energy and reserve scheduling of the next day should remain reliable through changing the uncertain variables of the network.

14.1.4 Chapter Organization

In Sect. 14.2, mathematical modeling including objective function and problem constraints is presented. In addition, RO method for modeling uncertainty is presented in this section. Information about the sample network is provided in Sect. 14.3.

The statistical results and charts related to the achievements of the problem are presented in Sect. 14.4. A summary of the work is presented in Sect. 14.5.

14.2 Mathematical Modeling

In this section, a complete mathematical formulation for ODAS of the smart SDS, including objective function and problem constraints, is presented. Also, modeling for RESs including WTs, DR programs, and BESSs is presented in this section.

14.2.1 The Objective Function

Energy and reserve scheduling for SDSs takes place by DSO, with the goal of minimizing the network operating costs over a 24-h period:

$$\begin{aligned}\text{Min}: &\sum_{t=1}^{24}\left\{P_{\text{grid}}(t)\times\lambda_g^E(t)\right\}\\ &+\sum_{j=1}^{N_{DG}}\left\{CE_{DG}(j,t)+CS_{DG}(j,t)+CR_{DG}(j,t)\right\}\\ &+\sum_{d=1}^{N_{\text{DRP}}}\left\{CE_{DRP}(d,t)+CR_{DRP}(d,t)\right\}\\ &+\sum_{i=1}^{N_{IL}}\left\{CE_{LL}(i,t)+CR_{LL}(i,t)\right\}\end{aligned} \tag{14.1}$$

The proposed objective function consists of four terms. The first term is the cost of supplying power and exchange with the upstream network, which is modeled as a multiplication of the hourly power purchased from the upstream network (P_{grid}) at the hourly power of the upstream network (λ_g^E). The second term refers to the costs of the DG units, including the cost of operation (CE_{DG}), the start-up cost (CS_{DG}), and the cost of the reservation provided by these units (CR_{DG}), which are subsequently introduced by Eqs. (14.6), (14.7), and (14.8), respectively. The third term relates to the cost of the DR providers, including energy costs (CE_{DRP}) and the cost of reservation (CR_{DRP}), which are introduced by Eqs. (14.24) and (14.26), respectively. The fourth term is the cost of the participation of industrial loads in DR programs including the cost of energy provision (CE_{LL}) and the cost of providing the reservation (CR_{LL}) by these units, which are modeled using Eqs. (14.28) and (14.29), respectively. The index $t = 1, \ldots, N_T$ denotes the time, the index $j = 1, \ldots, N_{DG}$ represents the DG units, the index $d = 1, \ldots, N_{DRP}$ for the DRPs, and the index $i = 1, \ldots, N_{IL}$ for the large industrial loads.

14.2.2 Constraints

The constraints associated with the ODAS of SDS including equal and unequal constraints are represented in this section.

14.2.2.1 Distribution Network Constraints

In order to ensure the safe and proper operation of the distribution network, constraints (14.2) and (14.3) are provided [19]. Equation (14.2) ensures that the voltage remains acceptable. The current range is also considered by (14.3):

$$V_{\min}(n) \le v(n,t) \le V_{\max}(n) \quad \forall n,t \tag{14.2}$$

$$I(m,n,t) \le I_{\max}(m,n) \quad \forall m,n,t \tag{14.3}$$

where $V_{\min}$, $V_{\max}$, and v are the minimum, maximum, and hourly values of the bus voltages. Also, $I_{\max}$ and I are the maximum tolerable current and the hourly current of the feeder between the m and n buses, respectively.

14.2.2.2 Active and Reactive Power Balance Constraints

Reliable operation of distribution networks can be obtained by continues balance of generated power and power load demand of the network [20]. Accordingly, the following constraints should be considered for load balance at bus n at time t:

$$\begin{aligned} &P_{ug}(t) + \sum_{j\in n} P_{DG}(j,t) + \sum_{w\in n} P_{\text{Wind}}(w,t) - P_{ch}(t) + P_{dis}(t) + \sum_{i\in n} P_{LL}(i,t) \\ &+ \sum_{d\in n} P_{DRA}(d,t) - P_{\text{load}}(n,t) = V_n \sum_{n} V_{n,t}(G_{nm}\cos\delta_{n,t} + B_{nm}\sin\delta_{m,t}) \end{aligned} \tag{14.4}$$

$$\begin{aligned} &Q_{ug}(t) + \sum_{j\in n} Q_{DG}(j,t) + \sum_{w\in n} Q_{\text{Wind}}(w,t) + \sum_{d\in n} Q_{DRA}(d,t) + \sum_{i\in n} Q_{LL}(i,t) \\ &- Q_{\text{load}}(n,t) = V_{n,t} \sum_{n} V_{n,t}(G_{nm}\cos\delta_{n,t} - B_{nm}\sin\delta_{m,t}) \end{aligned} \tag{14.5}$$

where P_{Load} and Q_{Load} are the respective indicators for active and reactive power. The active and reactive power generation of each DG unit are defined by P_{DG} and Q_{DG}, respectively. P_{Wind} and Q_{Wind} are the respective active and reactive power generation of WTs. The active power charge/discharge of the storage unit is P_{ug} and P_{dis}. The reactive power charge/discharge of the storage unit is Q_{ug} and Q_{dis}. The active/reactive power reduced by large industrial load is P_{LL} and Q_{LL}. The active/reactive power reduced by DR aggregator is P_{DRA} and Q_{DRA}.

14.2.2.3 DG Units Constraints

The constraints of DG units are presented through (14.6, 14.7, 14.8, 14.9, 14.10, 14.11, 14.12, 14.13, and 14.14) [21]. The operation cost of the DG units is considered as a quadratic function of the power generated by such units, which can be stated as follows:

$$CE_{DG}(j,t) = a_j + b_j \times P_{DG}(j,t) + c_j \times {P_{DG}}^2(j,t) \quad \forall j,t \tag{14.6}$$

where the cost coefficients of the DG unit are indicated by a_j, b_j, and c_j. The start-up cost of DG units is taken into account in this study, which can be formulated as:

$$CS_{DG}(j,t) = SUC(j) \times (u(j,t) - u(j,t-1)); \qquad CS_{DG}(j,t) \geq 0; \quad \forall j,t \tag{14.7}$$

where u is a binary variable used to define the operation of DG units. The cost of providing required reserve of the network by DG units is considered as 20% of marginal price of DG units:

$$CR_{DG}(j,t) = 0.2 \times \left(b_j + 2 \times c_j \times {P_{DG}}^{\max}(j,t)\right) \quad \forall j,t \tag{14.8}$$

The power generation limits of the DG units should be considered in the scheduling of such units. Such constraint should be studied for both power and reserve scheduling of DG units, which can be stated as follows:

$${P_{DG}}^{\min}(j) \times u(j,t) \leq P_{DG}(j,t) \leq {P_{DG}}^{\max}(j) \times u(j,t) \quad \forall j,t \tag{14.9}$$

$$P_{DG}(j,t) + R_{DG}(j,t) \leq {P_{DG}}^{\max}(j) \times u(j,t) \quad \forall j,t \tag{14.10}$$

Equation (14.11) defines that the sum of power and reserve generated by DG units should be limited to maximum generation of such units. The ramp-up/ramp-down limits of the DG units can be studied using the following equations:

$$\begin{aligned} &P_{DG}(j,t) - P_{DG}(j,t-1) \leq \\ &UR(j) \times (1 - y(j,t)) + {P_{DG}}^{\min}(j) \times y(j,t) \quad \forall j,t \end{aligned} \tag{14.11}$$

$$\begin{aligned} &P_{DG}(j,t-1) - P_{DG}(j,t) \leq \\ &DR(j) \times (1 - z(j,t)) + {P_{DG}}^{\min}(j) \times z(j,t) \quad \forall j,t \end{aligned} \tag{14.12}$$

where the ramp-up/ramp-down limits of the DG units are defined by $UR(j)$ and $DR(j)$. The minimum up/down time of DG units should be considered in the scheduling of units, which can be formulated as follows:

$$\sum_{h=t}^{t+UT(j)-1} u(j,h) \geq UT(j) \times y(j,t) \quad \forall j,t \tag{14.13}$$

$$\sum_{h=t}^{t+DT(j)-1} \left(1 - u(j,h) \geq DT(j) \times z(j,t) \quad \forall j,t \right. \tag{14.14}$$

where the respective indicators of minimum up/down time of DG units are $UT(j)$ and $DT(j)$.

14.2.2.4 Wind Turbine Modeling

The power output of WTs is considered as a function of wind speed, which is formulated as (14.15) [22]:

$$P_{wind}(t) = \begin{cases} P_r \times \dfrac{(v(t) - v_{ci})}{(v_r - v_{ci})} & v_{ci} \leq v(t) \leq v_r \\ P_r & v_r \leq v(t) \leq v_{co} \\ 0 & \text{otherwise} \end{cases} \tag{14.15}$$

where $V(t)$ is wind speed, V_{ci} is cut-in speed, V_{co} is cut-out speed, and V_r is the rated speed of WT.

14.2.2.5 Modeling Battery Energy Storage System

Energy storage technology is studied in the proposed model for charging power at off-peak hours and recharging it at on-peak hours [23]. The energy balance of the storage unit is as follows:

$$SOC(b,t) = SOC(b,t-1) + \eta^{ch} \times P_{ch}(b,t) - \eta^{dis} \times P_{dis}(b,t) \tag{14.16}$$

where SOC is the energy storage at the storage unit. The charge/discharge efficiencies of the storage units are defined by η^{ch}/η^{dis}. The energy charged in the storage unit should be limited to its minimum and maximum values as follows:

$$\underline{SOC(b)} \leq SOC(b,t) \leq \overline{SOC(b)} \tag{14.17}$$

where the minimum and maximum energy stored in the storage unit is defined by $\underline{SOC}/\overline{SOC}$. The power charge/discharge of the storage units should be limited to its lower and upper limitations as Eqs. (14.18) and (14.19):

$$0 \leq P_{ch}(b,t) \leq \overline{P_{ch}} \times bs_c(b,t) \tag{14.18}$$

$$0 \le P_{\text{dis}}(b,t) \le \overline{P_{\text{dis}}} \times bs_d(b,t) \tag{14.19}$$

$$bs_c(b,t) + bs_d(b,t) \le 1; \quad bs_c, bs_d \in \{0,1\}, \forall t \tag{14.20}$$

Equation (14.20) is used to limit the operation of storage unit in one of the charge/discharge/idle modes.

14.2.2.6 Modeling Demand Response Programs

In this chapter, consumers have been involved in DR programs in two ways. In the first way, in order to create a position for the participation of home-grown consumers or small-scale commercial and industrial consumers, two DR aggregators have been utilized. Aggregated entities examine the possibility of customer participation in DR programs, and after aggregating and integrating the responses of consumers, it is possible to connect these with the wholesale market [24]. The cost of this DR program is modeled by (14.21, 14.22, 14.23, and 14.24):

$$O^d_{\min} \le o^d_1 \le O^d_1 \tag{14.21}$$

$$0 \le o^d_k \le \left(o^d_{k+1} - o^d_k\right) \forall k = 2, 3, \ldots, k \tag{14.22}$$

$$P_{DRA}(d,t) = \sum_k o^d_k \tag{14.23}$$

$$CE_{DRA}(d,t) = \sum_k \pi^d_k \times o^d_k \tag{14.24}$$

Equation (14.21) limits the acceptance value of the load reduction by the aggregator d (o^d_1) between the minimum of decreasing value ($O^d_{\min}$) and the proposed load reduction by aggregator (O^d_1) in step 1. According to (14.22), in the other steps, the proposed acceptance of the aggregator can be between zero and proposed load reduction in the related steps. According to (14.23), the sum of the power reduced by the aggregator d at hour t (P_{DRA}) is equal to the sum of all accepted reductions in that hour. Also, the cost of reducing the load through the aggregator is calculated by (14.24), which is equal to the product of the energy reduction cost (π^d_k) in the accepted demand reduction of consumer d.

Load reduction which is not accepted by the aggregators can be utilized in reserve scheduling. In accordance with (14.25), the total amount of energy (P_{DRA}) and scheduled reserve (R_{DRA}) by decreasing the load should be limited to the maximum proposition of aggregators ($P^{\max}{}_{DRA}$). In addition, the cost of providing reserve by aggregator entities is calculated by (14.26). (KR_{DRA}) is the cost of each reservation unit provided by the aggregators:

$$P_{DRA}(d,t) + R_{DRA}(d,t) \le P^{\max}{}_{DRA}(d,t) \tag{14.25}$$

$$CR_{DRA}(d,t) = R_{DRA}(d,t) \times KR_{DRA}(d,t) \tag{14.26}$$

The second type of DR programs which are used in this chapter is related to load reduction by large individual consumers. The power and reserve scheduling through large consumers is restricted by (14.27), and the energy and reserve costs are divided from (14.28) and (14.29):

$$P_{LL}(i,t) + R_{LL}(i,t) \leq P^{\max}{}_{LL}(i,t) \tag{14.27}$$

$$CE_{LL}(i,t) = P_{LL}(i,t) \times KE_{LL}(i,t) \tag{14.28}$$

$$CR_{LL}(i,t) = R_{LL}(i,t) \times KR_{LL}(i,t) \tag{14.29}$$

In accordance with (14.27), the sum of the energy (P_{LL}) and the reserve (R_{LL}) of large industrial loads should be lower than the maximum amount of energy that can be reduced ($P^{\max}{}_{LL}$). Equation (14.28) states that the cost of reducing the energy by large consumers (CE_{LL}) is equal to the product of reduced energy (P_{LL}) at the cost of each unit of power reduction (KE_{LL}). Equation (14.29) states that the cost of providing required reserve by large consumers (CR_{IL}) is equal to the cost of the intended reservation (R_{LL}) at the intended cost for each unit of reserve scheduling (KR_{LL}).

14.2.3 The Proposed Robust Method

The robust optimization (RO) was firstly proposed by Soyster in 1973 to deal with uncertainties associated with power system parameters [25]. The RO is effective in solving the problems with a series of uncertain parameters specially when there is incomplete information on the uncertain parameters [26]. In this study, the price of power purchased from the upstream grid is considered uncertainty, which is handled using RO method. The objective function of the studied problem in (14.1), which is deterministic, can be updated as follows considering the uncertainty of price of power purchased from the upstream grid [27]:

$$\begin{aligned}
&\text{Min}: \sum_{j=1}^{N_{DG}} \{CE_{DG}(j,t) + CS_{DG}(j,t) + CR_{DG}(j,t)\} \\
&+\sum_{d=1}^{N_{DRP}} \left\{CE_{DRP}(d,t) + CR_{DRP}(d,t)\right\} + \sum_{i=1}^{N_{IL}} \left\{CE_{IL}(i,t) + CR_{IL}(i,t)\right\} \\
&+\min \quad \max \sum_{t=1}^{24} \left\{P_{\text{grid}}(t) \times \lambda_g^{RO,E}(t)\right\}
\end{aligned} \tag{14.30}$$

where $\lambda_g^{RO,E}(t)$ is the uncertain price of upstream grid. The second term of objective function should be considered in solving the problem using the dual process.

The power price is the sum of the forecasted price and deviation of price with respect to the forecasted value:

$$\begin{aligned}
&\max \sum_{t=1}^{24}\left\{P_{\text{grid}}(t)\times(1+z^t)\lambda_g^{\text{forecasted},E}(t)\right\}\\
&\text{subject to}\\
&z^t\le 1 \quad :\zeta^t\\
&\sum_{t=1}^{24} z^t\le \Gamma \quad :\beta\\
&z^t\ge 0
\end{aligned} \tag{14.31}$$

where β and ζ^t are dual variables of the problem. Γ is the robust level. The Karush Kuhn Tucker (KKT) condition can be utilized to providing the robust formulation. Accordingly, the objective function of the problem can be updated as follows:

$$\begin{aligned}
&\text{Min}: \Gamma\beta+\sum_{t=1}^{24}\zeta^t+\sum_{t=1}^{24}\left\{P_{\text{grid}}(t)\times\lambda_g^{\text{forecasted},E}(t)\right\}\\
&+\sum_{j=1}^{N_{DG}}\{CE_{DG}(j,t)+CS_{DG}(j,t)+CR_{DG}(j,t)\}\\
&+\sum_{d=1}^{N_{DRP}}\left\{CE_{DRP}(d,t)+CR_{DRP}\left(d,t\right)\right\}+\sum_{i=1}^{N_{IL}}\left\{CE_{IL}(i,t)+CR_{IL}\left(i,t\right)\right\}\\
&\text{Constraints (14.2)}-\text{(14.29)}\\
&\zeta^t+\beta\ge \text{dev}\times\lambda_g^{\text{forecasted},E}(t)\times P_{\text{grid}}(t)\\
&\zeta^t\ge 0\\
&\beta\ge 0
\end{aligned} \tag{14.32}$$

14.3 Case Study

In this chapter, the IEEE 33-bus standard network has been used to examine the effectiveness of the proposed method. Based on the results of [28], DG units are connected to the appropriate buses. Three WTs are used in this network, connected to the buses 13, 15, and 30. The rated power of WTs is 3 MW, and the cut-in, cut-out, and rated speed of these turbines are 3, 25, and 13 m/s, respectively. The prediction of wind speed over the next 24 h is shown in Fig. 14.1 [29].

Also, in the distribution network, there are four diesel generators that are connected to the buses 8, 13, 16, and 25. The coefficients for the cost of these generators and the information of the maximum and minimum power, the rate of

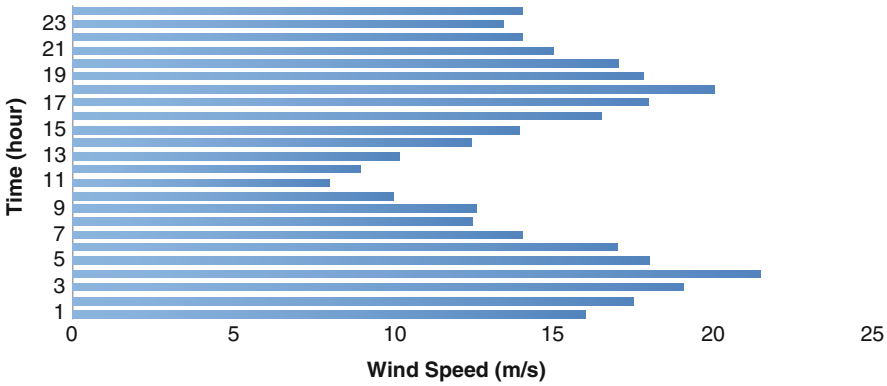

Fig. 14.1 Wind speed predicted for the next 24 h

Table 14.1 Information of DG's cost coefficients

Cost coefficients			
Units	a_i ($)	b_i ($/MWh)	c_i ($/MWh^2)
DG1	33	87	0.0025
DG2	25	87	0.0025
DG3	28	92	0.0035
DG4	26	81	0.184

power increase and power decrease, and the minimum up time and minimum down time are given in Tables 14.1 and 14.2 [30]. Also, the prediction of the hourly load during the day-ahead is shown in Fig. 14.2 [31]. Also, the 33-bus network is shown in Fig. 14.3 [32].

Also, the hourly forecast for the wholesale electricity price is assumed for day-ahead as shown in Fig. 14.4.

The battery power system with a capacity of 0.5 MW is connected to the bus 21. The minimum and maximum capacity of the energy storage system is 20% and 80% of its nominal capacity. The maximum charge and discharge rates for each hour are equal to 0.1 MW.

14.4 Results

The proposed model provides an optimal energy and reserve scheduling for distributed resources and DR programs in the studied network. Also, in order to demonstrate the effect of DR programs on the economic performance of the network, a robust ODAS has been carried out in two modes of presence and absence of DR programs, and the results have been compared.

Table 14.2 Information of the DG's technical data

Technical data					
Units	SUT ($)	MUT/MDT (h)	RU/ RD (MW/h)	Pmax (MW)	Pmin (MW)
DG1	15	2	1.8	3.5	1
DG2	25	1	1.5	3	0.75
DG3	28	1	1.5	3	0.75
DG4	26	2	1.8	4.1	1

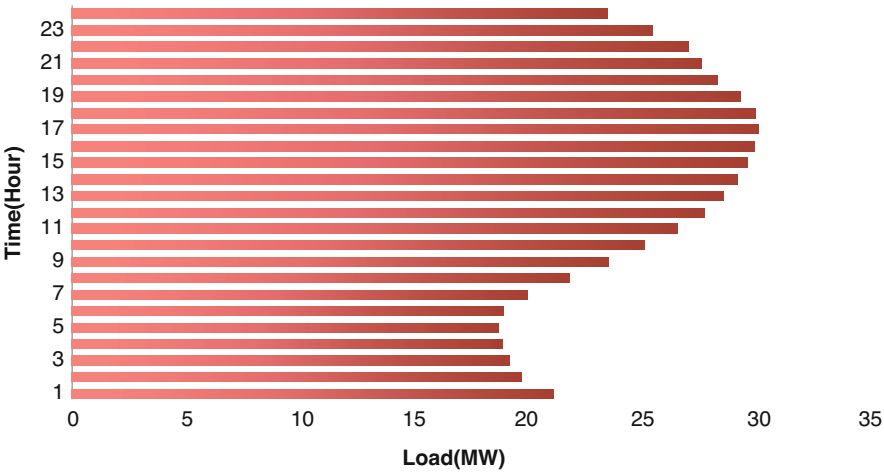

Fig. 14.2 Estimated hourly load for next 24 h

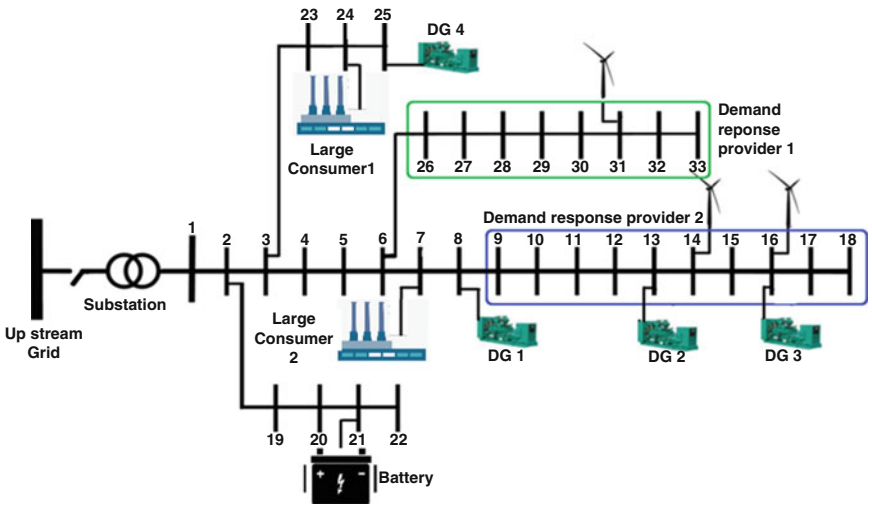

Fig. 14.3 IEEE 33-bus distribution network

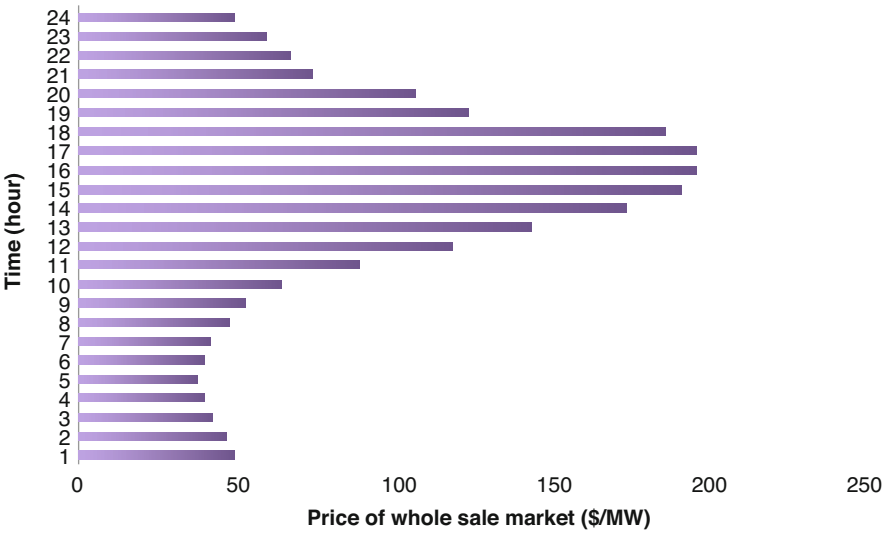

Fig. 14.4 The wholesale market price forecast for the next 24 h

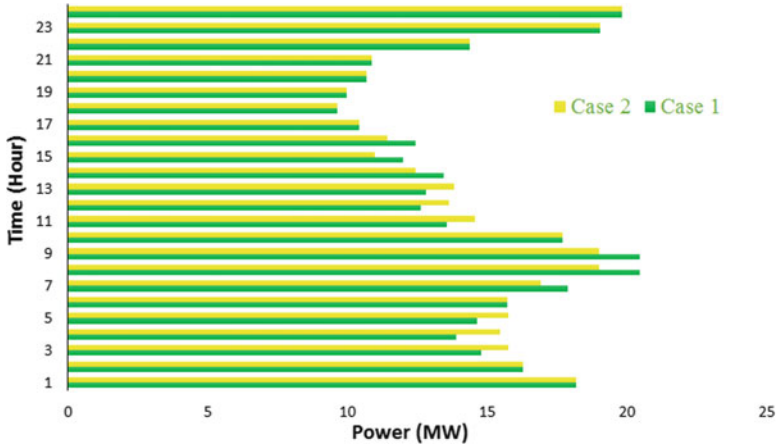

Fig. 14.5 Power scheduled to purchase from the upstream network in the next 24 h

14.4.1 First Mode (Absence of Demand Response Programs)

As seen in Fig. 14.5, during the hours when the energy price of the upstream grid is low, especially at $t = 24$ h and during the hours from 1 to 9, the required energy is purchased from the upstream grid. Also, at hours when the energy prices of DG units are lower than the wholesale market, especially during the hours from 10 to 24, the energy purchased from the upstream network is reduced. The scheduling done in this

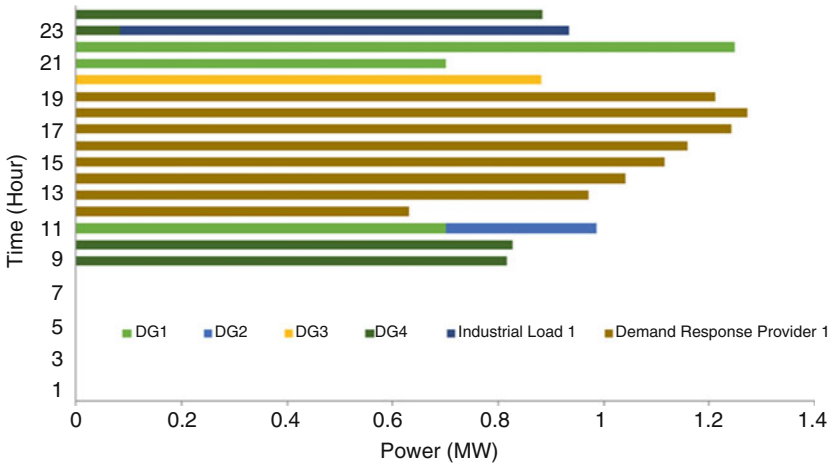

Fig. 14.6 Reservation scheduled to provide by DGs and DR programs in the next 24 h

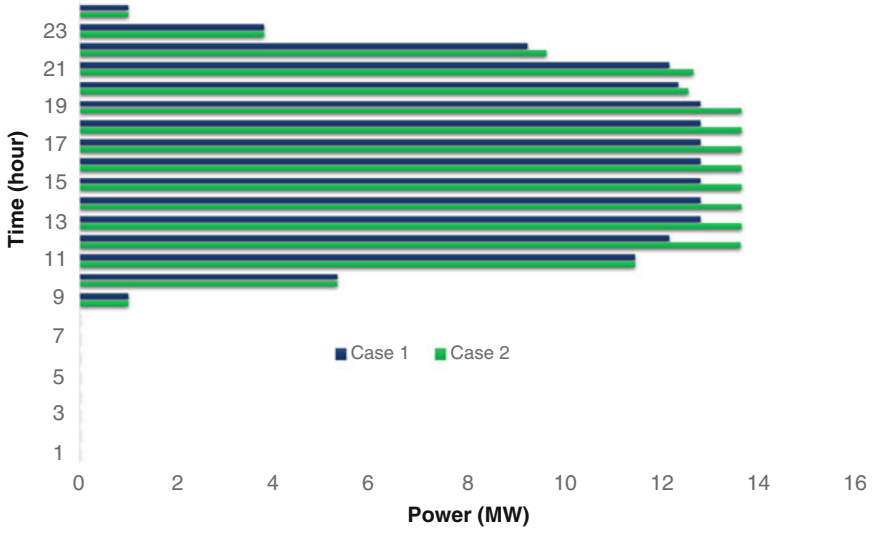

Fig. 14.7 The power scheduled to generate by DG units in the next 24 h

chapter tends to reduce the functional costs of the distribution network, and the results are more economical. As shown in Figs. 14.6 and 14.7, in the absence of DR programs, all reservations required for the distribution network are provided by DG units. It is also evident that one or more of DG units should be in standby mode at peak hours, especially times 14–21 in order to provide the required reserve capacity. Also, during the hours from 10 to 23, where the price of the wholesale market is high, it is the best time to sell the energy of the DG units, but the need to provide the required reserve would force the distribution network operator to buy energy from

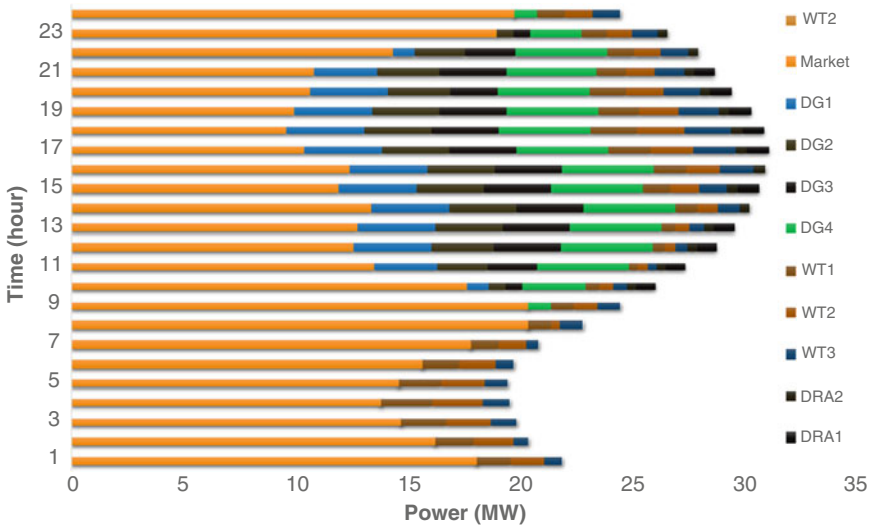

Fig. 14.8 Energy scheduled to provide by all instruments in the next 24 h

the upstream network at a higher price in the absence of DR programs. Also, at $t = 1$–9 and $t = 24$ h, when the energy price of the wholesale market is low, providing the required reserve, forces a number of DG units to remain at standby at a higher cost. As can be seen, the cost of providing reserve is increased and the operational costs of the distributed network increase.

14.4.2 Second Mode (Presence of Demand Response Programs)

In the second case, in order to demonstrate the effectiveness of DR programs, the ODAS of the SDS is taken place considering DR programs. As shown in Fig. 14.5, during the hours from $t = 10$ to $t = 23$ h, when the network upstream price is high, the reduction in consumption is taken place using DR programs by the distribution network operator. Also, the results of network reserve scheduling that is provided by DG units, DR providers, and large-scale consumer are presented in Fig. 14.6. It is also shown in Fig. 14.6 that the network DR programs meet the required reserve, and therefore as can be seen in Fig. 14.7 in case 2, DG capacity is freed up and can be fully utilized to supply the network's energy. Thus, considering load response programs, as can be seen in Figs. 14.7 and 14.8, DGs does not occupy the capacity of the DG units and can fully participate in providing the required demand of network at a lower cost.

The operation of WTs has no cost, and therefore the WTs are working in their maximum capacity of power production in both cases as can be seen in Fig. 14.9.

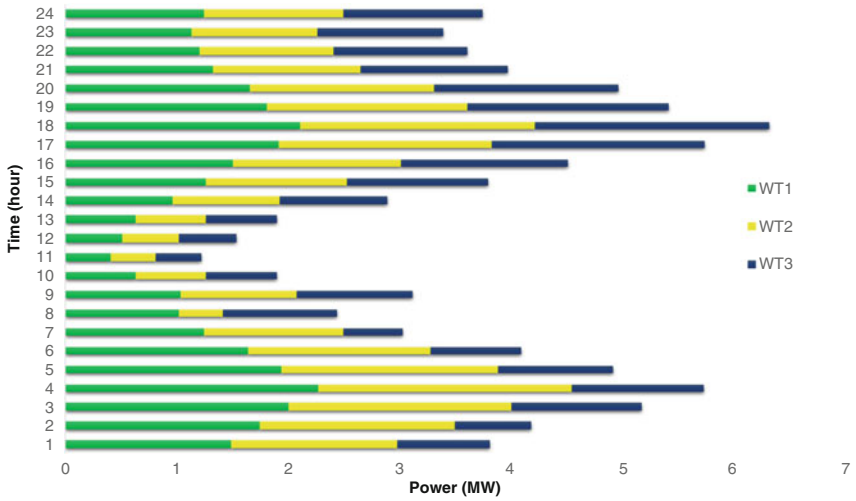

Fig. 14.9 Energy scheduled to provide by WTs in the next 24 h

14.5 Conclusions

The optimal scheduling of distribution networks considering renewable resources and DR programs has attracted much attention in recent years. In this chapter, the effect of the application of DR programs along with the presence of nonrenewable and distributed sources on optimal operation of distribution networks has been investigated. Also, a robust optimization method is used in this chapter for considering price uncertainties. This method ensures that the results will remain optimal for the worst uncertainty conditions. An IEEE 33-bus distribution network has been used to evaluate the performance of the proposed method. It also can be seen from the results that in high-priced hours, purchases from the wholesale market are reduced, and the BESS, distributed generation sources, and DR programs provide the required energy of distribution network. It can also be seen that the proposed model has the ability of ODAS of SDS. In addition, it can be seen that application of DR programs reduces the cost of network operation.

References

1. Saber, A. Y., & Venayagamoorthy, G. K. (2011). Plug-in vehicles and renewable energy sources for cost and emission reductions. *IEEE Transactions on Industrial Electronics, 58*(4), 1229–1238.
2. Zhang, N., et al. (2016). Unit commitment model in smart grid environment considering carbon emissions trading. *IEEE Transactions on Smart Grid, 7*(1), 420–427.
3. Milligan, M., et al. (2015). Alternatives no more: Wind and solar power are mainstays of a clean, reliable, affordable grid. *IEEE Power and Energy Magazine, 13*(6), 78–87.

4. Wandhare, R. G., & Agarwal, V. (2015). Novel integration of a PV-wind energy system with enhanced efficiency. *IEEE Transactions on Power Electronics, 30*(7), 3638–3649.
5. Liu, C., et al. (2016). Fuzzy energy and reserve co-optimization with high penetration of renewable energy. *IEEE Transactions on Sustainable Energy, 8*(2), 782–791.
6. Alipour, M., Mohammadi-Ivatloo, B., & Zare, K. (2014). Stochastic risk-constrained short-term scheduling of industrial cogeneration systems considering demand response programs. *Applied Energy, 136*, 393–404.
7. Algarni, A. A. S., & Bhattacharya, K. (2009). A generic operations framework for discos in retail electricity markets. *IEEE Transactions on Power Apparatus and Systems, 24*(1), 356–367.
8. Cecati, C., Citro, C., & Siano, P. (2011). Smart operation of wind turbines and diesel generators according to economic criteria. *IEEE Transactions on Industrial Electronics, 58*(10), 4514–4525.
9. Chakraborty, S., Ito, T., Senjyu, T., & Saber, A. Y. (2013). Intelligent economic operation of smart-grid facilitating fuzzy advanced quantum evolutionary method. *IEEE Transactions on Sustainable Energy, 4*(4), 905–916.
10. Nojavan, S., Mohammadi-Ivatloo, B., & Zare, K. (2015). Optimal bidding strategy of electricity retailers using robust optimisation approach considering time-of-use rate demand response programs under market price uncertainties. *IET Generation, Transmission & Distribution, 9* (4), 328–338.
11. Neves, D., Pina, A., & Silva, C. A. (2015). Demand response modeling: A comparison between tools. *Applied Energy, 146*, 288–297.
12. Zhou, Y., Mancarella, P., & Mutale, J. (2015). Modelling and assessment of the contribution of demand response and electrical energy storage to adequacy of supply. *Sustainable Energy, Grids and Networks, 3*, 12–23.
13. Zakariazadeh, A., Jadid, S., & Siano, P. (2014). Stochastic operational scheduling of smart distribution system considering wind generation and demand response programs. *International Journal Electrical Power Energy System, 63*, 218–225.
14. Safdarian, A., Fotuhi-Firuzabad, M., & Lehtonen, M. (2013). A stochastic framework for short-term 597 operation of a distribution company. *IEEE Transactions on Power Apparatus and Systems, 28*(4), 4712–4721.
15. Nojavan, S., Jalali, M., & Zare, K. (2014). Optimal allocation of capacitors in radial/mesh distribution systems using mixed integer nonlinear programming approach. *Electric Power Systems Research, 107*, 119–124.
16. Zakariazadeh, A., Jadid, S., & Siano, P. (2014). Stochastic multi-objective operational planning of smart distribution systems considering demand response programs. *Electric Power Systems Research, 111*, 156–168.
17. Zakariazadeh, A., Jadid, S., & Siano, P. (2014). Economic-environmental energy and reserve scheduling of smart distribution systems: A multi-objective mathematical programming approach. *International Journal Energy Conversion Management, 78*, 151–164. 601.
18. Nazari-Heris, M., Madadi, S., & Mohammadi-Ivatloo, B. (2018). Optimal management of hydrothermal-based micro-grids employing robust optimization method. In *Classical and recent aspects of power system optimization* (pp. 407–420). Elsevier, London, United Kingdom
19. Paudyal, S., Cañizares, C. A., & Bhattacharya, K. (2011). Optimal operation of distribution feeders in smart grids. *IEEE Transactions on Industrial Electronics, 58*(10), 4495–4503.
20. Kekatos, V., Wang, G., Conejo, A. J., & Giannakis, G. B. (2015). Stochastic reactive power management in microgrids with renewables. *IEEE Transactions on Power Systems, 30*(6), 3386–3395.
21. Bahramirad, S., Reder, W., & Khodaei, A. (2012). Reliability-constrained optimal sizing of energy storage system in a microgrid. *IEEE Transactions on Smart Grid, 3*(4), 2056–2062.
22. Ghahramani, M., Nazari Heris, M., Zare, K., & Mohammadi Ivatloo, B. (2016). Incorporation of demand response programs and wind turbines in optimal scheduling of smart distribution networks: A case study. *International Journal of Smart Electrical Engineering, 05*(04), 199–206. IJSEE-1705-1043.

23. Majidi, M., Nojavan, S., Esfetanaj, N. N., Najafi-Ghalelou, A., & Zare, K. (2017). A multi-objective model for optimal operation of a battery/PV/fuel cell/grid hybrid energy system using weighted sum technique and fuzzy satisfying approach considering responsible load management. *Solar Energy, 144*, 79–89.
24. Nojavan, S., Majidi, M., Najafi-Ghalelou, A., Ghahramani, M., & Zare, K. (2017). A cost-emission model for fuel cell/PV/battery hybrid energy system considering demand response program: ε-constraint method and fuzzy satisfying approach. *Energy Conversion and Management, 138*, 383–392.
25. Soyster, A. L. (1973). Convex programming with set-inclusive constraints and applications to inexact linear programming. *Journal of Operations Research, 21*(2), 1154e7.
26. Nazari-Heris, M., Mohammadi-Ivatloo, B., Gharehpetian, G. B., & Shahidehpour, M. (2018). Robust short-term scheduling of integrated heat and power microgrids. *IEEE Systems Journal, PP*(99), 1–9.
27. Nazari-Heris, M., & Mohammadi-Ivatloo, B. (2018). Application of robust optimization method to power system problems. In *Classical and recent aspects of power system optimization* (pp. 19–32). Elsevier, London, United Kingdom
28. Wong, S., Bhattacharya, K., & Fuller, J. D. (2009). Electric power distribution system design and planning in a deregulated environment. *IET Generation, Transmission & Distribution, 3* (12), 1061.
29. Willy Online Pty Ltd, online available at: http://wind.willyweather.com.au/
30. Diesel generators specification sheets, Kohler Power Systems Company, online available at: http://www.yestramski.com/industrial/generatorsdiesel/industrial-diesel-generators-all.htm
31. New York Independent System Operator. (2013, July 18). Online available at: http://www.nyiso.com/public/markets_operations/index.jsp
32. Baran, M. E., & Wu, F. F. (1989). Optimal capacitor placement on radial distribution systems. *IEEE Transactions on Power Delivery, 4*(1), 725–734.

Chapter 15
Risk-Based Performance of Multi-carrier Energy Systems: Robust Optimization Framework

Majid Majidi, Sayyad Nojavan, and Kazem Zare

Nomenclature

Indices	
t	Index of time horizon
Variables	
Cost	Total operation cost of multi-carrier energy system
$C_t^{st,e}$	Available stored energy level of electrical storage
$C_t^{st,h}$	Available stored energy level of thermal storage
g_t^{CHP}	Consumed gas by CHP unit
g_t^{B}	Consumed gas by boiler
g_t^{net}	Total injected gas to hub energy system
$I_t^{ch,e}$,$I_t^{dis,e}$	Charging/discharging condition binary variables of electrical storage
$I_t^{ch,h}$,$I_t^{dis,h}$	Charging/discharging condition binary variables of thermal storage
p_t^{e}	Total power procurement of hub energy system
$p_t^{ch,e}$,$p_t^{dis,e}$	Charging/discharging power of electrical storage
$p_t^{ch,h}$,$p_t^{dis,h}$	Charging/discharging heat of thermal storage
$p_t^{loss,e}$	Loss of power in electrical storage
$p_t^{loss,h}$	Loss of heat in thermal storage
p_t^{wi}	Produced power by wind unit
wa_t^{net}	Total water procurement of hub energy system
x_t	Decision variable in the standard MIP problem
z_0,q_{ot}	Dual variables of standard MIP problem

(continued)

M. Majidi (✉) · K. Zare
Faculty of Electrical and Computer Engineering, University of Tabriz, Tabriz, Iran
e-mail: majidmajidi95@ms.tabrizu.ac.ir; kazem.zare@tabrizu.ac.ir

S. Nojavan
Department of Electrical Engineering, University of Bonab, Bonab, Iran
e-mail: sayyad.nojavan@bonabu.ac.ir

B. Mohammadi-ivatloo, M. Nazari-Heris (eds.), *Robust Optimal Planning and Operation of Electrical Energy Systems*,
https://doi.org/10.1007/978-3-030-04296-7_15

Parameters	
η_{ee}^{T}	Efficiency of net transformer
η_{ge}^{CHP}	Gas to electric efficiency of CHP unit
η_{ee}^{CON}	Efficiency of wind turbine converter
$\eta_{ch}^{e},\eta_{dis}^{e}$	Charge and discharge efficiency of electrical storage
$\eta_{ch}^{h},\eta_{dis}^{h}$	Charge and discharge efficiency of thermal storage
$\alpha_{\min}^{e},\alpha_{\max}^{e}$	Minimum/maximum charging/discharging coefficients of electrical storage
$\alpha_{\min}^{h},\alpha_{\max}^{h}$	Minimum/maximum charging/discharging coefficients of thermal storage
α_{loss}^{e}	Coefficient modeling loss of power in electrical storage
α_{loss}^{h}	Coefficient modeling loss of power in thermal storage
a_{mt},b_{m}	Constraints coefficients in the standard MIP problem
A^{NET}	Upstream network availability value
A^{CHP}	CHP unit availability value
A^{WIND}	Wind turbine availability value
$C_{c}^{st,e}$	Nominal predefined capacity of stored energy in electrical storage
$C_{c}^{st,h}$	Nominal predefined capacity of stored heat in thermal storage
d_{t}	Deviance from nominal coefficient, e_{n}
e_{t}	Objective function coefficients in the standard MIP problem
$g_{\min}^{net},g_{\max}^{net}$	Minimum/maximum nominal capacity of gas network
G_{t}^{l}	Hourly gas demand
J_{0}	Cost deviation of objective function calculated by $J_{0}=\{t\,\vert\,d_{t}>0\}$
$p_{\min}^{e},p_{\max}^{e}$	Minimum/maximum nominal capacity of upstream network
p_{c}^{T}	Rated capacity of net transformer
p_{c}^{CHP}	CHP unit rated capacity
p_{c}^{B}	Boiler rated capacity
p_{r}	Nominal electric power of wind turbine
$P_{t}^{e,l}$	Electrical demand
$P_{t}^{l,h}$	Heating demand
Wa_{t}^{l}	Water demand
$wa_{\min},wa_{\max}$	Minimum/maximum nominal capacity of water network
w_{ci},w_{co},w_{r}	Cut-in, cutout, and rated wind speeds of wind turbine
w_{t}	Actual wind speed
x,y,z	Coefficients used for modeling generation of wind turbine
λ_{t}^{e}	Upstream network price
λ^{wi}	Generation cost of wind turbine
λ^{g}	Price of gas network
λ^{wa}	Price of water network
λ_{s}^{e}	Operation cost of electrical storage
λ_{s}^{h}	Operation cost of thermal storage
Γ_{0}	Integer value used for robustness level controlling in the objective function
Abbreviations	
CHP	Combined heat and power
GAMS	General algebraic modeling system

15.1 Introduction

Efficiency of energy systems especially power systems has been always a critical issue. Recently, in order to attain energy systems with higher efficiencies, multi-carrier energy systems have been propounded to be used instead of traditional power systems. Multi-carrier energy systems or so-called hub energy systems usually benefit from renewable/nonrenewable local generation units like CHP system [1–4], boiler [5, 6] and wind turbine [7–9], and storage systems [10–12] to supply several types of energy demands [13–15]. In addition to efficiency, uncertainty-based operation of power systems is another important factor that needs to be investigated. There are many parameters in power systems like market price which uncertainty modeling should be taken into account to avoid further disorders in the operation of such systems.

15.1.1 Literature Review

In this section, researches published in the field of hub energy systems are briefly summarized from various viewpoints in below:

Different types of pricing models are available in energy market environment. Operation of hub energy system has been analyzed in the presence of time-of-use and dynamic pricings in [16]. Optimal performance of multi-carrier energy system has been investigated in the presence of intelligent agents in [17]. Optimal dispatch problem of multi-carrier energy system has been analyzed using a new developed model called self-adoptive learning with time varying acceleration coefficient-gravitational search algorithm (SAL-TVAC-GSA) in [18]. Renewable-based energy sources like wind and solar systems have been integrated into a combined cycle power plant using energy hub concept in [19]. New formulations with high accuracies have been developed for optimal operation of multi-carrier energy system in [20]. In order to provide economic benefits for costumers and electricity and gas utilities, demand response program has been developed for electrical and gas networks in a smart multi-carrier energy system in [21]. A new extensive model based on mixed integer nonlinear programming has been developed for optimal operation of multi-carrier energy system in [22]. In order to investigate adequacy of hub energy system, a new framework considering capacity outage probability tables of various energy infrastructure components and resources limitation has been presented in [23]. Optimal operation of residential multi-carrier energy system has been studied in the presence of electric vehicles and renewable distributed energy resources in [24]. Similar problem has been studied under electric vehicle and demand response program in [25]. Business concepts have been presented for multi-carrier energy system in [26]. Optimal operation of a hub energy microgrid has been investigated through a hierarchical energy management system in [27]. District heating network impact has been studied on the optimal performance of hub

energy system in [28]. Concept of hub energy systems has been used to develop an integrated energy system at neighborhood level in [29]. Optimal operation and power flow problem of hub energy microgrid has been studied in [30]. Optimal thermal and electrical operation of hub energy system has been evaluated under energy storage system and demand response program in [31]. Optimal performance of hub energy system has been investigated using SAL-TVAC-GSA in [32]. In order to represent microgrid in steady-state analysis, hub energy system has been molded using a new developed approach in [33]. Hub energy concept has been utilized to integrate renewable-based resources to handle energy consumption as well as generated emission in [34].

Performance of multi-carrier energy system has been analyzed in the presence of price and wind uncertainty using stochastic programming in [35]. Multi-carrier energy system has been planned and scheduled under uncertainties of price, demand, and wind using stochastic programming in [36, 37]. Also, stochastic programming has been employed to model uncertainties of wind, price, and load in the presence of demand response and thermal energy market in [38]. Using hyper-spherical search algorithm, uncertainty-based economic dispatch problem of residential multi-carrier energy system has been investigated in [39].

Well-known reliability evaluation approach called Markov chain technique has been used in [40, 41] to study optimal operation of multi-carrier energy system from reliability viewpoint.

In [42], a multi-objective optimization model has been developed for multi-carrier energy system in which grid integration level and levelized energy cost have been set to be objective functions. Modified teaching-learning-based algorithm has been used to solve the proposed multi-objective problem for economic-emission problem of hub energy system in [43]. Weighted sum approach has been employed to solve cost-emission problem of multi-carrier energy system networks in [44]. Similar cost-environmental problem of hub energy system has been studied in the presence of demand response program in [7]. Proposed multi-objective model for active electrical losses, energy costs, and natural gas losses has been solved using goal programming technique in [45].

Finally, multi-carrier energy systems have been investigated from viewpoints of recently used models and concepts in [46].

15.1.2 Novelty and Contributions

In this chapter, robust performance of hub energy system is studied under uncertainty of upstream network price using robust optimization approach. Employing robust optimization technique, appropriate operational strategies are obtained for robust performance of hub energy system against uncertain behavior of upstream network price. In comparison with other uncertainty modeling techniques like stochastic programming, robust optimization approach determines operational strategies to assess uncertainty-based operation of power system. Therefore, novelty and contributions of proposed chapter can be summarized as follows:

- Economic performance of multi-carrier energy system
- Optimal configuration of heat and electricity hub energy system
- Robust operation of multi-carrier energy system under uncertainty of upstream network price through robust optimization approach

15.1.3 Structure of Chapter

The remainder of proposed chapter is structured as follows: Base formulation of optimal operation problem of hub energy system is presented in Sect. 15.2. Robust optimization approach is briefly explained and then applied to the base problem in Sect. 15.3. Case studies as well as simulation results are presented in Sect. 15.4. Finally, the proposed chapter is concluded in Sect. 15.5.

15.2 Formulation

Optimal performance of hub energy system has been formulated without considering upstream network uncertainty in this section.

15.2.1 Objective Function

Total cost of multi-carrier energy system is due to be minimized as the objective function of proposed chapter (15.1). Mentioned objective function consists of costs of imported electric power, water, and gas from electricity, water, and gas networks as well as operation costs of boiler, CHP system, and electrical and thermal storage systems plus the cost/revenue of exchanged power.

$$\text{Min}\, Cost = \sum_{t}^{H} \begin{pmatrix} \lambda_t^e \times p_t^e + \lambda^{wi} \times p_t^{wi} + \lambda_s^e \times \left(p_t^{ch,e} + p_t^{dis,e}\right) \\ +\lambda_t^e \times \left(p_t^{ch,e} - p_t^{dis,e}\right) + \lambda^g \times g_t^B + \lambda^g \times g_t^{CHP} \\ +\lambda_s^h \times \left(p_t^{ch,h} + p_t^{dis,h}\right) + \lambda^{wa} \times wa_t \end{pmatrix} \tag{15.1}$$

15.2.2 Constraints

Electrical and thermal energy balance limitations are provided in Eqs. (15.2) and (15.3), respectively.

$$P_t^{e,l} = \begin{pmatrix} A^{NET} \times \eta_{ee}^{T} \times p_t^{e} + A^{CHP} \times \eta_{ge}^{CHP} \times g_t^{CHP} \\ +A^{WIND} \times \eta_{ee}^{CON} \times p_t^{wi} + p_t^{dis,e} - p_t^{ch,e} \end{pmatrix} \tag{15.2}$$

$$P_t^{l,h} = \left(A^{CHP} \times \eta_{gh}^{CHP} \times g_t^{CHP} + \eta_{gh}^{B} \times g_t^{B} + p_t^{dis,h} - p_t^{ch,h} \right) \tag{15.3}$$

Electrical storage system is designed based on Eqs. (15.4, 15.5, 15.6, 15.7, 15.8, and 15.9). As expressed in Eq. (15.4), available energy of electrical storage system is equal to the energy in former hour plus the charging power minus power losses and discharging power of the storage system. Stored energy in electrical storage is limited through Eq. (15.5). Charging/discharging power of electrical storage is limited through Eqs. (15.6) and (15.7), respectively. Finally, in order to prevent storage system from simultaneous charge and discharge processes, Eq. (15.8) is employed.

$$C_t^{st,e} = C_{t-1}^{st,e} + p_t^{ch,e} \times \eta_{ch}^{e} - p_t^{dis,e} / \eta_{dis}^{e} - \alpha_{loss}^{e} \times C_t^{st,e} \tag{15.4}$$

$$\alpha_{\min}^{e} \times C_c^{st,e} \le C_t^{st,e} \le \alpha_{\max}^{e} \times C_c^{st,e} \tag{15.5}$$

$$\frac{\alpha_{\min}^{e} \times C_c^{st,e} \times I_t^{ch,e}}{\eta_{ch}^{e}} \le p_t^{ch,e} \le \frac{\alpha_{\max}^{e} \times C_c^{st,e} \times I_t^{ch,e}}{\eta_{ch}^{e}} \tag{15.6}$$

$$\alpha_{\min}^{e} \times C_c^{st,e} \times I_t^{dis,e} \times \eta_{dis}^{e} \le p_t^{dis,e} \le \alpha_{\max}^{e} \times C_c^{st,e} \times I_t^{dis,e} \times \eta_{dis}^{e} \tag{15.7}$$

$$I_t^{ch,e} + I_t^{dis,e} \le 1 \tag{15.8}$$

Thermal storage system is also designed based on Eqs. (15.9, 15.10, 15.11, 15.12, and 15.13).

$$C_t^{st,h} = C_{t-1}^{st,h} + p_t^{ch,h} \times \eta_{ch}^{h} - p_t^{dis,h} / \eta_{dis}^{h} - \alpha_{loss}^{h} \times C_t^{st,h} \tag{15.9}$$

$$\alpha_{\min}^{h} \times C_c^{st,h} \le C_t^{st,h} \le \alpha_{\max}^{h} \times C_c^{st,h} \tag{15.10}$$

$$\frac{\alpha_{\min}^{h} \times C_c^{st,h} \times I_t^{ch,h}}{\eta_{ch}^{h}} \le p_t^{ch,h} \le \frac{\alpha_{\max}^{h} \times C_c^{st,h} \times I_t^{ch,h}}{\eta_{ch}^{h}} \tag{15.11}$$

$$\alpha_{\min}^{h} \times C_c^{st,h} \times I_t^{dis,h} \times \eta_{dis}^{h} \le p_t^{dis,h} \le \alpha_{\max}^{h} \times C_c^{st,h} \times I_t^{dis,h} \times \eta_{dis}^{h} \tag{15.12}$$

$$I_t^{ch,h} + I_t^{dis,h} \le 1 \tag{15.13}$$

Available heat in the thermal storage is equal to the stored heat at previous hour plus the charging heat minus heat losses and discharging heat (15.9). Stored heat is constrained through Eq. (15.10). Charging/discharging heat of thermal storage system is constrained through Eqs. (15.11) and (15.12), respectively. Finally, in order to prevent thermal storage from simultaneous charging and discharging, Eq. (15.13) is used.

Power generated by wind turbine is based on the pattern presented in Eq. (15.14).

$$p_t^{wi} = \begin{cases} 0 & w < w_{ci} \\ p_r(z - y.w(t) + x.w^2(t)) & w_{ci} \le w < w_r \\ p_r & w_r \le w < w_{co} \\ 0 & w \ge w_{co} \end{cases} \tag{15.14}$$

Imported power from upstream network cannot exceed the nominal power (15.15). Also, transformer limitation should be taken into account (15.16).

$$p_{\min}^e \le p_t^e \le p_{\max}^e \tag{15.15}$$

$$\eta_{ee}^T \times p_t^e \le p_c^T \tag{15.16}$$

Operational limitations of boiler and CHP unit are presented in Eqs. (15.17) and (15.18), respectively.

$$\eta_{gh}^B \times g_t^B \le p_c^B \tag{15.17}$$

$$\eta_{ge}^{CHP} \times g_t^{CHP} \le p_c^{CHP} \tag{15.18}$$

Gas demand balance limitation is presented in (15.19) in which gas demand is satisfied through the imported gas from gas network deducing the gas used for operation of boiler and CHP system.

$$G_t^l = g_t^{net} - g_t^B - g_t^{CHP} \tag{15.19}$$

It should be noted that purchased gas is not allowed to exceed rated capacity of gas network.

$$g_{\min}^{net} \le g_t^{net} \le g_{\max}^{net} \tag{15.20}$$

According to the water demand balance equations expressed in (15.21), imported water from water network should satisfy water demand. It should be noted that imported water from water network is restricted through (15.22).

$$Wa_t^l = wa_t^{net} \tag{15.21}$$

$$wa_{\min} \le wa_t^{net} \le wa_{\max} \tag{15.22}$$

15.3 Robust Operation of Hub Energy System

Robust performance of multi-carrier energy system under uncertainty of upstream network price is studied through robust optimization technique in this section. Robust optimization approach is briefly explained first, and then it is applied to the base problem [47–49].

15.3.1 Robust Optimization Technique

Robust optimization approach determines appropriate operational strategies to be used by the operators to guarantee stable performance of operating system under various conditions of uncertainty. Standard form of a simple optimization problem can be modeled using Eqs. (15.23, 15.24, 15.25, and 15.26).

$$\underset{X_t,\forall t}{\text{Minimize}} \quad \sum_{t=1}^{H} e_t x_t \tag{15.23}$$

S.t

$$\sum_{t=1}^{H} a_{mt} x_t \le b_m, \quad m = 1, \ldots, M \tag{15.24}$$

$$x_t \ge 0, \quad t = 1, \ldots, H \tag{15.25}$$

$$x_t \in \{0, 1\} \quad \text{for some } t = 1, \ldots, H \tag{15.26}$$

For modeling robust optimization problem, the whole coefficients are set to be between e_t and e_t+d_t, where d_t is the deviance from nominal coefficient, e_t. Then, an integer parameter (Γ_0) considering values between 0 and $|J_0|$ is defined. It should be noted that$J_0 = \{t | d_t > 0\}$. The effect of cost deviations in the objective function of problem is ignored if the defined integer parameter is zero. In simple words if $\Gamma_0 = |J_0|$, the whole cost deviations of objective function are considered.

Therefore, robust optimization problem can be expressed as follows:

$$\underset{x_t,\forall t}{\text{Minimize}} \quad \sum_{t=1}^{H} e_t x_t + \underset{\{S_0 | \ S_0 \subseteq J_0, |S_0| = \Gamma_0\}}{\text{Maximize}} \left\{ \sum_{t \in S_0} d_t |x_t| \right\} \tag{15.27}$$

S.t

$$Eqs. \ (15.24) - (15.26) \tag{15.28}$$

It should be noted that mentioned robust optimization problem above can be reformulated in a new form as follows [50]:

$$\underset{x_t, q_{ot}, y_t, \forall t; z_0}{\text{Minimize}} \quad \sum_{t=1}^{H} e_t x_t + z_0 \Gamma_0 + \sum_{t=1}^{H} q_{ot} \tag{15.29}$$

S.t

$$Eqs.\ (15.24) - (15.26) \tag{15.30}$$

$$z_0 + q_{ot} \geq d_t y_t, \quad t = 1, \ldots, H \tag{15.31}$$

$$q_{ot} \geq 0, \quad t = 1, \ldots, H \tag{15.32}$$

$$y_t \geq 0, \quad t = 1, \ldots, H \tag{15.33}$$

$$z_0 \geq 0 \tag{15.34}$$

$$x_t \leq y_t, \quad t = 1, \ldots, H \tag{15.35}$$

It should be noted that z_0 and q_{ot} are dual variables of optimization problem (15.23, 15.24, 15.25, and 15.26).

15.3.2 Robust Performance of Hub Energy System Under Uncertainty of Upstream Network Price

According to the explanation of robust optimization approach, robust performance of multi-carrier energy system using robust optimization technique can be modeled as follows:

$$\text{Min} \left(\sum_{t=1}^{H} \begin{pmatrix} \hat{\lambda}_t^e \times p_t^e + \lambda^{wi} \times p_t^{wi} + \lambda_s^e \times \left(p_t^{ch,e} + p_t^{dis,e} \right) \\ + \lambda_t^e \times \left(p_t^{ch,e} - p_t^{dis,e} \right) + \lambda^g \times g_t^B + \lambda^g \times g_t^{CHP} \\ + \lambda_s^h \times \left(p_t^{ch,h} + p_t^{dis,h} \right) + \lambda^{wa} \times wa_t \end{pmatrix} + z_0 \Gamma_0 + \sum_{t=1}^{H} q_{ot} \right) \tag{15.36}$$

S.t

$$Eqs.\ (15.2) - (15.22) \tag{15.37}$$

$$z_0 + q_{ot} \geq d_t y_t, \quad t = 1, \ldots, H \tag{15.38}$$

$$q_{ot} \geq 0, \quad t = 1, \ldots, H \tag{15.39}$$

$$y_t \geq 0, \quad t = 1, \ldots, H \tag{15.40}$$

$$z_0 \geq 0 \tag{15.41}$$

$$p_t^e + p_t^{ch,e} - p_t^{dis,e} \leq y_t, \quad t = 1, \ldots, 24 \tag{15.42}$$

15.4 Case Study

In this section, a sample multi-carrier energy system containing renewables and nonrenewable generation units, CHP, and boiler as well as electrical and thermal storage systems (ESS and TES) is studied. Studied system is shown in Fig. 15.1.

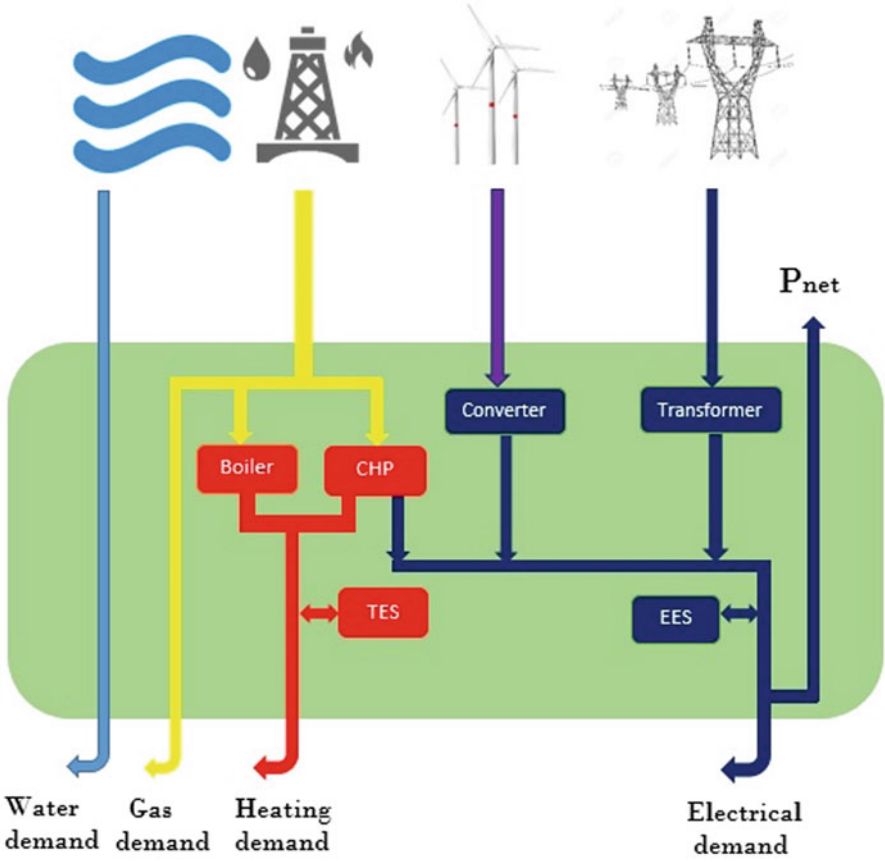

Fig. 15.1 Sample multi-carrier energy system

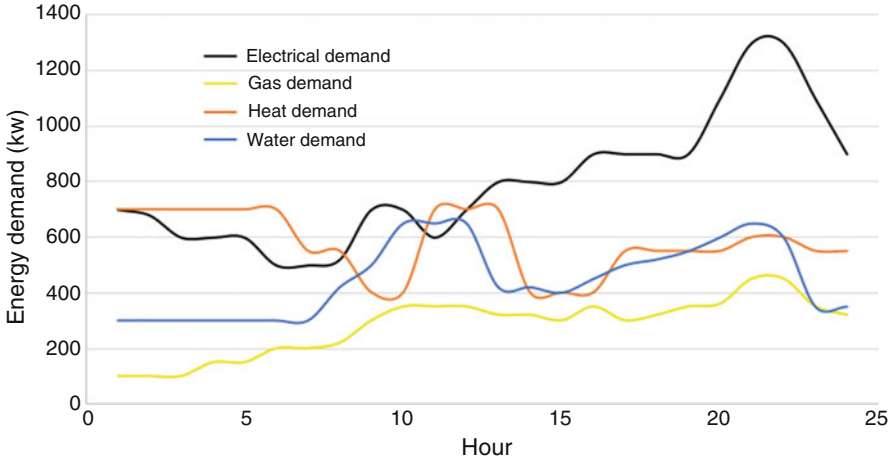

Fig. 15.2 Energy demand of multi-carrier energy system [7, 37]

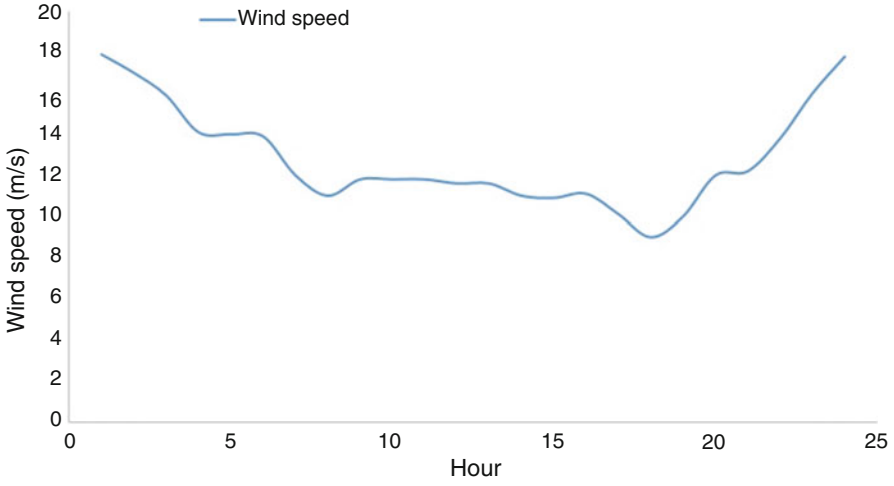

Fig. 15.3 Wind speed [7, 37]

15.4.1 Data

Simulations are done according to the data given in the following: Electrical, thermal, gas, and water demands of multi-carrier energy system are illustrated in Fig. 15.2 [7, 37]. Also, hourly wind speed according to which wind power is generated is illustrated in Fig. 15.3 [7, 37]. Finally, Fig. 15.4 illustrates the upper, expected, and lower limits of upstream network price [7, 37].

Technical limitations and data of upstream network as well as gas and water networks are presented in Table 15.1. As mentioned before, upstream network is one of the resources providing power for supplying electrical demand. Technical

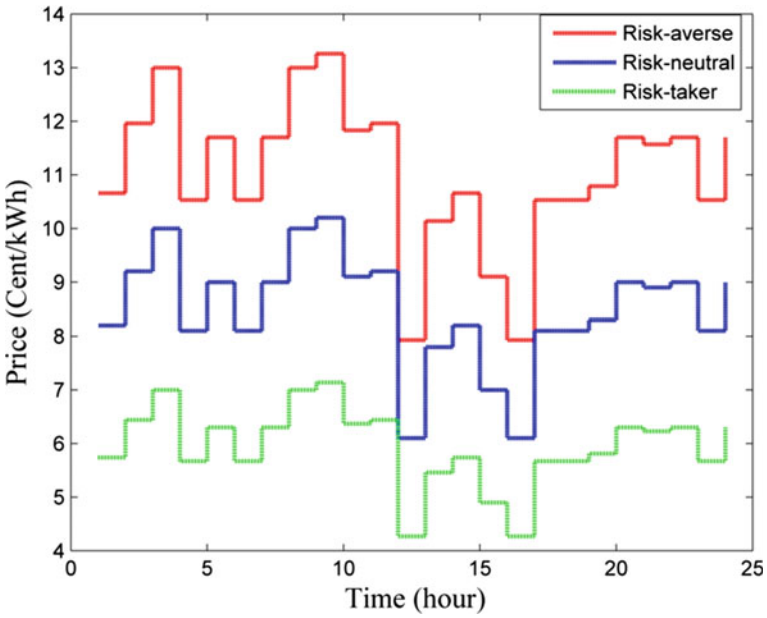

Fig. 15.4 Upstream network price [7, 37]

Table 15.1 Technical limitations related to upstream, gas, and water networks [3, 26]

Upstream network parameter			Gas and water network parameters		
#	Unit	Value	#	Unit	Value
A^{NET}	–	0.99	$g^{net}_{\max}$	kW	1800
$p^{e}_{\max}$	kW	1000	$g^{net}_{\min}$	kW	0
$p^{e}_{\min}$	kW	0	$wa_{\max}$	kW	1000
p^{T}_{c}	kW	800	$wa_{\min}$	kW	0

constraints of electrical and thermal storage systems are presented in Table 15.2. Operational limitations of local distribution generation systems are presented through Table 15.3. Finally, operation costs of wind turbine, electrical and thermal storages, as well as prices of procured gas and water are presented in Table 15.4.

Setting the time step to be 1 hour, robust performance problem of multi-carrier energy system under uncertainty of price of upstream network is simulated using GAMS optimization package under CPLEX 11.0 [51].

15.4.2 Results

Solving the objective function (15.36) subject to constraints (15.37, 15.38, 15.39, 15.40, 15.41, and 15.42), robust costs of multi-carrier energy system are obtained. Figure 15.5 shows robust cost in various iterations including minimum, expected,

Table 15.2 Technical limitation of electrical and thermal storage systems [3, 26]

Electrical storage parameter			Thermal storage parameter		
#	Unit	Value	#	Unit	Value
$\alpha^{e}_{\min}$	–	0.05	$\alpha^{h}_{\min}$	–	0.05
$\alpha^{e}_{\max}$	–	0.9	$\alpha^{h}_{\max}$	–	0.9
α^{e}_{loss}	–	0.2	α^{h}_{loss}	–	0.2
η^{e}_{ch}	%	90	η^{h}_{ch}	%	90
η^{e}_{dis}	%	90	η^{h}_{dis}	%	90
$C^{st,e}_{c}$	kW	300	$C^{st,h}_{c}$	kW	200

Table 15.3 Technical constraints of distribution generation units [3, 26]

Wind turbine parameter			CHP and boiler parameters		
#	Unit	Value	#	Unit	Value
A^{WIND}	–	0.96	A^{CHP}	–	0.96
x, y, z	–	0.07, 0.01, 0.03	η^{CHP}_{ge}	%	40
w_{ci}	m/s	4	η^{CHP}_{gh}	%	35
w_{co}	m/s	22	p^{CHP}_{c}	kW	800
p_r	kW	400	η^{B}_{gh}	%	85
			p^{B}_{c}	kW	800

Table 15.4 Data of generation units [3, 26]

Parameter	Value	Unit
λ^{g}	6	Cent/kWh
λ^{wa}	4	Cent/kWh
λ^{wi}	0	Cent/kWh
λ^{e}_{s}	2	Cent/kWh
λ^{h}_{s}	2	Cent/kWh

and maximum robust levels. Iteration 6 represents deterministic case excluding uncertainty in which total operation cost of hub energy system is equal to 2677.41 $. As shown in Fig. 15.5, iteration 1 is related to the case in which the ideal outcome is obtained for the hub energy system due to the lower prices of upstream network. It can be seen that total operation cost of hub energy system in this level is 2417.97 $ which is reduced by 9.69% in comparison with deterministic condition. Also, due to the higher prices of upstream network, the worst case for the hub energy system is obtained in iteration 11 according to which hub energy system experienced total cost of 2771.77 $ which is 3.52% more in comparison with deterministic case. In other words, in order to guarantee stable operation of hub energy system against increase of upstream network up to 30%, the operation cost of hub energy system is increased by 3.52%.

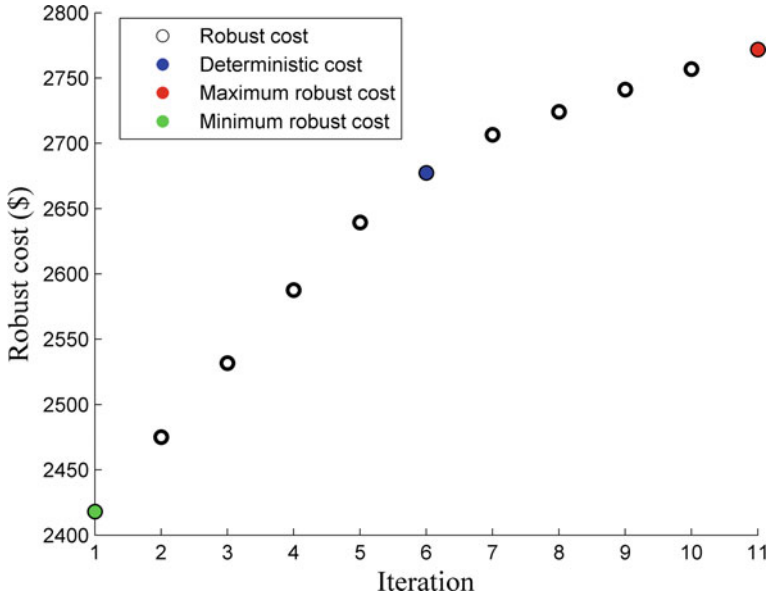

Fig. 15.5 Robust cost of multi-carrier energy system

Imported power from upstream network is declared in Fig. 15.6. As shown in this figure, multi-carrier energy system has purchased less power from upstream network in the worst case containing the highest upstream network prices, and on the other hand, because of lower prices, multi-carrier energy system has attempted to buy more power from upstream network in minimum robust condition.

CHP unit has been mostly used for electric power generation due to the lack of electric power for supplying electrical load in maximum robust condition, and this has led to more gas consumption of this unit in the mentioned condition. Moreover, since heat generation of CHP system is proportional with its electrical generation, generated heat by this unit is increased in the maximum robust condition. Reverse explanation is also true for minimum robust condition. Total consumed gas, electrical generation, and generated heat by CHP unit are shown in Figs. 15.7, 15.8, and 15.9, respectively.

Since generated heat by CHP system in the minimum robust condition is insufficient to meet heating demand, lack of heat in this condition has been made up by heat generation of boiler which has led to the increase of gas consumption of this unit in the mentioned condition. Finally, total consumed gas and generated heat by boiler are illustrated through Figs. 15.10 and 15.11, respectively.

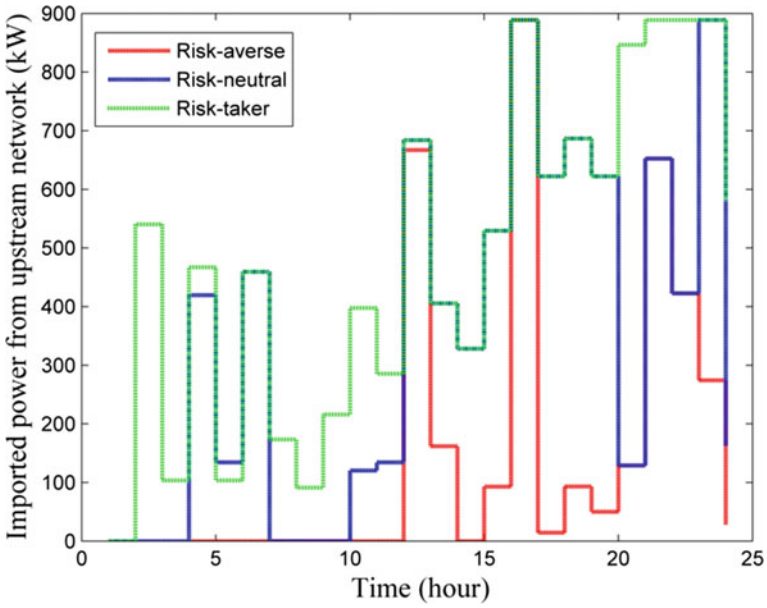

Fig. 15.6 Imported power from upstream network

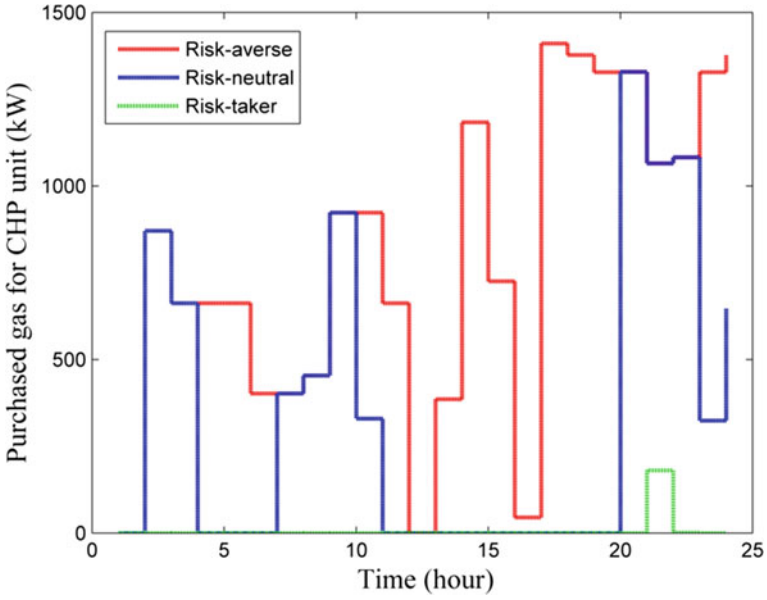

Fig. 15.7 Gas consumption of CHP unit

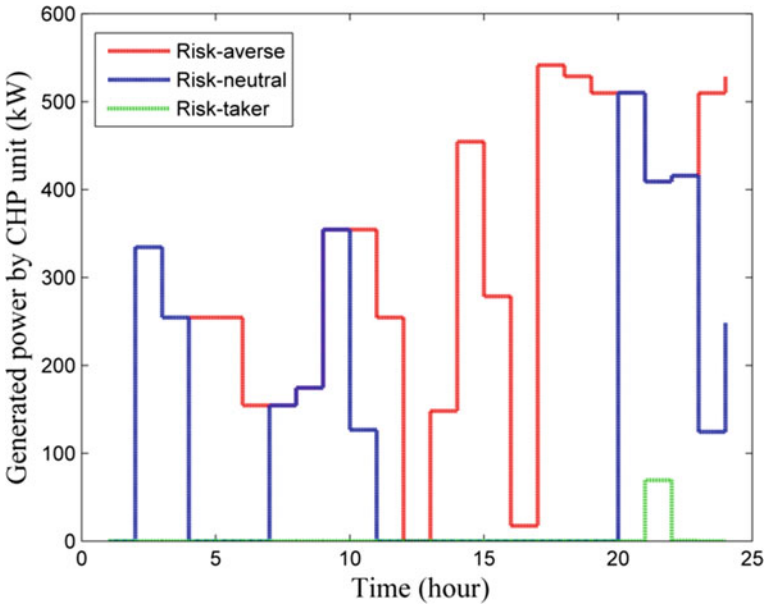

Fig. 15.8 Electric power generation of CHP unit

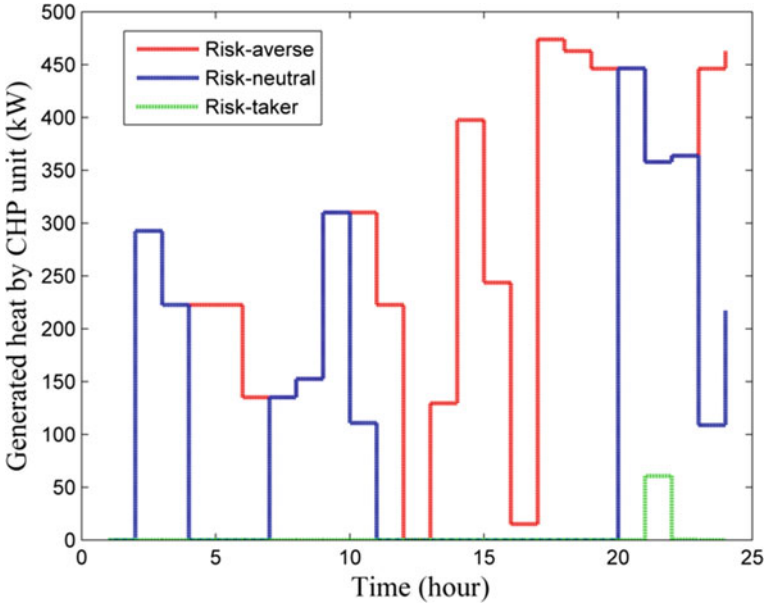

Fig. 15.9 Heat generation of CHP unit

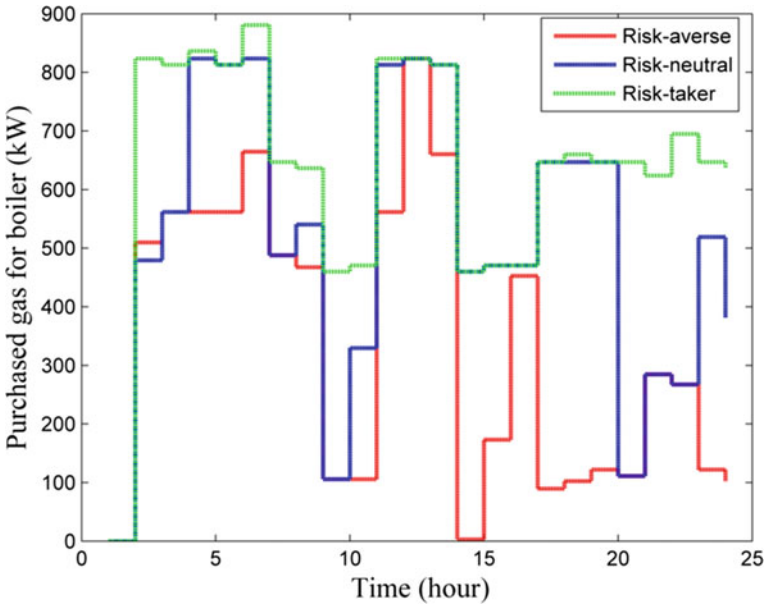

Fig. 15.10 Gas consumption of boiler

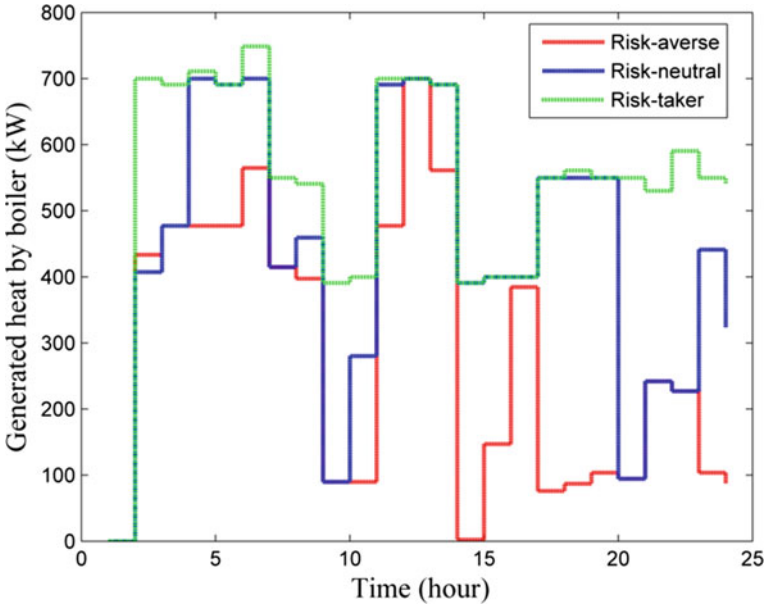

Fig. 15.11 Heat generation of boiler

15.5 Conclusions

In this chapter, risk-based performance of multi-carrier energy system has been studied using robust optimization approach under uncertainty of upstream network price. Upstream network price can either increase or decrease in different uncertainty conditions which can challenge stable operation of operating system. So, robust optimization technique is applied to determine the appropriate operating strategies. The possible outcomes that can be caused by uncertainty are investigated, and the results are presented for comparison. According to the obtained results from simulations, robust operation of hub energy system can be guaranteed against 30% increase of upstream network price through experiencing 3.52% more operation cost in comparison with the normal operating condition. This increase is mainly due to the taken risk-averse strategy by the operator of operating system. On the other hand, the operator can take risk-seeking strategy to benefit from the possible reduction of price. According to the results, the operator can gain 9.69% economic benefit through reduction of price up to 30%. So, it can be concluded that by using the provided operating strategies through robust optimization method, the whole possible consequences of uncertainties can be taken into account.

References

1. Nojavan, S., Majidi, M., & Zare, K. (2018). Optimal scheduling of heating and power hubs under economic and environment issues in the presence of peak load management. *Energy Conversion and Management, 156*, 34–44.
2. Nazari-Heris, M., Abapour, S., & Mohammadi-Ivatloo, B. (2017). Optimal economic dispatch of FC-CHP based heat and power micro-grids. *Applied Thermal Engineering, 114*, 756–769.
3. Nazari-Heris, M., Mohammadi-Ivatloo, B., & Gharehpetian, G. (2017). A comprehensive review of heuristic optimization algorithms for optimal combined heat and power dispatch from economic and environmental perspectives. *Renewable and Sustainable Energy Reviews, 81*, 2128–2143.
4. Nazari-Heris, M., Mohammadi-Ivatloo, B., Gharehpetian, G. B., & Shahidehpour, M. (2018). Robust short-term scheduling of integrated heat and power microgrids. *IEEE Systems Journal*, (99), 1–9. https://doi.org/10.1109/JSYST.2018.2837224 (early access)
5. Majidi, M., Nojavan, S., Esfetanaj, N. N., Najafi-Ghalelou, A., & Zare, K. (2017). A multi-objective model for optimal operation of a battery/PV/fuel cell/grid hybrid energy system using weighted sum technique and fuzzy satisfying approach considering responsible load management. *Solar Energy, 144*, 79–89.
6. Haghrah, A., Nazari-Heris, M., & Mohammadi-Ivatloo, B. (2016). Solving combined heat and power economic dispatch problem using real coded genetic algorithm with improved Mühlenbein mutation. *Applied Thermal Engineering, 99*, 465–475.
7. Majidi, M., Nojavan, S., & Zare, K. (2017). A cost-emission framework for hub energy system under demand response program. *Energy, 134*, 157–166.
8. Nojavan, S., Majidi, M., Najafi-Ghalelou, A., & Zare, K. (2018). Supply side management in renewable energy hubs. In *Operation, planning, and analysis of energy storage systems in smart energy hubs* (pp. 163–187). Cham: Springer.
9. Majidi, M., Nojavan, S., & Zare, K. (2018). Multi-objective optimization framework for electricity and natural gas energy hubs under hydrogen storage system and demand response

program. In *Operation, planning, and analysis of energy storage systems in smart energy hubs* (pp. 425–446). Cham: Springer.
10. Nojavan, S., Majidi, M., & Esfetanaj, N. N. (2017). An efficient cost-reliability optimization model for optimal siting and sizing of energy storage system in a microgrid in the presence of responsible load management. *Energy, 139*, 89–97.
11. Majidi, M., & Nojavan, S. (2017). Optimal sizing of energy storage system in a renewable-based microgrid under flexible demand side management considering reliability and uncertainties. *Journal of Operation and Automation in Power Engineering, 5*(2), 205–214.
12. Nojavan, S., Majidi, M., & Zare, K. (2017). Stochastic multi-objective model for optimal sizing of energy storage system in a microgrid under demand response program considering reliability: A weighted sum method and fuzzy satisfying approach. *Journal of Energy Management and Technology, 1*(1), 61–70.
13. Majidi, M., Nojavan, S., & Zare, K. (2017). Optimal stochastic short-term thermal and electrical operation of fuel cell/photovoltaic/battery/grid hybrid energy system in the presence of demand response program. *Energy Conversion and Management, 144*, 132–142.
14. Nazari-Heris, M., Mehdinejad, M., Mohammadi-Ivatloo, B., & Babamalek-Gharehpetian, G. (2017). Combined heat and power economic dispatch problem solution by implementation of whale optimization method. *Neural Computing and Applications*, 1–16. https://doi.org/10.1007/s00521-017-3074-9.
15. Nojavan, S., Majidi, M., & Zare, K. (2017). Risk-based optimal performance of a PV/fuel cell/battery/grid hybrid energy system using information gap decision theory in the presence of demand response program. *International Journal of Hydrogen Energy, 42*(16), 11857–11867.
16. Kamyab, F., & Bahrami, S. (2016). Efficient operation of energy hubs in time-of-use and dynamic pricing electricity markets. *Energy, 106*, 343–355. https://doi.org/10.1016/j.energy.2016.03.074.
17. Skarvelis-Kazakos, S., Papadopoulos, P., Grau Unda, I., Gorman, T., Belaidi, A., & Zigan, S. (2016). Multiple energy carrier optimisation with intelligent agents. *Applied Energy, 167*, 323–335. https://doi.org/10.1016/j.apenergy.2015.10.130.
18. Beigvand, S. D., Abdi, H., & La Scala, M. (2017). A general model for energy hub economic dispatch. *Applied Energy, 190*, 1090–1111. https://doi.org/10.1016/j.apenergy.2016.12.126.
19. AlRafea, K., Fowler, M., Elkamel, A., & Hajimiragha, A. (2016). Integration of renewable energy sources into combined cycle power plants through electrolysis generated hydrogen in a new designed energy hub. *International Journal of Hydrogen Energy, 41*(38), 16718–16728. https://doi.org/10.1016/j.ijhydene.2016.06.256.
20. Evins, R., Orehounig, K., Dorer, V., & Carmeliet, J. (2014). New formulations of the 'energy hub' model to address operational constraints. *Energy, 73*, 387–398. https://doi.org/10.1016/j.energy.2014.06.029.
21. Sheikhi, A., Bahrami, S., & Ranjbar, A. M. (2015). An autonomous demand response program for electricity and natural gas networks in smart energy hubs. *Energy, 89*, 490–499. https://doi.org/10.1016/j.energy.2015.05.109.
22. Moghaddam, I. G., Saniei, M., & Mashhour, E. (2016). A comprehensive model for self-scheduling an energy hub to supply cooling, heating and electrical demands of a building. *Energy, 94*, 157–170. https://doi.org/10.1016/j.energy.2015.10.137.
23. Shariatkhah, M.-H., Haghifam, M.-R., Chicco, G., & Parsa-Moghaddam, M. (2016). Adequacy modeling and evaluation of multi-carrier energy systems to supply energy services from different infrastructures. *Energy, 109*, 1095–1106. https://doi.org/10.1016/j.energy.2016.04.116.
24. Rastegar, M., & Fotuhi-Firuzabad, M. (2015). Load management in a residential energy hub with renewable distributed energy resources. *Energy and Buildings, 107*, 234–242. https://doi.org/10.1016/j.enbuild.2015.07.028.
25. Rastegar, M., Fotuhi-Firuzabad, M., & Lehtonen, M. (2015). Home load management in a residential energy hub. *Electric Power Systems Research, 119*, 322–328. https://doi.org/10.1016/j.epsr.2014.10.011.

26. Sepponen, M., & Heimonen, I. (2016). Business concepts for districts' energy hub systems with maximised share of renewable energy. *Energy and Buildings, 124*, 273–280. https://doi.org/10.1016/j.enbuild.2015.07.066.
27. Xu, X., Jia, H., Wang, D., Yu, D. C., & Chiang, H.-D. (2015). Hierarchical energy management system for multi-source multi-product microgrids. *Renewable Energy, 78*, 621–630. https://doi.org/10.1016/j.renene.2015.01.039.
28. Shabanpour-Haghighi, A., & Seifi, A. R. (2016). Effects of district heating networks on optimal energy flow of multi-carrier systems. *Renewable and Sustainable Energy Reviews, 59*, 379–387. https://doi.org/10.1016/j.rser.2015.12.349.
29. Orehounig, K., Evins, R., & Dorer, V. (2015). Integration of decentralized energy systems in neighbourhoods using the energy hub approach. *Applied Energy, 154*, 277–289. https://doi.org/10.1016/j.apenergy.2015.04.114.
30. Ma, T., Wu, J., & Hao, L. (2017). Energy flow modeling and optimal operation analysis of the micro energy grid based on energy hub. *Energy Conversion and Management, 133*, 292–306. https://doi.org/10.1016/j.enconman.2016.12.011.
31. Brahman, F., Honarmand, M., & Jadid, S. (2015). Optimal electrical and thermal energy management of a residential energy hub, integrating demand response and energy storage system. *Energy and Buildings, 90*, 65–75. https://doi.org/10.1016/j.enbuild.2014.12.039.
32. Derafshi Beigvand, S., Abdi, H., & La Scala, M. (2016). Optimal operation of multicarrier energy systems using time varying acceleration coefficient gravitational search algorithm. *Energy, 114*, 253–265. https://doi.org/10.1016/j.energy.2016.07.155.
33. Wasilewski, J. (2015). Integrated modeling of microgrid for steady-state analysis using modified concept of multi-carrier energy hub. *International Journal of Electrical Power & Energy Systems, 73*, 891–898. https://doi.org/10.1016/j.ijepes.2015.06.022.
34. Orehounig, K., Evins, R., Dorer, V., & Carmeliet, J. (2014). Assessment of renewable energy integration for a village using the energy hub concept. *Energy Procedia, 57*, 940–949. https://doi.org/10.1016/j.egypro.2014.10.076.
35. Najafi, A., Falaghi, H., Contreras, J., & Ramezani, M. (2016). Medium-term energy hub management subject to electricity price and wind uncertainty. *Applied Energy, 168*, 418–433. https://doi.org/10.1016/j.apenergy.2016.01.074.
36. Pazouki, S., & Haghifam, M.-R. (2016). Optimal planning and scheduling of energy hub in presence of wind, storage and demand response under uncertainty. *International Journal of Electrical Power & Energy Systems, 80*, 219–239. https://doi.org/10.1016/j.ijepes.2016.01.044.
37. Pazouki, S., Haghifam, M.-R., & Moser, A. (2014). Uncertainty modeling in optimal operation of energy hub in presence of wind, storage and demand response. *International Journal of Electrical Power & Energy Systems, 61*, 335–345.
38. Vahid-Pakdel, M., Nojavan, S., Mohammadi-ivatloo, B., & Zare, K. (2017). Stochastic optimization of energy hub operation with consideration of thermal energy market and demand response. *Energy Conversion and Management, 145*, 117–128.
39. Sanjari, M., Karami, H., & Gooi, H. (2016). Micro-generation dispatch in a smart residential multi-carrier energy system considering demand forecast error. *Energy Conversion and Management, 120*, 90–99.
40. Shariatkhah, M.-H., Haghifam, M.-R., Parsa-Moghaddam, M., & Siano, P. (2015). Modeling the reliability of multi-carrier energy systems considering dynamic behavior of thermal loads. *Energy and Buildings, 103*, 375–383. https://doi.org/10.1016/j.enbuild.2015.06.001.
41. Koeppel, G., & Andersson, G. (2009). Reliability modeling of multi-carrier energy systems. *Energy, 34*(3), 235–244. https://doi.org/10.1016/j.energy.2008.04.012.
42. Perera, A. T. D., Nik, V. M., Mauree, D., & Scartezzini, J.-L. (2017). Electrical hubs: An effective way to integrate non-dispatchable renewable energy sources with minimum impact to the grid. *Applied Energy, 190*, 232–248. https://doi.org/10.1016/j.apenergy.2016.12.127.
43. Shabanpour-Haghighi, A., & Seifi, A. R. (2015). Multi-objective operation management of a multi-carrier energy system. *Energy, 88*, 430–442. https://doi.org/10.1016/j.energy.2015.05.063.

44. Maroufmashat, A., Elkamel, A., Fowler, M., Sattari, S., Roshandel, R., Hajimiragha, A., Walker, S., & Entchev, E. (2015). Modeling and optimization of a network of energy hubs to improve economic and emission considerations. *Energy, 93*, 2546–2558. https://doi.org/10.1016/j.energy.2015.10.079.
45. La Scala, M., Vaccaro, A., & Zobaa, A. F. (2014). A goal programming methodology for multiobjective optimization of distributed energy hubs operation. *Applied Thermal Engineering, 71*(2), 658–666. https://doi.org/10.1016/j.applthermaleng.2013.10.031.
46. Mancarella, P. (2014). MES (multi-energy systems): An overview of concepts and evaluation models. *Energy, 65*, 1–17. https://doi.org/10.1016/j.energy.2013.10.041.
47. Nojavan, S., Najafi-Ghalelou, A., Majidi, M., & Zare, K. (2018). Optimal bidding and offering strategies of merchant compressed air energy storage in deregulated electricity market using robust optimization approach. *Energy, 142*, 250–257.
48. Nazari-Heris, M., Madadi, S., & Mohammadi-Ivatloo, B. (2018). Optimal management of hydrothermal-based micro-grids employing robust optimization method. In *Classical and recent aspects of power system optimization* (pp. 407–420). Elsevier.
49. Nazari-Heris, M., & Mohammadi-Ivatloo, B. (2018). Application of robust optimization method to power system problems. In *Classical and recent aspects of power system optimization* (pp. 19–32). Elsevier.
50. Bertsimas, D., & Sim, M. (2003). Robust discrete optimization and network flows. *Mathematical Programming, 98*(1–3), 49–71.
51. The GAMS Software Website. (2017). [Online]. Available: http://www.gams.com/help/index.jsp?topic=%2Fgams.doc%2Fsolvers%2Findex.html

Chapter 16
Robust Optimization Method for Obtaining Optimal Scheduling of Active Distribution Systems Considering Uncertain Power Market Price

Morteza Nazari-Heris, Saeed Abapour, and Behnam Mohammadi-ivatloo

16.1 Introduction

The optimal scheduling of electricity distribution networks is accomplished by network operators to provide the optimal set points of the network components and improving the utilization of alternative energy technologies. Active network management (ANM) is introduced as an effective approach for coordinating the interconnection and operation of distributed generators (DGS) and electricity distribution networks [1]. The application of ANM in distribution networks takes advantages of decreasing power loss of the network, modifying the load profile of the network, controlling the voltage profile, and reducing the curtailment of DGs in the network. Both DG owner (DGO) and distribution company (DisCo) are responsible in providing reliable electrical energy and improving the efficiency of the power network [2, 3].

It is important to be mentioned that the application of ANM is not fully enough according to load demand increment and conditions with full load. The requirement of electricity networks to renewable energy sources and energy storage systems has been more sensible by the issues appeared as limitation of oil and gas sources and emission of pollutant gases. Different energy storage technologies have been introduced including fuel cell [4], battery technologies for electrical energy storage units [5], pumped storage units [6], ice storage [7], and compressed air energy storage [8]. Moreover, development of smart grids in distribution networks and improvements of the energy technologies have clarified the role of demand response programs (DRPs). DRPs are introduced as demand side management approach for changing the customer loads from peak hours to off-peak hours and receiving incentives for participating in DRPs. The application of DRPs in distribution

M. Nazari-Heris · S. Abapour (✉) · B. Mohammadi-ivatloo
Faculty of Electrical and Computer Engineering, University of Tabriz, Tabriz, Iran
e-mail: mnazari@tabrizu.ac.ir; bmohammadi@tabrizu.ac.ir

B. Mohammadi-ivatloo, M. Nazari-Heris (eds.), *Robust Optimal Planning and Operation of Electrical Energy Systems*,
https://doi.org/10.1007/978-3-030-04296-7_16

networks is impactful in improving the stability of power systems [9]. The employment of time-of-use DRPs on bidding strategy of electrical energy retailers has been studied in [10]. The proposed model in this reference has investigated the effect of system flexibility in improvement of generation dispatch and reduction of electricity bills for the supply and demand sections, respectively. Various modeling approaches with different strategies for fixed and flexible loads in obtaining optimal dispatch of power networks have been compared in [11]. In addition, the utilization of energy storage units and their advantages in ancillary services have been discussed in the area of improving system reliability indexes and modifying the load profile [12]. The application of energy storage technologies has been studied in the system planning [13], energy markets [14], joint energy and reserve markets [15], and operation of micro-grids [16].

The smart distribution network can be attained by adjustment of transformer tap changer and reactive power compensators hourly. Such adjustment will be effective in decreasing voltage deviation and operational cost of the network. The ANM of distribution networks can be accomplished by controlling and managing by using a control center placed in the primary substation of the network. State estimation process is proceeded in the distribution network by receiving the load data by local and remote measurements. Three ANM strategies implemented in the distribution networks can be defined as [17]:

(a) Active power regulation of DG
(b) Active management of on-load-tap changer (OLTC)
(c) Using reactive power compensators (RPCs)

This chapter aims to study robust optimal scheduling of active distribution networks considering the uncertainty associated with power market price. The robust optimization (RO) method has been implemented to deal with uncertain price maximizing benefit of distribution company (DisCo) and maximizing benefit of distributed generation owner (DGO). Accordingly, ε-constraint is applied to handle multi-objective profit maximization of DisCo and DGO, and a fuzzy satisfying method is used to define the best compromise solution. The application of time-of-use DRP and energy storage units has been investigated in the proposed robust model. The proposed model is tested on 33-bus radial distribution network to evaluate and conform the performance of the model.

The organization of this chapter is as follows: The problem formulation of the proposed robust scheduling of distribution networks is prepared in Sect. 16.2. The case study and solution method have been provided in Sect. 16.3. Section 16.4 discusses and investigated the simulation results. Finally, the summary of this chapter is provided in Sect. 16.5.

16.2 Problem Formulation

16.2.1 Objective Functions of DisCo and DGO

The objective function of DisCo is obtaining maximum benefit by obtaining optimal short-term scheduling of the network, which can be calculated as follows:

$$OF_1 = \max \sum_{h=1}^{N_h} \left\{ \begin{array}{l} \sum_{i=1}^{N_{\text{load}}} \rho_{\text{sell}}^{P} \times P_{i,h}^{D} + \sum_{i=1}^{N_{\text{load}}} \rho_{\text{sell}}^{Q} \times Q_{i,h}^{D} - \sum_{ss=1}^{N_{SS}} \lambda_h \times P_h^{ss} - \sum_{ss=1}^{N_{SS}} \lambda_{Qfix} \times Q_h^{ss} \\ -\lambda_h \times P_{\text{loss}}^{\text{tot}} - \sum_{n=1}^{N_{DG}} \rho_{\text{sell}}^{PDGO} \times P_{n,h}^{DG} - \sum_{n=1}^{N_{DG}} \rho_{\text{sell}}^{QDGO} \times Q_{n,h}^{DG} \end{array} \right\} \tag{16.1}$$

where ρ_{sell}^{P} and ρ_{sell}^{Q} are the price of selling active and reactive power of DisCo to consumers, respectively. The indicators of active and reactive power sold to the consumers are $P_{i,h}^{D}$ and $Q_{i,h}^{D}$. The power market price and power exchanged between the network and power market are defined by λ_h and P_h^{ss}, respectively. The fixed reactive power price and its corresponding reactive power are defined by λ_{Qfix} and Q_h^{ss}, respectively. Total active power loss is defined by $P_{\text{loss}}^{\text{tot}}$. The active and reactive power injected by a diesel generator are defined by $P_{n,h}^{DG}$ and $Q_{n,h}^{DG}$, respectively. In addition, the price of active and reactive power of the generators are indicated by $\rho_{\text{sell}}^{PDGO}$ and $\rho_{\text{sell}}^{QDGO}$, respectively. The revenue of selling power to the consumers is the first and second terms of (16.1). The cost of purchased power from the power market is the third term of this equation. The cost of purchasing reactive power from the external network is the fourth term of (16.1). Benefits or costs related to variation of network power losses are defined as fifth term of the equation. The respective terms for purchasing active and reactive energy from DGO by DisCo are provided as sixth and seventh terms of (16.1). Considering the uncertain power market price, Eq. (16.1) can be reformulated as a max-min-max robust optimization problem as follows [18]:

$$\begin{aligned} OF_1 = \quad & \max \sum_{h=1}^{N_h} \left\{ \begin{array}{l} \sum_{i=1}^{N_{\text{load}}} \rho_{\text{sell}}^{P} \times P_{i,h}^{D} + \sum_{i=1}^{N_{\text{load}}} \rho_{\text{sell}}^{Q} \times Q_{i,h}^{D} - \sum_{ss=1}^{N_{SS}} \lambda_h \times P_h^{ss} - \sum_{ss=1}^{N_{SS}} \lambda_{Qfix} \times Q_h^{ss} \\ -\lambda \times P_{\text{loss}}^{\text{tot}} - \sum_{n=1}^{N_{DG}} \rho_{\text{sell}}^{PDGO} \times P_{n,h}^{DG} - \sum_{n=1}^{N_{DG}} \rho_{\text{sell}}^{QDGO} \times Q_{n,h}^{DG} \end{array} \right\} \\ & + \min \quad \max \sum_{h=1}^{N_h} \lambda_h \times P_h^{ss} \end{aligned} \tag{16.2}$$

where the price of power market is assumed to be uncertain. The objective of the proposed RO model is to obtain the optimal solution in robust condition, where the operation cost of the network will be preserved considering probable deviation of power market price from the forecasted values [19]. The inner problem equivalently can be reformulated as the following:

$$\begin{aligned} &\max \quad \left(\lambda_h + z_h, \hat{\lambda}_h\right) \times P_h^{ss} \\ &\text{s.t.} \quad z_h \le 1 \quad : \quad \xi_h, \quad \forall h, \\ &\sum_{h=1}^{N_h} (z_h) \le \Gamma \quad : \quad \beta, \\ &z_h \ge 0 \end{aligned} \tag{16.3}$$

where Γ is the robust budget of the proposed RO model. Deviation of the power market price from the forecasted value for each time interval is defined by $z_h \hat{\lambda}_h$. The dual variables for the inner problem of Eq. (16.1) are defined by ξ_h and β. Accordingly, the objective function of robust optimal scheduling of distribution network for maximizing profit of DisCO can be reformulated as:

$$\begin{aligned} OF_1 = \max \sum_{h=1}^{N_h} &\left\{ \begin{array}{l} \sum_{i=1}^{N_{\text{load}}} \rho_{\text{sell}}^{P} \times P_{i,h}^{D} + \sum_{i=1}^{N_{\text{load}}} \rho_{\text{sell}}^{Q} \times Q_{i,h}^{D} - \sum_{ss=1}^{N_{SS}} \lambda_h \times P_h^{ss} - \sum_{ss=1}^{N_{SS}} \lambda_{Qfix} \times Q_h^{ss} \\ -\lambda_h \times P_{\text{loss}}^{\text{tot}} - \sum_{n=1}^{N_{DG}} \rho_{\text{sell}}^{PDGO} \times P_{n,h}^{DG} - \sum_{n=1}^{N_{DG}} \rho_{\text{sell}}^{QDGO} \times Q_{n,h}^{DG} \end{array} \right\} - \Gamma\beta - \sum_{h=1}^{N_h} \xi_h \\ \text{s.t.} \quad & \xi_h + \beta \ge \hat{\lambda}_h P_h^{ss} \\ & \xi_h \ge 0 \\ & \beta \ge 0 \end{aligned} \tag{16.4}$$

The objective function of DGO is maximizing its own profit by selling electricity to DisCo. In addition, DGO is the owner of energy storage units. The DGO sells power to the network at power market price. The following formulation can be written for calculating the DGO profit:

$$\begin{aligned} OF_2 = \max \\ \sum_{h=1}^{N_h} &\left\{ \begin{array}{l} \sum_{n=1}^{N_{DG}} \rho_{\text{sell}}^{PDGO} \times P_{n,h}^{DG} + \sum_{j=1}^{N_{DG}} \rho_{\text{sell}}^{QDGO} \times Q_{n,h}^{DG} + \sum_{k=1}^{N_k} \rho_{\text{sell}}^{PDGO} \times P_{k,h}^{\text{disc}} - \sum_{k=1}^{N_k} \lambda_h \times P_{k,h}^{c} \\ -\sum_{n=1}^{N_{DG}} \left(A_n P_{n,h}^{2_{DG}} + B_n P_{n,h}^{DG} + C_n \right) - \sum_{n=1}^{N_{DG}} Q_{n,h}^{DG} \times CT_n^{Q} - C_k^{\text{deg}} \left(\sum_{k=1}^{N_k} \frac{P_{k,h}^{\text{disc}}}{\eta_k^{\text{disc}}} + \eta_k^{C} \times P_{k,h}^{c} \right) \end{array} \right\} \end{aligned} \tag{16.5}$$

where the cost coefficients of diesel generators are defined by A_n, B_n, and C_n. The power charge and discharge of the EES unit are indicated by $P_{k,h}^{c}$ and $P_{k,h}^{\text{disc}}$, respectively. The respective indicators of charge and discharge efficiencies are

indicated by η_k^C and η_k^{disc}. Degradation cost of the EES unit is defined by C_k^{deg}. Reactive power of the diesel generator and the corresponding cost are defined by $Q_{n,h}^{DG}$ and CT_n^Q. The revenues of selling power to DisCo are the first and second terms of (16.2). The revenues of discharged energy and cost of charged energy of batteries are the third and fourth terms of (16.2). The operation cost of DG units is the fifth term of (16.2). Degradation cost of energy storage units is defined as the sixth term of this equation. Considering the uncertain power market price, Eq. (16.5) can be reformulated as a max-min-max robust optimization problem as follows:

$$\begin{aligned} OF_2 = \max & \sum_{h=1}^{N_h} \left\{ \begin{array}{l} \sum_{n=1}^{N_{DG}} \rho_{\text{sell}}^{PDGO} \times P_{n,h}^{DG} + \sum_{j=1}^{N_{DG}} \rho_{\text{sell}}^{QDGO} \times Q_{n,h}^{DG} + \sum_{k=1}^{N_k} \rho_{\text{sell}}^{PDGO} \times P_{k,h}^{\text{disc}} - \sum_{k=1}^{N_k} \lambda_h \times P_{k,h}^{c} \\ -\sum_{n=1}^{N_{DG}} \left(A_n P_{n,h}^{2_{DG}} + B_n P_{n,h}^{DG} + C_n \right) - \sum_{n=1}^{N_{DG}} Q_{n,h}^{DG} \times CT_n^Q - C_k^{\text{deg}} \left(\sum_{k=1}^{N_k} \frac{P_{k,h}^{\text{disc}}}{\eta_k^{\text{disc}}} + \eta_k^C \times P_{k,h}^{c} \right) \end{array} \right\} \\ & + \min \quad \max \sum_{h=1}^{N_h} \sum_{k=1}^{N_k} \lambda_h \times P_{k,h}^{c} \end{aligned} \tag{16.6}$$

Similar to the operation of DisCo, the RO model of the DGO can be solved. The inner problem equivalently can be reformulated as the following:

$$\begin{aligned} \max \quad & \sum_{h=1}^{N_h} \sum_{k=1}^{N_k} \left(\lambda_h + z_h \hat{\lambda}_h \right) \times P_{k,h}^{c} \\ \text{s.t.} \quad & z_h \le 1 : \xi_h, \forall h, \\ & \sum_{h=1}^{N_h} (z_h) \le \Gamma : \beta, \\ & z_h \ge 0 \end{aligned} \tag{16.7}$$

Accordingly, the objective function of robust optimal scheduling of distribution network for maximizing profit of DisCO can be reformulated as:

$$\begin{aligned} OF_2 = \max & \sum_{h=1}^{N_h} \left\{ \begin{array}{l} \sum_{n=1}^{N_{DG}} \rho_{\text{sell}}^{PDGO} \times P_{n,h}^{DG} + \sum_{j=1}^{N_{DG}} \rho_{\text{sell}}^{QDGO} \times Q_{n,h}^{DG} + \sum_{k=1}^{N_k} \rho_{\text{sell}}^{PDGO} \times P_{k,h}^{\text{disc}} - \sum_{k=1}^{N_k} \lambda_h \times P_{k,h}^{c} \\ -\sum_{n=1}^{N_{DG}} \left(A_n P_{n,h}^{2_{DG}} + B_n P_{n,h}^{DG} + C_n \right) - \sum_{n=1}^{N_{DG}} Q_{n,h}^{DG} \times CT_n^Q - C_k^{\text{deg}} \left(\sum_{k=1}^{N_k} \frac{P_{k,h}^{\text{disc}}}{\eta_k^{\text{disc}}} + \eta_k^C \times P_{k,h}^{c} \right) \end{array} \right\} \\ & - \Gamma\beta - \sum_{h=1}^{N_h} \xi_h \\ \text{s.t.} \quad & \xi_h + \beta \ge \hat{\lambda}_h P_h^{ss} \\ & \xi_h \ge 0 \\ & \beta \ge 0 \end{aligned} \tag{16.8}$$

16.2.2 Constraints and Optimal Power Flow Equations

The active and reactive power flow of the distribution network should be considered as:

$$P_h^{ss} + P_{i,h}^{DG} - \left((1 - DR_h) \times P_{i,h}^{D} + ldr_h\right) + \sum_{k=1}^{N_k} \left(P_{k,h}^{\text{disc}} - P_{k,h}^{c}\right) = V_{i,h} \sum_{j} V_{j,h}\left(G_{ij} \cos \delta_{i,h} + B_{ij} \sin \delta_{j,h}\right) \tag{16.9}$$

$$Q_h^{ss} + Q_{i,h}^{DG} - Q_{i,h}^{D} = V_{i,h} \sum_{j} V_{j,h}\left(G_{ij} \cos \delta_{i,h} - B_{ij} \sin \delta_{j,h}\right) \tag{16.10}$$

where the voltage value and voltage angle for each node of the network are defined by $V_{i,h}$ and $\delta_{i,h}$, respectively. Conductance and substance of the network lines are indicated by G_{ij} and B_{ij}, respectively. The active and reactive load demand of the network in each node are defined by $P_{i,h}^{D}$ and $Q_{i,h}^{D}$, respectively.

The limitations of each node voltage and active and reactive power transmission can be stated as follows:

$$V_i^{\min} \le V_{i,h} \le V_i^{\max} \tag{16.11}$$

$$P_{ss}^{\min} \le P_h^{ss} \le P_{ss}^{\max} \tag{16.12}$$

$$Q_{ss}^{\min} \le Q_h^{ss} \le Q_{ss}^{\max} \tag{16.13}$$

$$S_{ij,h} \le S_{ij}^{\max} \tag{16.14}$$

The minimum and maximum values of node voltages are defined by $V_i^{\min}$ and $V_i^{\max}$, respectively. In addition, the respective indicators for lower and upper bounds of the active power exchange between the network and power market are $P_{ss}^{\min}$ and $P_{ss}^{\max}$. The minimum and maximum reactive power exchange between the network and power market are indicated by $Q_{ss}^{\min}$ and $Q_{ss}^{\max}$, respectively. Maximum thermal limit of each line of the network is defined by a, and power flow in network branches is defined by $S_{ij,h}$. The generation of active and reactive power of each generation units should be limited to its minimum and maximum values as follows:

$$P_{DG}^{\min} \le P_{i,h}^{DG} \le P_{DG}^{\max} \tag{16.15}$$

$$Q_{DG}^{\min} \le Q_{i,h}^{DG} \le Q_{DG}^{\max} \tag{16.16}$$

The minimum and maximum generations of each generator are defined by $P_{DG}^{\min}$ and $P_{DG}^{\max}$, respectively. In addition, the respective indicators of minimum and

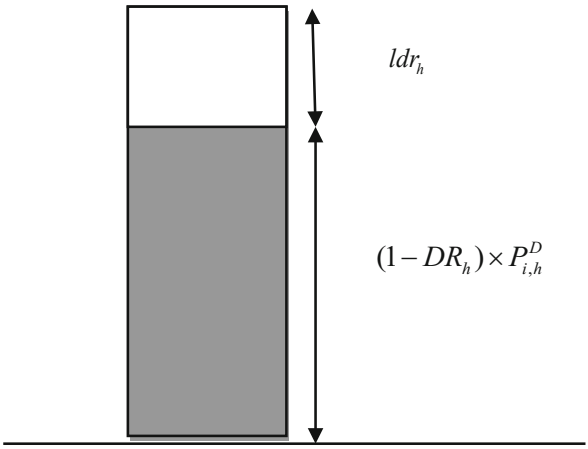

Fig. 16.1 DRP load modeling

maximum amounts of reactive power generation of such units are $Q_{DG}^{\min}$ and $Q_{DG}^{\max}$. It is assumed that the power factor for each generation unit is constant:

$$\cos\phi = \frac{P_{i,h}^{DG}}{\sqrt{\left(P_{i,h}^{DG}\right)^2 + \left(Q_{i,h}^{DG}\right)}} = \text{const.} \tag{16.17}$$

The tap setting of tap changer is stated as:

$$T_l^{\min} \le T_{l,h} \le T_l^{\max} \tag{16.18}$$

where tap setting of tap changer is defined by $T_{l,h}$ and its corresponding minimum and maximum values are indicated by $T_l^{\min}$ and $T_l^{\max}$.

The application of DRPs has been studied in this paper to shift load demands of the consumers from on-peak hours to off-peak hours. Time-of-use program is selected as DRP in this chapter, which is shown in Fig. 16.1.

The load demand of the network is classified to two parts, where the dashed section does not participate in the program and the other can shift load from on-peak hours to off-peak hours, which can be formulated as follows:

$$P_{i,h}^{D} = (1 - DR_h) \times P_{i,h}^{D} + ldr_h \tag{16.19}$$

$$P_{i,h}^{D} - P_{i,h}^{DR} = ldr_h = DR_h \times P_{i,h}^{D} \tag{16.20}$$

where the costumers' participation in DRP is defined by DR_h and the load value shifted by DRP is indicated by ldr_h. It should be considered that total demand during the scheduling time interval before application of DRP should be equal to the sum of demand by employing DRP, which can be stated as:

$$\sum_{h=1}^{N_h} ldr_h = \sum_{h=1}^{N_h} DR_h \times P_{i,h}^{D} \tag{16.21}$$

$$DR_h \leq DR_{\max} \tag{16.22}$$

where the maximum rate for costumers' participation in DRP is defined by $DR_{\max}$. Demand increment by employing DRP should be limited as follows:

$$P_{i,h}^{D(inc)} \leq inc_h \times P_{i,h}^{D} \tag{16.23}$$

$$inc_h \leq inc_{\max} \tag{16.24}$$

As mentioned before, it is assumed that the DGO owns energy storage unit. The constraints of the storage units have been provided in the following. The limitations of charge/discharge of the storage units are as (16.19). The energy stored in the energy storage units is limited to its minimum and maximum limits as (16.20). The storage can be operated only in one of the states of charge, discharge, or ideal, which is stated as (16.21). The energy balance of the energy storage unit is provided in (16.22):

$$0 \leq P_{k,h}^{c} \leq b_{k,h}^{c} P_{k,h}^{c,\max}, 0 \leq P_{k,h}^{\text{disc}} \leq b_{k,h}^{\text{disc}} P_{k,h}^{\text{disc},\max} \tag{16.25}$$

$$E_k^{\min} \leq E_{k,h} \leq E_k^{\max} \tag{16.26}$$

$$b_{k,h}^{c} + b_{k,h}^{\text{disc}} \leq 1; b_{k,h}^{c}, b_{k,h}^{\text{disc}} \in \{1, 0\} \tag{16.27}$$

$$E_{k,h+1} = E_{k,h} + \left(\eta_k^{C} \times P_{k,h}^{c} - \frac{P_{k,h}^{\text{disc}}}{\eta_k^{\text{disc}}} \right) \tag{16.28}$$

where the maximum charge and discharge power rates of the EES unit at each time interval are defined by $P_{k,h}^{c,\max}$ and $P_{k,h}^{\text{disc},\max}$, respectively. The energy charged at the EES unit is indicated by $E_{k,h}$, and its corresponding minimum and maximum values are indicated by $E_k^{\min}$ and $E_k^{\max}$, respectively. The binary variables $b_{k,h}^{c}$ and $b_{k,h}^{\text{disc}}$ are used to define the operation of EES unit in charge, discharge, or ideal modes.

16.3 Solution Method and Case Study

16.3.1 ε-Constraint Method

The multi-objective problems have been handled using different methods in recent publications. In this chapter, ε-constraint method is used to solve the proposed robust optimal scheduling of distribution networks. Such method considers one of the

multi-objectives as main objective and the other objectives as the constraints of main objective, which can be stated as [4]:

$$\begin{aligned} &OF = \max(\text{of}_1) \\ &\text{s.t.} \\ &\begin{cases} \text{of}_2 \geq \varepsilon \\ \text{Eqs.}(16.9) - (16.27) \end{cases} \end{aligned} \tag{16.29}$$

Fuzzy satisfying approach is selected as the solution method to select the best compromise solution among the provided Pareto optimal solutions. Considering a problem with N objectives, linear membership function for the sth solution of the wth function can be stated as [20]:

$$\mu_w^s = \begin{cases} 1 & of_w^s \leq f_w^{\min} \\ \dfrac{\text{OF}_w^{\max} - \text{of}_w^s}{\text{OF}_w^{\max} - \text{OF}_w^{\min}} & \text{OF}_w^{\min} \leq of_w^s \leq \text{OF}_w^{\max} \\ 0 & of_w^s \geq \text{OF}_w^{\max} \end{cases} \tag{16.30}$$

where the maximum and minimum values of the objective function w are indicated by $\text{OF}_k^{\max}$ and $\text{OF}_k^{\min}$ are in solutions of Pareto optimal set. μ_w^s defines the optimality degree of the sth solution of wth objective function. The membership function of sth solution can be obtained as:

$$\begin{aligned} &\mu^s = \min\left(\mu_1^s, \ldots, \mu_N^s\right) \\ &\text{s} = 1, \ldots, \text{N}_P \end{aligned} \tag{16.31}$$

The best compromise solution will be selected as the solution with maximum weakest membership function. The corresponding membership function of this solution ($\mu^{\max}$) can be obtained as:

$$\mu^{\max} = \max\left(\mu^1, \ldots, \mu^{Np}\right) \tag{16.32}$$

16.3.2 Case Study and Problem Assumptions

The proposed model has been applied on 33-bus distribution network, which is demonstrated in Fig. 16.2. The hypothetical voltage level of the substation and the hypothetical capacity of the feeders are 12.66 kV and 8 MVA, respectively. In addition, the peak load is 4460 kW and 2760 kVar.

As mentioned before, the DGO is the owner of distributed generators, which are DG1 and DG2 with a capacity of 1.5 MW installed at the nodes 11 and 33 in the studied test system, respectively. In addition, reactive power compensations RPC1

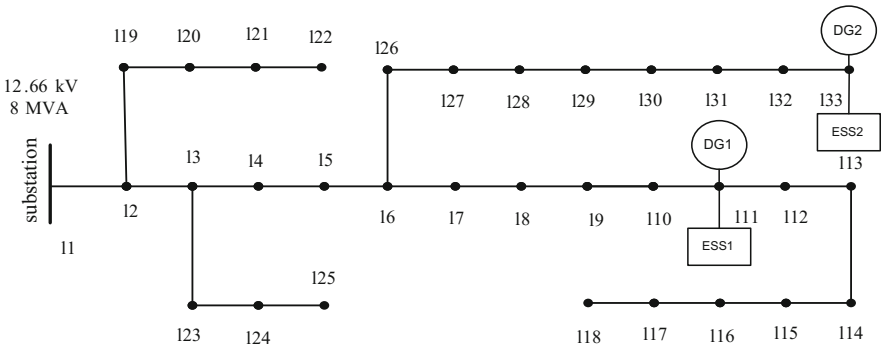

Fig. 16.2 The studied test system

Table 16.1 Characteristics of DG units

Bus with DG	A ($/MW^2)	B ($/MW)	C ($)	CT_j^Q($/MVar)
11	0.0075	36	28.5	4.28
33	0.0075	40	22	8.5

Table 16.2 Economic and technical data

Parameters	Values	Parameters	Values
$V_i^{\max}$ (p.u.)	1.05	ρ_{sell}^{P} ($/MWh)	85
$V_i^{\min}$ (p.u.)	0.95	ρ_{sell}^{Q} ($/Mvarh)	52
PF_{DG}	0.95	$\rho^{\text{sell}}{}_{PDGO}$ ($/MWh)	67
ρ_{base}	72	λ_{Qfix} ($/Mvarh)	42

Table 16.3 Characteristics of the energy storage units

E_k^{cap} (MWh)	0.5	$P_{k,h}^{c,\max}$ (MW)	0.2
$E_k^{\min}$ (MWh)	0.1	$P_{k,h}^{\text{disc},\max}$ (MW)	0.2
$E_k^{\max}$ (MWh)	0.45	η_k^{C}	0.95
C_k^{deg} ($/MWh)	2.7	η_k^{disc}	0.85

and RPC2 are located in buses 17 and 33 with capacities of 0.8 MVar and 1.7 MVar, respectively. Two storage units are located in parallel with DG plants with capacity of 0.5 MW and charge/discharge rate of 200 kW. The lower and upper bounds of energy storage of the battery are 100 kWh and 500 kWh, respectively.

The characteristics of DG units are provided in Table 16.1. Table 16.2 prepared the economic and technical data of the studied network. The characteristics of the energy storage units are provided in Table 16.3.

16.4 Assumptions and Simulation Results

In this section, the simulation results of the proposed robust model for optimal scheduling of distribution networks have been reported and analyzed. The robust short-term scheduling is accomplished for a daily 24-h time interval considering demand response programs. The robust budget is considered to be 10, and 20% deviation is considered for the forecasted values of the power market price for 24 h. The forecasted, minimum and maximum power market prices are provided in Table 16.4. The Pareto solutions provided for the multi-objective problem are reported in Table 16.5. The ε-constraint method has solved the problem for 20 iterations, which is obvious from this table. By using the fuzzy satisfying method, the best compromise solution is related to Solution#12, where the benefit of DisCO and DGO are $6035.132 and $1575.873, respectively. It should be mentioned that the optimal benefit of the DisCO and DGO for the studied network without implementing RO method is as $6176.782 and $1687.76, which are reduced by the proposed model due to considering the worst case of the uncertain price.

The obtained optimal scheduling of the distribution network for the best compromise solution is investigated. Figure 16.3 shows the electrical energy purchased from the upstream grid during the 24-h scheduling time horizon.

The optimal generation scheduling of DG1 and DG2 during the 24-h scheduling time interval is demonstrated in Fig. 16.4, which shows that DG1 has participated in power demand supply more than DG2.

The optimal charge/discharge power of the batteries 1 and 2 is depicted in Fig. 16.5. The analysis shows that energy storage units have charged power during on-peak hours and have discharged the power in off-peak hours to supply the load demand when required.

Load demand of the studied distribution network with and without consideration of demand response program has been demonstrated in Fig. 16.6, which shows the effectiveness of the demand response program on modifying the load demand profile of the network.

Table 16.4 Forecasted, minimum and maximum power market price

h	Forecasted	Minimum	Maximum	*h*	Forecasted	Minimum	Maximum
1	53.96	43.17	64.76	13	52.97	42.38	63.56
2	41.9	33.52	50.28	14	53.32	42.66	63.99
3	36.38	29.11	43.66	15	57.53	46.03	69.04
4	34.27	27.42	41.13	16	56.63	45.30	67.95
5	34.62	27.7	41.54	17	55.29	44.23	66.35
6	34.01	27.21	40.82	18	56.42	45.14	67.71
7	37.03	29.62	44.44	19	57.38	45.90	68.85
8	37.146	29.72	44.58	20	59.64	47.71	71.57
9	40.75	32.6	48.9	21	67.19	53.76	80.63
10	46.90	37.53	56.29	22	72	57.6	86.4
11	49.99	39.99	59.99	23	68.49	54.79	82.19
12	50.09	40.08	60.11	24	63.88	51.10	76.65

Table 16.5 Pareto optimal solutions for optimal robust scheduling of active distribution network

#	DisCo profit ($/day)	DGO profit ($/day)	$\mu_1(p.u.)$	$\mu_2(p.u.)$	$\min(\mu_1, \mu_2)$
1	6333.116	399.184	0.759	0.035	0.035
2	6332.883	434.1791	0.758	0.05	0.05
3	6325.504	548.3485	0.753	0.1	0.1
4	6317.749	662.5178	0.747	0.15	0.15
5	6299.751	776.6872	0.733	0.2	0.2
6	6275.487	890.8566	0.714	0.25	0.25
7	6251.245	1005.026	0.695	0.3	0.3
8	6218.831	1119.195	0.667	0.35	0.35
9	6178.841	1233.365	0.639	0.4	0.4
10	6134.358	1347.534	0.604	0.45	0.45
11	6086.15	1461.703	0.567	0.5	0.5
12	**6035.132**	**1575.873**	**0.527**	**0.55**	**0.527**
13	5980.843	1690.042	0.485	0.6	0.485
14	5923.55	1804.211	0.440	0.65	0.440
15	5863.299	1918.381	0.393	0.7	0.393
16	5799.832	2032.55	0.344	0.75	0.344
17	5732.331	2146.72	0.291	0.8	0.291
18	5655.338	2260.889	0.232	0.85	0.232
19	5584.698	2375.058	0.177	0.9	0.177
20	5477.487	2489.228	0.093	0.95	0.093

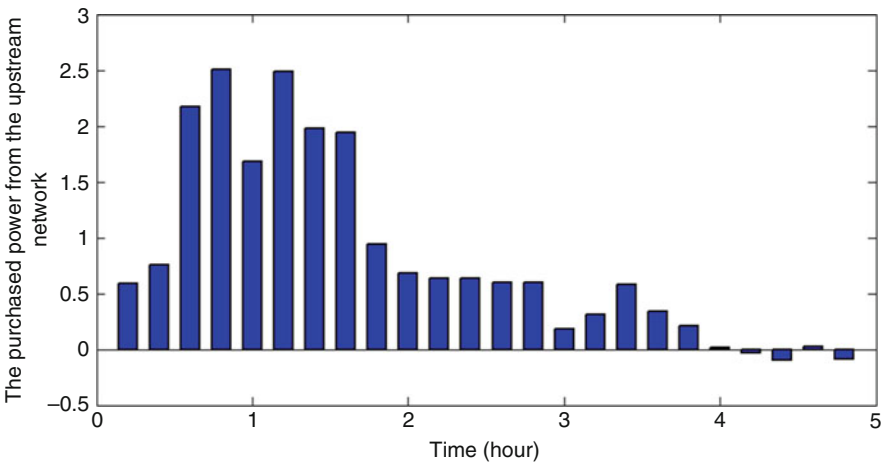

Fig. 16.3 Purchased electrical energy from the upstream grid

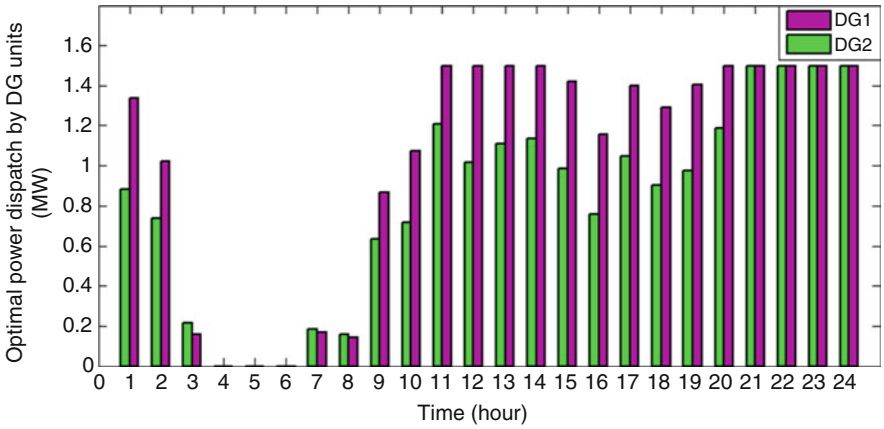

Fig. 16.4 Optimal economic dispatch of distribution generators

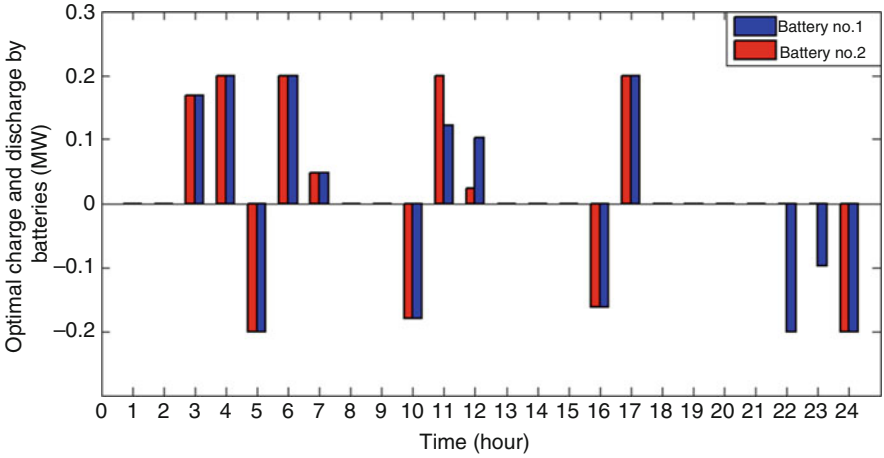

Fig. 16.5 Optimal charge/discharge power of the energy storage units

The optimal set points of OLTC and RPCs for the studied test system of active distribution network are reported in Table 16.6. The application of DRP has been considered in the obtained solution for this case study.

16.5 Conclusions

This chapter aimed to study the robust scheduling of active distribution network considering maximization of benefit of distribution company and benefit of distributed generation owner. The uncertainty associated with forecasted power market

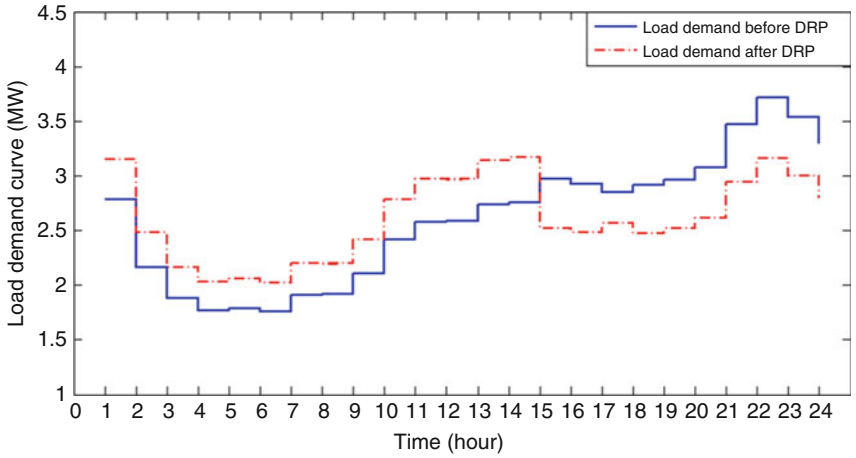

Fig. 16.6 Load demand of the studied network with and without consideration of DRP

Table 16.6 Optimal set points of OLTC and RPCs of active distribution network

h	RPC1 (MVar)	RPC2 (MVar)	OLTC (p. u)	*h*	RPC1 (MVar)	RPC2 (MVar)	OLTC (p. u)
1	0.559	1.220	1.024	13	0.548	1.2	1.007
2	0.421	0.945	1.05	14	0.551	1.208	1.006
3	0.359	0.840	1.05	15	0.596	1.300	1.004
4	0.343	0.803	1.05	16	0.581	1.279	1.008
5	0.338	0.791	1.05	17	0.563	1.248	1.013
6	0.340	0.797	1.05	18	0.578	1.274	1.009
7	0.363	0.850	1.05	19	0.593	1.296	1.004
8	0.364	0.852	1.030	20	0.622	1.355	0.995
9	0.407	0.918	1.017	21	0.7	1.547	0.98
10	0.478	1.059	1.012	22	0.761	1.658	0.974
11	0.513	1.131	1.012	23	0.717	1.568	0.983
12	0.515	1.132	1.024	24	0.667	1.466	0.983

price has been investigated. Robust optimization method has been implemented as an effective method to deal with such uncertainty. The provided optimal scheduling of the network using robust optimization method prevents the distribution company and distributed generation owner from being exposed to low benefit considering undesired deviation of market power prices from the forecasted values. A robust budget of 10 and 20% deviation of power market price from the forecasted values is taken into account. By using the proposed model, the benefit of distribution company and distributed generation owner is obtained as \$6035.132 and \$1575.873, respectively.

References

1. Saint-Pierre, A., & Mancarella, P. (2017). Active distribution system management: A dual-horizon scheduling framework for DSO/TSO interface under uncertainty. *IEEE Transactions on Smart Grid, 8*(5), 2186–2197.
2. Wang, F., Xu, H., Xu, T., Li, K., Shafie-Khah, M., & Catalão, J. P. (2017). The values of market-based demand response on improving power system reliability under extreme circumstances. *Applied Energy, 193*, 220–231.
3. Abapour, S., Nojavan, S., & Abapour, M. (2018). Multi-objective short-term scheduling of active distribution networks for benefit maximization of DisCos and DG owners considering demand response programs and energy storage system. *Journal of Modern Power Systems and Clean Energy, 6*(1), 95–106.
4. Nazari-Heris, M., Abapour, S., & Mohammadi-Ivatloo, B. (2017). Optimal economic dispatch of FC-CHP based heat and power micro-grids. *Applied Thermal Engineering, 114*, 756–769.
5. Cho, J., Jeong, S., & Kim, Y. (2015). Commercial and research battery technologies for electrical energy storage applications. *Progress in Energy and Combustion Science, 48*, 84–101.
6. Wu, Y., Liu, L., Gao, J., Chu, H., & Xu, C. (2017). An extended VIKOR-based approach for pumped hydro energy storage plant site selection with heterogeneous information. *Information, 8*(3), 106.
7. Nazari-Heris, M., & Kalavani, F. (2017). Evaluation of peak shifting and energy saving potential of ice storage based air conditioning systems in Iran. *Journal of Operation and Automation in Power Engineering, 5*(2), 163–170.
8. Budt, M., Wolf, D., Span, R., & Yan, J. (2016). A review on compressed air energy storage: Basic principles, past milestones and recent developments. *Applied Energy, 170*, 250–268.
9. Siano, P. (2014). Demand response and smart grids—A survey. *Renewable and Sustainable Energy Reviews, 30*, 461–478.
10. Nojavan, S., Mohammadi-Ivatloo, B., & Zare, K. (2015). Optimal bidding strategy of electricity retailers using robust optimisation approach considering time-of-use rate demand response programs under market price uncertainties. *IET Generation, Transmission & Distribution, 9* (4), 328–338.
11. Neves, D., Pina, A., & Silva, C. A. (2015). Demand response modeling: A comparison between tools. *Applied Energy, 146*, 288–297.
12. Zhou, Y., Mancarella, P., & Mutale, J. (2015). Modelling and assessment of the contribution of demand response and electrical energy storage to adequacy of supply. *Sustainable Energy, Grids and Networks, 3*, 12–23.
13. Luo, F., Meng, K., Dong, Z. Y., Zheng, Y., Chen, Y., & Wong, K. P. (2015). Coordinated operational planning for wind farm with battery energy storage system. *IEEE Transactions on Sustainable Energy, 6*(1), 253–262.
14. Palizban, O., Kauhaniemi, K., & Guerrero, J. M. (2014). Microgrids in active network management—Part I: Hierarchical control, energy storage, virtual power plants, and market participation. *Renewable and Sustainable Energy Reviews, 36*, 428–439.
15. Parastegari, M., Hooshmand, R. A., Khodabakhshian, A., & Zare, A. H. (2015). Joint operation of wind farm, photovoltaic, pump-storage and energy storage devices in energy and reserve markets. *International Journal of Electrical Power & Energy Systems, 64*, 275–284.
16. Rahbar, K., Xu, J., & Zhang, R. (2015). Real-time energy storage management for renewable integration in microgrid: An off-line optimization approach. *IEEE Transactions on Smart Grid, 6*(1), 124–134.
17. Abapour, S., Zare, K., & Mohammadi-Ivatloo, B. (2015). Dynamic planning of distributed generation units in active distribution network. *IET Generation, Transmission & Distribution, 9* (12), 1455–1463.

18. Nazari-Heris, M., Mohammadi-Ivatloo, B., Gharehpetian, G. B., & Shahidehpour, M. (2018). Robust short-term scheduling of integrated heat and power microgrids. *IEEE Systems Journal, PP*(99), 1–9.
19. Nazari-Heris, M., & Mohammadi-Ivatloo, B. (2018). Application of robust optimization method to power system problems. In *Classical and recent aspects of power system optimization* (pp. 19–32). Elsevier Publisher
20. Soroudi, A., Mohammadi-Ivatloo, B., & Rabiee, A. (2014). Energy hub management with intermittent wind power. In *Large scale renewable power generation* (pp. 413–438). Singapore: Springer.

Index

B. Mohammadi-ivatloo, M. Nazari-Heris (eds.), *Robust Optimal Planning and Operation of Electrical Energy Systems*,
https://doi.org/10.1007/978-3-030-04296-7